

NOTE TO USERS

This reproduction is the best copy available.

UMI[®]

**The relationship of transgressive systems tracts to sea-floor diagenesis,
Lower Cretaceous, Scotian Basin**

By

Ann Chioma Okwese

**A Thesis Submitted to Saint Mary's University, Halifax, Nova Scotia,
in Partial Fulfillment of the Requirements for the Degree of Masters of Science**

June, 2010, Halifax, Nova Scotia

© Ann Okwese, 2010

Approved: Dr. Peir K. Pufahl
External Examiner

Approved: Dr. Georgia Pe-Piper
Senior Supervisor

Approved: Dr. Danika van Proosdji
Supervisory Committee Member

Approved: Dr. Andrew MacRae
Supervisory Committee Member

Approved: Dr. David J.W. Piper
Supervisory Committee Member

Approved: Dr. Cristian Suteanu
Program Representative

Approved: Dr. Pierre Jutras
Graduate Studies Representative

June 11, 2010



Library and Archives
Canada

Published Heritage
Branch

395 Wellington Street
Ottawa ON K1A 0N4
Canada

Bibliothèque et
Archives Canada

Direction du
Patrimoine de l'édition

395, rue Wellington
Ottawa ON K1A 0N4
Canada

Your file *Votre référence*

ISBN: 978-0-494-68811-3

Our file *Notre référence*

ISBN: 978-0-494-68811-3

NOTICE:

The author has granted a non-exclusive license allowing Library and Archives Canada to reproduce, publish, archive, preserve, conserve, communicate to the public by telecommunication or on the Internet, loan, distribute and sell theses worldwide, for commercial or non-commercial purposes, in microform, paper, electronic and/or any other formats.

The author retains copyright ownership and moral rights in this thesis. Neither the thesis nor substantial extracts from it may be printed or otherwise reproduced without the author's permission.

AVIS:

L'auteur a accordé une licence non exclusive permettant à la Bibliothèque et Archives Canada de reproduire, publier, archiver, sauvegarder, conserver, transmettre au public par télécommunication ou par l'Internet, prêter, distribuer et vendre des thèses partout dans le monde, à des fins commerciales ou autres, sur support microforme, papier, électronique et/ou autres formats.

L'auteur conserve la propriété du droit d'auteur et des droits moraux qui protègent cette thèse. Ni la thèse ni des extraits substantiels de celle-ci ne doivent être imprimés ou autrement reproduits sans son autorisation.

In compliance with the Canadian Privacy Act some supporting forms may have been removed from this thesis.

While these forms may be included in the document page count, their removal does not represent any loss of content from the thesis.

Conformément à la loi canadienne sur la protection de la vie privée, quelques formulaires secondaires ont été enlevés de cette thèse.

Bien que ces formulaires aient inclus dans la pagination, il n'y aura aucun contenu manquant.

■ ■ ■
Canada

The relationship of transgressive systems tracts to sea-floor diagenesis, Lower Cretaceous, Scotian Basin

By Ann Okwese

Abstract

The Lower Cretaceous rocks of the Scotian Basin are deltaic, with cycles of delta progradation with relatively high sedimentation rates, capped by a transgressive unit with lower sedimentation rates. The diagenetic mineral phases in the sea-floor diagenetic system are commonly preserved where there is abrupt change in sedimentation rates, and also in coated grains found in the transgressive unit. This study assesses the role of seafloor diagenesis in the overall diagenetic system of the Lower Cretaceous of the Scotian Basin by studying the sedimentology, mineralogy, and geochemistry of the transgressive unit and underlying sediments from conventional core in two wells.

The observed variation in mineralogy and geochemistry of the different transgressive units can be tentatively related to their different facies associations. Those in younger strata at Peskowsk can be compared with modern sea-floor diagenetic systems in areas of high Fe availability. In shelf-edge deltaic deposits at Thebaud, there was higher Ca and Mg availability.

June 11, 2010.

ACKNOWLEDGEMENTS

I am heartily thankful to my supervisor, Georgia Pe-Piper for providing me the opportunity and finances to work on this project. Her encouragement, guidance and support from the initial to the final level enabled me to develop an understanding of the subject.

It is a pleasure to thank those who made this thesis possible. David Piper, your advice and feedback through draft after draft increased my knowledge and made completing this thesis possible. Danika van Proosdji, your feedback from the beginning of the thesis to the very end was very helpful. Andrew MacRae, thank you for your constructive feedback, that helped broaden my horizons and gave my work a more in-depth meaning.

The funding for this thesis came from a collaborative Research and Development Grant from the Petroleum Research-Atlantic Canada (PR-AC) and NSERC.

This thesis would not have been possible without the assistance of the Canada-Nova Scotia Petroleum Board whom provided samples and arranged for time in the lab.

I am grateful to William LeBlanc of the Geological Survey of Canada (Bedford Institute of Oceanography) for his assistance in conducting X-ray diffraction and Carbon analysis.

I would like to show my gratitude to the Dalhousie University Regional Electron Microprobe and Image Analysis facility and the Saint Mary's University Regional Analytic Centre. These facilities made completing the petrography aspect of my project possible. I am would like to thank Randolph Corney and Barbara Meunier for assistance throughout the course of my program.

Thank you to my family for their never ending love, and words of encouragement. I would like to show my gratitude to Maryanne and Maureen for their ear, and shoulder whenever I needed it. Your support has been more than amazing and I could not have finished without the constant push I get from you.

I offer my regards and blessings to all of those who supported me in any respect during the completion of the project, and I owe my deepest gratitude to God for giving me the strength to complete this project.

TABLE OF CONTENTS	PAGES
Title	i
Abstract	ii
Acknowledgements	iii
Table of Contents	iv-vi
List of Tables	vii-viii
List of Figures	ix-xx
List of Abbreviations	xxi
 Chapter 1: Introduction	 1-23
1.1 General Statement	1-4
1.2 Previous Work on Early Diagenesis in the Cretaceous of the Scotian Basin	5-10
1.3 The Modern Sea-floor Diagenetic System	11-20
1.3.1 Introduction	11
1.3.2 Redox Reactions	11-13
1.3.3 Precipitation and Preservation of Phosphorus	13-15
1.3.4 Carbonate Fluorapatite	15
1.3.5 Coated Grains and Ooids	16-19
1.3.6 Rare Earth Elements	19-20
1.4 Research Objectives	21-22
1.4.1 Research Problem	21
1.4.2 Research Objectives	21-22
1.4.3 Expected Significance of the Research	22
1.5 Chapter Summary	23
 Chapter 2: Background and Study Area	 24-48
2.1 Evolution of the Scotian Basin	24-26
2.2 The Sedimentary Environment of the Uppermost Jurassic-Lower Cretaceous	27-31
2.2.1 Introduction	27-28
2.2.2 Mic Mac Formation	28-29
2.2.3 Missisauga Formation	29
2.2.4 Verrill Canyon Formation	29
2.2.5 Logan Canyon Formation	30
2.2.6 Dawson Canyon Formation	30
2.2.7 Wyandot Formation	31
2.3 Sequence Stratigraphy of the Lower Cretaceous	32-36
2.4 Wells Studied	37-41
2.4.1 General Strategy	37
2.4.2 Peskowesk A-99; location, general stratigraphy, location of cores	37-39
2.4.3 Thebaud C-74; location, general stratigraphy, location of cores	40-41
2.5 Gamma Log Interpretations of Cores	42-47
2.6 Chapter Summary	48
 Chapter 3: Results (Stratigraphy and Sedimentology)	 49-124
3.1 Introduction	49

3.2 Methods	53-54
3.3 Sediment Lithofacies	55-66
3.3.1 Identified Lithofacies	56-66
3.4 Description of core intervals	67-112
3.4.1 Peskowsk A-99	67-90
3.4.2 Thebaud C-74	91-101
3.5 Detailed character of Transgressive Units	113-124
3.5.1 Introduction	113-114
3.5.2 Identified Packets in Thebaud C-74	114-117
3.5.3 Identified Packets in Peskowsk A-99	117-120
3.6 Chapter Summary	120
Chapter 4: Results (Petrography)	125-170
4.1 Laboratory Methods	125
4.1.1 Electron Microprobe, Scanning Electron and Petrographic Microscope	125
4.1.2 X-ray Diffraction	126
4.2 Petrographic Results	130-163
4.2.1 Introduction	130
4.2.2 Coated Grains	130-138
4.2.3 Carbonate Cement	138-144
4.2.4 Pyrite and Phosphorite Cements	144-149
4.2.5 Kaolinite Cement and Concretions	149-152
4.2.6 Chlorite Cement	152-159
4.2.7 Quartz Overgrowth	159-161
4.2.8 Titanium Minerals	159-165
4.3 Paragenetic Sequence	166-170
4.3.1 Thebaud C-74	166-168
4.3.2 Peskowsk A-99	168-170
4.4 Chapter Summary	171
Chapter 5: Results (Geochemistry)	172-232
5.1 Laboratory Methods	172-191
5.1.1 Carbon Analysis	192-196
5.2 Results: Statistical Analyses	198-215
5.2.1 Introduction	198
5.2.2 Correlation Coefficient Correlations at Peskowsk A-99	198-202
5.2.3 Correlation Coefficient Correlations at Thebaud C-74	202
5.2.4 Principal Component Analysis (PCA)	203-215
5.3 Results: Variation of Elements with Minerals and Facies	216-224
5.3.1 Effects of Diagenetic Cements	216-217
5.3.2 Variations in Geochemistry with Facies	217
5.3.3 Behavior of P and Ti	217-219
5.3.4 Mineralogical Control of Key Elements	222
5.3.5 Stratigraphical Variations in Ca, Fe, Mg, Ti, P, Rb, and K ₂ O	222
5.4 Results: Downcore Variation of Elements	225-232

5.4.1 Geochemical Differences	225-232
5.5 Chapter Summary	232
Chapter 6: Discussion and Conclusions	233-267
6.1 Introduction and Review of Objectives	233-234
6.1.1 Paleogeographic Setting	234
6.2 Diagenetic Minerals and Paragenetic Sequence	235-239
6.3 Paragenetic Sequence at and near the Sea-floor	240-243
6.4 The Role of Burial Diagenesis	243
6.4.1 Early Meteoric Water	243
6.4.2 Deeper or Later Diagenesis	243
6.5 Stratigraphic and Geographical Variations in Chemistry and Mineralogy	244-249
6.5.1 Detrital Mineralogy and Geochemistry	244
6.5.2 Bulk Geochemistry of Major Elements involved in Early Diagenesis	244-246
6.5.3 Variation in Abundance of Early Diagenetic Mineralogy	246-250
6.6 Comparison of Transgressive Units	251-255
6.6.1 Facies and the Sedimentation rates	251
6.6.2 Thebaud C-74	251-253
6.6.3 Peskowsk A-99	253-254
6.7 Fossilization of the Sea-Floor Diagenetic Sequence	256-259
6.7.1 The Sampling Problem	257
6.8 An Integrated Diagenetic Model	259-264
6.8.1 Introduction	259
6.8.2 Distribution of Diagenetic Carbonates	259-260
6.8.3 Principal Component Analysis of Whole-rock Geochemistry	260
6.8.4 Depositional Model for Studied Wells	261-264
6.8.5 Reservoir Quality	264-265
6.9 Conclusions	266-267
References	269-275
Appendices	refer to CD

LIST OF TABLES

Table 3.1: Characteristics of lithofacies used for both studied wells.	50-52
Table 3.2: Conventional core information for both studied wells. Modified from Natural Resources Canada, Geological Survey of Canada, Geoscience Data Repository, BASIN Database: http://basin.gdr.nrcan.gc.ca/index_e.php	54
Table 3.3: Summary of observations from packets in Thebaud C-74 and Peskowesk A-99.	115
Table 4.1: Summary of petrography with lithofacies at Thebaud C-74.	127-128
Table 4.2: Summary of petrography with lithofacies at Peskowesk A-99.	129
Table 4.3: Detailed description of coated grains types in studied wells.	131-132
Table 4.4: Stratigraphic distribution of coated grains in studied wells.	133-134
Table 5.1a: Location and other information of analytical samples from Thebaud C-74.	173-174
Table 5.1b: Location and other information of analytical samples from Peskowesk A-99.	175-178
Table 5.2a: Representative whole rock geochemical analyses for Thebaud C-74.	179-183
Table 5.2b: Representative whole rock analyses for Peskowesk A-99.	184-191
Table 5.3a: Carbon analysis results for Thebaud C-74.	193-194
Table 5.3b: Carbon analysis results for Peskowesk A-99.	195-197
Table 5.4a: Correlation coefficient matrix, Peskowesk A-99.	199
Table 5.4b: Correlation coefficient matrix, Thebaud C-74.	200
Table 5.5a: Major elements PCA data with variables loadings for Thebaud C-74.	205
Table 5.5b: Major elements PCA data with variables loadings for Peskowesk A-99.	206
Table 5.6a: Major and trace element, facies and grain size PCA data	

with variable loadings for Thebaud C-74.	207
Table 5.6b: Major and trace element, facies and grain size PCA data with variable loadings for Peskowsk A-99.	208
Table 5.7: Facies re-numbering chart for both studied wells.	209
Table 6.1: Stratigraphic and geographic variations of diagenetic minerals for both studied wells.	245

LIST OF FIGURES

Figure 1.1: General map of the Scotian Basin (modified from Williams and Grant 1998) showing depth to basement in kilometres.	2
Figure 1.2: Paragenetic sequences from the Scotian Basin (modified from Gould <i>et al.</i> , 2010).	8
Figure 1.3: Fossilization of diagenetic sea-floor minerals in the Scotian Basin (modified from Gould 2007).	10
Figure 1.4: Diagenetic chemical reactions (modified from Fisher, 1982).	12
Figure 1.5: Pore-water chemistry of element within the diagenetic chemical reaction profile (modified from Burns, 1997).	12
Figure 1.6: Mode of formation of the Fe ooid (modified from Collin <i>et al.</i> , 2005).	19
Figure 2.1: Cross section of the Scotian Basin near Peskowsk A-99 (modified from Wade <i>et al.</i> 1995).	25
Figure 2.2: Generalized paleogeography of large deltas in the Scotian Basin in the Late Jurassic (GSC, 2004).	26
Figure 2.3: Generalized stratigraphy of the Cretaceous (modified from Wade and Maclean, 1993).	28
Figure 2.4: Lithostratigraphy, core locations, gamma and sonic logs at the Peskowsk A-99 well.	38
Figure 2.5: Lithostratigraphy, core locations, gamma and sonic logs at the Thebaud C-74 well.	41
Figure 2.6: Legend for lithologies depicted in Figures 2.7 to 2.11.	42
Figure 2.7: Gamma and core plots for cores 1-6 at Thebaud C-74.	43
Figure 2.8: Gamma and core plots for cores 1-4 at Peskowsk A-99.	45
Figure 2.9: Gamma and core plot for core 5 at Peskowsk A-99.	46
Figure 2.10: Gamma and core plot for core 6 at Peskowsk A-99.	47
Figure 2.11: Gamma and core plot for core 7 at Peskowsk A-99.	47

Figure 3.1: Graphical interpretation of lithofacies in the specific environments (modified from Gould, 2007).	55
Figure 3.2: 2220.41 m: facies 0m with sharp-based siltstone beds with pervasive chondrites bioturbation in predominantly mudstone at Thebaud C-74.	63
Figure 3.3: 3870.56 m, facies 0s showing the muddiest interval after transgression.	63
Figure 3.4: 2491.94 m, facies 1 shale.	63
Figure 3.5: 3808.85 m, facies 1c calcareous shale overlying bioclastic limestone.	63
Figure 3.6: 2272.28 m, facies 2b with interbedded fine-grained sandstone and silty mudstone with uncommon bioturbation at the base.	63
Figure 3.7 2275.56 m, facies 2c showing bioturbated medium-grained sandstone with siderite cementation and sparse shelly fragments.	63
Figures 3.8: 2481.20 m, facies 3a with large shelly fragments in commonly bioturbated fine-grained sandstone with mudstone laminae at Peskowsk A-99.	64
Figure 3.9: 3902.55 m, facies 3b with fine-grained sandstone with siderite intraclast and lithic granules and common bioturbation at Thebaud C-74.	64
Figure 3.10: 2492.84 m, facies 3c with siderite cemented coarse-grained sandstone with thick-shelled shelly fragments at Peskowsk A-99.	64
Figure 3.11: 3808.85 m, facies 3l, bioclastic limestone underlying calcareous shale in facies 1c at Peskowsk A-99.	64
Figure 3.12: 3801.60 m, facies 3m, thick mudstone beds with siderite cementation at Peskowsk A-99.	64
Figure 3.13: 3813.50 m, facies 3o with oolitic limestone with fine-grained sandstone at Peskowsk A-99.	64
Figure 3.14: 3872.44 m, facies 3s with rapidly alternating very coarse and fine-grained sandstone and siderite cementation at Thebaud C-74.	64
Figure 3.15: 2938.20 m, facies 4g with slightly cross-bedded fine-grained sandstone with muddy burrows at Peskowsk A-99.	65
Figure 3.16: 3919.45 m, facies 4o showing fine-grained sandstone rich in	

<i>Ophiomorpha</i> , mud drapes, and rare horizontal burrows at Thebaud C-74.	65
Figure 3.17: 2210.47 m, facies 4x showing cross-bedded medium-grained sandstone with phytodetritus, lacking mudstone at Peskowsk A-99.	65
Figure 3.18: 2209.64 m, facies 5 with fine-grained sandstone with common bioturbation interbedded with mudstone at Peskowsk A-99.	65
Figure 3.19: 2935.99 m, facies 5s showing fine-grained sandstone with parallel lamination, mud drapes, and plant detritus at Peskowsk A-99.	65
Figure 3.20: 2493.19 m, facies 8 showing greenish bioturbated mudstone at Peskowsk A-99.	66
Figure 3.21: 3913.73 m, facies 9, massive coarse-grained sandstone at Thebaud C-74.	66
Figure 3.22: 2273.15 m, facies 9b showing fine-grained sandstone with lenticular beds and siderite cementation at Peskowsk A-99.	66
Figure 3.23: 2935.35 m, facies 9f showing graded sandstone units with muddy burrows and mud drapes at Peskowsk A-99.	66
Figure 3.24: 2482.74 m, facies 9g showing fine-grained sandstone with thin wood fragments at Peskowsk A-99.	66
Figure 3.25: Legend for interpreted core stratigraphy, extent of bioturbation (after MacEachern et al., 2005) and other interpreted diagenetic features including packets.	68
Figure 3.26: Core 7 at Peskowsk A-99. Detailed core stratigraphy with sample and appendix photo location with interpreted diagenetic features and lithofacies including additional interpretation like the presence of bioclasts, nodules, phytodetritus and bioturbation.	69-70
Figure 3.27: Core 6 at Peskowsk A-99. Detailed core stratigraphy with sample and appendix photo location with interpreted diagenetic features and lithofacies including additional interpretation like the presence of bioclasts, nodules, phytodetritus and bioturbation.	71-72
Figure 3.28: Core 5 at Peskowsk A-99. Detailed core stratigraphy with sample and appendix photo location with interpreted diagenetic features and lithofacies including additional interpretation like the presence of bioclasts, phytodetritus and bioturbation.	73-74
Figure 3.29: Core 4 at Peskowsk A-99. Detailed core stratigraphy with	

sample and appendix photo location with interpreted diagenetic features and lithofacies including additional interpretation like the presence of bioclasts, nodules, phytodetritus and bioturbation.	75
Figure 3.30: Core 3 at Peskowsk A-99. Detailed core stratigraphy with sample location and lithofacies including additional interpretation like the presence of bioclasts, and phytodetritus.	76
Figure 3.31: Core 2 at Peskowsk A-99. Detailed core stratigraphy with sample and appendix photo location with interpreted diagenetic features and lithofacies including additional interpretation like the presence of bioclasts, phytodetritus and bioturbation.	77
Figure 3.32: Core 1 at Peskowsk A-99. Detailed core stratigraphy with sample and appendix photo location with interpreted diagenetic features and lithofacies including additional interpretation like the presence of bioclasts, phytodetritus and bioturbation.	78
Figure 3.33 (Appx. 3.2 photo 63): Thick mudstone bed with siderite cementation.	102
Figure 3.34 (Appx. 3.2 photos 61 & 62): Mudstone lacking sandstone overlying interbedded mudstone and siderite cemented fine-grained sandstone.	102
Figure 3.35 (Appx. 3.2 photo 43): Graded sandstone unit with muddy burrow and mud drapes.	103
Figure 3.36 (Appx. 3.2 photos 56, 58 & 59): (A) 2935.99 m has parallel laminated sandstone with mud clast and minor phytodetritus; (B) 2936.30 m has sandstone lamination picked out by siderite, plus siderite cemented mud drapes; (C) 2938.07 m shows a diagenetic contact, which is also present in 2939.03 m but with siderite cemented mud drapes.	103
Figure 3.37 (Appx. 3.2 photo 54): Diagenetic contact between grey and beige medium-grained sandstone.	104
Figure 3.38 (Appx. 3.2 photo 52): mudstone with interbedded fine-grained sandstone, very patchy siderite cementation, and abundant bioturbation.	104
Figure 3.39(Appx. 3.2 photo 51): Bioturbated sandstone with greenish concretions	104
Figure 3.40 (Appx. 3.2 photo 46): Facies 1 shale overlying bioturbated facies 3 sandstone (sideritic diagenesis).	104

Figure 3.41 (Appx. 3.2 photo 47): Bioturbated sandstone with patchy siderite cementation.	105
Figure 3.42 (Appx. 3.2 photo 48): Bioturbated sandstone with patchy siderite cementation and shelly fragments.	105
Figure 3.43 (Appx. 3.2 photo 49): Bioturbated sandstone with patchy siderite cementation and abundant shelly fragments that appear undisturbed.	105
Figure 3.44 (Appx. 3.2 photo 41): Bioturbation on the top of facies 9 fine-grained sandstone with some wood fragments.	105
Figure 3.45 (Appx. 3.2 photos 42a-d): Fine grained sandstone with thinner beds showing wood fragments, cross lamination, complex laminations, and erosional surfaces.	106
Figure 3.46a (Appx. 3.2 photos 39 & 40): Facies 1 shale overlying facies 3 fine-grained sandstones with some shelly fragments, and 3.46b: Large shell fragments at the base of the unit.	106
Figure 3.47 (Appx. 3.2 photo 37): Bioturbated fine grained sandstone with considerable siderite cement.	107
Figure 3.48 (Appx. 3.2 photo 38a): Fine grained sandstone with abundant shells and areas with and without siderite cementation.	107
Figure 3.49 (Appx. 3.2 photo 36): Bioturbated medium grained sandstone with siderite cementation and few shelly fragments.	107
Figure 3.50 (Appx. 3.2 photo 35): Facies 1 black shale with bioclasts overlying sideritic mudstone.	107
Figure 3.51 (Appx. 3.2 photo 32): Sandstone with lenticular beds and siderite concretions.	108
Figure 3.52 (Appx. 3.2 photo 33): Sideritic sandstone with common bioturbation.	108
Figure 3.53 (Appx. 3.2 photo 31): Interbedded fine grained sandstone and mudstone with sparse bioturbation at the base.	108
Figure 3.54 (Appx. 3.2 photos 27, 28a, & 30): (A) 2266.33 m: Coarse sandstone with low angle cross-bedding and phytodetritus, ~5 mm lithic granules, a large mud clast and an erosional base. (B) 2266.94 m: Coarse sandstone interbedded with sideritic silty mudstone. (C) 2271.42 m:	

Conglomerate of siderite intraclasts and granules <5 mm.	109
Figure 3.55 (Appx. 3.2 photo 19): Coarse-grained sandstone with erosional base and muddy laminae over sparsely bioturbated brown mudstone and laminated fine grained sandstone beds.	109
Figure 3.56 (Appx. 3.2 photo 6): Moderately bioturbated mudstone with fine-grained sandstone, mud fragments and brown staining.	109
Figure 3.57 (Appx. 3.2 photo 3): Bioturbated mudstone with beds of very fine-grained sandstone to siltstone with some siderite concretions.	110
Figure 3.58 (Appx. 3.2 photo 18): Abundant phytodetritus and fine siderite intraclasts in fine to medium grained sandstone, with trough cross-bedding in the sandstone.	110
Figure 3.59a (Appx. 3.2 photo 14): Black shale over laminated and bioturbated fine-grained sandstone with coal layers and coarse-grained sandstone. This is interpreted as a possible maximum flooding surface.	110
Figure 3.59b (Appx. 3.2 photo 15): Fine-grained sandstone with common bioturbation interbedded with mudstone.	110
Figure 3.60 (Appx. 3.1 photo 26): Fine to medium grained sandstone in a fining upwards succession.	111
Figure 3.61 (Appx. 3.1 photo 27): Fine-grained sandstone rich in <i>Ophiomorpha</i> , mud drapes and the rare horizontal burrows.	111
Figure 3.62: Core 6 at Thebaud C-74. Detailed core stratigraphy with sample and appendix photo location with interpreted diagenetic features and lithofacies including additional interpretation like the presence of bioclasts, nodules, phytodetritus and bioturbation.	92
Figure 3.63: Core 5 at Thebaud C-74. Detailed core stratigraphy with sample and appendix photo location with interpreted diagenetic features and lithofacies including additional interpretation like the presence of bioclasts, phytodetritus and bioturbation.	93
Figure 3.64: Core 4 at Thebaud C-74. Detailed core stratigraphy with sample and appendix photo location with interpreted diagenetic features and lithofacies including additional interpretation like the presence of bioclasts, phytodetritus and bioturbation.	94
Figure 3.65: Core 2 at Thebaud C-74. Detailed core stratigraphy with sample and appendix photo location lithofacies including additional	

interpretation like the presence of bioclasts, and bioturbation.	95
Figure 3.66: Core 1 at Thebaud C-74. Detailed core stratigraphy with sample and appendix photo location with interpreted diagenetic features and lithofacies including additional interpretation like the presence of bioclasts, nodules, phytodetritus and bioturbation.	96
Figure 3.67 (Appx. 3.1 photo 28): Sandy mudstone with <i>Ophiomorpha</i> .	109
Figure 3.68 (Appx. 3.1 photo 29): Abundantly bioturbated mudstone with fine-grained sandstone laminae with sparsely distributed mud drapes.	109
Figure 3.69 (Appx. 3.1 photo 31): Commonly bioturbated fine-grained sandstone with mud drapes, burrows, and <i>Ophiomorpha</i> .	110
Figure 3.70: A conceptual “packet” as defined in this study.	112
Figure 3.71: Core photo of packet 1 at Thebaud C-74.	121
Figure 3.72: Core photo of packet 4 at Peskowsk A-99.	122
Figure 3.73: Core photo of packet 7 at Peskowsk A-99.	123
Figure 3.74: Core photo of packet 9 at Peskowsk A-99.	124
Figure 4.1: Various BSE images from both studied wells. <u>Thebaud C-74</u> (A) 3859.95 m: mudstone with siderite cementation and few shelly fragments. (B) 3862.91 m: very coarse-grained sandstone (pebble sized sand present) with siderite cementation and fecal pellet. <u>Peskowsk A-99</u> (C) 2275.64: reddish brown mudstone as a result of siderite cementation. (D) 2493.15: sandstone with sparse shelly fragments and siderite cementation. (E) 2482.68 m: sandstone with 15% shelly fragments (some shale removed from sample). (F) 3813.15 m: muddy TST sandstone with shelly fragments.	136-137
Figure 4.2: Various BSE images from the Thebaud C-74 well. (A) 3862.91 m: very coarse-grained sandstone (pebble sized sand present) with siderite cementation and fecal pellet. (B) 3864.51 m: fine grained sandstone with thick beds of mudstone. (C) 3859.95 m: mudstone with siderite burrows and shelly fragments. (D) 3914.34 m: fine to coarse-grained sandstone with rare pebbles and siderite-cemented nodules. (E) 3871.05 m: fine-grained sandstone with silty mudstone and burrows.	140-141
Figure 4.3: Various BSE images from the Peskowsk A-99 well. (A & B) 2209.83 m: homogeneous sandstone with dispersed wood fragments. (C & D) 2221.17 m: mudstone with several whitish brown nodules (not shown on both images). (E & F) 2275.64 m: reddish brown mudstone as a result of	

siderite cementation. 142-143

Figure 4.4: Various BSE images from the Peskowesk A-99 well.

(A) 2482.68 m: sandstone with 15% shelly fragments (some shale removed from sample). (B) 2492.25 m: sandstone with thin beds of siderite cement and extensive Fe-calcite cementation. (C) 2931.91 m: fine-grained sandstone with prominent greenish burrows. Image of calcite cement in contact with quartz overgrowths. (D & E) 2942.02 m: fine grained sandstone with shelly fragments. (F) 3813.15 m: muddy TST sandstone with shelly fragments.

145-146

Figure 4.5: microphotographs and BSE images from the Thebaud C-74 well.

(A) 3859.95 m (microphotograph): Framboidal pyrite cluster. (B) 3868.39 m (microphotograph): Platy pyrite crystals. (C) 3902.65 m (BSE image): Bioturbated fine to medium-grained sandstone with burrows and siderite cementation. (D) 3863.09 m (BSE image): fine to medium- grained sandstone. (E) 3866.79 m (BSE image): fine grained sandstone with a few coal fragments and burrows. (F) 3868.38 m (BSE image): bioturbated fine grained sandstone interbedded with silty mudstone with burrows and siderite cementation.

147-148

Figure 4.6: microphotographs and BSE images from the Peskowesk A-99 well.

(A) 2942.02 m (microphotograph): Platy and framboidal pyrite grains occurring within an intraclast. (B) 2482.68 m (microphotograph): pore-filing framboidal pyrite. (C) 2482.68 m (BSE image): sandstone with 15% shelly fragments (some shale removed from sample). (D) 2209.83 m (BSE image): sandstone with dispersed wood fragments. Microcrystalline siderite filling some pores between detrital quartz grains.

150-151

Figure 4.7: Two BSE images from the Thebaud C-74 well. (A) 3859.95 m: mudstone with siderite burrows and shelly fragments. (B) 3914.34 m: fine to coarse-grained sandstone with rare pebbles and siderite-cemented nodules.

153

Figure 4.8: microphotographs and BSE images from the Peskowesk A-99 well. (A) 2482.68 m (microphotograph: kaolinite grains and small pieces of lithic clasts. (B & C) 2209.83 m (BSE image): homogeneous sandstone with dispersed wood fragments. (D) Coated grain has a quartz nucleus and three concentric layers. (E) Coated grain with three concentric layers.

154-155

Figure 4.9: Various BSE images from both studied wells. Thebaud C-74 (A) 3921.98 m: fine to medium-grained sandstone with siderite cementation and burrows. (B) 3862.91 m: very coarse-grained sandstone (pebble sized sand present) with siderite cementation. (C) 3859.95 m: mudstone with siderite burrows and shelly fragments. Peskowesk A-99 (D) 2481.34 m: sandstone with sparse shelly fragments and siderite cementation. (E) 2221.17 m: mudstone with a whitish brown nodule. (F) 2945.38 m: fine grained sandstone.

157-158

Figure 4.10: Various BSE images from both studied wells. Thebaud C-74

(A) 3864.51 m: fine-grained sandstone with thick beds of mudstone.

<u>Peskowesk A-99</u> (B) 2209.83 m: homogeneous sandstone with dispersed wood fragments. (C) 2492.25 m: sandstone with thin beds of siderite cementation.	160-161
Figure 4.11: Various BSE images from both studied wells. <u>Thebaud C-74</u> (A) 3866.79 m: fine-grained sandstone with a few coal fragments and burrows. <u>Peskowesk A-99</u> (B) 2221.17 m: mudstone with several whitish brown nodules. (C) 2249.39 m: medium-grained sandstone. (D) 2493.19 m: greenish sandstone with shelly and wood fragments. (E) 3813.63 m: muddy TST sandstone with shelly fragments.	163-164
Figure 4.12: X-ray diffraction stacking of high versus low TiO_2 from geochemical analysis for anatase and rutile identification. Low titanium samples have < 1.00 wt. % and high titanium samples have > 1.00 wt. %.	165
Figure 4.13: Carbonate classification diagram from the Thebaud C-74 well. Fields were created using carbonate analyses from Chang et al. (1996).	166
Figure 4.14: Paragenetic sequence deduced from textural relationship in sandstones from the Thebaud C-74 well.	168
Figure 4.15: Carbonate classification diagram from the Peskowesk A-99 well. Fields were created using carbonate analyses from Chang et al. (1996).	169
Figure 4.16: Paragenetic sequence deduced from textural relationship in sandstones from the Peskowesk A-99 well.	170
Figure 5.1: Histogram showing the variance of principal components for major elements at Thebaud C-74 (A) and Peskowesk A-99 (B).	210
Figure 5.2: Histogram showing the variance of principal components for major and trace elements, facies and grain size at Thebaud C-74 (A) and Peskowesk A-99 (B).	211
Figure 5.3: PCA biplot of major elements loading at the Thebaud C-74 well.	214
Figure 5.4: PCA biplot of major and trace elements, facies and grain size loading at the Thebaud C-74 well.	214
Figure 5.5: PCA biplot of major elements loading at the Peskowesk A-99 well.	215
Figure 5.6: PCA biplot of major and trace elements, facies and grain size loading at the Peskowesk A-99 well.	215
Figure 5.7: Ratio plot of $\text{P}_2\text{O}_5/\text{Al}_2\text{O}_3$ against $\text{CaO}/\text{Al}_2\text{O}_3$ presented on a logarithmic scale.	218

Figure 5.8: Aluminum plots against silica in weight percentage.	218
Figure 5.9: CaO plotted against calcite.	218
Figure 5.10: Strontium in ppm plotted against CaO in weight percentage.	218
Figure 5.11: Ratio plot with P_2O_5/Al_2O_3 against Ce/Al_2O_3 .	218
Figure 5.12: MgO is plotted against ankerite and dolomite (no separate XRD peaks of the minerals).	220
Figure 5.13: MgO plotted against total FeO in weight percentage.	220
Figure 5.14: Phosphorus plotted against TiO_2 in weight percentage.	220
Figure 5.15: Ratio plot of $FeOT/Al_2O_3$ against P_2O_5/Al_2O_3 presented on a logarithmic scale.	220
Figure 5.16: Ratio plot of $FeOT/Al_2O_3$ against TiO_2/Al_2O_3 .	220
Figure 5.17: A plot of CaO against silica in weight percentage.	220
Figure 5.18: Calcite normalized total FeO plotted against calcite normalized silica in weight percentage.	220
Figure 5.19: A plot of CaO versus silica in weight percentage	222
Figure 5.20: Calcite free FeO_T versus calcite free silica weight percentage.	222
Figure 5.21: Calcite free TiO_2 versus calcite free silica weight percentage.	222
Figure 5.22: Calcite free P_2O_5 versus calcite free silica weight percentage.	222
Figure 5.23: Plot of Fe against siderite from XRD analysis.	223
Figure 5.24: Plot of pyrite from XRD analysis against sulphur in weight percentage.	223
Figure 5.25: Strontium in ppm plotted against inorganic carbon (assuming $CaCO_3$) in weight percentage.	223
Figure 5.26: Stratigraphic plot of total FeO against depths for both studied wells.	224
Figure 5.27: Stratigraphic plot of TiO_2 against depths for both studied wells.	224

Figure 5.28: Stratigraphic plot of P_2O_5 against depths for both studied wells.	224
Figure 5.29: Stratigraphic plot of CaO against depths for both studied wells.	224
Figure 5.30: Stratigraphic plot of MgO against depths for both studied wells.	224
Figure 5.31: K_2O plotted against Rb (alumina normalized).	224
Figure 5.32: Lithology legend for figures 5.34 to 5.38.	225
Figure 5.33: Binary plot of sulphur plotted against SiO_2 in weight percentage.	226
Figure 5.34: Cores 1 to 6 at Thebaud C-74. Stratigraphic variation of selected major and trace elements and inorganic carbon (assuming $CaCO_3$).	227
Figure 5.35: Cores 1 to 4 at Peskowsk A-99. Stratigraphic variation of selected major and trace elements and inorganic carbon (assuming $CaCO_3$).	228
Figure 5.36: Core 5 at Peskowsk A-99. Stratigraphic variation of selected major and trace elements and inorganic carbon (assuming $CaCO_3$).	229
Figure 5.37: Core 6 at Peskowsk A-99. Stratigraphic variation of selected major and trace elements and inorganic carbon (assuming $CaCO_3$).	230
Figure 5.38: Core 7 at Peskowsk A-99. Stratigraphic variation of selected major and trace elements and inorganic carbon (assuming $CaCO_3$).	231
Figure 6.1: Pore-water profile for a high sedimentation rate environment (Burns, 1997) with zones showing expected mineral precipitation for coated grains forming in a low sedimentation rate environment over a few cm.	241
Figure 6.2: Thebaud C-74 with interpreted core stratigraphy, lithofacies and identified diagenetic features, showing geochemical differences.	247
Figure 6.3: Peskowsk A-99 (Cores 1-4) with interpreted core stratigraphy, lithofacies and identified diagenetic features, showing geochemical differences.	248
Figure 6.4: Various binary plots for selected diagenetic minerals (quartz normalized) for both studied wells showing facies variation. (A) Calcite plotted against depth (B) Ankerite + Dolomite plotted against depth (C) Siderite plotted against depth (D) Chlorite plotted against depth (E) Pyrite plotted against depth (F) Kaolinite plotted against depth.	250
Figure 6.5: Various binary plots above and below the TS. (A) Plot of FeO_T against SiO_2 showing TS change variations at Thebaud C-74 above the TS. (B) Plot of FeO_T against SiO_2 showing TS change variations at Peskowsk	

A-99 above the TS. (C) Plot of FeO_T against SiO_2 showing TS change variations at Thebaud C-74 below the TS. (D) Plot of FeO_T against SiO_2 showing TS change variations at Peskowsk A-99 below the TS.	255
Figure 6.6: Cores 4, 5, and 6 at Thebaud C-74 with interpreted core stratigraphy, lithofaices and identified diagenetis features, showing evidence of fossilization below the TS.	258
Figure 6.7: Cores 1 and 2 at Peskowsk A-99 with interpreted core stratigraphy, lithofaices and identified diagenetis features, showing evidence of the lack of fossilization below the TS.	259
Figure 6.8: Accommodation and diagenesis model for both studied wells.	262
Figure 6.9: Diagenetic minerals within pore-water profiles in the Scotian Basin for the fluvially dominated Peskowsk A-99.	263
Figure 6.10: Diagenetic minerals within pore-water profiles in the Scotian Basin for the mixing zone between studied wells.	264
Figure 6.11: Diagenetic minerals within pore-water profiles in the Scotian Basin for the deep water shelf edge at Thebaud C-74.	264
Figure 6.12: Integrated Model for Studied Wells.	265

LIST OF ABBREVIATIONS

BSE: Back Scattered Electron
EDS: Energy Dispersion Detector
EMP: Electron Microprobe
FSST: Falling Stage System Tract
HST: Highstand Systems Tract
KB: Kelly Bushing
MFS: Maximum Flooding Surface
SEM: Scanning Electron Microscope
TS: Transgressive Surface
TST: Transgressive Systems Tracts
REE: Rare Earth Elements
CFA: Carbonate Fluorapatite

CHAPTER 1: INTRODUCTION

1.1 GENERAL STATEMENT

Most hydrocarbon discoveries in the Scotian Basin are in the Lower Cretaceous deltaic sandstone reservoirs, including the Sable project gas fields (CNSOPB, 2000). New commercial discoveries in the Lower Cretaceous sandstone are important to the future of the Nova Scotia petroleum industry. Principal risks in these plays are (1) reservoir effectiveness due to diagenetic processes, (2) the presence of suitable net pay and its relationship to the breaching of seals by faults, and (3) the distribution of coarser thick-bedded permeable sandstone.

The Scotian Basin is a Mesozoic to Quaternary passive margin, influenced by salt tectonics, and initiated by the formation of rift basins in the Triassic and early Jurassic when a new phase of crustal motion began. The Scotian Basin encompasses an area over 300,000 square kilometres. The Sable, Abenaki and Laurentian subbasins developed in the eastern Scotian shelf as a result of greater subsidence of the rift basins formed in the Triassic, which were filled with continental clastic rocks, salt and basal Jurassic basalts.

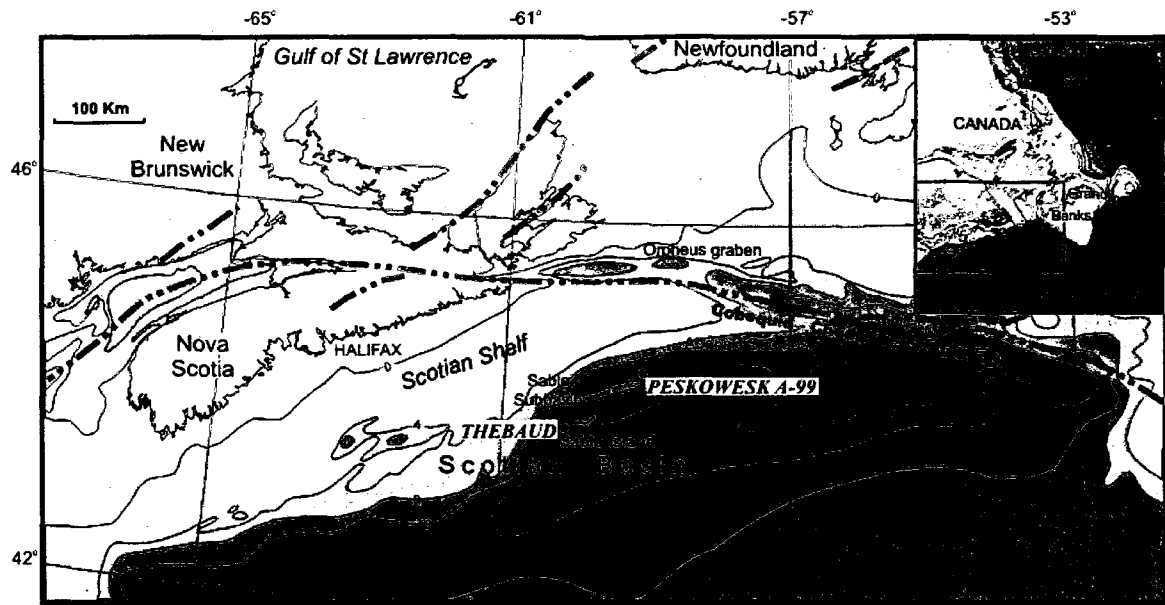


Figure 1.1: General map of the Scotian Basin (modified from Williams and Grant 1998) showing depth to basement in kilometres.

This study addresses one aspect of the first risk presented above: reservoir effectiveness due to diagenetic processes. It follows up on observations by Gould *et al.* (2010) about the importance of early diagenetic processes in determining the distribution of late diagenetic minerals. In many reservoir sandstones in the Scotian Basin, highly porous sandstones have diagenetic chlorite rims that appear to have inhibited silica cementation (Drummond 1992). Gould *et al.* (2010) showed that formation of chlorite rims resulted from the presence of Fe-rich clay formed by sea-floor diagenesis. They also presented evidence that there was a strong correlation between the abundance of P and Ti in sandstones and the presence of good quality chlorite rims. They speculated that the breakdown of detrital ilmenite (FeTiO_3) supplied labile Fe for the formation of early Fe-rich clay and that P and Fe were concentrated together in the sea-floor diagenetic system. Gould *et al.* (2009) also proposed that changing rates of sedimentation had an important influence on the sea-floor diagenetic system.

This study investigates early diagenetic processes in the Lower Cretaceous deltaic sediments of the Scotian Basin. Conventional core from two wells, Thebaud C-74 and Peskowsk A-99, with contrasting sediment types have been studied. Early diagenetic minerals have been characterized with the help of sedimentological, geochemical, and petrographic interpretations. Particular emphasis is placed on the preservation of early diagenetic minerals, either as coated grains, or as a result of precipitation during adjustment of pore-water profiles at times of rapid change in sedimentation rates. Detailed objectives are presented at the end of this chapter, following a review of previous work and the principles of the modern sea-floor diagenetic system.

The anticipated outcome of this study is a new understanding of the influence of sea-floor diagenesis on the later diagenetic history and reservoir quality in the Scotian Basin. This work can be used as a predictive tool for reservoir management.

In an attempt to reach textural and geochemical equilibrium, sediment assemblages and their interstitial pore waters go through a broad spectrum of physical, chemical and biological post-depositional processes. These are the processes that make up diagenesis (Worden and Burley, 2003). Diagenesis could be said to be responsible for what makes sediments change to sedimentary rocks (from weathering to metamorphism). Diagenetic reactions take place due to changes in ambient pore-fluid chemistry, temperature, and pressure. Without the presence of aqueous pore fluids, diagenesis cannot occur. Early diagenesis relates to the time component. Time is critical, and early reactions can be rapid. Early diagenetic reactions, like marine cementation in sandstones or carbonates,

take place in mere decades (Taylor and Illing, 1969; Pyre *et al.*, 1990; Al-Agha *et al.*, 1995 in Worden and Burley, 2003).

A number of terms used to describe aspects of diagenesis are defined here. Authigenesis is the growth of a mineral in situ (growth in the location the mineral has been ultimately preserved). Cementation refers to the growth of a mineral in sediment pore spaces.

Dissolution involves a mineral going into solution from a solid state. The order in which diagenetic processes occur in sediments is known as a paragenetic sequence. Precipitation is growth of a mineral from a solution. Re-crystallization involves changes in crystal size or habit of a specific mineral, generally resulting from solid-state change rather than dissolution followed by re-precipitation. Replacement is the growth of a chemically different authigenic mineral within the body of a pre-existing mineral.

1.2 PREVIOUS WORK ON EARLY DIAGENESIS IN THE CRETACEOUS OF THE SCOTIAN BASIN

In the Scotian Basin, most previous work has been done on burial diagenesis (e.g. Jansa and Noguera, 1990; Drummond, 1992) and such studies have emphasized the role of chlorite rims on detrital quartz in terms of preserving porosity. Work by Pe-Piper and Weir-Murphy (2007) and Gould *et al.* (2010) showed the importance of verdine facies (green clay facies) and berthierine (an Fe-rich silicate), as a precursor of chlorite. Karim *et al.* (2008) focused on carbonate diagenesis in the western Sable Subbasin.

Early diagenetic phosphorites and iron-silicate (Fe-silicate) minerals are common in the Lower Cretaceous of the Orpheus Graben, the most inboard part of the Scotian Basin. Pe-Piper and Weir Murphy (2007) studied how the distribution of phosphate minerals may be an indicator for the formation of early diagenetic berthierine.

The types of phosphorites present in the Cretaceous sandstones of the Orpheus graben were in the form of either cement or nodules. Pe-Piper and Weir-Murphy (2007) noted that the phosphorite cuttings had a brownish color and a variety of shapes.

Microscopically, they occurred either as clasts or nodules, in coated grains, but the most common occurrence were as phosphatic cements identified in cuttings of silty mudstones, siltstones, and very fine-grained quartzwacke. These phosphorites also have a relationship with siderite, as the cement or nodular types identified occur with siderite, and berthierine. The siderite is a replacement of Fe-rich silicates and forms discrete microscopic layers. Glauconite-dominated coated grains were found in a more distal well

(Peskowesk A-99) in bioturbated transgressive sandstone, and the remaining layers in the coated grains contained chamosite or kaolinite with the outer surface rimmed by Mg-rich siderite (Pe-Piper and Weir Murphy, 2007).

Based on the co-occurrence of berthierine and phosphorite in coated grains, Pe-Piper and Weir Murphy (2007) suggested that both these minerals formed during sea-floor diagenesis and under similar conditions in the Fe-reduction zone (depth where Fe^{2+} is present). Phosphorus from organic matter or detrital minerals is released into pore-water during sea-floor diagenesis. It is absorbed by Fe-oxides and hydroxides that form at the top of the Fe-reduction zone and may thus be mineralized. This increase in phosphorus mineralization is favored by the same sea-floor diagenetic conditions that allowed the precipitation of berthierine.

Pe-Piper and Weir-Murphy (2007) identified chamosite (Fe-rich chlorite) rims on detrital quartz grains in thick-bedded prograded sandstones that underlie a transgressive system tract. Phosphorites were also identified to be associated with this Fe-rich chlorite in the Lower Cretaceous rocks of the Scotian Basin (Weir-Murphy, 2004); it appeared that both the precursor of the Fe-rich chlorite and phosphorites were precipitating under similar conditions.

More studies of the relationship between phosphorus and Fe-rich silicates have been carried out in the Jurassic sandstone reservoirs of Norway by Ehrenberg *et al.* (1998). High amounts of phosphorus (~ 15 %) were seen to occur in close stratigraphic proximity

to zones with well-developed chlorite rims in rapidly deposited medium-grained sandstones. Marine organic matter from bacterial blooms was proposed as the possible source of the high phosphorus in this Jurassic sandstone, however, no evidence was given for the high input of marine organic matter (Ehrenberg *et al.*, 1998).

Berthierine is suggested by some authors to form chamosite rims after burial (Aargaard *et al.*, 2000). A recent study by Gould (2007) identified diagenetic chlorite rims on detrital quartz in the Venture wells of the Scotian Basin that preserve porosity by preventing the formation of secondary pore-filling quartz overgrowth on detrital grains. These Fe-rich chlorite rims had been previously studied by Jansa and Noguera (1990) and Drummond (1992). More cases of cementation inhibition has also been studied in the North Sea, where authigenic Fe-rich clays (odinite) altered to berthierine during sea-floor diagenesis (Humphrey *et al.*, 1989).

Karim *et al.* (2008) studied the formation of some diagenetic cements (principally clay minerals, carbonate and quartz), and how these cements influence reservoir quality. The study focused on diagenetic changes and the spatial and temporal distribution of the diagenetic cements in relation to lithofacies and sequence stratigraphy. An example is the presence of chlorite and illite coated grains cemented by Fe-calcite in transgressive systems tracts (TST) versus the presence of early kaolinite booklets with vermicular stacking textures principally in sandstones immediately beneath the TSTs, particularly in cross-bedded, coarse-grained, channel sandstone (Karim *et al.*, 2008).

From their studies, both Gould (2007) and Karim *et al.* (2008) inferred a similar paragenetic sequence of diagenetic cements (Fig. 1.2). Carbonate cements (e.g. calcite, the most common cement type in the studies) tend to fill intergranular pores. Fe-calcite and ankerite occur in the later stages of the diagenetic sequence, and siderite is identified as two types. Siderite (I) occurs early with a fine-grained texture filling intergranular pores and siderite (II) occurs later with a microcrystalline texture that forms euhedral small crystals. Pyrite was identified as early framboids and late individual crystals.

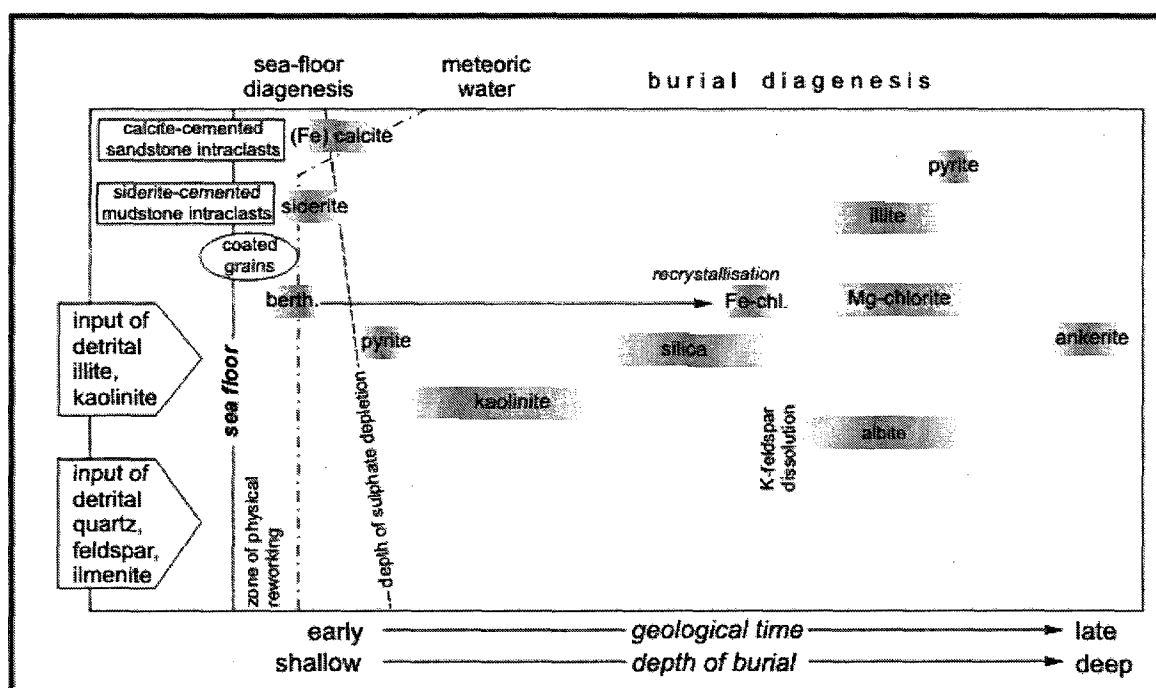


Figure 1.2: Paragenetic sequences from the Scotian Basin (modified from Gould *et al.*, 2010).

In the Venture and Thebaud fields, Gould (2007) studied the relationship between diagenetic minerals and whole-rock geochemistry. Statistical analysis on whole rock geochemical data from sandstone samples showed that P correlates strongly with Ti, and each correlates with the other more strongly than with any other element. These elements

also correlate well with the quality of chlorite rims. Gould *et al.* (2010) related abundant Ti to the supply of detrital ilmenite and its alteration products to the basin and suggested that where Ti was high, so too was Fe, which was available for the formation of odinite. They further suggested that precipitation of odinite and phosphate minerals took place at the top of the Fe-reduction zone of sea-floor diagenesis (Fig. 1.3). Gould *et al.* (2010) also pointed out that the abrupt changes in sedimentation rates at transgressive surfaces would lead to upward migration of the sea-floor diagenetic succession and result in the precipitation of early diagenetic minerals of the sea-floor, as shown elsewhere by Burns (1997). These hypotheses are tested in this present thesis.

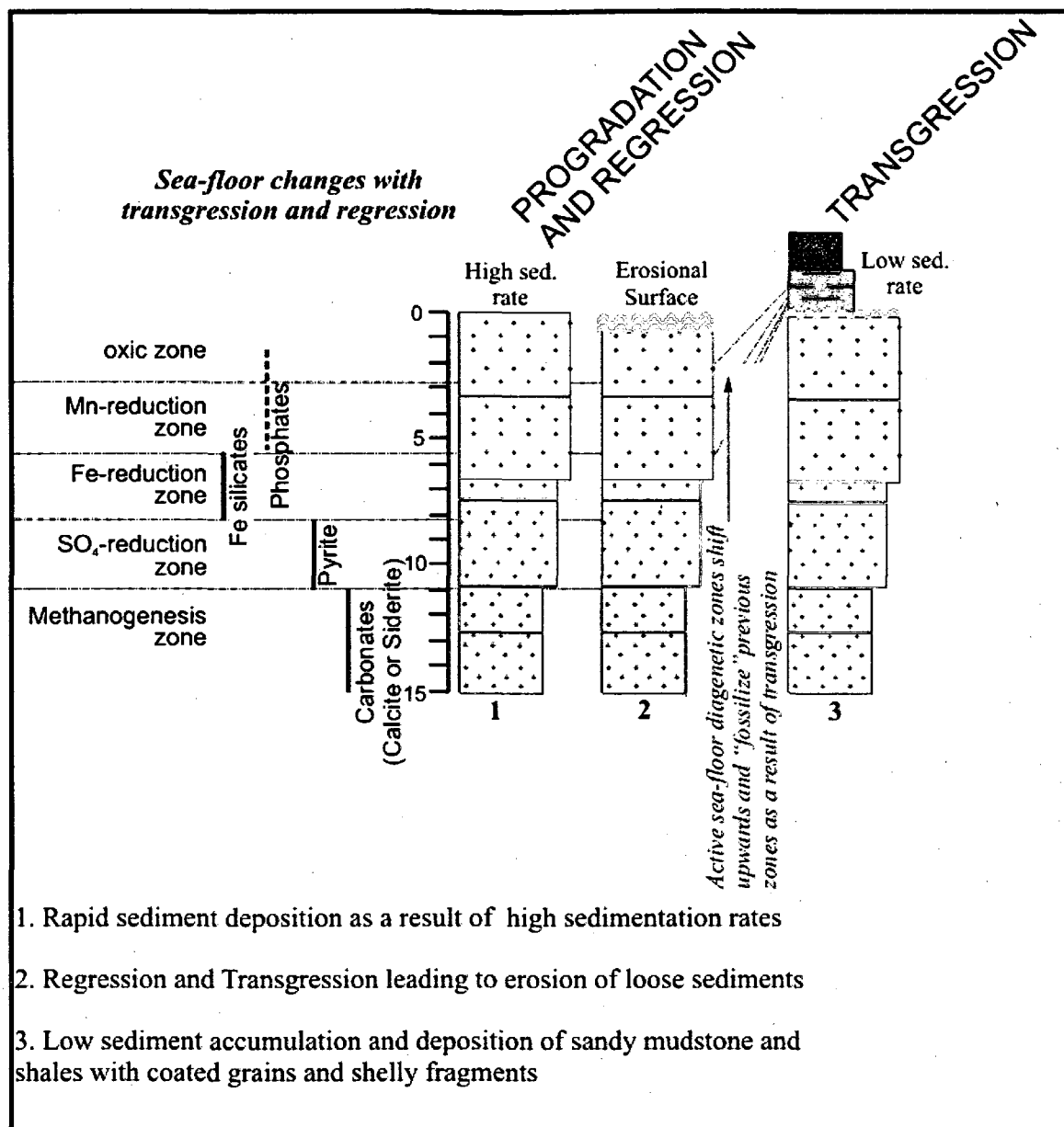


Figure 1.3: Fossilization of diagenetic sea-floor minerals in the Scotian Basin (modified from Gould 2007).

1.3 THE MODERN SEA-FLOOR DIAGENETIC SYSTEM

1.3.1 Introduction

An investigation of modern sea-floor diagenetic systems is required to further understand the Cretaceous early diagenetic systems suggested by previous work described in section 1.2. In the Lower Cretaceous of the Scotian Basin, terrigenous sediment rich in Fe (Piper *et al.*, 2008) was supplied by rivers to a warm marine environment (Karim *et al.*, 2010).

1.3.2 Redox Reactions

Chemical diagenesis of sediments results from reactions such as redox reactions, but it takes place after sediment deposition, during and after burial of the sedimentary material. Most sea-floor diagenetic reactions start with the decomposition of organic matter (mediated by bacteria), which causes redox reactions that involve some ionic species in seawater, notably reduction of SO_4^{++} to S^- , and the production of HCO_3^- , and the redox state of some solid phases e.g. Mn and Fe.

The metabolic activities of microorganisms tend to create a vertical arrangement of biogenically mediated diagenetic reactions along a gradient aligned with the diffusion of oxygen from the overlying seawater.

These reactions are presented in Fig. 1.4, showing various redox reactions for sediments at the sediment-water interface mediated by bacteria. It starts with the decay of organic

carbon (most important early diagenetic process) that then drives most other biogeochemical transformations in sediments (Berner, 1980 in Tromp *et al.*, 1995).

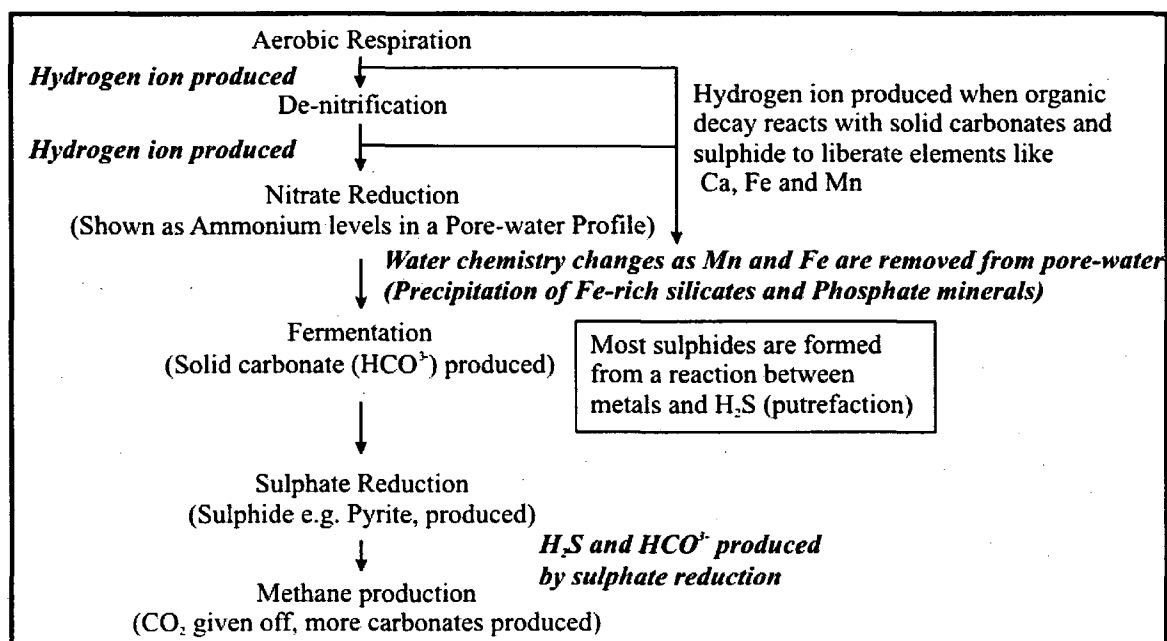


Figure 1.4: Diagenetic chemical reactions (modified from Fisher, 1982)

The pore-water chemistry of ionic specific represented in Fig. 1.4 is shown in Fig. 1.5, which shows pore-water profiles from modern sea-floor in areas with high sedimentation rates, presence of abundant terrestrial carbon and Fe.

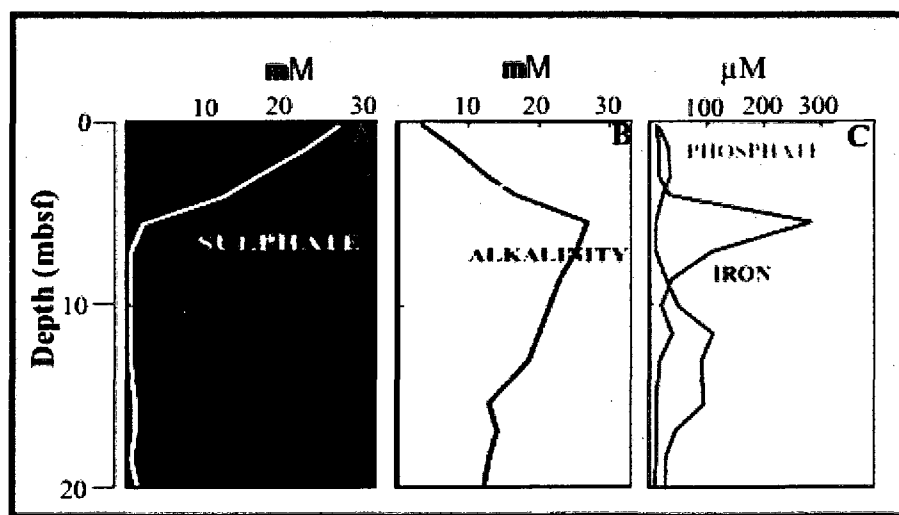


Figure 1.5: Pore-water chemistry of element within a typical diagenetic chemical reaction profile (modified from Burns, 1997).

Figure 1.5A represents a sulphate reduction zone showing sulphate highest at shallow depths, decreasing downwards as it changes to sulphide (e.g. precipitation of pyrite) deeper down in the profile. Part B represents a combination of the sulphate and alkalinity profile showing how alkalinity peaks then reduces with depth as more HCO_3^- are produced which leads to the precipitation of carbonate minerals. Part C shows a peak in Fe^{2+} which represents the zone of Fe reduction.

The effects of transgression on redox profiles, as illustrated in Figs. 1.3 and 1.4, includes the fossilization of the sequence of mineral types. During progradation and regression the rate of sedimentation is rapid so that the depth of complete sulphate reduction may be tens of metres deep (Berner, 1980) and when transgression abruptly occurs with slower rates of sedimentation, it causes the pore-water zones to migrate upwards (Burns (1997) so that mineral types (e.g. phosphorite, Fe-silicates, pyrite, and carbonates) precipitate in the overlying muddy sandstone. Coated grains precipitate as a result of the slow rate of sediment burial and erosional exposure. Such abrupt changes in sedimentation and the presence of coated grains are preserved in sea-floor diagenetic phases.

1.3.3 Precipitation and Preservation of Phosphorus

Phosphorus (P) is brought into the ocean mainly by rivers, in both dissolved form and as particulate matter (Froelich *et al.*, 1982; Cha *et al.*, 2005). The P is then removed from the ocean by phytoplankton (primary production), adsorption on Fe oxides, hydroxides and oxyhydroxides (referred in this study generally as Fe-oxides) and through the

formation of authigenic minerals such as carbonate fluorapatite (Cha *et al.*, 2005).

However, P is also released back into pore-water due to organic matter decay.

Numerous authors (Ingall and Van Cappellan, 1990; Ruttenberg and Berner, 1993; Schenad and DeLange, 2001 in Cha *et al.*, 2005) have studied the supply and preservation of phosphorus (P). Determining the sources of P and the eventual burial in sediments depends on a number of parameters. These parameters are different for different sedimentary environments, so that the burial of P depends greatly on its depositional environment. In terms of P burial, the following are the parameters that should be understood (Cha *et al.*, 2005):

- Nature of the P compounds supplied to the sediments
- Sedimentation rates (low rates favors P precipitation as such environments have Fe-rich conditions, most important in non-upwelling environments)
- Bioturbation
- Oxygen availability (also with regard to benthic biological activity)
- Diagenetic processes (early diagenesis at the sediment-water interface)
- Organic carbon content in sediments

P is influenced by Fe solubility, which changes due to the redox state. Fe acts as a trap for P in what is known as Fe redox-adsorbed P cycling (termed by Froelich *et al.*, 1988 as the phosphate pumping trap) and it is an important process in the precipitation of phosphate cement. After the P and Fe are dissolved in sediment pore-waters, the P migrates upwards and and the Fe re-precipitates under oxic conditions in the upper parts of the sediment

(Cha *et al.*, 2005). On the other hand, the dissolved Fe either precipitates into glauconite grains, a phyllosilicate mineral that develops as a consequence of the diagenetic alteration of sedimentary deposits, or into Fe sulphides like pyrite (Froelich *et al.*, 1988). The presence of glauconite signals an environment with suboxic conditions, hence making glauconite an important accessory diagenetic mineral in many phosphorite deposits.

1.3.4 Carbonate Fluorapatite (CFA)

Carbonate fluorapatite (CFA) is an authigenic P-bearing mineral formed diagenetically in marine sediments, and its formation reduces benthic flow of the dissolved P, released from organic matter decay. Precipitation of CFA is indicated by an increase with depth in the authigenic fraction of P (Cha *et al.*, 2005). A few processes have been shown to hinder or assist in the precipitation of CFA. One is the presence of high concentration of calcite in sediments, which does not allow for the precipitation of CFA, whereas pyrite formation is able to occur simultaneously with CFA, thereby assisting with the precipitation of CFA (Louchouart *et al.*, 1997).

CFA formation is important because studies have shown that its authigenic formation helps with the retention of P in marine sediments. The other process that helps with P retention is the storage of remobilized phosphates on Fe oxyhydroxide at the oxic-anoxic boundary discussed in section 1.3.3 (Sundby *et al.* 1992 in Louchouart *et al.* 1997).

1.3.5 Coated Grains and Ooids

Coated grains consist of a nucleus with a cortex generally made up carbonates, but can have an iron moneral or phosphate cortex. There are commonly two types of coated grains, ooids and oncoids (Tucker *et al.*, 1990). Ooids have a smooth and evenly laminated cortex, and are commonly spherical and small (about < 2 mm). Ooids can be of two types: (a) superficial ooids with a thin coating, where the nucleus controls its shape, and (b) mature ooids with a thick coating that tends to be more in shape (Davies *et al.*, 1978).

An important occurrence of phosphorite is as coated phosphate grains. Many ancient phosphorite deposits are dominated by sand-sized pellets, ooids and intraclasts rather than larger nodules (Sheldon, 1981; Cook, 1984, Rigg, 1984 in Froelich *et al.*, 1988). Coated phosphate grains give better insight into depositional and diagenetic processes (Riggs *et al.*, 1997 in Collin *et al.*, 2005). Coated phosphates grains form authigenically just below the sediment-water interface and consist of circumgranular apatite layers (Garrison and Kastner, 1990; Soudry, 2000 in Collin *et al.*, 2005). This characteristic is highly important because the coated grains preserve a record of physical and chemical properties from the environments they have formed.

Pufahl and Grimm (2003) studied phosphate grains whose depositional environment was related to a period of relative low and/or negative sedimentation rates. These authors identified two types of cortices (outer rims of grains): unconformity bounded grains (UB grains) and the redox aggraded grains (RA grains). The UB grains identified show

evidence of reworking on the sea-floor surface on which benthic organisms live. The substrate reworking shown by the UB grains indicate that there was an interruption in quiet water sediment deposition, which could suggest intermittent storm currents and/or shallow water currents associated with sea-level lowstands or shoreline transgression.

The RA grains identified by Pufahl and Grimm (2003) are important because they have been found to consist of authigenic minerals like sedimentary apatite (francolite), pyrite, plus chamosite and barite. The occurrence of these authigenic minerals has been attributed to seasonal fluctuations in the export of sedimentary organic matter. These fluctuations have also been suggested to account for the variability of the minerals identified in the RA grains. In addition, these fluctuations indicate that the RA grains have formed in seawater settings with low organic productivity. In low productivity settings, pore-water phosphate concentration is regulated by the seasonal changes in productivity and Fe redox pumping of phosphorus, and phosphorus absorbed into Fe oxyhydroxides (Heggie *et al.*, 1990 in Pufahl *et al.*, 2003).

When ooids are not the result of a single primary mineral, the secondary mineralogy can be determined if (a) there was a replacement of a carbonate ooid, (b) there was a transformation of a mineral by oxidation (an early diagenetic process), and (c) there was a replacement of clay mineral e.g. kaolinite. It is possible to interpret earlier mineralogy because the original mineralogy of ooids influences their subsequent diagenesis and their microfabric (Collin *et al.*, 2005).

Recent marine ooids studied by Tucker *et al.* (1990) have aragonite mineralogy in a radial or concentric fabric. High Mg calcite ooids have been identified in the same marine environment, whereas low Mg calcite ooids occur in present day lakes, streams, caves and calcareous soils. Both the high and low Mg calcite ooids, occur with concentric fabric.

Fe-ooids found in condensed sections (e.g. Paris Basin) have been identified to range in size from 125 μm to 2 mm. According to Collin *et al.* (2005), the ooids found in the Paris Basin are composed almost entirely of primary goethite (FeOOH). Low sedimentation rates in a condensed section could have caused the sediment accumulation to remain above the redox boundary for a long time, which allowed prolonged diagenesis in the oxic zone, causing oxidation of the major part of the buried material. This is suitable for goethite formation. Fe precipitates as goethite on the surface layer of sediments at the boundary of Fe-reduction and oxidation zones. At the surface layer of the sediment, there is microbial activity that has been known to play a significant role in the formation of Fe coated grains, and this microbial activity helps in the precipitation of Fe oxyhydroxide. The mode of formation for the Callovian-Oxfordian Fe-ooids of the Paris Basin was suggested by Collin *et al.* (2005) and can be represented by the following chart (Figure 1.5).

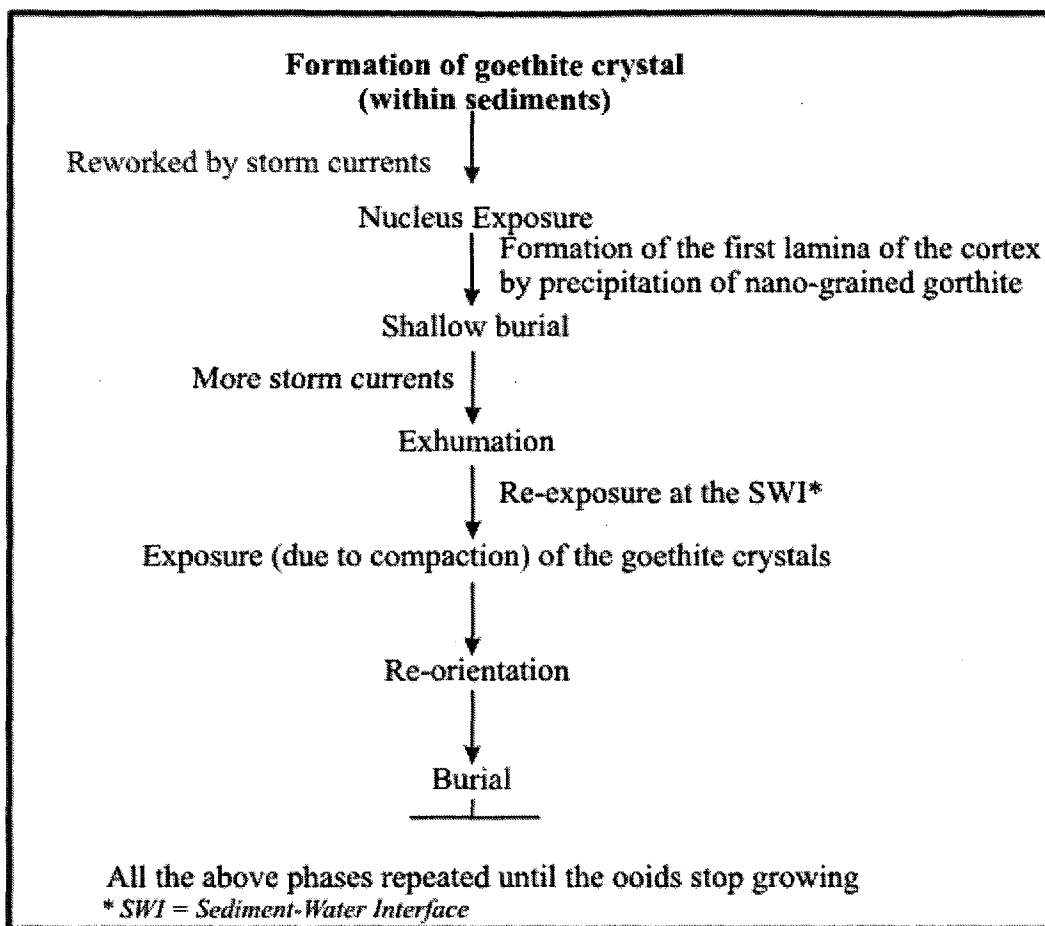


Figure 1.6: Mode of formation of Jurassic Fe ooids in the Paris Basin (modified from Collin *et al.*, 2005)

1.3.6 Rare Earth Elements

The presence of solid-phase phosphate influences rare earth element (REE) abundance.

Different REE patterns are found in different environments, especially in marine

depositional settings. This is why REE geochemistry of phosphorites provides an

interesting tool to understand their depositional environment. Moreover, recent work by

Haley *et al.* (2004) in Fazio *et al.* (2007) demonstrated that the pore-water could acquire

characteristic REE patterns in different early diagenetic environments. These are possible

because the REEs are abundant in marine sediments, and their abundance, despite the low

REE seawater contents, is due to the long residence time of the sediment at the sea floor. However, processes like weathering, burial diagenesis, and metamorphism can also alter abundance and seawater patterns of REEs.

Two early diagenetic processes can be recognized for REE abundance: (a) impoverishment of phosphatic solution by Y/La ratios when REEs are released to the phosphatic solution from organic matter, (b) the precipitation of phosphate from oxic to suboxic pore-waters that create a linear (flat) REE pattern. The linear pattern of REEs may be present in oxic to anoxic environments, but it usually appears near the sediment-water interface where pore-water is oxic to suboxic. In addition, light REEs (e.g. Ce) have weak mobility during diagenesis and Ce in particular tends to accumulate in Fe and Mn-rich layers and gets reduced with manganese in the Mn-reduction zone.

1.4 RESEARCH STRATEGY

1.4.1 Research Problem

Gould (2007) identified a correlation between phosphorus (P) and titanium (Ti) and the quality of diagenetic chlorite rims that suggested early diagenesis was an important control on later diagenetic processes. Gould *et al.* (2010) hypothesized that sea-floor mineralization was controlled by rapid changes in sedimentation rate from progradational deltaic successions into transgressive units. The research problem in this study is to determine how the change from progradation to transgression influences early diagenetic cementation by focusing on the interval across transgressive surfaces in the deltaic Lower Cretaceous of the Scotian Margin. This research will be based on two observations:

- Sea-floor diagenetic phases are commonly preserved where there is an abrupt change in sedimentation rate;
- Sea-floor diagenetic phases are also preserved in coated grains found in transgressive units.

1.4.2 Research Objectives

The working hypothesis is that due to the abrupt changes caused by the beginning of transgression, mineralization in the sediment-water (near seabed) redox profile is interrupted and the sequence of mineral types is “fossilized” (Fig. 1.3). In addition, Fe-rich minerals like diagenetic pyrite are precipitated within and below the Transgressive surface of erosion, with the presence of other cements (carbonates and quartz overgrowths). Specific research objectives were developed to address this model:

1. To determine whether there is a general relationship between P and Ti below the transgressive surface (TS), as suggested by Gould (2007). In particular, to determine whether the distribution of P is an indicator of chlorite rims.
2. To infer sea-floor diagenetic processes from coated grains that occur in sediments immediately above the TS.
3. To determine why the sediments immediately above the TS are often siderite-rich, and to evaluate the role of bioturbation.
4. To compare the sequence of early diagenetic minerals in the TST and underlying deltaic sediments with literature on modern sea-floor diagenesis.
5. To determine the nature of the early diagenetic system in the overall diagenesis of sandstone reservoirs in the Scotian Basin.

1.4.3 Expected Significance of the Research

Sea-floor diagenetic phases influence the entire diagenetic mineral assemblage and hence petroleum reservoir quality. This research is expected to (a) improve the understanding of early diagenetic processes in Fe-rich sea-floor environments and (b) because early diagenesis influences later diagenesis, improve the prediction of reservoir quality in the Scotian Basin.

1.5 CHAPTER SUMMARY

In this chapter, the relationship between the early diagenetic processes in Lower Cretaceous and the hydrocarbon discoveries in the Scotian Basin was reviewed with a focus on early diagenetic processes around transgressive units and the immediately underlying prograded sediments. Previous work on early diagenesis in the Scotian Basin was reviewed and an investigation of the modern sea-floor diagenetic system was used to further understand the Cretaceous early diagenetic processes suggested by previous work. Five specific objectives were then highlighted to help solve the research problem. The following chapter provides a broader perspective on the studied area and briefly introduces a few terms in sequence stratigraphy involved with diagenetic processes.

CHAPTER 2: GEOLOGY OF THE STUDY AREA

2.1 EVOLUTION OF THE SCOTIAN BASIN

The Scotian Basin (Fig. 1.1) is a passive margin sedimentary basin up to 20 km thick that developed in the Mesozoic and Cenozoic (Wade and MacLean, 1990). It encompasses an area of over 300, 000 square kilometres. The Scotian Margin initially formed by rifting about 200 million years ago, at the time of the opening of the North Atlantic. In the last 40 years, much has been learned about the margin through the use of geophysical surveying and drilling of exploration wells (Dehler *et al.*, 2004).

The formation of the Scotian Basin started with the onset of rifting in the Triassic and Early Jurassic. Small rift basins filled with continental clastic rocks, salt, and basal Jurassic basalt. In the mid Jurassic, the African plate started moving away from the North American plate (Dehler *et al.*, 2004). The oceanic crust of the central Atlantic Ocean formed as the magma that extruded at the spreading center cooled. The edge of the rift zone was at this stage no longer under extensional stress and lithospheric cooling eventually allowed further subsidence of the rifted margin. The Sable, Abenaki and Laurentian Subbasins developed in the eastern Scotian shelf as a result of further subsidence of these initial rift basins.

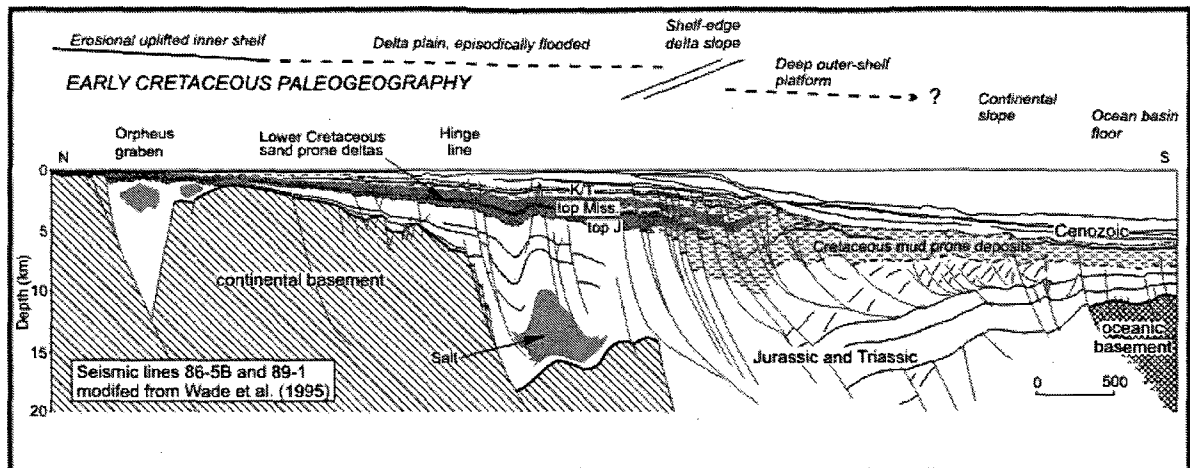


Figure 2.1: Cross section of the Scotian Basin near Peskowsk A-99 (modified from Wade et al. 1995).

Sands and muds brought to the coast by river systems began to fill the subsiding Scotian Basin, with thickest accumulation in large deltas, which formed in the Late Jurassic and Early Cretaceous (Figs. 2.1, 2.2). In the Jurassic, carbonate banks formed in warm shallow areas of the sea typically away from the main clastic inputs. Salt tectonic movement started by the mid Jurassic (Ings and Shimeld, 2006) and the movement recognized during the later Jurassic and Cretaceous is indicated by rapid changes in sediment thickness adjacent to salt structures.

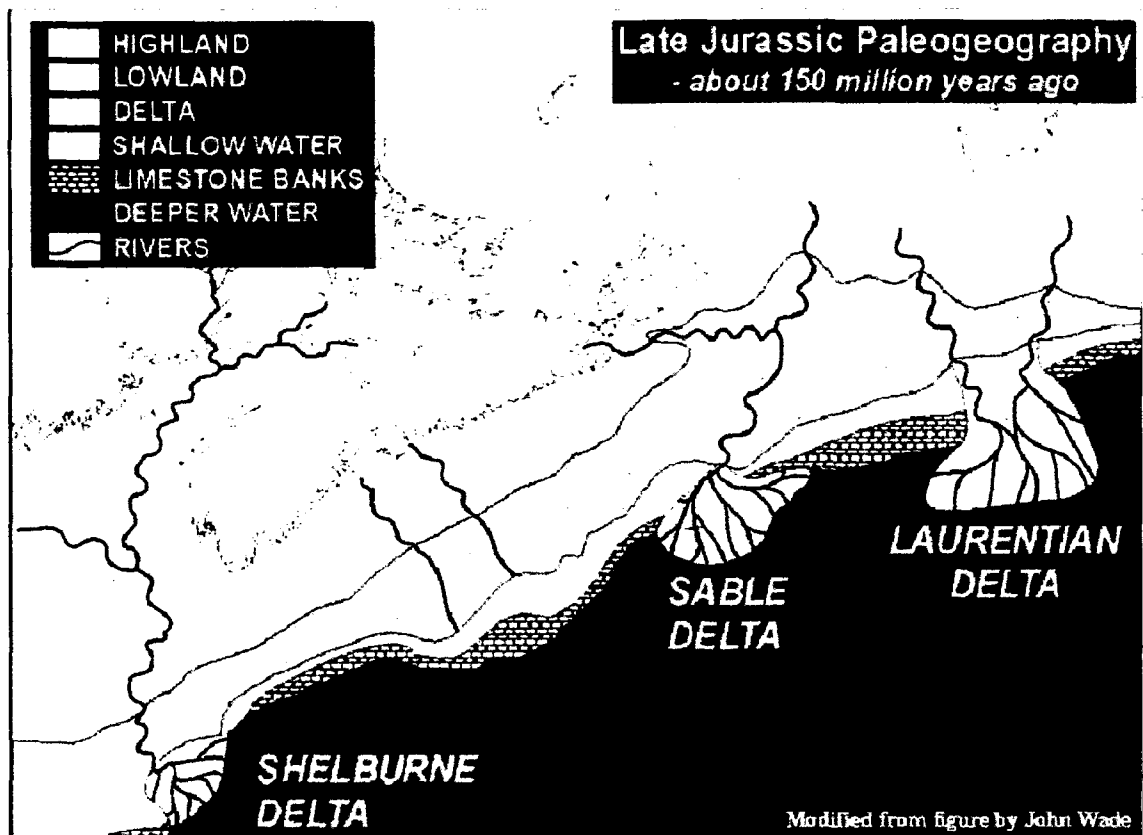


Figure 2.2: Generalized paleogeography of large deltas in the Scotian Basin in the Late Jurassic (GSC, 2004)

2.2 THE SEDIMENTARY ENVIRONMENT OF THE UPPERMOST JURASSIC- LOWER CRETACEOUS

2.2.1 Introduction

Already in the Upper Jurassic Mic Mac Formation, clastic deltaic sediments are found in the Scotian Basin, particularly near Sable Island and eastward (Figs. 2.2, 2.3). Deltaic sedimentation predominated throughout the Early Cretaceous, forming the Missisauga and Logan Canyon Formations. Subdivisions of these formations into members use the terminology of MacLean and Wade (1993). These units were followed in the Late Cretaceous by more a transgressive succession of shales (Dawson Canyon Formation) and chinks (Wyandot Formation).

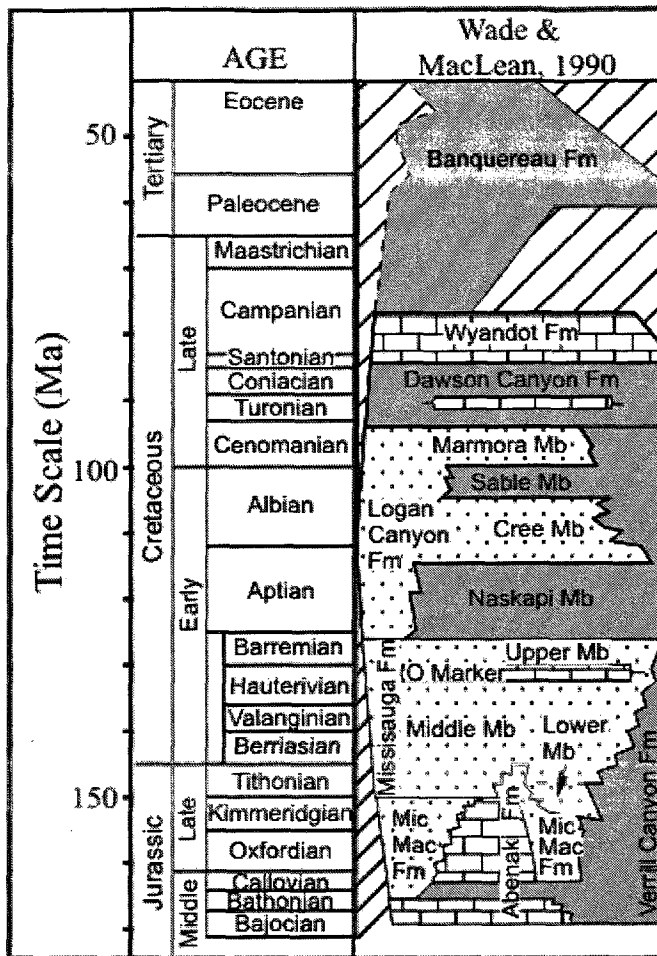


Figure 2.3: Generalized stratigraphy of the Middle Jurassic to Early Tertiary in the Scotian Basin (modified from Wade and Maclean, 1993).

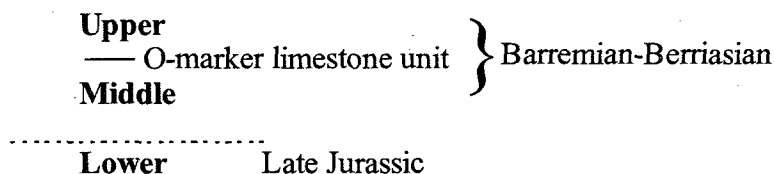
2.2.2 Mic Mac Formation

The Mic Mac Formation is a sequence of thick post rift sediments, predominantly clastic, underlying the Missisauga Formation and deposited in the late Jurassic from Bathonian to Kimmeridgian (144 Ma to 163 Ma). The overall thickness of the Mic Mac Formation varies from about 4 km of interbedded sandstone, shale, and limestone southeast of the Sable Island, to about 6 km in the Laurentian Subbasin. The Mic Mac Formation is interbedded with limestone of the Abenaki Formation to the north and west of the Sable

Island. The carbonate and clastic facies of the Mic Mac Formation pass seaward into fine-grained sediments of the Verrill Canyon Formation (Wade and MacLean, 1990).

2.2.3 Missisauga Formation

In the Scotian Basin, the Missisauga Formation is widespread and the formation shows variability in terms of sediment facies and thickness, being more than 2.1 km thick in the Sable Subbasin. The sandstones make up to 80 percent of the formation in some areas, with some significant amounts of local limestone facies in some locations. The Missisauga Formation is from Barremian to Tithonian (125 Ma to 147 Ma) in age and is divided into three informal members:



The Lower member is recognized only in parts of the Sable Subbasin and is laterally equivalent to the upper Mic Mac Formation (Wade and MacLean, 1990).

2.2.4 Verrill Canyon Formation

The fine-grained sediments of the Verrill Canyon Formation are deep water sediments of mid Jurassic to early Cretaceous age, approximately Bajocian to Barremian (170 Ma to 125 Ma), and were deposited on the outer shelf and slope. The Verrill Canyon Formation is the seaward equivalent of the Mic Mac and Missisauga Formations. It consists primarily of grey to brown calcareous shale, thinly bedded with siltstone, sandstone and limestone (Wade and MacLean, 1990).

2.2.5 Logan Canyon Formation

The Logan Canyon Formation is in the upper part of the Lower Cretaceous. This formation is in general an upward fining succession that has similar distribution of sedimentary facies as the Missisauga Formation, but generally with less sandstone and more shale. Sediment thickness in the Logan Canyon Formation reaches a maximum of 2.5 km. There are four subdivisions of the Logan Canyon Formation (Wade and MacLean 1990):

Marmora Member (Sandstone-dominated unit)

Sable Member (Shale-dominated unit)

Cree Member (Sandstone-dominated unit)

Naskapi Member (Shale-dominated unit)

The Logan Canyon Formation has a distal turbidite/shale equivalent known as the Shortland Shale unit (Wade and MacLean, 1990), and this consists of deep water facies that were deposited in a prodelta, outer shelf, and continental slope setting. It is thus an analogue of the deeper Verrill Canyon Formation (Wade and MacLean, 1990).

2.2.6 Dawson Canyon Formation

The Upper Cretaceous Dawson Canyon Formation consists of marine shales, chinks and minor limestones and it varies in thickness from 100 to 700 meters. The Dawson Canyon Formation was deposited between Cenomanian and Coniacian (95 Ma to 85 Ma) and it appears to be the most laterally extensive Cretaceous formation because of its transgressive nature (Wade and MacLean, 1990).

2.2.7 Wyandot Formation

The sediments of the Wyandot Formation are carbonates, and they range in composition through chalks, chalky mudstone, marls and minor limestones. They were deposited between Coniacian and Maastrichtian (85 Ma to 65 Ma). The Wyandot Formation ranges in thickness from about 50 meters in some wells of the Sable Subbasin, to ~ 400 metres in the southeastern corner of the Scotian Shelf. However, due to erosion the Wyandot Formation is thin or missing over extensive portions of the Scotian Basin (Wade and MacLean, 1990) but the formation has not been completely removed over most of the shelf. Like the Dawson Canyon Formation it is very widespread, more so than earlier Cretaceous and Jurassic units.

2.3 SEQUENCE STRATIGRAPHY AND ITS APPLICATION TO THE LOWER CRETACEOUS OF THE SCOTIAN BASIN

Sequence stratigraphy provides a system for analyzing stratal geometry and lithofacies in terms of relative changes in sea level (Catuneanu *et al.*, 2009). Using seismic reflection profiles, sediments are interpreted in a geometrical context from seismic reflectors.

Hence, emphasis is placed on the stratal geometry and unconformities seen in seismics, for the interpretation of sequence stratigraphy.

Sequences are large-scale units bounded by unconformities (Catuneanu *et al.*, 2009).

Sequence boundaries ideally form widespread unconformities on the basin margin, and these unconformities pass into correlative conformities on the basin floor. Sequence boundaries represent any surface in lithostratigraphy that separates older sequences from younger ones, and they may be recognized in core as a sharp erosional contact between unrelated facies. On the basin margin and floor, sequence boundaries underlie the Lowstand Systems Tract (LST). The Transgressive Systems Tract (TST) sediments are deposited as a result of relative sea-level rise, on a ravinement surface due to erosion on the shelf. The Highstand Systems Tract (HST) forms at highstands of relative sea-level, and the Falling Stage Systems Tract (FSST) is deposited during relative sea-level fall.

The frequencies at which changes occur in eustatic sea-level vary. These frequencies can be interpreted as orders of sequences and the higher a frequency the lower the assigned order. There is first order, second order, and third order changes in eustatic sea-level and they reflect the cyclic changes in the depositional trend. First orders represent large scale

changes in sea-level that also last longer. After each order with a higher frequency is recognized, various orders of sequences may then be recognized (Haq *et al.*, 1987).

Parasequences are the smallest order, the basic unit of a sequence stratigraphy that occurs in sets. Parasequences imply no change in sea-level and they are the result of the progradation of a delta distributary, followed by distributary abandonment.

When sediments are deposited during a relative sea level lowstand and initial rise, the deposits are termed a LST. These show a progradational (seaward) to retrogradational (landward) facies stacking. LST's are characteristically deposited below the level of the coastal plain or shelf and commonly may have a distal distribution. The LST may include lowstand shoreline, lowstand delta, and deep-water submarine fan (Posamentier and Allen, 1999).

The TST follows the LST and the type of sediments deposited shows an overall retrogradational facies stacking due to the influence of a relative sea level rise (Pemberton *et al.*, 1995; Droser *et al.*, 2002). The Transgressive surface (TS) or ravinement at the lower boundary of the TST, may be marked by erosion and associated early cementation. At the TS, when erosion occurs, stiff but uncemented sediments at the sediment-water interface may be exposed for a relative long period of time before being covered. These stiff but uncemented surfaces are known as "firm grounds" and they are sites for colonization by macro and microorganisms (Droser *et al.*, 2002).

The Maximum Flooding Surface (MFS) caps the TST and is characterized by a low rate of sediment deposition in distal parts of the basin, during a maximum relative sea-level highstand (Posamentier and Allen, 1999). The MFS is commonly characterized by extensive condensation or low net deposition and the widest landward extent of marine condensed facies. Such facies are commonly rich in biogenic and authigenic sediment components and may be represented by shales or limestones. Condensed sections are commonly enriched in normally rare authigenic minerals such as glauconite, phosphate, pyrite, and siderite (Al-Ramadan *et al.*, 2005).

Highstand Systems Tract (HST) sediments are deposited during relative sea-level highstand following the MFS and this may result initially in aggradational facies stacking, and later in progradational facies stacking. The HST involves a sea level still-stand accompanied by low rates of sedimentation that produces progradational onlapping. The Falling Stage Systems Tract (FSST) is interpreted as part of the HST by some authors and results from a falling sea-level accompanied by high sedimentation, which causes a forced regression (relative sea-level fall as a result of high sedimentation rates) and the formation of prograding clinoforms (Pemberton *et al.*, 1995).

Progradational parasequences consist of prograded sediments recognized by a coarsening upward succession, for example shale overlain by sandstone and then by conglomerates. Commonly, sequences bounded by sequence boundaries are made up of several parasequences (Posamentier and Allen, 1999). The facies succession in such a parasequence can therefore be interpreted as the presence of open marine shales overlain

by an interbedded sandstone/shale facies of shoreface or prodeltaic to river mouth facies, capped by fluvial or estuarine coarse-grained sandstone. Regressional parasequences consists of fining upwards successions and are the reverse of the progradational parasequence. Parasequences form by shifting delta disturbances under conditions of overall subsidence.

There are no published sequence stratigraphic interpretations of the entire Lower Cretaceous of the Scotian Basin. Several authors have suggested that second-order sequences can be recognized across the Scotian Shelf, such as the Upper member of the Missisauga Formation being bounded by MFS within the O-Marker and Naskapi Member intervals (Wade and MacLean, 1990; Karim *et al.*, 2010). In a detailed study of the Panuke field, Cummings *et al.* (2006) recognized two third-order sequences in the Upper Member of the Missisauga Formation. Third-order sequence boundaries have been recognized locally in some other fields (Cummings and Arnott, 2005; Karim *et al.*, 2010). In general, the distinction of third order sequences from local parasequences is difficult in the Scotian Basin.

According to Gould *et al.* (2010), a deltaic parasequence in the Lower Cretaceous of the Scotian Basin usually includes the presence of graded laminated sandstones with bioturbated mudstones interbedded in a progradational succession. Such a succession is seen to have abundant ($\pm 65\%$) mudstone beds with moderate to common bioturbation. Sandstone beds have sparse bioturbation, cross laminations, and wave ripples at the top of the beds. Thicker sandstone beds show the presence of phytodetritus, mica flakes, and

common shelly fragments are found in thinner sandstone beds. Parasequences (or small scale sequences) in the Scotian Basin are typically 3 m to ~50 m thick.

2.4 WELLS STUDIED

2.4.1 General Strategy

In order to be able to document the possible effect of geographic variation of sediment input in the Scotian Basin, conventional core from a well in the Abenaki Subbasin (Peskowesk A-99 well: location in Fig. 1.1 and lithostratigraphy in Fig. 2.4) and a well in the Sable Subbasin (Thebaud C-74 well: location in Fig. 1.1 and lithostratigraphy in Fig. 1.1 and 2.5) were studied. Petrographic and geochemical studies by Pe-Piper et al. (2008) suggested different sediment supply for the two wells. This thesis study is focused on the transgressive units and the immediately underlying prograded sediments.

2.4.2 Peskowesk A-99: location, general stratigraphy, and location of cores

Peskowesk A-99 (Fig. 2.4) is located in the southwest Abenaki Subbasin (Fig. 1.1) in the eastern part of the Scotian Basin. In this well, the Lower Cretaceous totals approximately 2100 m thick, predominantly of shale with interbedded siltstone to coarse-grained sandstone, and occasional granules and/or pebbles.

The Logan Canyon Formation at Peskowesk A-99 well is approximately 1100 m thick and the Missisauga Formation is approximately 1000 m thick. The sediments of the Mic Mac formation at the Peskowesk A-99 well are terrigenous clastics from 3500 m down to about 3750 m, and below that are predominantly carbonates (Fig. 2.4).

There are seven conventional cores in the Peskowesk A-99 well (Fig. 2.4). Cores one through four are from the lower part of the Cree Member of the Logan Canyon

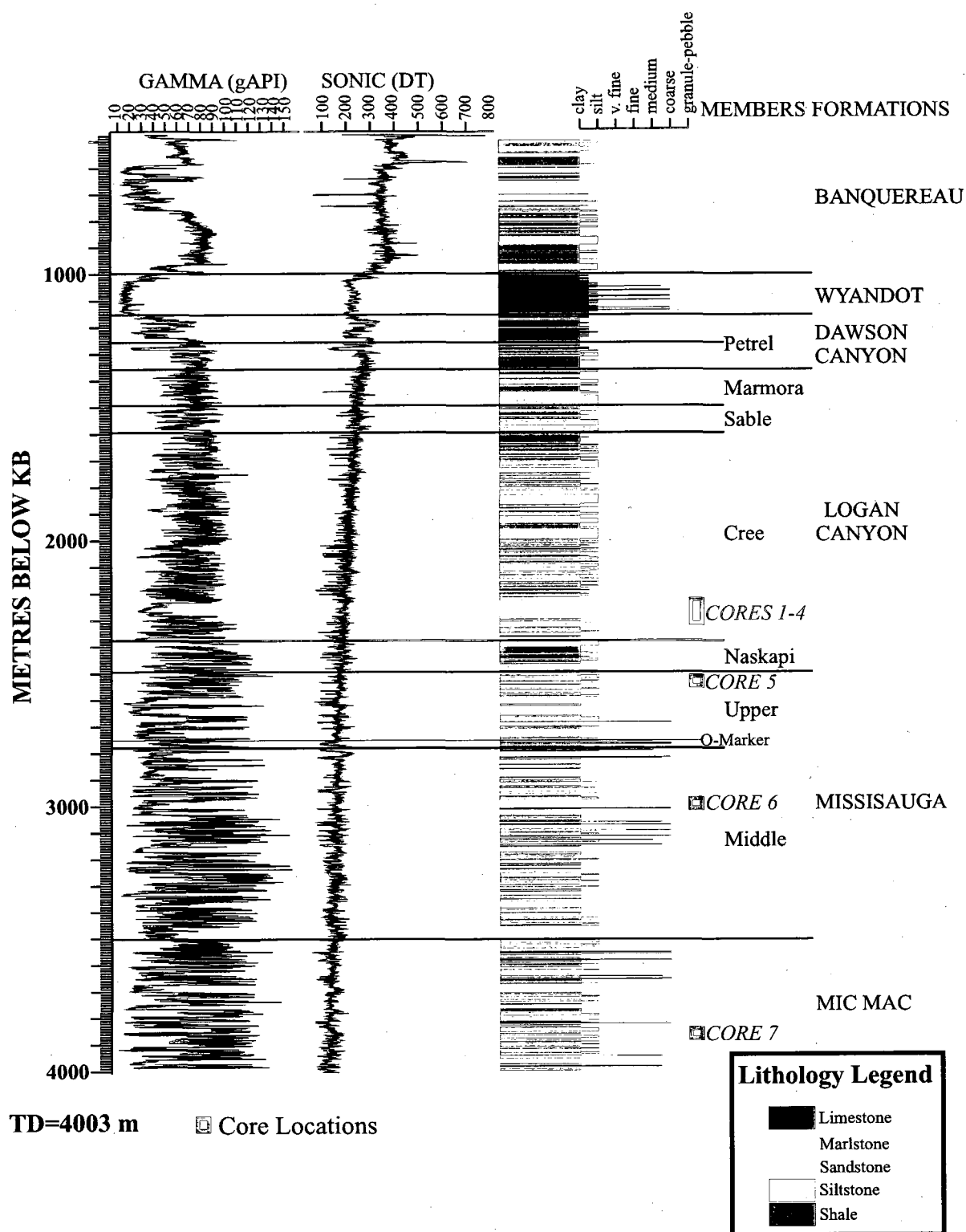


Figure 2.4: Lithostratigraphy, core locations, gamma and sonic logs at the Peskowesk A-99 well. Lithostratigraphic picks from MacLean and Wade, 1993. Lithology from Canadian Stratigraphic, wireline data from IHS Accumap. Diagram plotted with lithplot2.perl by A. MacRae, using data from BASIN database (http://basin.gdr.nrcan.gc.ca/index_english.php).

Formation, and core five is near the top of the Missisauga Formation. Core six is from the upper part of the middle member of the Missisauga Formation and core seven is from ~ 300 metres below the top of the Mic Mac Formation, at a level where calcareous shale and limestone predominate.

2.4.3 Thebaud C-74: location, general stratigraphy, and location of cores

Thebaud C-74 is an exploration well in the Thebaud field that is situated in the west central Sable Subbasin, about 10 km southwest of Sable Island. The thick, sand prone lower and middle members of the Missisauga Formation in Thebaud C-74 (Fig. 2.5) overlie upper Jurassic shales of uncertain lithostratigraphic affinity and they pass seaward into the shale-prone Verrill Canyon Formation. The O-marker, between the middle and upper member of the Missisauga Formation, is a transgressive to highstand limestone unit and it is a thin unit in the Thebaud field (MacLean and Wade, 1993). Sediments in the Thebaud field are deposited in a rollover anticline structure bounded by two large listric growth faults striking through from east to west, extending down into the basin. There are six conventional cores in Thebaud C-74, all of which are from the lower member of the Missisauga Formation. They consist of shale interbedded with siltstone to coarse-grained sandstone and rare granules and/or pebbles.

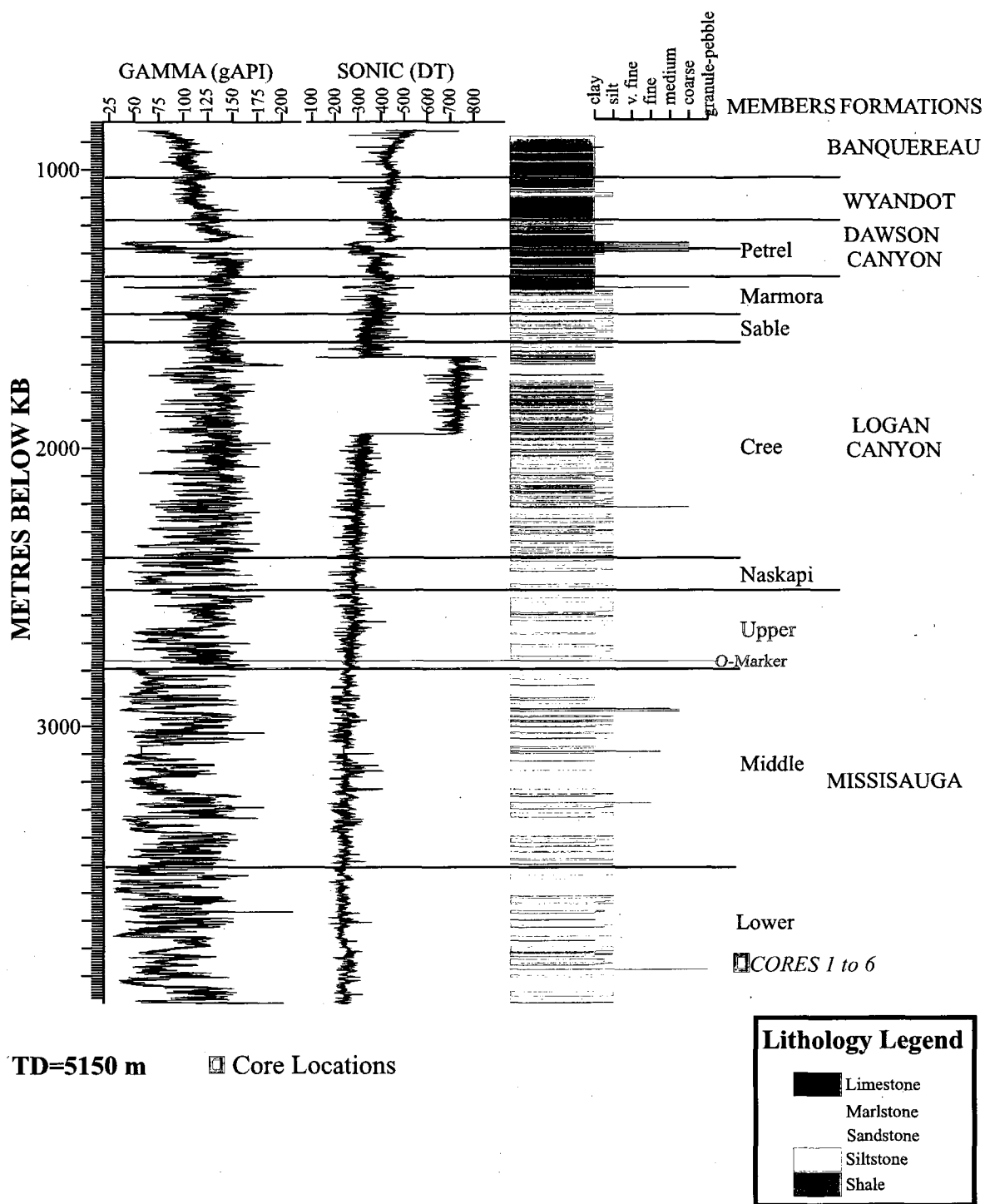


Figure 2.5: Lithostratigraphy, core locations, gamma and sonic logs at the Thebaud C-74 well. Lithostratigraphic picks from MacLean and Wade, 1993. Lithology from Canadian Stratigraphic, wireline data from IHS Accumap. Diagram plotted with lithplot2.perl by A. MacRae, using data from BASIN database (http://basin.gdr.nrcan.gc.ca/index_english).

2.5 GAMMA AND CONVENTIONAL CORE LOGS

Conventional cores may have gaps as a result of incomplete sampling. Gamma ray logs can be used to position sediment in the core relative to the suite of down-well logs (Figs. 2.4, 2.5). Gamma is higher in shales (generally above 100 API units; a measurement originated by the petroleum industry), while sandstones and carbonates are generally between 50 and 75 API units.

Aligning the core lithology with gamma log showed that for the cores at Thebaud C-74 (Fig. 2.7), the nominal core depths, used throughout this study including identifying sample depths, are offset about 3.5 m deeper than the log depth measured below KB. The abrupt change from thick sandstone in core 5 and base of core 4 to mudstone higher in core 4 is particularly clear on the gamma log (Fig. 2.7).

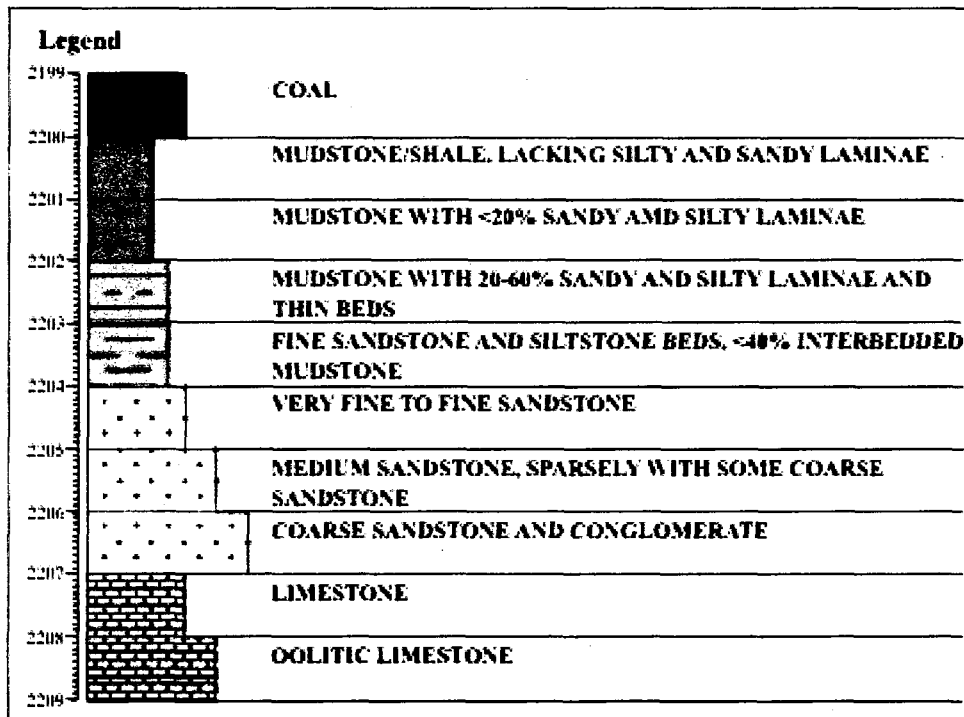


Figure 2.6: Legend for lithologies depicted in Figures 2.7 to 2.11

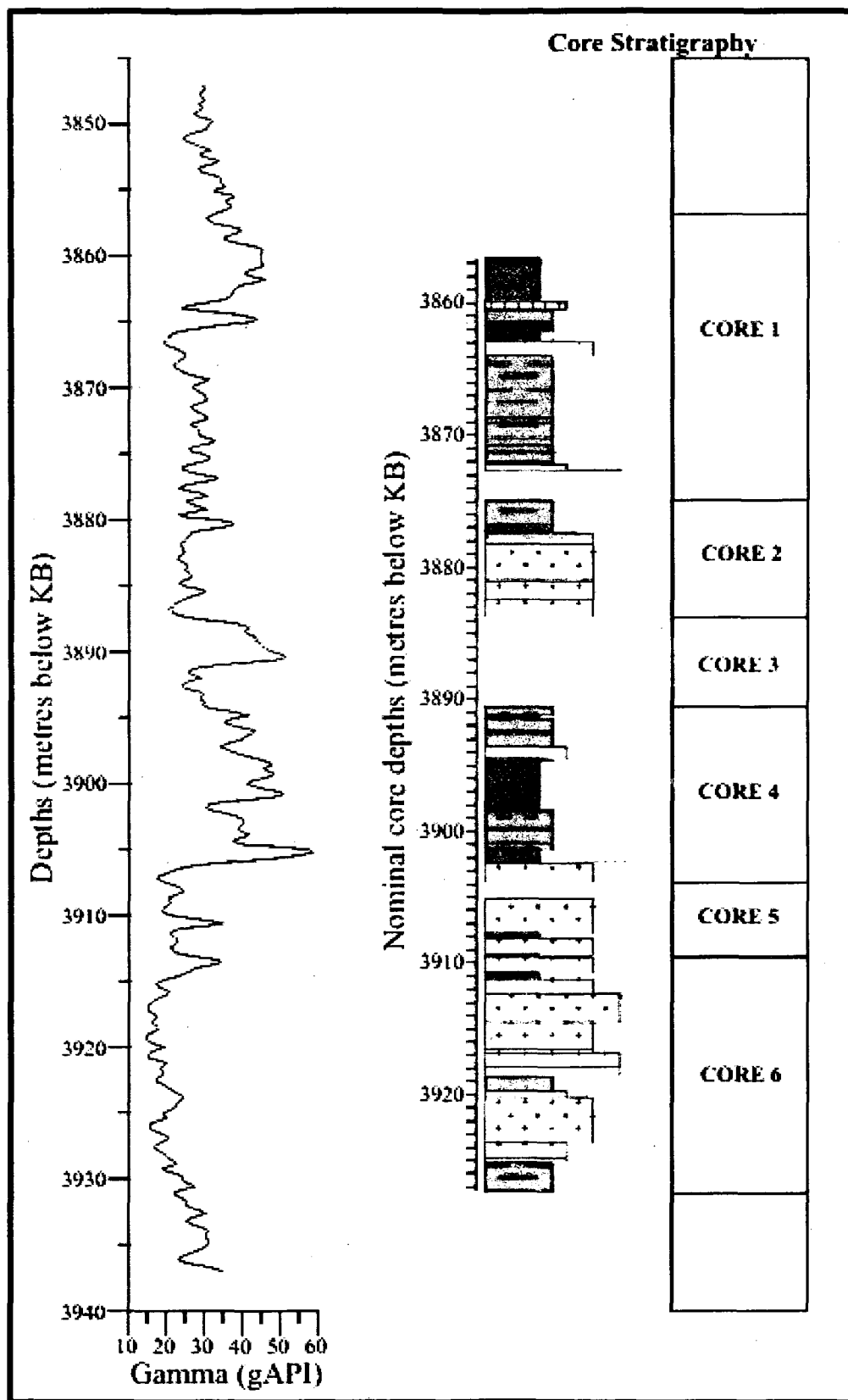


Figure 2.7: Gamma and core plots for cores 1-6 at Thebaud C-74.

For cores 1 to 4 at Peskowsk A-99, the nominal core depths are offset about 3 m deeper than the log depth measured below KB (Fig. 2.8). The gap between cores 3 and 4 in conventional core appears to be predominantly thick sandstones based on the gamma log.

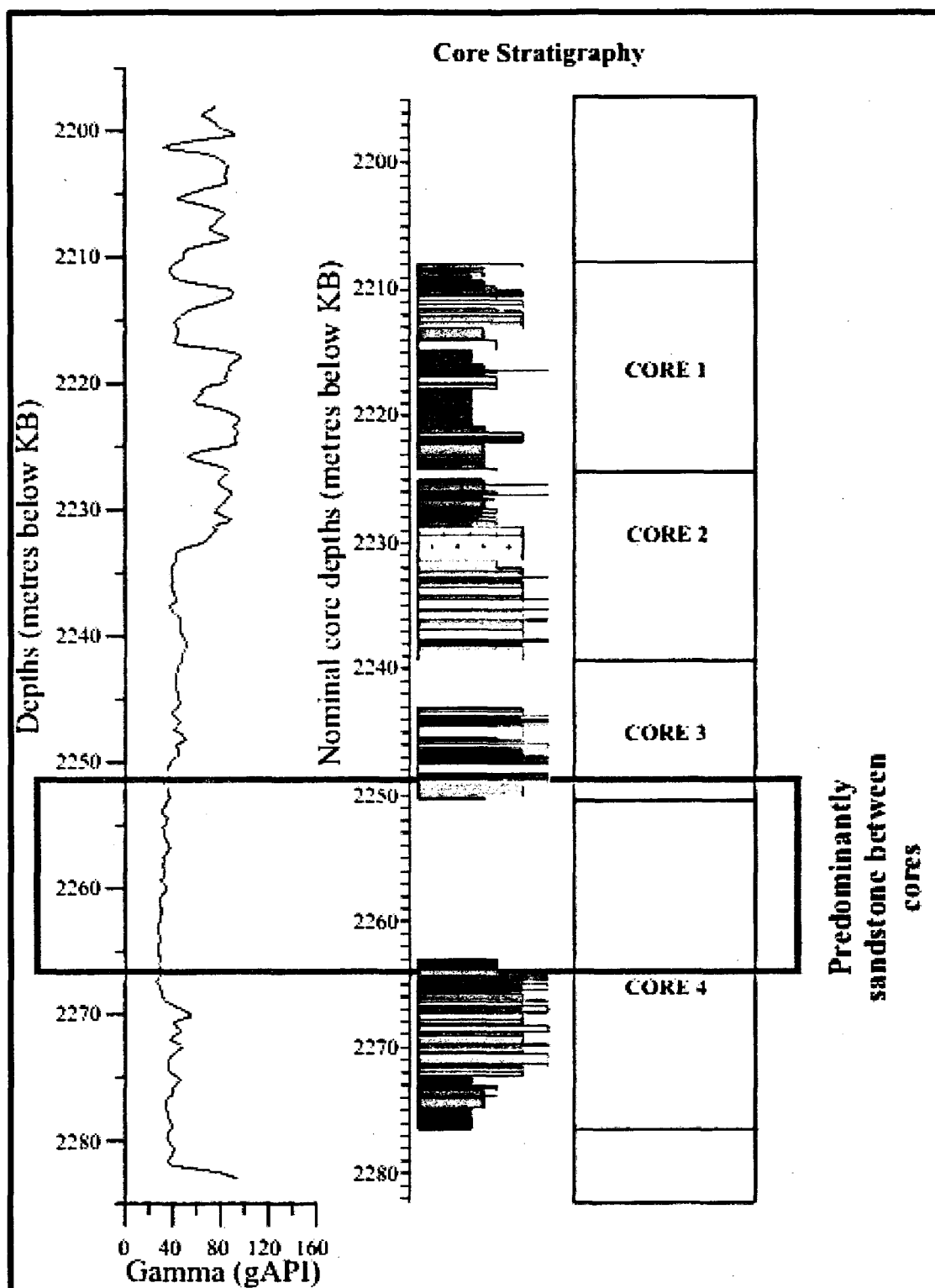


Figure 2.8: Gamma and core plots for cores 1-4 at Peskowsk A-99.

For the remaining individual cores at Peskowsk A-99 (cores 5, 6, and 7), the nominal core depths for are offset by about 4 m (Figs. 2.9, 2.10, 2.11). The limestone unit in core 7 is particularly clear on the gamma log.

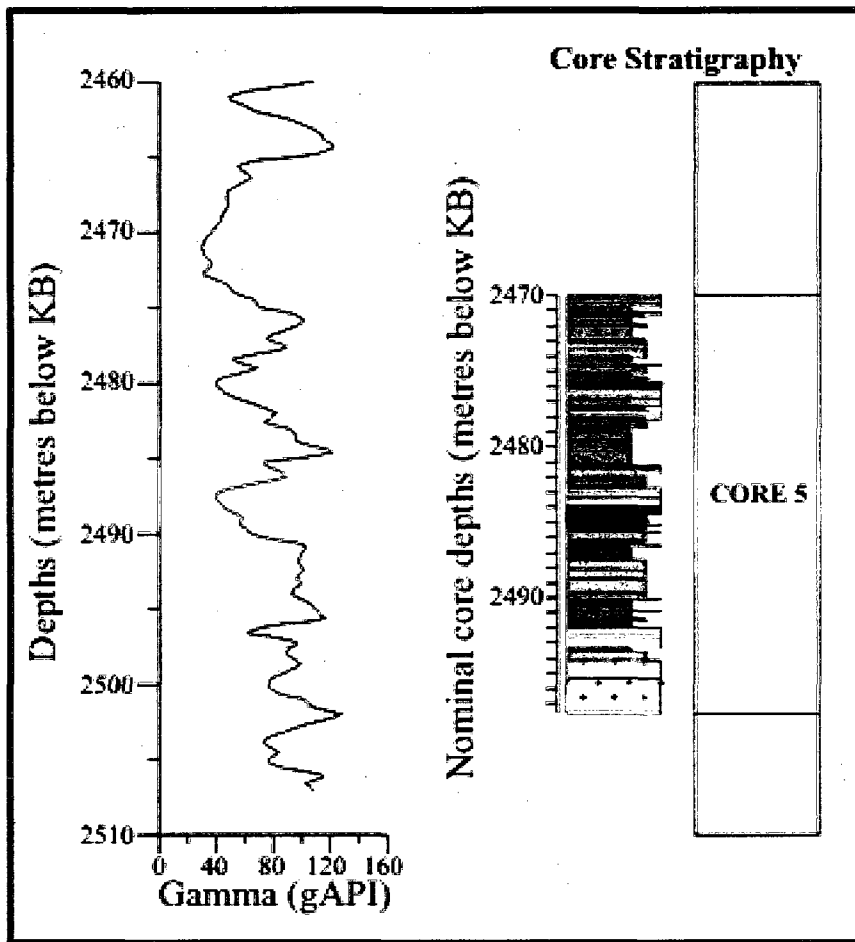


Figure 2.9: Gamma and core plot for core 5 at Peskowsk A-99.

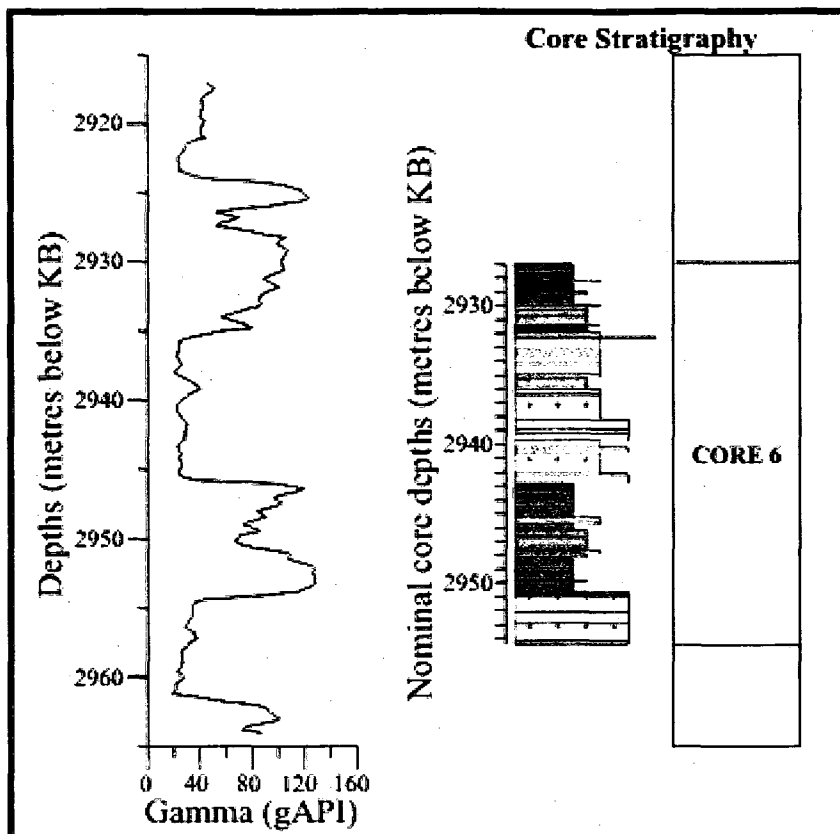


Figure 2.10: Gamma and core plot for core 6 at Peskowsk A-99.

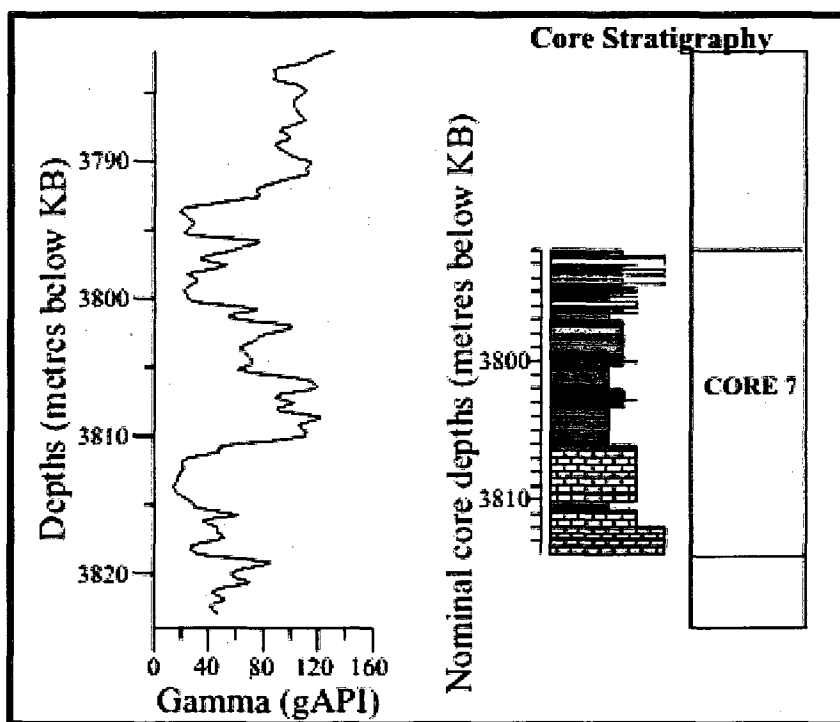


Figure 2.11: Gamma and core plot for core 7 at Peskowsk A-99.

2.6 CHAPTER SUMMARY

This chapter explains how the Scotian Basin evolved. The two wells of focus, one in the Sable Subbasin, and the other in the Abenaki Subbasin, have been interpreted based on lithostratigraphy. The role of sequence stratigraphy and its application to the Lower Cretaceous of the Scotian Basin was further reviewed. A background for the study area is established with the sections in this chapter. The following chapter is the beginning of the results section of this study. Chapter 3 provides a detailed sedimentological interpretation of conventional cores, and introduces the facies types that have been recognized.

CHAPTER 3: STRATIGRAPHY AND SEDIMENTOLOGY

3.1 INTRODUCTION

The purpose of this chapter is to describe the sedimentary facies in the conventional core in both studied wells and to evaluate how the sedimentary succession changes across Transgressive Surfaces (TS). The lithofacies classifications (Table 3.1) by Karim *et al.* (2008) for Lower Cretaceous conventional cores is used as the basis for description of the cores (with additions from this study). The environmental interpretations corresponding to particular lithofacies proposed by Karim *et al.* (2008) are used as a guide, but have not been evaluated in detail for the entire core section. The sediments immediately above and below the TS have been described and have been interpreted in more detail (section 3.5) because of their importance in the early diagenetic history of sandstones in this study.

Table 3.1: Characteristics of lithofacies used for both studied wells.

Facies	Lithology	Characteristics	Literature Reference	Specific Interpretation	General Interpretation	Figure References
0	mudstone with sandstone and siltstone beds (< 25 cm) and laminae, absent to moderate bioturbation	0a: alternation of coarse and fine sandstone beds with interbedded mudstone, bioturbation absent		Proximal	River mouth to shoreface	
		0c: Almost all sand, cut + fill, oblique bedding lacking interbedded mudstone		Transitional to facies 9		
		0g: common medium bedded graded sandstone beds lacking interbedded mudstone	G-(S4); C&A-(6)			
		0l: sandstone beds with parallel lamination at top and cross laminations at base	C&A-(5)	Proximal		
		0m: predominant mudstone, uncommon bioturbation, some silt or very fine sandstone laminae	G-(M1); C et al. (4); C&A-(4)	Distal		Fig. 3.2
		0n: distinctive graded silt to mud laminae interbedded with well sorted very fine sandstone laminae and lenticular beds, bioturbation absent	C&A-(2)			
		0s: sandstone beds (< 25 cm) with parallel and cross lamination and interbedded mudstone with fewer silt laminae than 0t , uncommon bioturbation, sharp base		Proximal		Fig. 3.3
		0t: graded sandstone beds, generally laminated to cross laminated with lesser interbedded mudstone with abundant silt laminae and some lenticular, sparse bioturbation, erosional base	G-(S2b); C&A-(3)			
1	bioturbated mudstones	may have uncommon thin-shelled fossils			Shelf	Fig. 3.4
		1c: calcareous shales				Fig. 3.5
		1d: MFS with ~ 70% sandstones				

Table 3.1: Characteristics of lithofacies used for both studied wells.

Facies	Lithology	Characteristics	Literature Reference	Specific Interpretation	General Interpretation	Figure References
2	fine sandstone, mudstone	2b: interbedded with moderate to common bioturbation, sharp base	G-(S4)	Closer to river mouth	Shoreface	Fig. 3.6
		2c: common to completely bioturbated sandstone and mudstone with sandstone predominant (60 - 90 %)- usually well bioturbated	C&A-(14)	Inshore		Fig. 3.7
		2d: as 2c but <60% sandstone		Offshore		
3	conglomerate formed with bioturbated shelly sandy mudstone to muddy sandstone generally with some coarse sand or granule sized intraclasts and/or lithic clasts. Commonly sideritic diagenesis. In other wells, bioclastic and oolitic limestones	3a: sandstone matrix and mud laminae, bioturbation absent to uncommon	G-(C1)		Transgressive Surface	Fig. 3.8
		3b: sandstone matrix, bioturbation absent, erosional base				Fig. 3.9
		3c: conglomerate				Fig. 3.10
		3l: bioclastic limestones	G-(L1); C et al. (7)			Fig. 3.11
		3m: mud matrix predominant, moderate to common bioturbation	G-(M2); C&A-(13)			Fig. 3.12
		3o: oolitic limestones				Fig. 3.13
		3s: medium sandstone matrix, bioturbation absent, sharp base				Fig. 3.14
4	fine to coarse sandstone (general medium to coarse), interbedded mudstone with siltstone laminae, and cross-bedding are characteristic	4g: medium to coarse sandstone, minor mud drapes, bioturbation absent, base of sandstone may be erosional	G-(S1); C et al. (2); C&A-(10, 12)	Main estuary channel	Fluvial to tidal estuary	Fig. 3.15
		4o: fine to medium sandstone rich in <i>Ophiomorpha</i> and mud drapes		Seaward part of an estuary		Fig. 3.16
		4s: sandstone and siltstone commonly lenticular, mudstone drapes		Margin of estuary channel		
		4x: thick beds medium to coarse sandstone, not "graded", some cross-bedding	C et al. (1)	Fluvial		Fig. 3.17

Table 3.1: Characteristics of lithofacies used for both studied wells.

Facies	Lithology	Characteristics	Literature Reference	Specific Interpretation	General Interpretation	Figure References
5	bioturbated fine sandstone	5: with uncommon to moderate bioturbation, muddy linings to some burrows, transitional to 4o	G-(S3); C et al. (5); C&A-(7)		Sandy tidal flat	Fig. 3.18
		5s: > 70 % fine-grained sandstone with some bioclasts, burrow traces and sparse mud drapes				Fig. 3.19
6	laminated mudstone and siltstone	with root traces, tidal flat structure	C et al. (3); C&A-(11)		Muddy tidal flat	Appendix 3.2, P20
7	coal				Tidal marsh	
8	grey-green sandy highly bioturbated	with heavy shelly fossils			Lagoon	Fig. 3.20
9	thick (> 25 cm) bedded sandstones in "graded" beds, moderate bioturbation at top, plant debris, minor interbedded facies 0	9b: diffuse siderite cement and diagenetic siderite concretions			River mouth to turbidite	Fig. 3.22
		9f: fine sandstone with mud drapes		Transitional to facies 4o		Fig. 3.23
		9g: graded sandstone beds lacking interbedded mudstone	G-(S2c); C&A-(8)	More proximal		Fig. 3.24
		9s: sharp base, parallel lamination at base and cross lamination at top. Some beds have abundant mud intraclasts generally near base	G-(S2a)	More tidal		

Literature reference abbreviation: G: Gould 2007, C et al: Cummings et al. (2006) C&A: Cummings and Arnott (2005).

3.2 METHODS

The lithostratigraphy of conventional cores provided by the Canada Nova Scotia Offshore Petroleum Board (CNSOPB) was described. The cores were laid out and the labeling of the cores were checked by comparing the ends of each box. For Peskowesk A-99 (Table 3.2), there were seven conventional cores with an average of 16 boxes available for each core, and for Thebaud C-74 (Table 3.2) there were six cores with an average of 15 boxes available to each core (except core 3, which is only one box). The cores were set against a one-metre ruler, which was aligned with the top of the core box. It was important to line up the ruler with the top of the box because most cores have missing parts.

The principal sediment type present based on grain size and composition was identified and the core was divided into major lithological units, making note of the top and bottom depths for each unit. More detailed interpretation was also recorded e.g. presence of siderite cementation (or the general presence of brown staining), bioclasts, nodules, phytodetritus, bioturbation, cross bedding, graded beds and other features in the core.

For the purpose of this study, the character of upper and lower contacts for the different units (e.g. erosional, sharp, or gradation contacts) was also recorded. Every specific feature was photographed at least once (e.g. complex laminations), and sub-sampling of the core was done after units were described. 53 samples were collected from Peskowesk A-99 and for Thebaud C-74 six samples were collected and added to the 23 previous samples collected by Gould (2007).

Wells	Samples	Top (m)	Bottom (m)	Formation Cored	Comments
Peskowesk A-99	Core 1	2208	2225	Logan Canyon Fm (Cree Mb)	Recovered 15.8 m
	Core 2	2225	2243	Logan Canyon Fm (Cree Mb)	Recovered 14.0 m
	Core 3	2243	2263	Logan Canyon Fm (Cree Mb)	Recovered 7.35 m
	Core 4	2263	2282	Logan Canyon Fm (Cree Mb)	Recovered 13.5 m
	Core 5	2470	2498	Missisauga Fm (Upper Mb)	Recovered 27.64 m
	Core 6	2927	2956	Missisauga Fm (Upper Mb)	Recovered 27.36 m
	Core 7	3791	3814	Mic Mac Fm	Recovered 21.91 m
Thebaud C-74	Core 1	3856.63	3873.26	Missisauga Fm (Lower Mb)	Recovered 16.63 m
	Core 2	3874.92	3883.86	Missisauga Fm (Lower Mb)	Recovered 8.94 m
	Core 3	3890.52	3891.08	Missisauga Fm (Lower Mb)	Recovered 0.56 m
	Core 4	3891.08	3903.92	Missisauga Fm (Lower Mb)	Recovered 12.84 m
	Core 5	3905.1	3909.35	Missisauga Fm (Lower Mb)	Recovered 4.25 m
	Core 6	3909.67	3926.83	Missisauga Fm (Lower Mb)	Recovered 17.16 m

Table 3.2: Conventional core information for both studied wells. Modified from Natural Resources Canada, Geological Survey of Canada, Geological Survey of Canada, Geoscience Data Repository, BASIN Database (<http://basin.gdr.nrcan.gc.ca>).

3.3 SEDIMENT LITHOFACIES

Karim *et al.* (2008) recognized eleven lithofacies for Lower Cretaceous conventional cores, most of which were sandstone or interbedded sandstone and mudstone. Each of the lithofacies was assigned a number between 0 and 10 (Table 3.1). The main characteristics for distinguishing the lithofacies include: bedding structures, grain size, sedimentary structures, degree of bioturbation, and the abundance of mudstone beds or laminae. A small letter denotes subdivisions of the lithofacies, e.g. Facies 2 can be divided into 2c, with abundant sandstone and bioturbation, and 2b has lesser sandstones and bioturbation. Figure 3.1 shows a graphical general interpretation of the distribution of the facies in a deltaic environmental model. A full description of each facies is given in section 3.3.1, as well as comparison to other published lithofacies classifications (e.g. Cummings and Arnott, 2005).

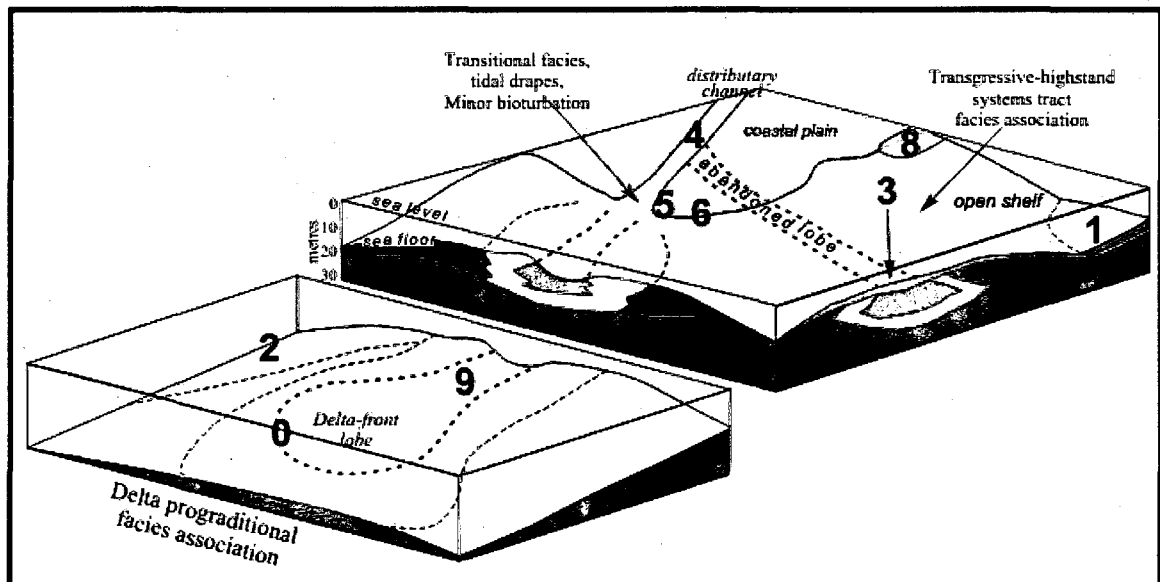


Figure 3.1: Graphical interpretation of lithofacies in the specific environments (modified from Gould, 2007).

3.3.1 Identified Lithofacies in Both Studied Wells

Facies 0: Rivermouth to shoreface – mudstone with sandstone and siltstone beds (< 25 cm in thickness) and laminae with absent to uncommon bioturbation.

This facies is recognized on the basis of its lithology, consisting of mudstone with thin-bedded sandstones and siltstones (beds <25 cm thick). Bioturbation ranges from absent to uncommon and it is never sufficient to completely obscure sandstone beds. The grain size of the sands ranges from very fine to medium-grained. Siltstone and sandstone beds have sharp bases, generally with parallel to cross laminations and lenticular beds. This facies lacks mud drapes, and plant detritus is not uncommon. Facies 0 differs from facies 9 in the thickness of individual sandstone beds.

Two sub-facies are recognized in this study: 0m and 0s. Sub-facies 0m (Fig. 3.2) with predominantly mudstone showing the highest intensity of bioturbation as the sandstone beds are uncommonly bioturbated. Sub-facies 0s (Fig. 3.3) consists of predominantly sandstone beds with sharp bases, parallel and cross laminations, and interbedded mudstone. Bioturbation is uncommon in this sub-facies.

Facies 0 resembles facies 2 and 4 of Cummings and Arnott (2005) and facies Ss1 and Ms of Gould *et al.* (2010). Cummings and Arnott (2005) interpreted this facies as a distal shoreface because of the wave-formed ripples. Sub-facies 0s is in the more proximal part of the shoreface based on the presence of more sandstone. Gould *et al.* (2010) suggested that sediments of facies 0 are not shoreface, but delta-front turbidites similar to those described by Lamb *et al.* (2008).

Facies 1: Shelf – bioturbated mudstone

This facies consists of mudstone that lacks interbedded sandstone (Fig. 3.4). Calcareous shales are classified as sub-facies 1c (Fig. 3.5). Bioturbation has obliterated any primary sedimentary structures. Thin shelled fossils are common and include echinoderms and ammonites.

The lack of sandstone suggests conditions from a remote delta or shoreline. The presence of thin-shelled fossils such as echinoderms, implies fully marine conditions. The abundance of fossils suggests relatively low sedimentation rates. Piper *et al.* (2004) identified a similar facies to facies 1, which was interpreted to be wave-dominated shoreface to offshore (prodelta muds) deposit.

Facies 2: Shoreface – bioturbated fine-grained sandstone with minor to major interbedded mudstone

This facies comprise very fine to fine-grained sandstone, interbedded with mudstone, in the presence of common to complete bioturbation. Sub-facies are defined on the basis of proportions of sandstone and intensity of bioturbation. Sub-facies 2b comprise commonly bioturbated sandstone with about 60% mudstone (Fig. 3.6). Many sandstone beds have a concentration of shelly fragments at the base of the bed. Sub-facies 2c comprises 60-90% completely bioturbated sandstone, 10-40% mudstone, commonly with patchy siderite cementation (Fig. 3.7). Sub-facies 2d (no photos available) is similar to facies 2c but with less than 60% sandstone. Wave ripples are common in facies 2, and are identified at the

top of sand beds. Sandstone beds have sharp bases, commonly with lenticular to parallel laminations.

Facies 2 corresponds to facies 7 of Cummings and Arnott (2005) and facies Ss2 of Gould *et al.* (2010). Cummings and Arnott (2005) showed evidence of storm-wave deposition including: (a) sharp-based event beds, (b) reworking of shells, and (c) presence of wave ripples at the top of sand beds.

The presence of highly burrowed zones suggests a considerable variation in sedimentation rate, which could be associated with storm related deposition in offshore settings. Sub-facies 2d, with the most mudstone was probably deposited farthest offshore. Sub-facies 2b (e.g. Fig. 3.6) represents a lower shoreface setting that commonly has thinner mudstone beds. Sub-facies 2c (e.g. Fig. 3.7) represents an upper shoreface setting that generally has a predominance of sandstone. The presence of less mudstone and higher bioturbation intensity differentiates facies 2 from facies 0.

Facies 3: Transgressive highstand sediments –conglomerate, sandstone and sandy mudstone with thin-shelled shelly fragments

The facies is recognized as poorly sorted fine to coarse-grained sandstone and conglomerate consisting of pebble-sized, carbonate cemented intraclasts. The facies shows patchy siderite cementation. The base of this facies is generally an erosion contact with the underlying facies. Bioturbation ranges from absent to complete. Bioclastic and oolitic limestones are also included in facies 3.

There are seven sub facies within facies 3 (i.e. 3a, 3b, 3c, 3l, 3m, 3o, and 3s). Sub facies 3a (Fig. 3.8) consists of fine-grained sandstone with interbedded mud laminae.

Bioturbation is absent to uncommon. Sub-facies 3b (Fig. 3.9) consists of fine to medium-grained sandstone with an erosional base. Bioturbation is generally absent. Sub facies 3c (Fig. 3.10) consists of conglomerate formed with bioturbated shelly sandy mudstone.

Bioturbation is common. Sub-facies 3l (Fig. 3.11) consists of bioclastic limestone. Sub facies 3m (Fig. 3.12) consists predominantly of mudstone. Bioturbation is moderate to common. Sub-facies 3o (Fig. 3.13) consists of oolitic limestone. Sub-facies 3s (Fig. 3.14) consists predominantly of medium-grained sandstone with a sharp base. Bioturbation is generally absent.

Facies 3 corresponds to facies Ct, SMt, and SLt in Gould *et al.* (2010), all of which are categorized under the transgressive facies association, and to facies 13 in Cummings and Arnott (2005). Both authors have interpreted this facies as transgressive lag deposits.

The erosive base of the facies results from coastal ravinement. The sediments of facies 3 commonly pass up into deeper-water deposits of facies 1. Generally, the presence of complete bioturbation suggests low sedimentation rates relative to bioturbation activity. The abundance of thick-shelled shelly fragments also suggest low net sedimentation rates, but with intermittent high energy conditions suggesting a shallow water environment.

Facies 4: Fluvial to Tidal Estuary – fine to coarse-grained sandstone with interbedded mudstone and siltstone

Generally, this facies is made up of cross-bedded medium to coarse-grained sandstone with interbedded mudstone and siltstone laminae. The presence of mudstone (and/or mud drapes) appears to be associated with the presence of fine-grained sandstones.

Bioturbation in this facies is typically absent to uncommon. Three sub-facies are recognized (i.e. 4g, 4o, and 4x).

Sub-facies 4o is characterized by common *Ophiomorpha* (Fig. 3.16). Sub-facies 4x lacks mudstone and is characterized by thick beds generally made up of medium to coarse-grained sandstone, with common cross-bedding in sets of 0.1 m in thickness (Fig. 3.17).

Plant detritus and siderite cementation are common features in this sub-facies. Following the description of Gould *et al.* (2010), facies 4g consists of cross-bedded medium to coarse-grained sandstone (~ 15 cm thick) with mud drapes (Fig. 3.15). Granules (2-4 mm) and fine pebbles (4-8 mm) are common in sub-facies 4g and 4x.

Sub-facies 4g is interpreted as a tidally influenced fluvial sandstone based on the presence of mud drapes on cross beds, which suggests tidal sedimentation (Gould *et al.*, 2010). It may represent a main estuary channel. Sub-facies 4o may represent the seaward part of an estuary based on the presence of *Ophiomorpha* and the more bioturbated character, suggesting limited marine influence. The lack of mudstone or mud drapes in the cross-bedded, graded sandstone beds in sub-facies 4x suggests fluvial sedimentation. This is further supported by the lack of bioturbation in this sub-facies. Sediments in

facies 4 thus represent a range of depositional environments from continental to transitional. Similar interpretations have been made by Cummings and Arnott (2005) and Gould *et al.* (2010).

Facies 5: Sandy Tidal Flat – bioturbated fine-grained sandstone

This facies comprise entirely of sandstone, commonly massive or with thin parallel laminations. Bioturbation is uncommon to moderate. Fine-grained sandstones commonly have wave ripples (Fig. 3.18). The bioturbation is characterized by the presence of vertical mud lined burrows (*Skolithos* ?) and the lack of *Ophiomorpha* differentiates this facies from sub-facies 4o. Sub-facies 5s differ from typical facies 5 in having sparse mud drapes and rare bioclasts (Fig. 3.19). Facies 5 occurs interbedded with other shallow-water facies e.g. sub-facies 2c.

The presence of unusual vertical burrows and sands makes facies 5 similar to the facies 9 of Cummings and Arnott (2005). Cummings and Arnott (2005) interpreted this facies as tidal flat deposits.

Facies 8: Lagoon – grey to green sandy, commonly bioturbated mudstone

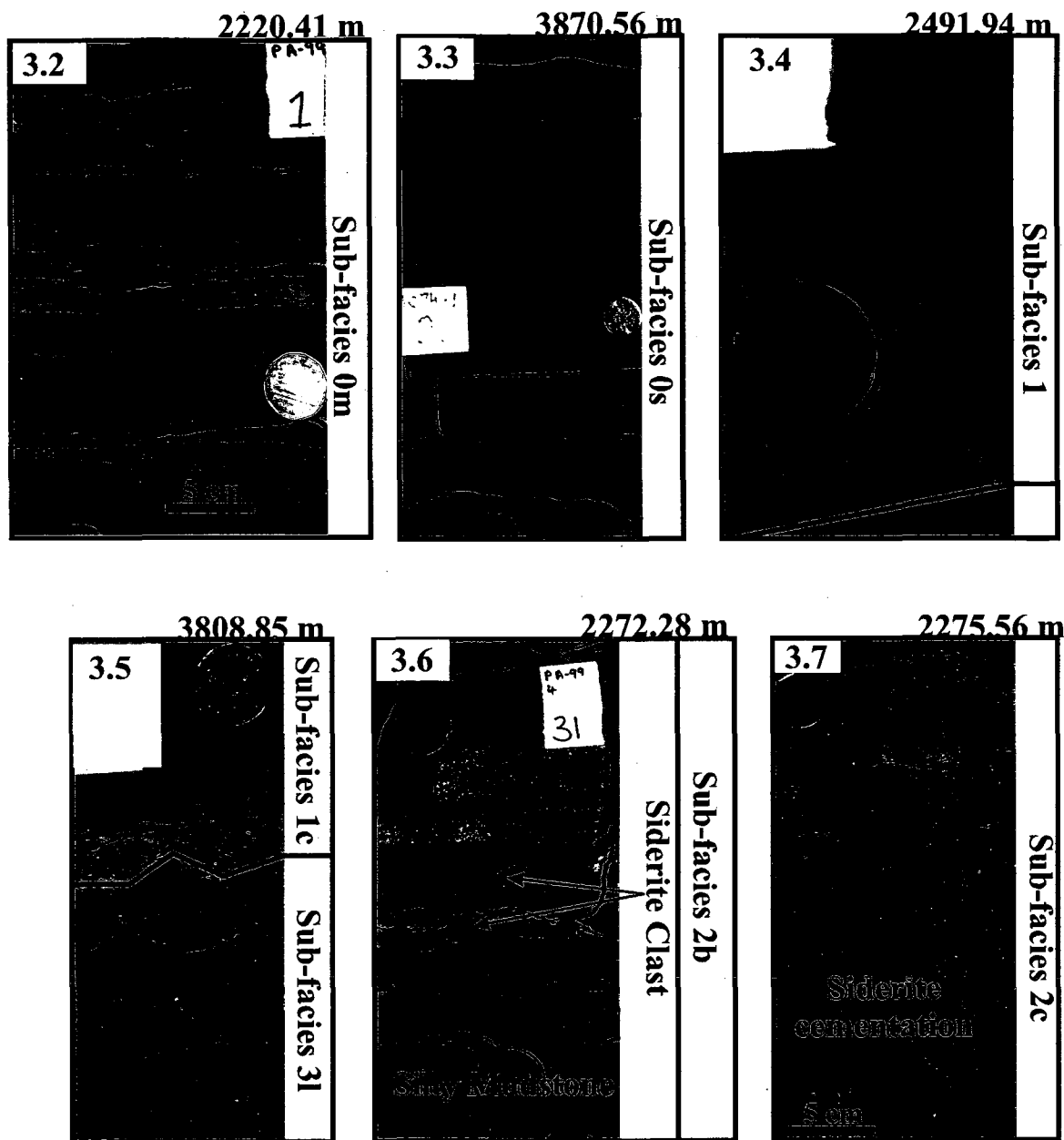
This facies is characterized by grayish green mudstone with interbedded siltstone to very fine-grained sandstone (Fig. 3.20). Bioturbation is common. Thick-shelled shelly fragments e.g. oysters are common. This facies is also characterized by the presence of greenish inclusions, identified in chapter 4. Piper *et al.* (2004) identified a similar facies as evidence of transgressive sequences in lagoons.

Facies 9: Rivermouth to turbidite – thick (> 25 cm), graded sandstone beds with minor interbedded facies 0, and plant detritus.

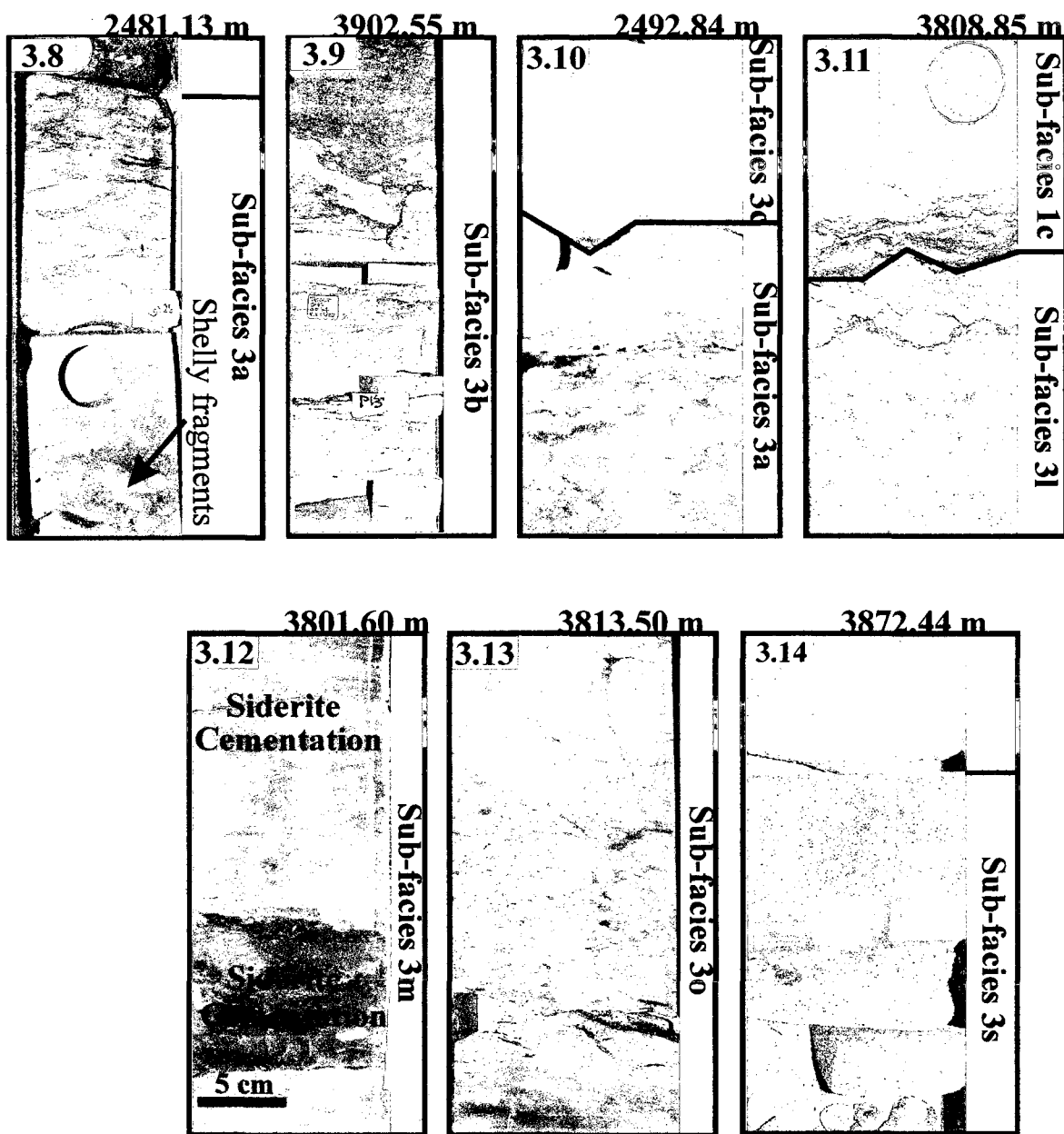
Generally, this facies is made up predominantly of thick normally graded sandstone beds greater than 25 cm in thickness (Fig. 3.21). Plant detritus is common. Bioturbation in facies 9 is generally absent to uncommon in the sandstones, but common in interbedded mudstone. Ungraded sandstone beds can be massive with a sharp contact common between beds or have parallel or cross laminations, with the presence of interbedded mudstones.

There are three sub-facies recognized in this study (i.e. 9b, 9f, and 9g). Sub-facies 9b (Fig. 3.22) consists of graded sandstone beds with diffuse siderite cement and diagenetic siderite concretions. Sub-facies 9f (Fig. 3.23) consists of fine-grained thick bedded sandstone resembling typical facies 9 but with mud drapes. Sub-facies 9g (Fig. 3.24) consists of graded sandstone beds lacking interbedded mudstone. The presence of thicker sandstone beds differentiates facies 9 from facies 0.

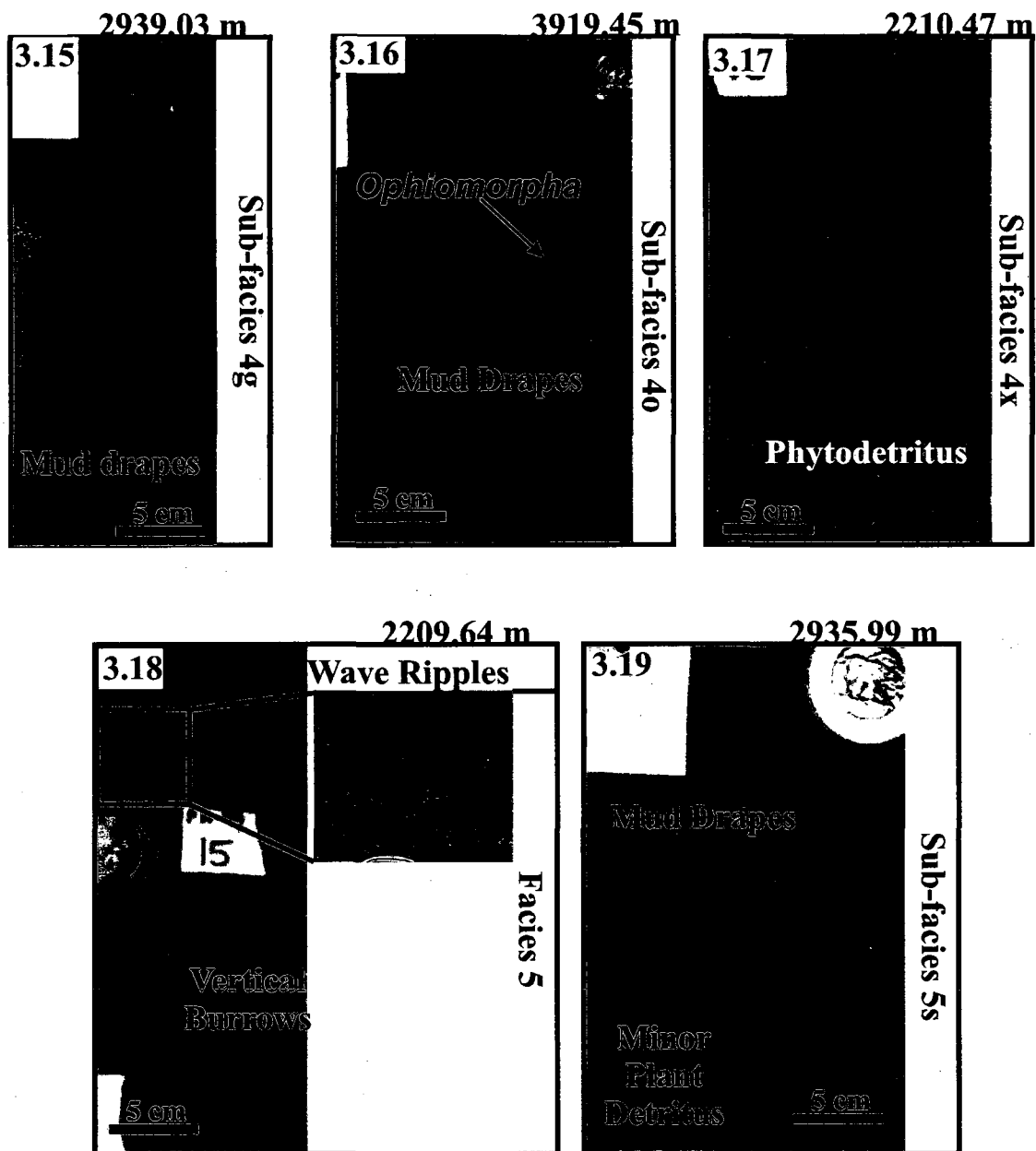
The presence of graded sandstone beds with abundant plant detritus in facies 9 has been interpreted by Gould *et al.* (2010) as evidence of delta front turbidites.



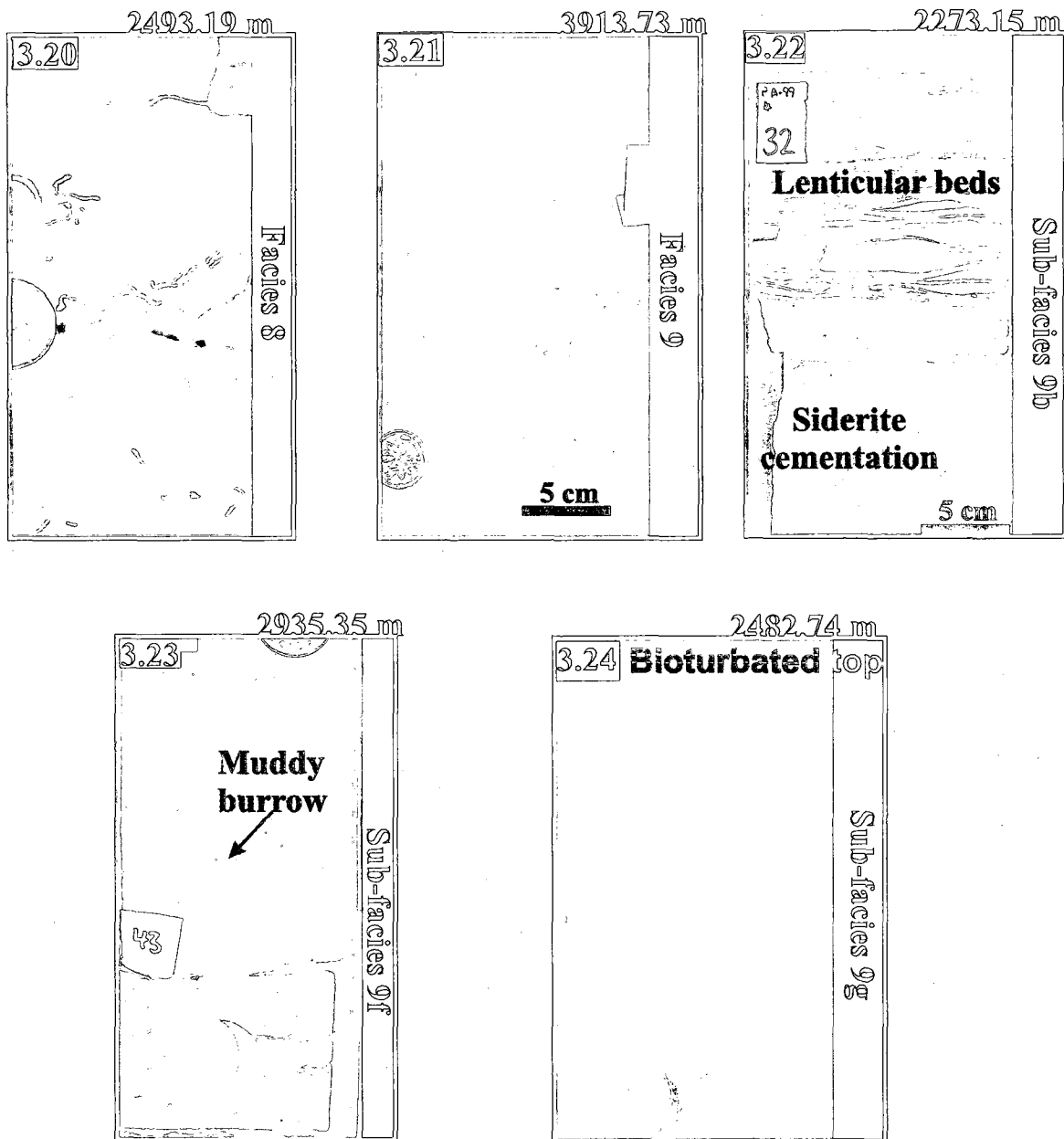
Figures: various core photographs from both studied wells with identified lithofacies. Peskowsk A-99. (3.2) 2220.41 m: Facies 0m with sharp-based siltstone beds with pervasive Chondrites bioturbation in predominantly mudstone. Thebaud C-74 (3.3) 3870.56 m: Facies 0s Showing the muddiest interval after transgression. (3.4) 2491.94 m: Facies 1 shale. (3.5) 3808.85 m: Facies 1c calcareous shale overlying bioclastic limestone. Peskowsk A-99. (3.6) 2272.28 m: facies 2b with interbedded fine-grained sandstone and silty mudstone with uncommon bioturbation at the base. (3.7) 2275.56 m: facies 2c showing bioturbated medium-Grained sandstone with siderite cementation and sparse shelly fragments.



Figures: various core photographs from both studied wells with identified lithofacies. Peskowsk A-99 (3.8) 2481.20 m: Facies 3a with large shelly fragments in commonly bioturbated fine-grained sandstone with mudstone laminae. Thebaud C-74. (3.9) 3902.55 m: Facies 3b with fine-grained sandstone with siderite intraclast and lithic granules and common bioturbation. Peskowsk A-99. (3.10) 2492.84 m: Facies 3c with siderite cemented coarse-grained sandstone with thick-shelled shelly fragments. (3.11) 3808.85 m: Facies 3l, bioclastic limestone underlying calcareous shale in facies 1c. (3.12) 3801.60 m: Facies 3m, thick mudstone beds with siderite cementation. (3.13) 3813.50 m: Facies 3o with oolitic limestone with fine-grained sandstone. (3.14) 3872.44 m: Facies 3s with rapidly alternating very coarse and fine-grained sandstone and siderite cementation.



Figures: various core photographs from both studied wells with identified lithofacies. Peskowsk A-99 (3.15) 2938.20 m: Facies 4g with slightly cross-bedded fine-grained sandstone with muddy burrows. Thebaud C-74.(3.16) 3919.45 m: Facies 4o showing fine-grained sandstone rich in Ophiomorpha, mud drapes, and rare horizontal burrows. Peskowsk A-99. (3.17) 2210.47 m: Facies 4x showing cross-bedded medium-grained sandstone with phytodetritus, lacking mudstone. (3.18) 2209.64 m: Facies 5 with fine-grained sandstone with common bioturbation interbedded with mudstone. (3.19) 2935.99 m: Facies 5s showing fine-grained sandstone with parallel lamination, mud drapes, and plant detritus.



Figures: various core photographs from both studied wells with identified lithofacies. Peskowsk A-99. (3.20) 2493.19 m: Facies 8 showing greenish bioturbated mudstone. Thebaud C-74. (3.21) 3913.73 m: Facies 9, massive coarse-grained sandstone. Peskowsk A-99. (3.22) 2273.15 m: Facies 9b showing fine-grained sandstone with lenticular beds and siderite cementation. (3.23) 2935.35 m: Facies 9f showing graded sandstone units with muddy burrows and mud drapes. (3.24) 2482.74 m: Facies 9g showing fine-grained sandstone with thin wood fragments and bioturbated top bed.

3.4 DESCRIPTION OF CORE INTERVALS

3.4.1 Peskowsk A-99

Core 7: Mic Mac Formation from 3791 m to 3814 m and a 21.91 m total recovery

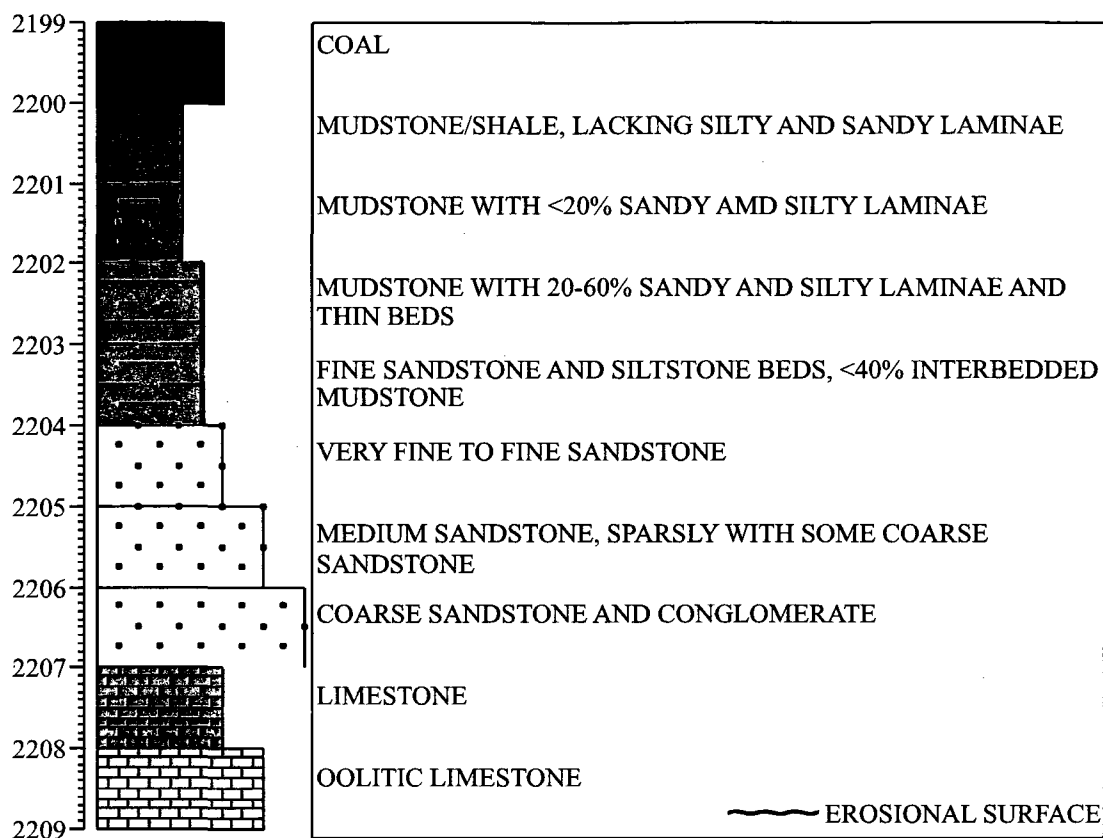
3812.05 m to 3813.91 m: the sediment is made up of a sandy limestone unit that is interpreted as sub-facies 3o. 3805.40 m to 3812.05 m: these sediments comprise bioclastic limestone (sub-facies 3l) interbedded with bioturbated mudstone (facies 1) and calcareous shales (sub-facies 1c). Core stratigraphy and interpreted diagenetic and other features are shown on the following pages.

3800.71 m to 3805.40 m: these sediments comprise a mudstone unit with parallel laminations and beds of siltstone and sharp based very fine-grained sandstone; but from 3802.50 m to 3805.40 m siderite cementation is present approximately every two metres.

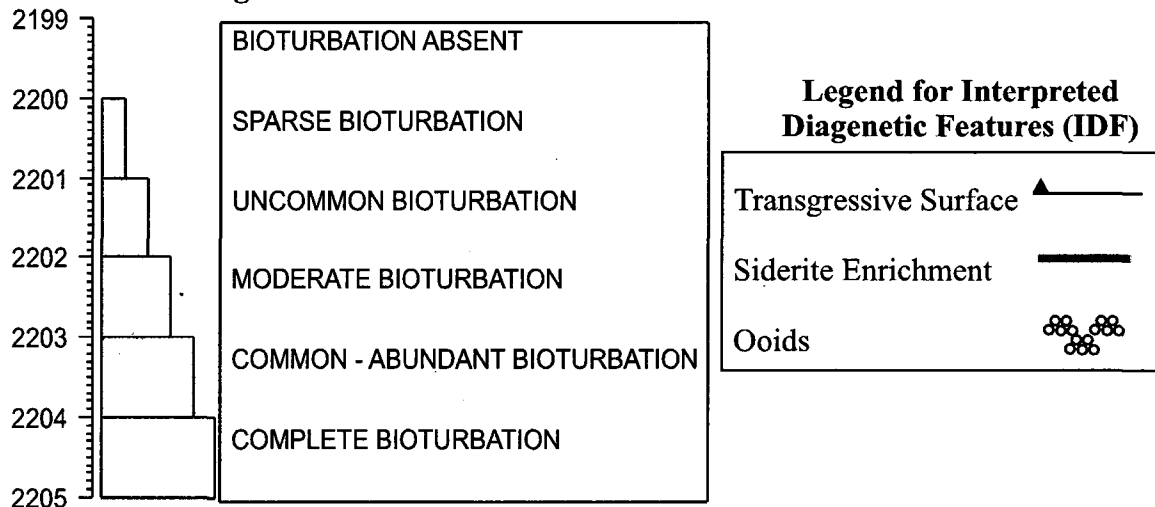
This unit is interpreted as sub-facies 0s on the basis of uncommon bioturbation and sharp based sandstone beds. From 3801.60 m to 3802.50 m, the sediment comprises siderite-cemented mudstone with fine-grained sandstone intraclasts, and well preserved shelly fragments. This unit is interpreted as facies 3; more specifically, it is interpreted as sub-facies 3m on the basis of predominantly mud matrix (Fig. 3.33).

The sub-facies 3m underlie a mudstone unit with < 1 mm siltstone laminae from 3800.71 m to 3801.60m. This unit is interpreted as facies 0m.

Stratigraphy Legend



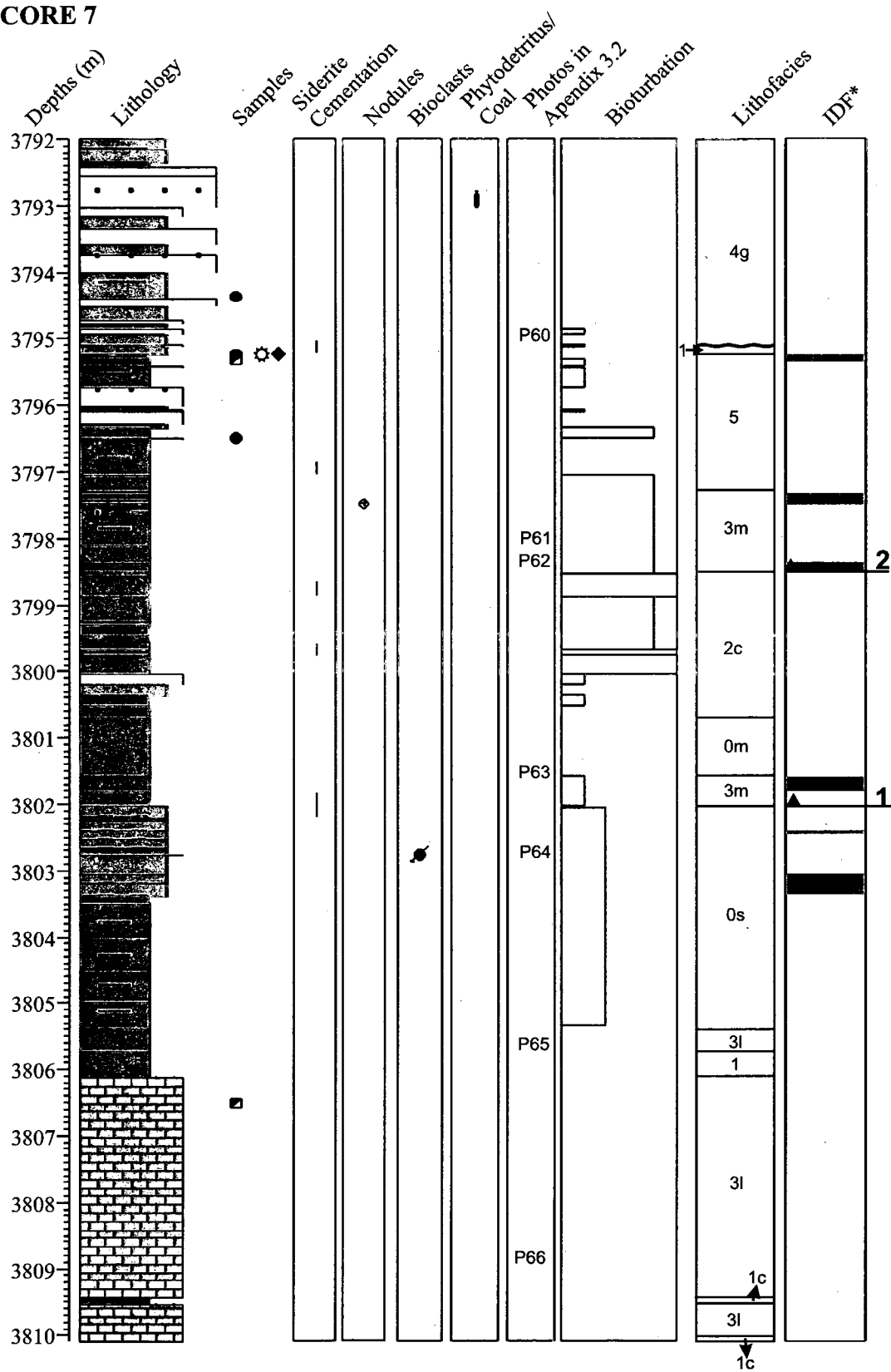
Bioturbation Legend



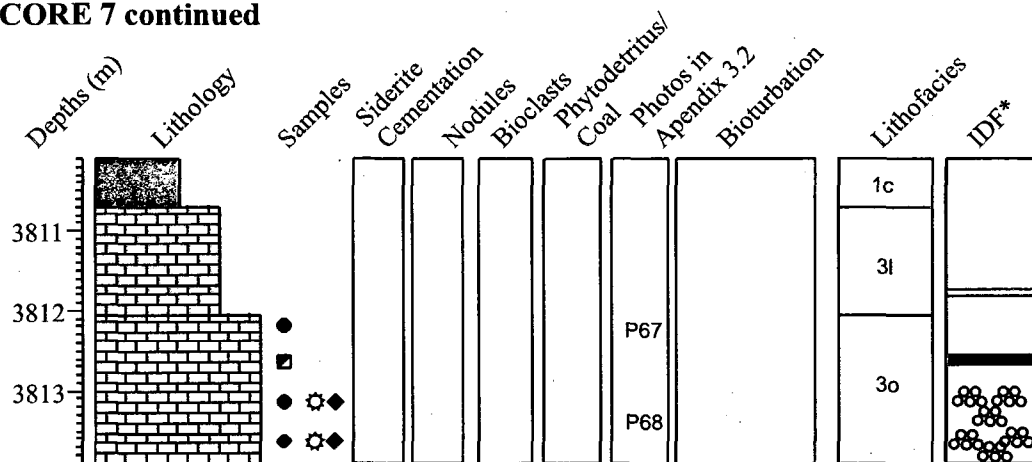
- Old Samples (samples already collected for other projects)
- New Samples (samples collected for the purpose of this thesis)
- ⊗ Samples used for Electron Microprobe Analysis
- ◆ Thin Section Samples

Figure 3.25: Legend for interpreted core stratigraphy, extent of bioturbation (after MacEachern et al., 2005) and other interpreted diagenetic features.

CORE 7



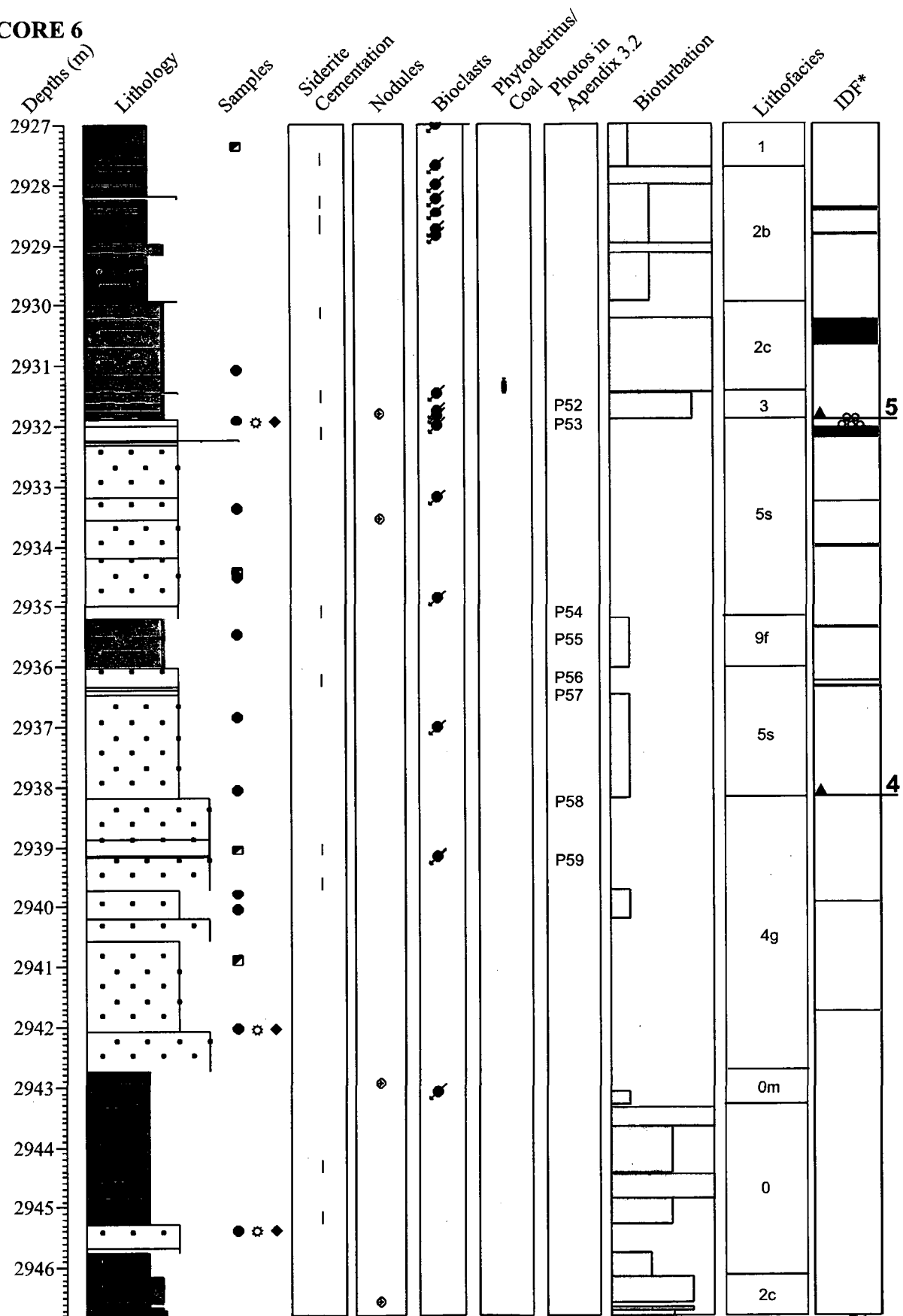
CORE 7 continued



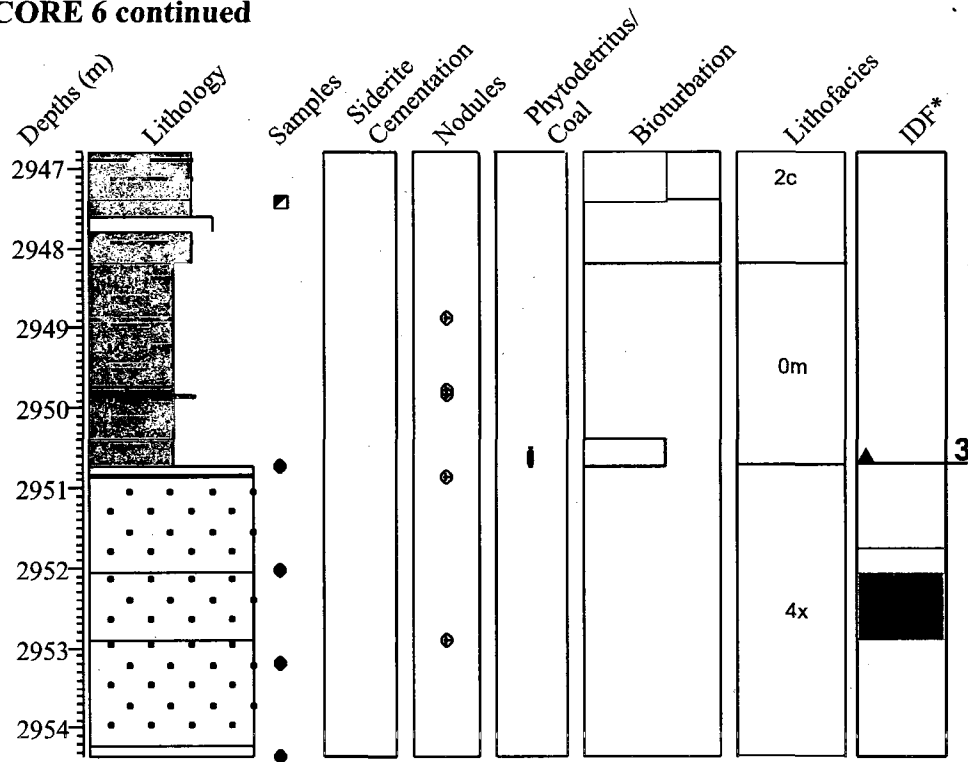
- Old Samples (samples already collected for other projects)
- New Samples (samples collected for the purpose of this thesis)
- ⚙ Samples used for Electron Microprobe Analysis
- ♦ Thin Section Samples

Figure 3.26: Core 7 at Peskowsk A-99. Detailed core stratigraphy with sample and appendix photo location with interpreted diagenetic features and lithofacies including additional interpretation like the presence of bioclasts, nodules, phytodetritus and bioturbation. IDF means interpreted diagenetic features.

CORE 6



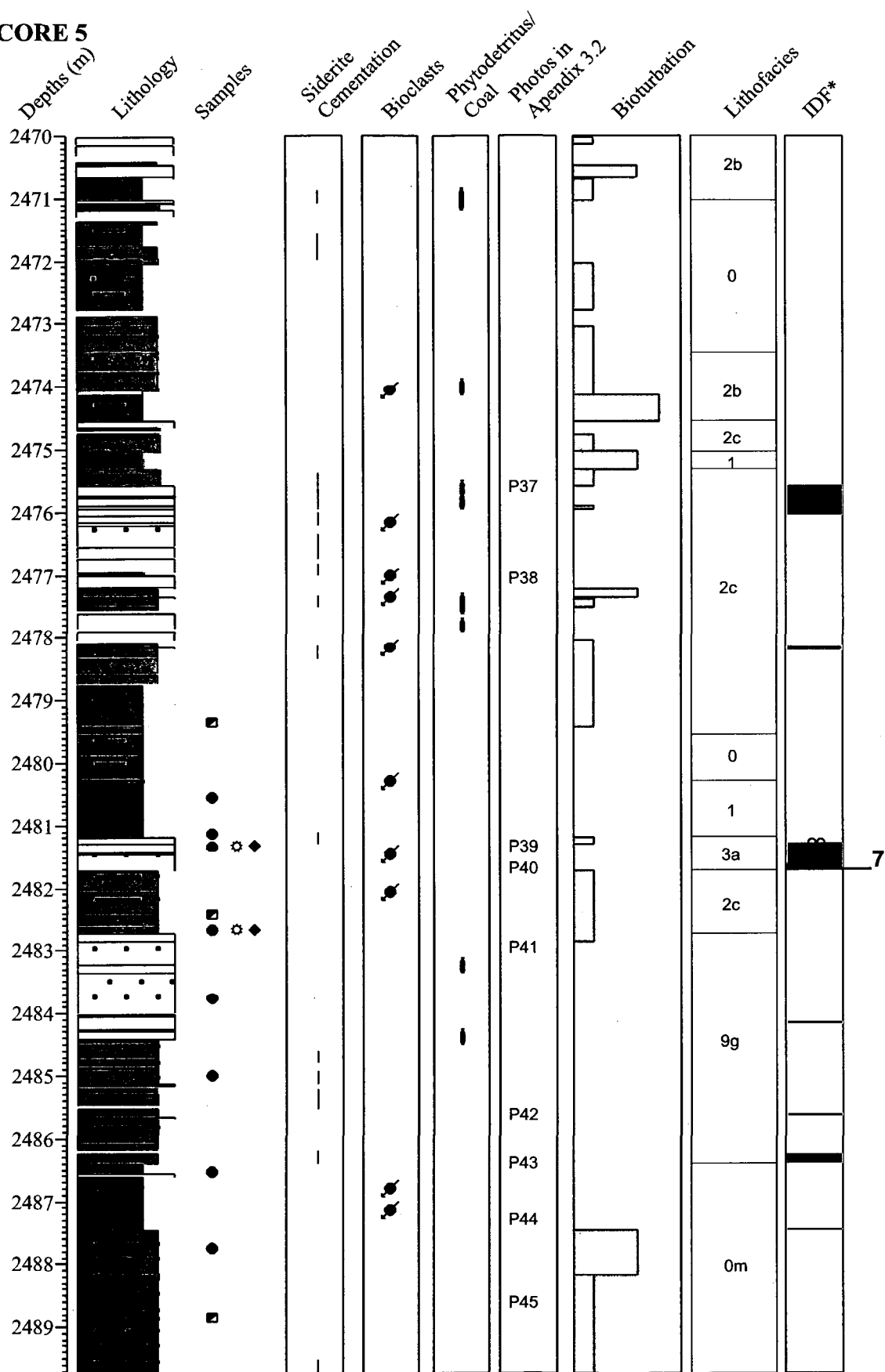
CORE 6 continued



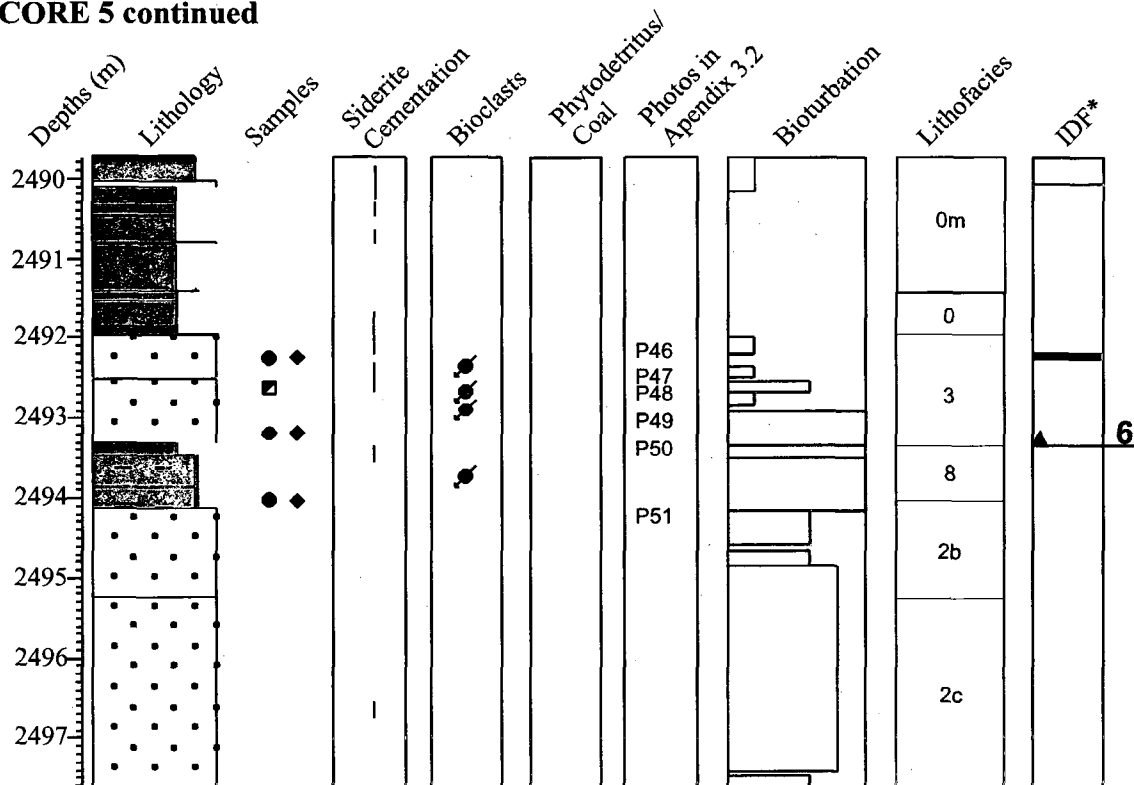
- Old Samples (samples already collected for other projects)
- New Samples (samples collected for the purpose of this thesis)
- ⊗ Samples used for Electron Microprobe Analysis
- ◆ Thin Section Samples

Figure 3.27: Core 6 at Peskowesk A-99. Detailed core stratigraphy with sample and appendix photo location with interpreted diagenetic features and lithofacies including additional interpretation like the presence of bioclasts, nodules, phytodetritus and bioturbation. IDF means interpreted diagenetic features.

CORE 5



CORE 5 continued



Rapid deposition of sst at this base

- Old Samples (samples already collected for other projects)
- New Samples (samples collected for the purpose of this thesis)
- ⊗ Samples used for Electron Microprobe Analysis
- ◆ Thin Section Samples

Figure 3.28: Core 5 at Peskowsk A-99. Detailed core stratigraphy with sample and appendix photo location with interpreted diagenetic features and lithofacies including additional interpretation like the presence of bioclasts, phytodetritus and bioturbation. IDF means interpreted diagenetic features.

CORE 4

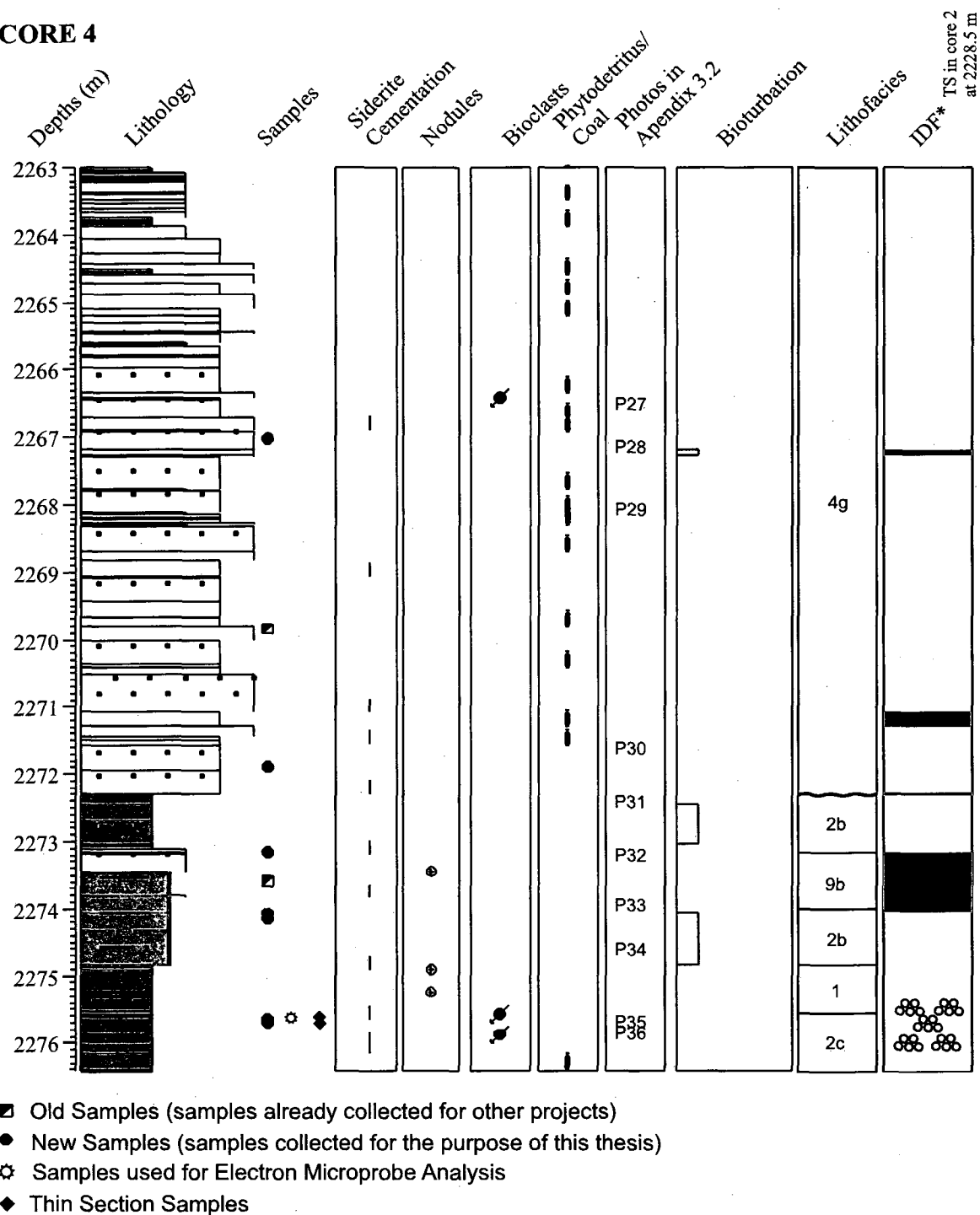
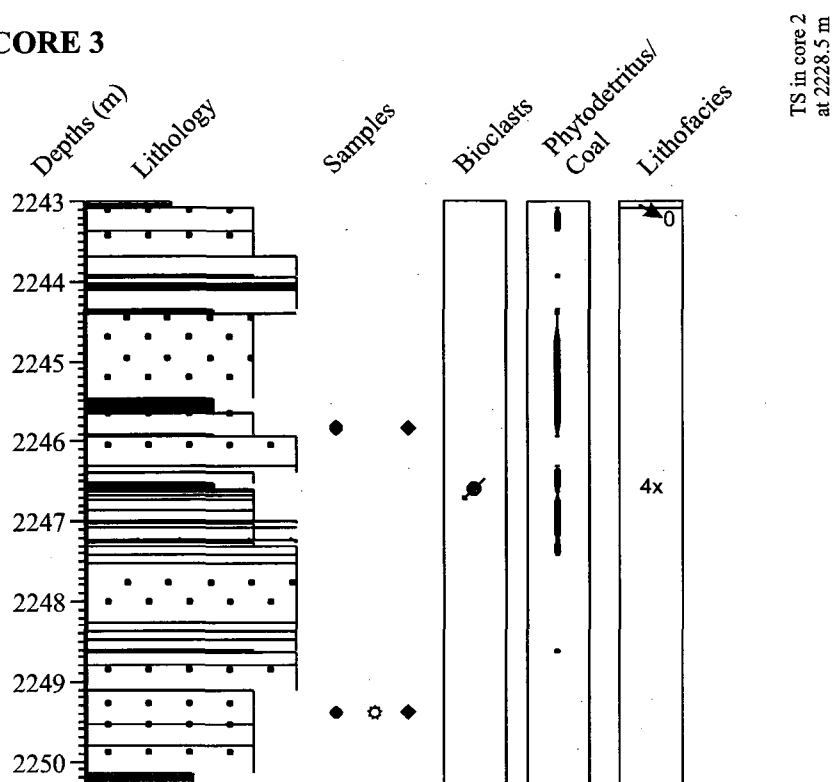


Figure 3.29: Core 4 at Peskowsk A-99. Detailed core stratigraphy with sample and appendix photo location with interpreted diagenetic features and lithofacies including additional interpretation like the presence of bioclasts, nodules, phytodetritus and bioturbation. IDF means interpreted diagenetic features.

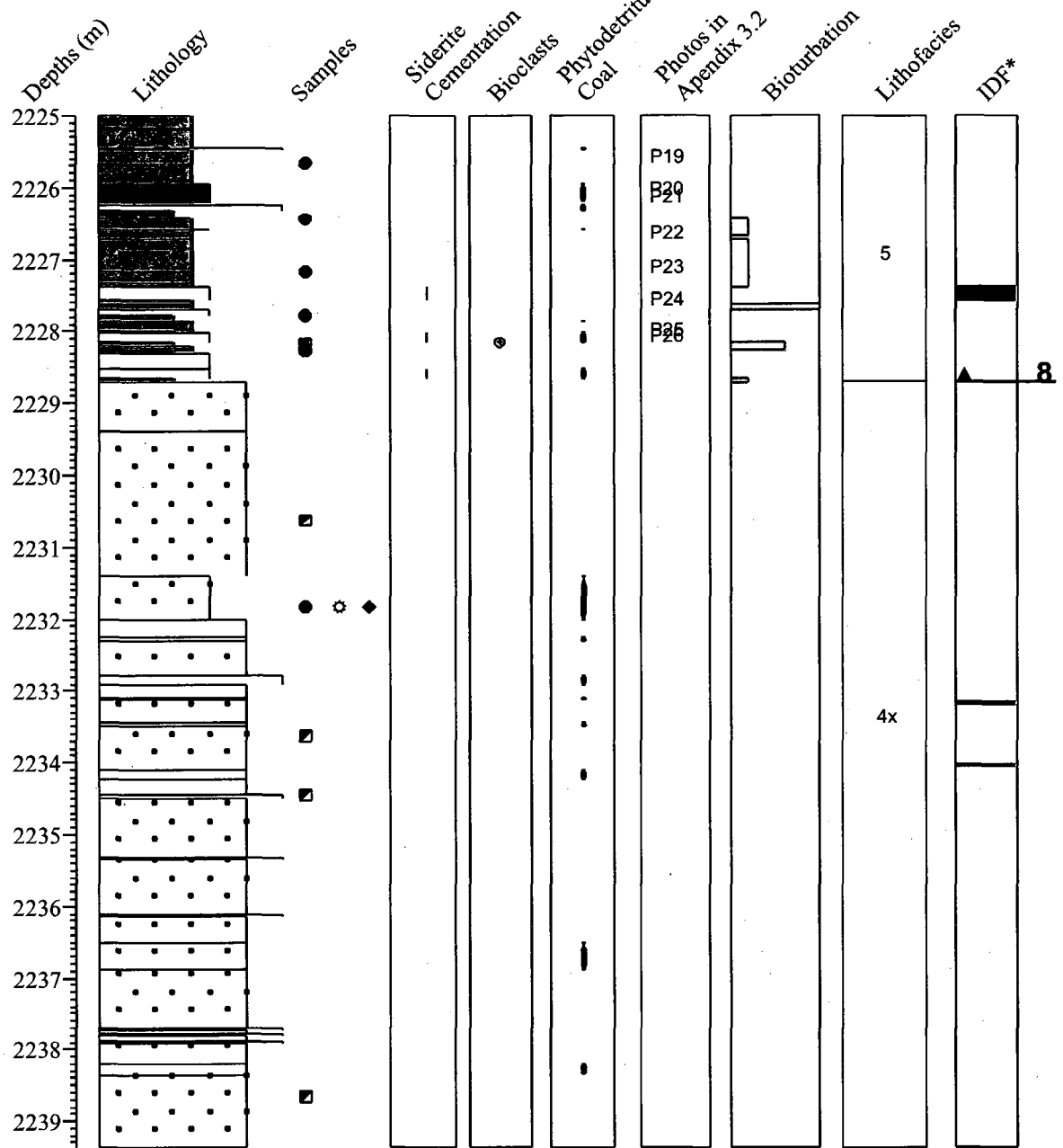
CORE 3



- Old Samples (samples already collected for other projects)
- New Samples (samples collected for the purpose of this thesis)
- ✱ Samples used for Electron Microprobe Analysis
- ◆ Thin Section Samples

Figure 3.30: Core 3 at Peskowsk A-99. Detailed core stratigraphy with sample location and lithofacies including additional interpretation like the presence of bioclasts, and phytodetritus. IDF means interpreted diagenetic features.

CORE 2



- Old Samples (samples already collected for other projects)
- New Samples (samples collected for the purpose of this thesis)
- ⚙ Samples used for Electron Microprobe Analysis
- ◆ Thin Section Samples

Figure 3.31: Core 2 at Peskowesk A-99. Detailed core stratigraphy with sample and appendix photo location with interpreted diagenetic features and lithofacies including additional interpretation like the presence of bioclasts, phytodetritus and bioturbation. IDF means interpreted diagenetic features.

CORE 1

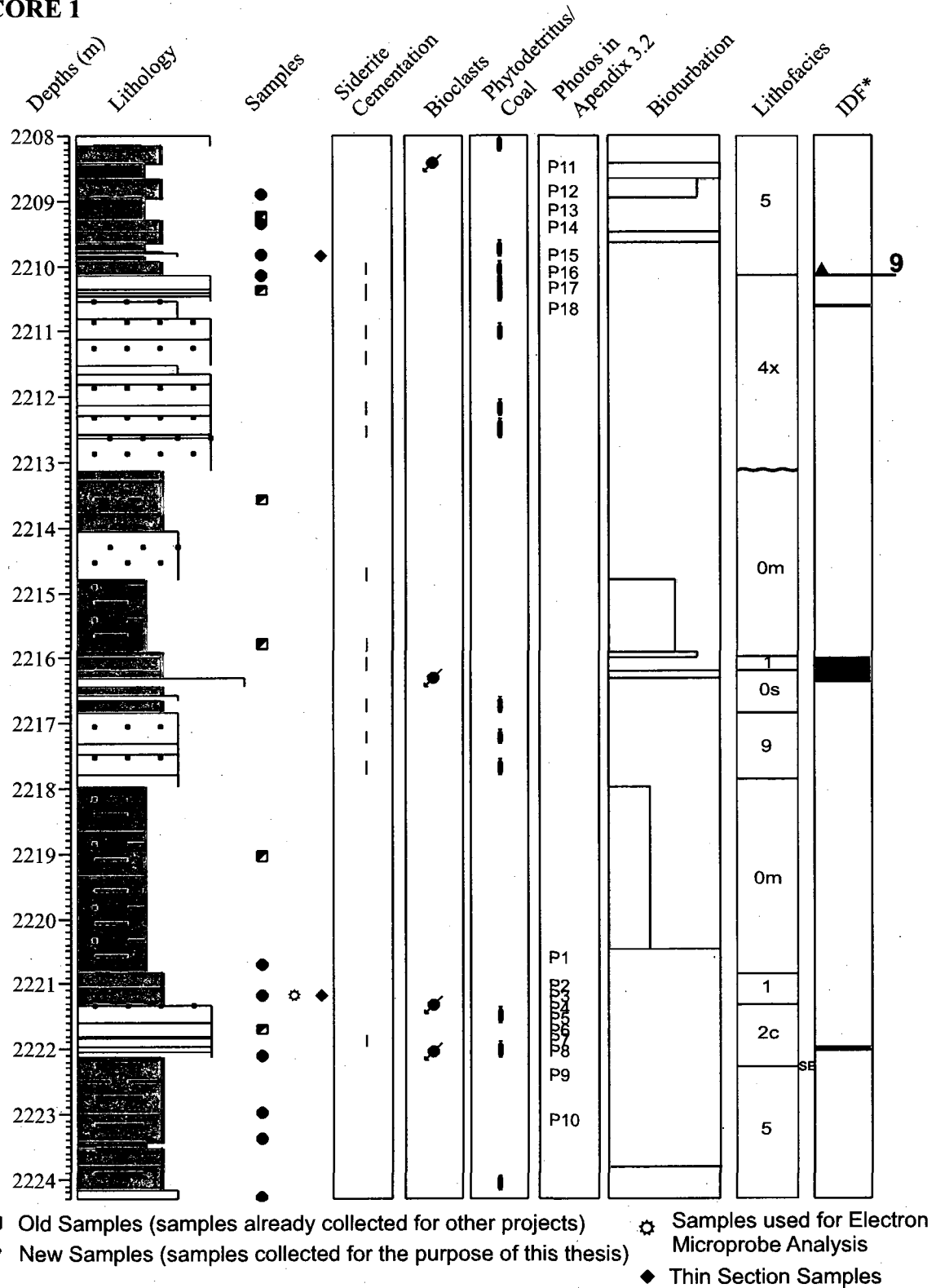


Figure 3.32: Core 1 at Peskowsk A-99. Detailed core stratigraphy with sample and appendix photo location with interpreted diagenetic features and lithofacies including additional interpretation like the presence of bioclasts, phytodetritus and bioturbation. IDF means interpreted diagenetic features.

The sediments from 3798.80 m to 3800.71 m comprise interbedded fine-grained sandstone and mudstone with common to abundant bioturbation. This unit is interpreted as sub-facies 2c on the basis of > 60% sandstone and abundant bioturbation. From 3797.28 m to 3798.80 m is a unit of siderite-cemented fine-grained sandstone with interbedded mudstone. Because it is similar to the sub-facies 3m 3802.50 m, it is also interpreted as sub-facies 3m on the basis of abundant bioturbation and the lack of thick (> 1 cm) sand beds (Fig 3.34).

From 3795.42 m to 3797.28 m sediments comprise fine-grained sandstone with mud drapes, vertical burrows, and climbing ripples. This unit is interpreted as facies 5, a sandy tidal flat deposit on the basis of the presence of mud drapes and vertical burrows.

Overlying this facies 5 is a mudstone unit from 3795.24 m to 3795.42 m with some siderite cementation. This unit is interpreted as facies 1.

3792.00 m to 3795.24 m: these sediments comprise fine to medium grained sandstone. This ~ 3 metres thick bed of sediments has mud drapes, plant detritus and distinct cross and parallel laminations and bedding in sets not thicker than 15 cm. This unit is interpreted as sub-facies 4g. At the bottom of this unit is an unconformity that suggests that the deposition of this estuarine sediment is unrelated to the underlying sediment.

Core 6: Upper member in the Mississauga Formation from 2927 m to 2956 m, and a 27.36 m total recovery

The sediments from 2950.72 m to 2954.10 m comprise massive beige, medium grained sandstone (~ 4m), with rare plant detritus, rare siderite patches, sparsely distributed siderite nodules, and cross bedding in sets < 10 cm thickness. This unit has a few mud laminae and a fining upward sequence with medium to coarse grains at the bottom and fine to medium grained sandstones towards the top. This unit is interpreted as sub-facies 4x.

2948.18 m to 2950.72 m: these sediments comprise an intercalated dark brown to black mudstone and light beige (in places grey) very fine-grained sandstone, with localized moderate bioturbation. This unit is interpreted as sub-facies 0m on the basis of the predominance of mudstones. The sediments from 2946.16 m to 2948.18 m comprise a light grey, very fine-grained sandstone unit with thin laminae of mudstone. This unit has moderate to common bioturbation, some greenish sandstone and more ovoid shaped nodules as in the above facies 0m. Bioturbation increases with depth (sandstone > mudstones). This unit is interpreted as sub-facies 2c

2943.67 m to 2946.16 m: the sediments in this unit comprise intercalated black mudstone and light grey siltstone to very fine-grained sandstone, with wavy lamination, through cross lamination in sandy beds, abundant silt laminae and localized moderate bioturbation. This unit is interpreted as facies 0, on the basis of cross lamination and abundant siltstone laminae. Overlying this facies 0 unit is a unit predominantly of

sparsely bioturbated mudstone, with rare siltstone beds, from 2942.74 m to 2943.67 m.

This unit has siderite as nodules (few cm in diameter) or as diffuse patches of brown staining. It also contains shell fragments. This unit is interpreted as sub-facies 0m.

2938.20 m to 2942.72 m: these sediments comprise a graded sandstone unit. The sandstone is mostly fine to medium grained, with some coarse-grained sandstone. Beds are typically 2-20 cm thick and show uncommon to moderate bioturbation. Individual beds have parallel or cross lamination (faint in places), mud drapes, shelly fragments and some siderite cementation (Fig. 3.35). This is interpreted as sub-facies 4g on the basis of mud drapes and cross laminations. Overlying this sub-facies 4g is a beige fine grained sandstone unit from 2936.03 m to 2938.20 m, with medium to coarse grained sandstone beds (~ 5 cm thick), some mudstone beds, uncommon bioturbation and localized siderite cements. This is interpreted as sub-facies 5s on the basis of the bioturbated fine-grained sandstone with muddy beds, and the presence of sparse shell fragments not visible in Fig. 3.36.

2935.19 m to 2936.03 m: these sediments comprise very fine-grained thick-bedded sandstones with mud drapes and uncommon bioturbation. This is interpreted as facies 9, specifically sub-facies 9g due to the lack of mudstone beds. The sediments from 2931.89 m to 2935.19 m comprise a massive light grey to beige, fine grained sandstone unit with sparse siderite cemented coarse grained sandstone (sometimes medium to coarse-grained), some shelly fragments dispersed through the unit, and very rare carbonate nodules. Figure 3.37 shows the diagenetic contact between the grey and beige sandstone.

This unit is interpreted as facies 5. Overlying this facies 5 unit is an abundantly bioturbated mudstone and fine grained sandstone unit from 2931.46 m to 2931.89 m, with very patchy siderite cementation (Fig. 3.38). This unit is interpreted as facies 3.

Overlying this facies 3 unit is a common to abundantly bioturbated mudstone unit from 2929.95 m to 2931.46 m, with >60% interbedded sandstone (Fig. 3.38). The unit has sparse shelly fragments, localized siderite cementation and rare plant detritus in brown stained sandstone. This unit is interpreted as sub-facies 2c.

2927.72 m to 2929.95 m: these sediments comprise interbedded black mudstone and light grey siltstone to very fine grained sandstone with sparse to common bioturbation. The unit has rare shelly fragments and sparse siderite cements. This unit is interpreted as sub-facies 2b (on the basis of few sand beds). This sub-facies 2b passes up into a unit of black mudstone from 2927.00 m to 2927.72 m, with sparse bioturbation (intensity increases with depth) and some siderite cementation. This unit is interpreted as facies 1.

Core 5: Upper member in the Mississauga Formation from 2470 m to 2498 m, and a 27.64 m total recovery

2495.27 m to 2497.64 m: these sediments comprise interbedded fine-grained sandstone (beds up to 5 cm and greater than 60%) and mudstone with common bioturbation. This unit is interpreted as sub-facies 2c. Overlying this unit is a silty mudstone unit from 2494.15 m to 2495.27 m with thick siltstone to very fine-grained sandstone beds (≥ 5 cm), but with an overall lesser amount of sands throughout the unit. This unit is interpreted as sub-facies 2b (on the basis of few sand beds).

The sediments from 2493.50 m to 2494.15 m comprise a greenish mudstone unit with some siltstone laminae and fine-grained sandstone with common bioturbation. This unit has a large siderite intraclast at the top and localized shelly fragments. The siltstone composition increases in the basal 10 cm of the unit, and occurs with greenish patches (Fig. 3.39). This unit is interpreted as sub-facies 3a on the basis of the sandstone matrix, and mud laminae. Overlying this sub-facies 3a unit is a thin black shale unit from 2493.33 m to 2493.50 m interpreted as facies 1.

Overlying this facies 1 unit is a fine-grained sandstone unit from 2491.98 m to 2493.33 m, with shelly fragments and siderite cementation and the presence of common bioturbation in the interbedded mudstone (Figs. 3.40 to 3.43). This unit is interpreted as facies 3.

From 2486.40 m to 2491.98, sediments in this unit consist predominantly of mudstone interbedded with thick (> 5 cm) sandstone beds, some of which are siderite cemented. The unit has ~ 40% siltstone laminae, some cross lamination (sets < 1 cm) in siltstone, rare shelly fragments and sparse bioturbation. This unit is interpreted as sub-facies 0m. At the base of this unit, there is black shale a few cm thick (as in Fig. 3.40) interpreted as facies 1.

Overlying this facies 0m unit is a thick (~4.5 m), uncommonly bioturbated sandstone unit from 2482.72 m to 2486.40 m with parallel laminations passing up into cross laminations in undivided sandstone beds. Generally, sandstone beds in this unit have a sharp base, however erosional bases are common. From 2484.42 to the base of the unit, the

sandstone beds are fine-grained with some plant detritus. From the top of the unit to 2484.42 m, the sandstone beds are finer grained, with mud laminae, more plant detritus, and some siderite cementation (Figs. 3.44 and 3.45). This unit is interpreted as facies 9 based on the abundance and thickness of sandstone beds, more specifically sub-facies 9g on the basis of the graded sandstone beds.

2481.71 m to 2482.72 m: these sediments comprise uncommonly bioturbated muddy sandstone with a few shelly fragments. This unit is interpreted as sub-facies 2c (> 60 % sandstone). From 2481.20 m to 2481.71 m, sediments are dark grey, very fine-grained sandstone with common bioturbation. This unit has siderite-cemented sandstone and shelly fragments (Fig. 3.46a) that increase in abundance with depth and thick shell fragments are the predominant component of the rock from 2481.48 m to 2481.71 m (Fig. 3.46b). This unit is interpreted as facies 3.

Overlying this facies 3 unit is a bioturbated mudstone unit with thin-shelled fossils from 2480.30 m to 2481.20 m. This unit is interpreted as facies 1. Overlying this facies 1 unit is a dark grey mudstone unit with siltstone laminations distributed through the unit from 2479.55 m to 2480.30 m. The unit shows about 50% of siltstone and very fine-grained sandstone, with parallel lamination at the base of the individual beds. This unit is interpreted as facies 0.

2475.32 m to 2479.55 m: these sediments comprise abundantly bioturbated very fine-grained sandstone with patchy siderite cementation that ranges in abundance from 40-

95% (Figs. 3.47, 3.48). The sandstone unit locally has sparse coaly fragments, and sparsely distributed shelly fragments, that become more abundant towards the base of the unit. Some of the shells are thick-shelled molluscs > 1 cm in size. Based on the abundance of bioclasts and fine-grained sandstone, this unit is interpreted as sub-facies 2c.

Overlying this sub-facies 2c unit is a silty mudstone unit with sparse to moderate bioturbation and mud laminae from 2475.03 m to 2475.32 m. The moderately bioturbated mud has 10% siltstone laminae. The unit is interpreted as facies 1. Sediments from 2474.56 m to 2475.03 m comprise fine-grained sandstone with a muddier base to the unit. This unit is interpreted as sub-facies 2c. From 2473.47 m to 2474.56 m, sediments comprise sparsely bioturbated mudstone with 40% siltstone laminae. This unit has concentrations of shelly fragments and sparsely distributed coaly fragments in bioturbated mudstone. This unit is interpreted as sub-facies 2b.

Overlying this sub-facies 2b unit is a thick (2.5 m) unit of mudstone with laminae and beds of siltstone and fine-grained sandstone from 2471.04 m to 2473.47 m. This unit has some siderite cemented siltstone laminae, with up to 5 cm thick siltstone laminae making up to 40% of the unit. This unit is interpreted as facies 0. This facies 0 passes up into a sparsely bioturbated, fine-grained sandstone unit from 2470.00 m to 2471.04 m. This unit has mudstone laminae with moderate bioturbation in places. This unit is interpreted as sub-facies 2b.

Core 4: Cree member in the Logan Canyon Formation from 2263 m to 2282 m, and a 13.5 m total recovery

2275.56 m to 2276.42 m: the sediments comprise greenish black and grey mudstone with bioturbated patchy sideritic medium-grained sandstone with some shelly fragments, and coaly fragments (~ 30%) in the top 3 cm of the unit (Fig. 3.49). The bioturbation is complete as the bedding structure has been completely disturbed. This unit is interpreted as sub-facies 2c on the basis of sandstone amount and bioturbation.

Overlying this sub-facies 2c unit is a mudstone unit with thin silt laminations and uncommon bioturbation, from 2274.82 m to 2275.56 m. This unit has a few nodules and the presence of siderite cement at 2275.23 m. This unit is interpreted as facies 1. The sediments from 2274.00 m to 2274.82 m comprise commonly bioturbated fine-grained sandstone and mudstone (Fig. 3.50). This is interpreted as sub-facies 2c on the basis of common bioturbation and the presence of >60% fine-grained sandstone.

From 2273.15 m to 2274.00 m, sediments comprise fine-grained sandstone with patches of siderite cements and nodules 1-2 mm thick. This unit is identified as facies 9 on the basis of thick (> 25 cm) bed of sandstone; specifically sub-facies 9b based on the presence of diffuse siderite cements and diagenetic siderite concretions in the sandstone with common bioturbation (Figs. 3.51 and 3.52). This development of sub-facies 9b resembles facies 3 when comparing two features; the abundance of bioturbation and the presence of siderite cement. However, it is sub-facies 9b due to the lack of mudstones.

Overlying this sub-facies 9b unit is a brownish black mudstone unit with thin siltstone laminae and sparse bioturbation from 2272.28 m to 2273.15 m. This unit contains large (2 cm) siderite clasts at the base of the sandstone bed at the top (Fig. 3.53), suggesting an erosional surface. Also present are siltstone nodules interbedded with mudstone and fine-grained sandstone. This unit is interpreted as sub-facies 2b on the basis of sparse bioturbation.

2263.00 m to 2272.28 m: sediments comprise a thick (> 25 cm) unit of medium-grained sandstone, with some fine and coarse-grained sandstone occurring in places. This unit has distinct plant detritus associated with rare siderite cementation, few lithic grains, sparse mudclasts in places and a 4 cm thick mudstone beds from 2267.18 m to 2267.27 (Fig. 3.54). This unit is interpreted as sub-facies 4g.

Cores 2 and 3: Cree members in the Logan Canyon Formation from 2225 m to 2263 m, and a 21.35 m total recovery

The facies 4 in core 4 continues into the whole of core 3, but as sub-facies 4x from 2243.00 m to 2250.34 m and from 2228.65 m to 2239.39 m in core 2, for a total of ~ 18 metres. Sediments from 2225.00 m to 2228.65 m comprise fine to medium grained sandstones, coarse-grained sandstones, drape-like laminated mudstone, and sparse bioturbation. From 2226.00 m to 2226.33 m there is thick bed of sandy coal interpreted as facies 5.

Core 1: Cree member in the Logan Canyon Formation from 2208 m to 2225 m, and a 15.8 m total recovery

The sediments from 2222.12 m to 2224.30 m comprise dark brown to black interbedded siltstone (in places very fine-grained sandstones) and mudstone with a few sandstone beds (a few mm to 2 cm). The majority of the siltstone has a greenish color. Thicker sandstone beds (~15cm) with cross lamination and plant detritus are more abundant closer to the base of the unit. This unit is interpreted as facies 5 on the basis of the burrow traces, and the presence of mud drapes (Fig. 3.55).

The sediments from 2221.34 to 2222.12 m comprise grey to beige medium-grained sandstone beds with patches of coarse-grained sandstone, showing moderate to complete bioturbation throughout the unit with medium to coarse-grained sandstone intercalated with dark grey mudstone from 2221.60 m and above. The unit contains coarse shelly fragments, rare to minor plant detritus and carbonate cemented sandstone clasts, and shows localized brown staining (Fig. 3.56). This unit is interpreted as sub-facies 2c on the basis of > 60% sandstones and the presence of shelly fragments.

2220.84 m to 2221.34 m: these sediments comprise interbedded thick dark, reddish-brown mudstone and minor light grey very fine grained sandstone with complete bioturbation, except for sparse bioturbation at the base of the unit. A few siderite concretions occur between 2220.90 and 2220.95 (Fig. 3.57) and siderite nodules are found at 2221.10 m, dispersed in the completely bioturbated sandstone. This unit has

been interpreted as facies 1 based on the amount of bioturbation in the mudstone, although shelly fossils appear to be absent.

Overlying this facies 1 is a very thick (4 metres) unit of mudstone with interbedded siltstone to very fine-grained sandstone in places, from 2217.97 m to 2220.84 m. The sandstone beds range from 1 mm to ~1 cm, with laminae <1 cm common throughout the unit. These beds have an erosional contact at the base with underlying mudstone. The unit has sparse bioturbation with mm-scale burrow traces in sandstone and some localized green colored sandstone. This unit is interpreted as sub-facies 0m. From 2216.83 to 2217.97, sediments comprise medium grained sandstone (1 m thick) with both cross and parallel laminations, minor plant detritus, and a few siderite intraclasts. This unit is interpreted as facies 9 on the basis of the sandstone bed thickness and sedimentary structures.

The sediments from 2216.19m to 2216.83 m comprise interbedded brown and greenish very fine-grained sandstone and light grey fine-grained sandstone, with brown to black mudstone making up about 15% of the unit. Parallel lamination occurs at a mm-scale, with some cross laminated sets ~1 cm thick and uncommon bioturbation in the top 3 cm of sharp-based sandstone beds. From 2216.53 m, the cross lamination occurs throughout sandstone beds and plant detritus occurs in some sandstone laminae. Bioturbation becomes moderate within the topmost 5 cm of this bed (at 2216.53 m). This unit is interpreted as sub-facies 0s on the basis of sedimentary structures in sandstone beds, the presence of plant detritus and uncommon bioturbation.

2216.10 m to 2216.19 m: these sediments comprise thin black shale lacking any siltstone laminae, interpreted as facies 1, and are overlain by a unit (2213.12 m to 2216.10 m) predominantly of mudstone, with siltstone and very fine- to fine-grained sandstone beds and laminae. This upper unit has minor siderite cementation (either as nodules or in some cases a more diffuse brown staining), some bioclasts and moderate bioturbation.

Generally, the sandstone beds are a few cm thick and they increase upwards from 5% at the base to approximately 15% near the top. Many sandstone beds have an erosional base and have both parallel and cross lamination. This unit is interpreted as sub-facies 0m, on the basis of sandstone bed character and moderate bioturbation.

From 2210.15 m to 2213.12 m is a 3-metre thick unit of medium grained sandstone with a sharp base. The unit varies from grey to beige sandstone with distinct cross bedding in sets <35 cm thick, with localized concentration of plant detritus commonly associated with siderite intraclasts <1 mm (Fig. 3.58). This unit is interpreted as sub-facies 4x, on the basis of large scale cross bedding and lack of bioturbation.

2208.00 m to 2210.15 m: the sediments in this unit are commonly bioturbated and these sediments comprise interbedded dark grey mudstone and laminated fine-grained sandstone with a coarse-grained sandstone bed present. Several coaly laminae are interbedded with mudstone (Figs. 3.59a and 3.59b). The sandstone ranges from fine-grained to medium grained (with rare coarse grained beds). This unit is interpreted as facies 5 on the basis of similarities to tidal flat facies of Cummings and Arnott (2005).

3.4.2 Thebaud C-74

Core 6: Lower member in the Missisauga Formation from 3909.67 m to 3926.83 m, and a 17.16 m total recovery

3925.40 m to 3927.28 m; these sediments comprise a massive fine sandstone unit interbedded with abundantly bioturbated silty mudstone bedsets (~ 2 cm). The unit shows minor amounts of plant detritus, sandstone nodules and siderite cement. This unit is interpreted as sub-facies 2b (< 60% sandstone) on the basis of sandstone character and abundant bioturbation. Core stratigraphy and interpreted diagenetic and other features are shown on the following pages.

From 3920 m to 3925.40 m, the sediments are predominantly fine-medium grained sandstone in a fining upwards succession with localized siderite cementation at the bottom and rare horizontal burrows sparsely distributed throughout the unit. This unit is interpreted as facies 9 based on the lack of interbedded mudstone in > 25 cm thick sandstone beds (Fig. 3.60).

Overlying this facies 9 unit is another sandy unit with more mudstone intervals from 3918.60 m to 3920.20 m. These sediments comprise fine-grained sandstone with mudstone and some parallel laminations. This unit is interpreted as sub-facies 4o, based in abundance of *Ophiomorpha*, presence of mud drapes and rare horizontal burrows (Fig. 3.61).

Core 6

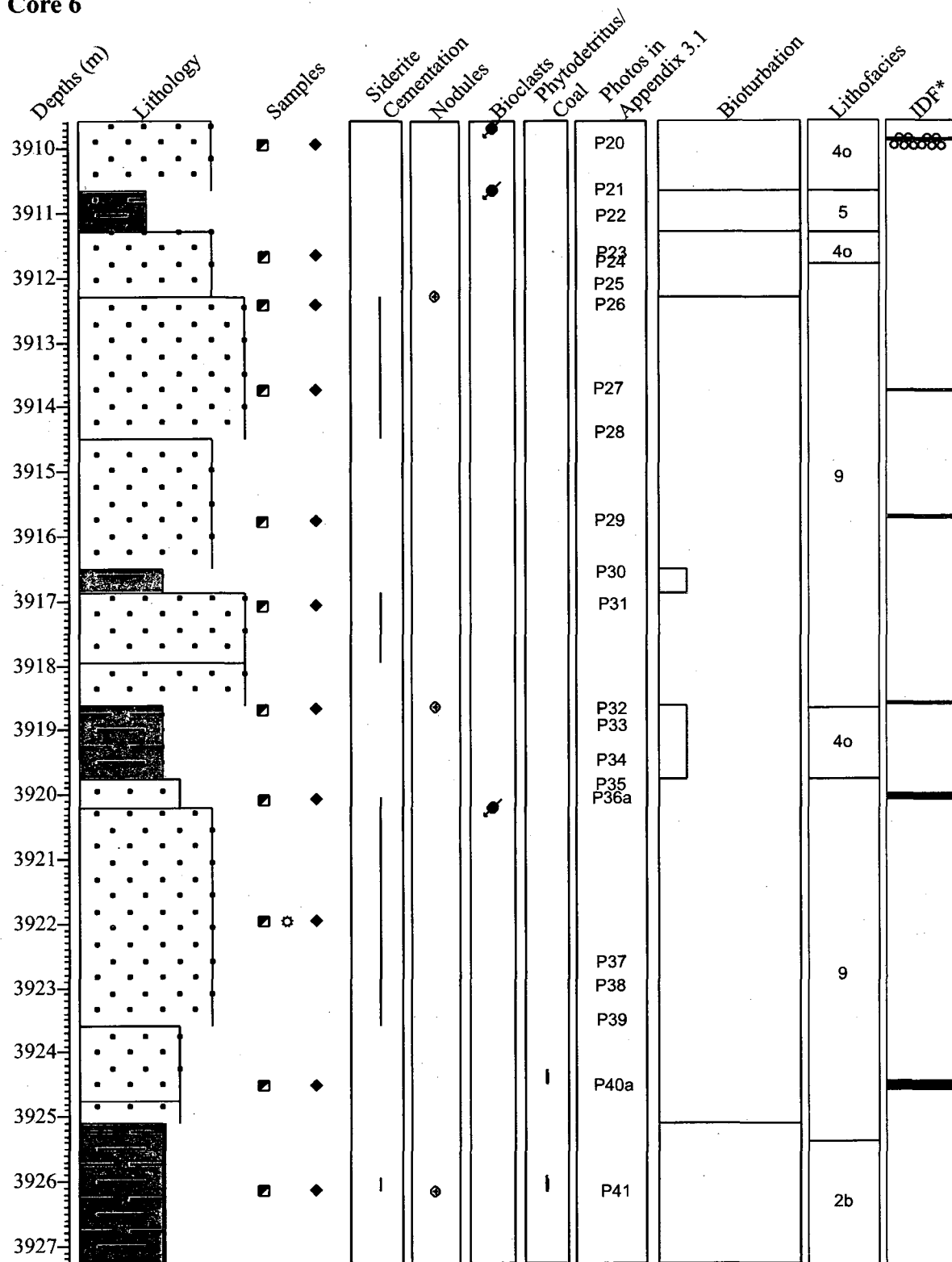
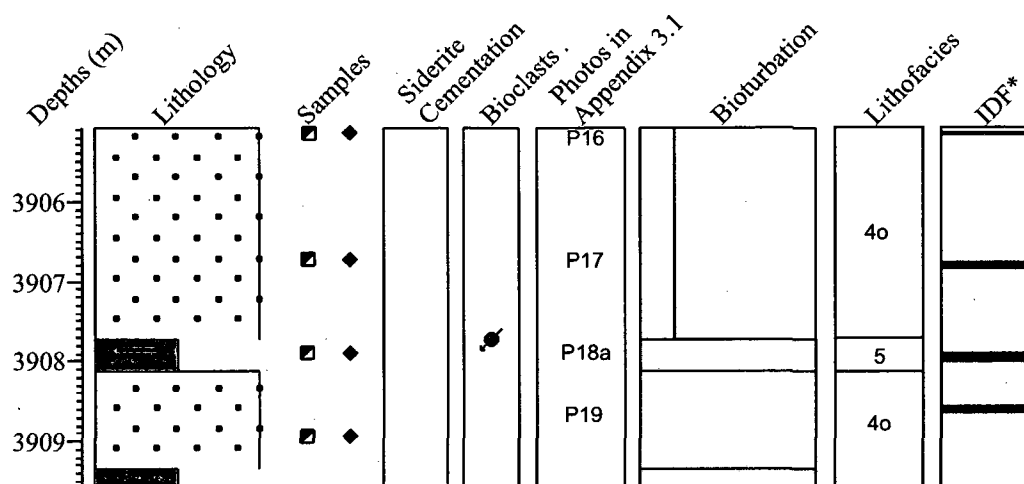


Figure 3.62: Core 6 at Thebaud C-74. Detailed core stratigraphy with sample and appendix photo location with interpreted diagenetic features and lithofacies including additional interpretation like the presence of bioclasts, nodules, phytodetritus and bioturbation. IDF means interpreted diagenetic features.

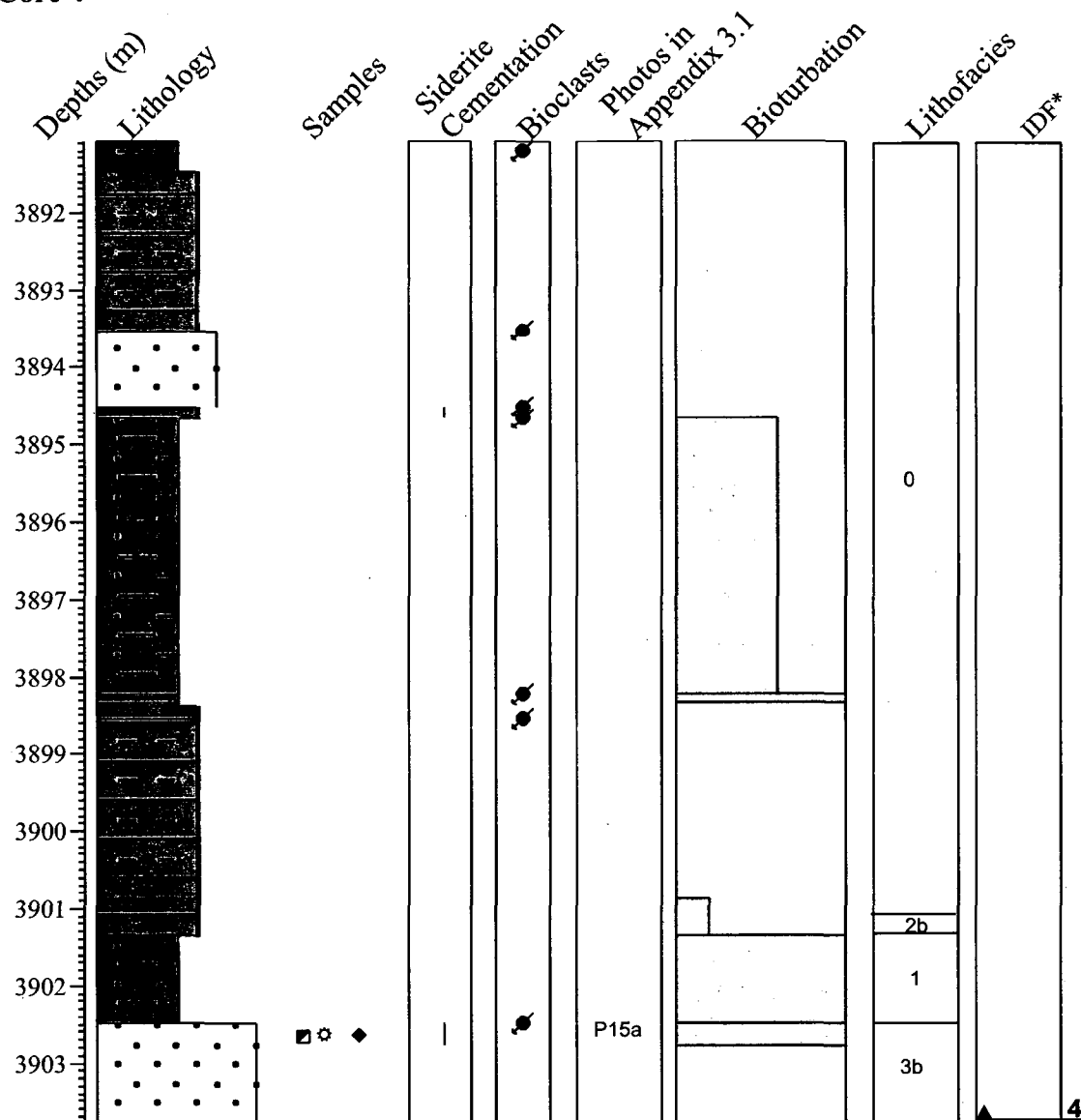
Core 5



- Old Samples (samples already collected for other projects)
- ◆ New Samples (samples collected for the purpose of this thesis)
- ⚙ Samples used for Electron Microprobe Analysis
- ◆ Thin Section Samples

Figure 3.63: Core 5 at Thebaud C-74. Detailed core stratigraphy with sample and appendix photo location with interpreted diagenetic features and lithofacies including additional interpretation like the presence of bioclasts, phytodetritus and bioturbation. IDF means interpreted diagenetic features.

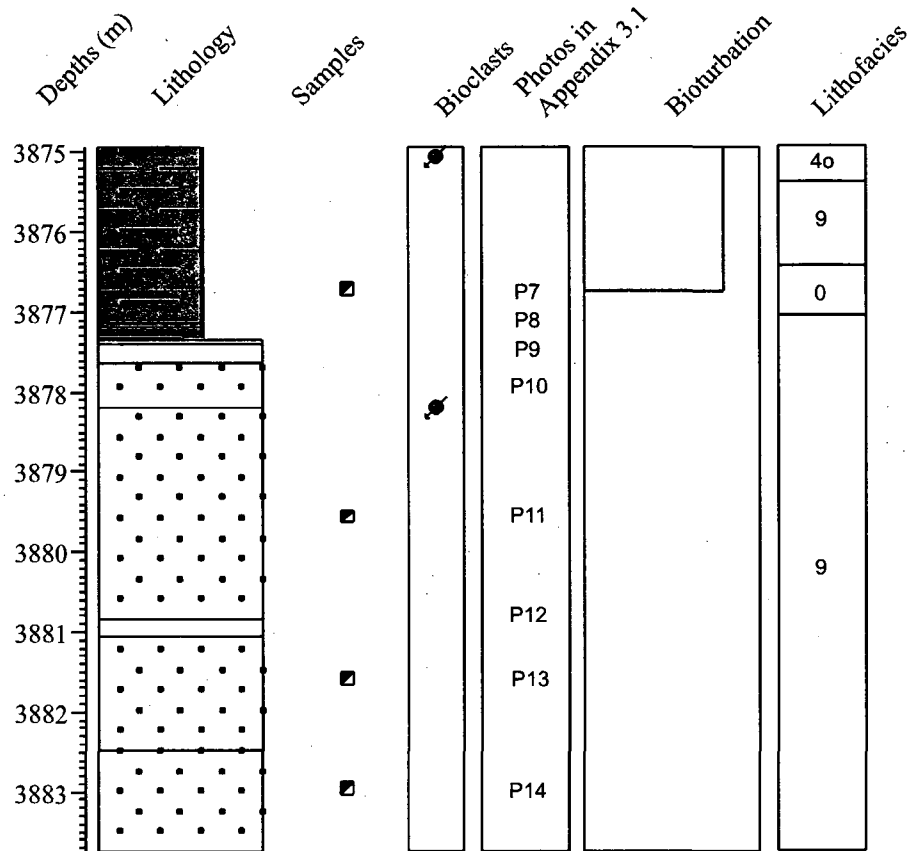
Core 4



- Old Samples (samples already collected for other projects)
- New Samples (samples collected for the purpose of this thesis)
- ⊛ Samples used for Electron Microprobe Analysis
- ◆ Thin Section Samples

Figure 3.64: Core 4 at Thebaud C-74. Detailed core stratigraphy with sample and appendix photo location with interpreted diagenetic features and lithofacies including additional interpretation like the presence of bioclots, phytodetritus and bioturbation. IDF means interpreted diagenetic features.

Core 2



- ☑ Old Samples (samples already collected for other projects)
- New Samples (samples collected for the purpose of this thesis)
- ⚙ Samples used for Electron Microprobe Analysis
- ◆ Thin Section Samples

Figure 3.65: Core 2 at Thebaud C-74. Detailed core stratigraphy with sample and appendix photo location lithofacies including additional interpretation like the presence of bioclasts, and bioturbation. IDF means interpreted diagenetic features.

Core 1

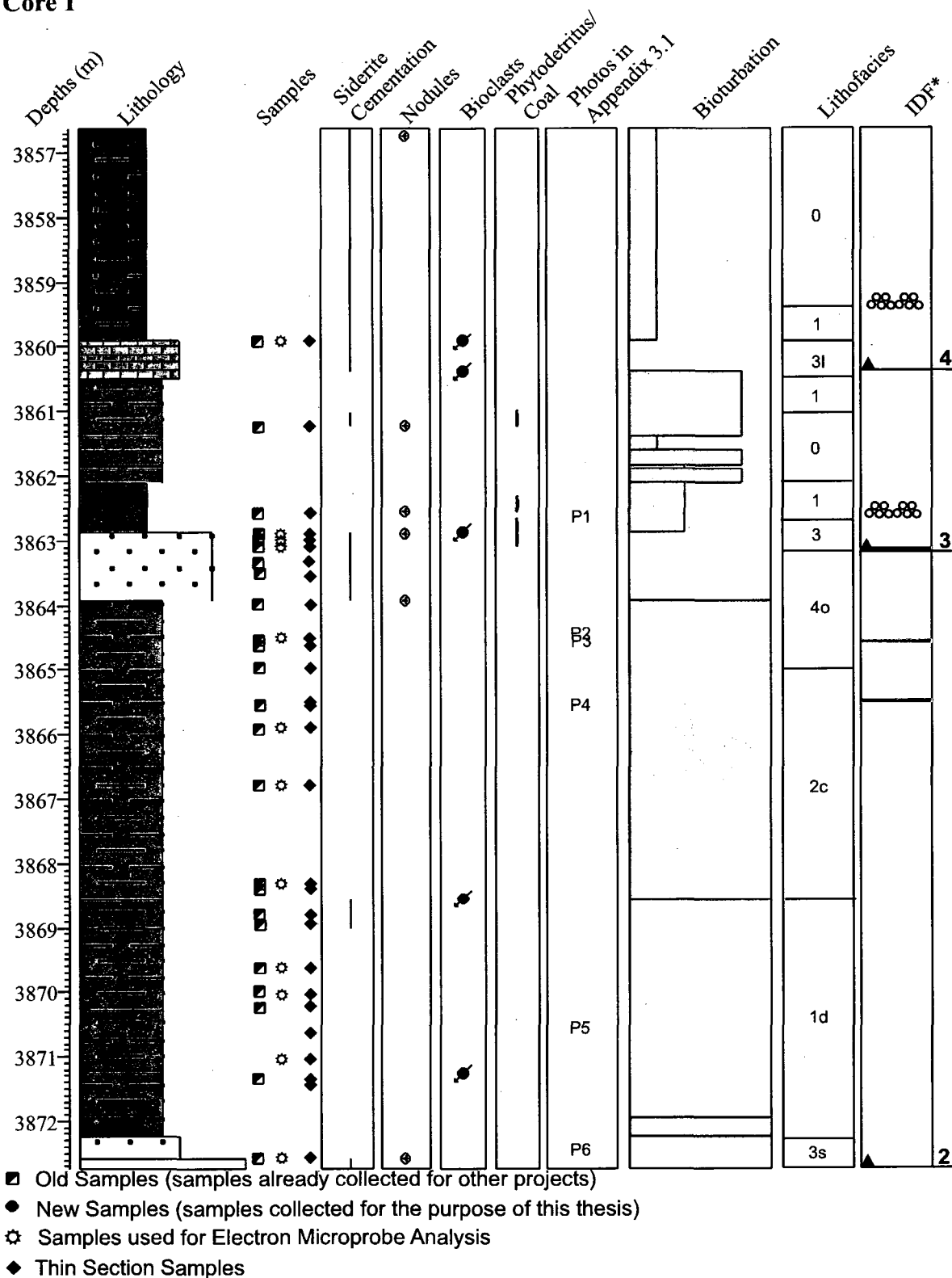


Figure 3.66: Core 1 at Thebaud C-74. Detailed core stratigraphy with sample and appendix photo location with interpreted diagenetic features and lithofacies including additional interpretation like the presence of bioclasts, nodules, phytodetritus and bioturbation. IDF means interpreted diagenetic features.

3911.80 m to 3918.60 m: these sediments comprise medium to coarse-grained sandstone beds > 25 cm in thickness. Bioturbation is complete at the top of the unit. This unit is interpreted as facies 9. The complete bioturbation in this facies 9 continues into the overlying sediment facies from 3911.28 m to 3911.80 m, which comprise fine-grained sandstone rich in *Ophiomorpha* and mud drapes. This unit is interpreted as sub-facies 4o.

3910.66 m to 3911.28 m: with a sharp contact at the bottom, this unit comprises mudstones abundantly bioturbated with very fine-grained sandstone lamination and some horizontal burrows and mud drapes sparsely distributed. This unit is interpreted as facies 5; a sandy tidal flat on the basis of mud drapes present in bioturbated sandy mudstones (Fig. 3.68). Sediments from 3909.57 m to 3910.66 m comprise a sandier unit with *Ophiomorpha* trace fossils; this latter unit is interpreted as sub-facies 4o (Fig. 3.67).

Core 5: Lower member in the Mississauga Formation from 3905.10 m to 3909.35 m, and a 4.25 m total recovery

The sub-facies 4o in core 6 continues into the adjacent core 5 from 3908.12 m to 3909.57 m.

The sediments from 3907.73 m to 3908.12 m comprise interbedded fine-grained sandstone and mudstone with abundant bioturbation and some vertical burrows. The bottom of the unit has a bioturbated contact with the underlying unit. This unit is interpreted as facies 5 as described by Cummings and Arnott (2005). From 3905.10 m to

3907.73 m, the sediments comprise medium-grained sandstone rich in *Ophiomorpha* and mud drapes. This unit is interpreted as sub-facies 4o

Core 4: Lower member in the Missisauga Formation from 3891.08 m to 3903.92 m, and a 12.84 m total recovery

3902.48 m to 3903.79 m: these sediments comprise medium-grained sandstone with uncommon bioturbation and some carbonate intraclasts. The presence of large burrows at the bottom of the unit suggests the presence of an erosional gap. This is interpreted as facies 3; more specifically sub-facies 3b on the basis of sandstone matrix, uncommon bioturbation and the presence of an erosional base.

From 3901.34 m to 3902.48 m, the sediments comprise completely bioturbated mudstone with rare lamination of siltstone. This unit is interpreted as facies 1. Overlying this facies 1 unit from 3901.08 m to 3901.34 m is a few centimeters of commonly bioturbated fine-grained sandstone interbedded with mudstone. This unit is interpreted as sub-facies 2b on the basis of lesser sandstone amount (< 60%).

3891.08 m to 3901.08 m: these sediments comprise interbedded siltstone to fine-grained sandstone and mudstone with a sharp contact between the sandstone and mudstone beds. The unit has a predominance of mudstone. The sandstones have cross lamination. Bioturbation is common with some vertical and horizontal burrows, and siderite cementation dispersed through the unit. This unit is interpreted as facies 0 based on the

predominance of mudstone. This facies 0 is continuous through the entire thickness of core 3 from 3890.52 m to 3891.08 m.

Core 2: Lower member in the Missisauga Formation from 3874.92 m to 3883.86 m, and an 8.94 m total recovery

3877.06 m to 3883.73 m: these sediments comprise predominantly medium-grained sandstone with common siltstone laminations, faint cross laminations (low angle) and very rare burrows. This massive unit is interpreted as facies 9 on the basis of > 25 cm sandstone beds. Overlying this facies 9 unit is a commonly bioturbated fine-grained sandstone unit from 3876.41 m to 3877.06 m with parallel siltstone laminations. This unit is interpreted as facies 0, and is overlain by more of facies 9 from 3875.38 m to 3876.41 m.

3874.94 m to 3875.38 m; these sediments comprise a fine-grained sandstone unit with mud drapes, common bioturbation with vertical and horizontal burrows, and is rich in *Ophiomorpha*. This unit is interpreted as sub-facies 4o (Fig. 3.69).

Core 1: Lower member in the Missisauga Formation from 3856.63 m to 3873.26 m, and a 16.63 m total recovery

The sediments from 3870.53 m to 3872.83 comprise fine to coarse-grained sandstone in a downward coarsening succession, with mm-scale mud intraclasts locally and abundant bioturbation from 3871.96 m to 3872.24 m, with a gradational contact at the bottom. This unit also has sand in-filled horizontal burrows in the coarser-grained sandstone. This unit is interpreted as facies 3; however, based on the peculiar nature of the TS facies (lack of

thin-shelled fossils and sideritic diagenesis); the unit is interpreted as sub-facies 3s, confirmed by the presence of a sharp base in the sandstone.

3868.58 m to 3870.53 m; sediments in this unit are made up of fine-grained sandstone with interbedded mudstone (~ 30%). This unit is interpreted as facies 2d, on the basis of this interval being the muddiest unit immediately above the transgressive surface with sub-facies 3s.

3865.00 m to 3868.58 m: these sediments comprise abundantly bioturbated fine-grained sandstone with interbedded mudstone with a gradational contact. This unit is interpreted as sub-facies 2c on the basis of sandstone amount (> 60%) and abundant bioturbation.

This sub-facies 2c is underlying a fine to medium grained sandstone unit from 3853.18 m to 3865.00 m in a coarsening upwards succession. There is abundant bioturbation in the bottom one meter of the unit, and the presence of vertical burrows, *Ophiomorpha* and siderite cementation (with some nodules) throughout. This unit is interpreted as sub-facies 4o.

The sediments from 3862.82 m to 3863.18 m comprise fine- to medium-grained sandstone with a few coarse lithic grains and a gradational contact at the bottom of the unit. Vertical burrows are present with some siderite cemented sandstones and a few siderite nodules. This unit is interpreted as facies 3 on the basis of the sideritic diagenesis, burrow traces, and coarseness of sandstones. Overlying the facies 3 unit is an

uncommonly bioturbated mudstone unit from 3862.10 m to 3862.88 m with some coarse lithic grains. This unit is interpreted as facies 1.

3861.03 m to 3862.10 m: these sediments comprise commonly bioturbated very fine to fine-grained sandstone with parallel and cross lamination of siltstone and mudstone, with a sharp contact at the top of the sandstone. This unit has rare thin-shelled fossils and rare siderite cementation. The unit is interpreted as facies 0. Overlying this facies 0 unit is a unit of interbedded very fine-grained sandstone and mudstones (with parallel laminations) unit from 3860.49 m to 3861.03 m. This unit is interpreted as facies 1 on the basis of the muddy nature of the beds.

From 3859.92 m to 3861.03 m, the sediments comprise limestone with shelly fragments. This is interpreted as sub-facies 31 on the basis of the bioclastic nature of the unit. From 3859.58 m to 3859.92 m, the sediments comprise a bioclastic mudstone unit with uncommon bioturbation. This unit is interpreted as facies 1. Overlying this facies 1 is an interbedded mudstone and very fine-grained sandstone unit with siderite cementation. This unit is interpreted as facies 0 on the basis of predominant mudstone with sandstone beds.

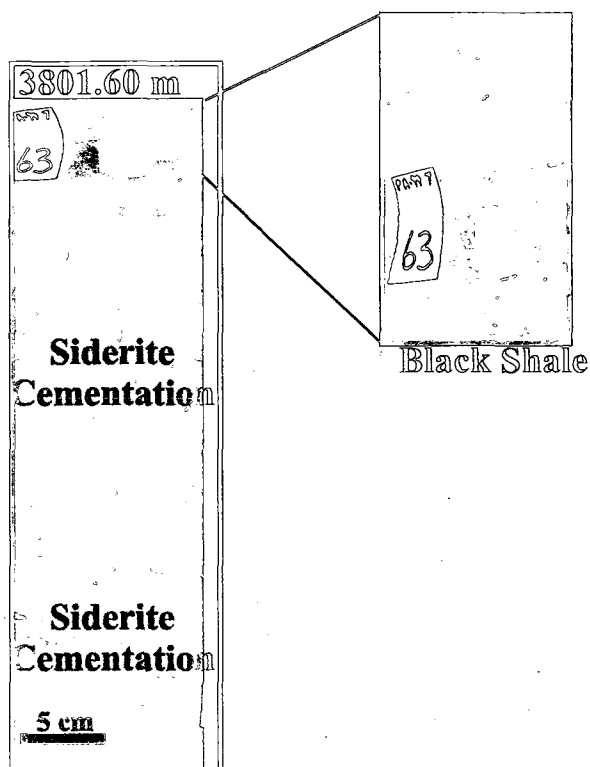


Figure 3.33 (Appx. 3.2 photo 63): Thick mudstone bed with siderite cementation.

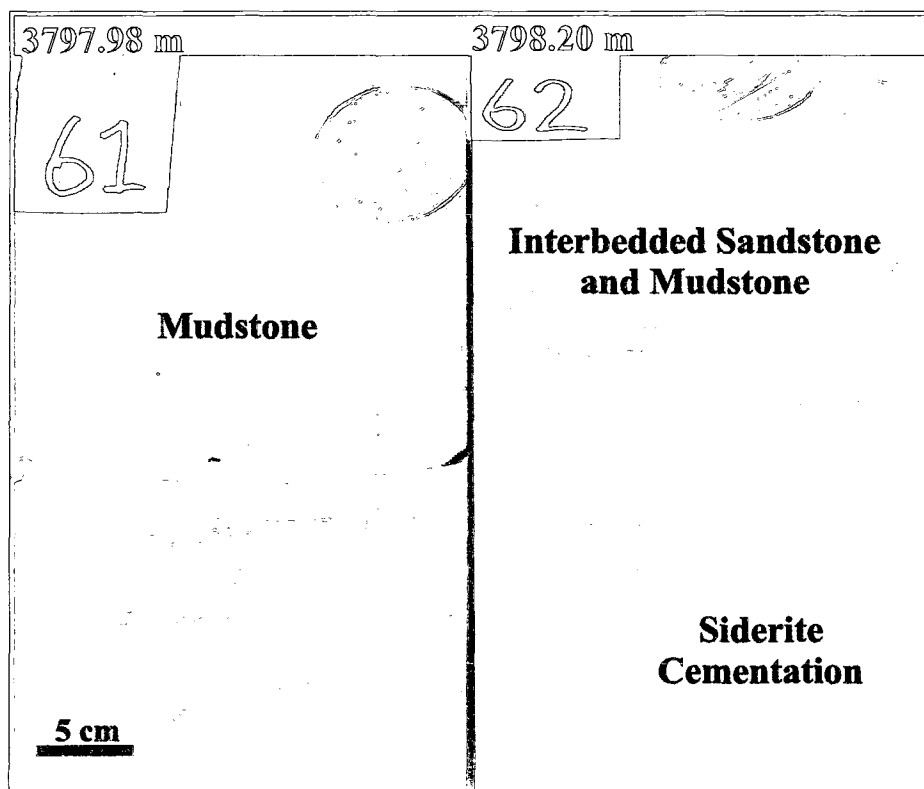


Figure 3.34 (Appx. 3.2 photos 61 & 62): Mudstone lacking sandstone overlying interbedded mudstone and siderite cemented fine-grained sandstone.

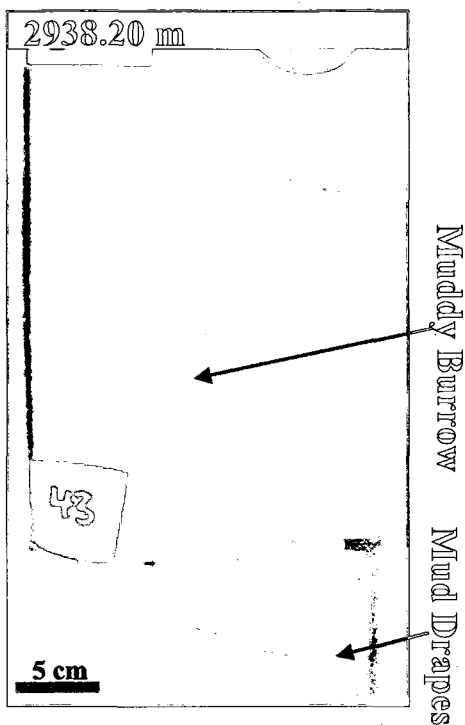


Figure 3.35 (Appx. 3.2 photo 43): Graded sandstone unit with muddy burrow and mud drapes

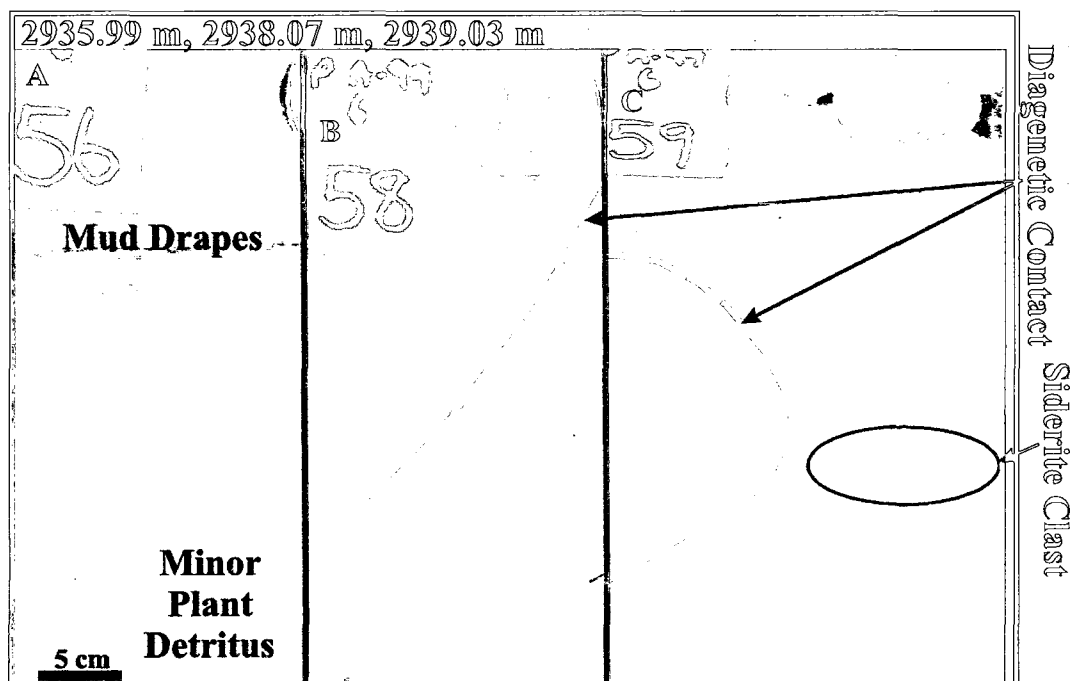


Figure 3.36 (Appx. 3.2 photos 56, 58 & 59): (A) 2935.99 m has parallel laminated sandstone with mud clast and minor phytodetritus; (B) 2936.30 m has sandstone lamination picked out by siderite, plus siderite cemented mud drapes; (C) 2938.07 m shows a diagenetic contact, which is also present in 2939.03 m but with siderite cemented mud drapes.

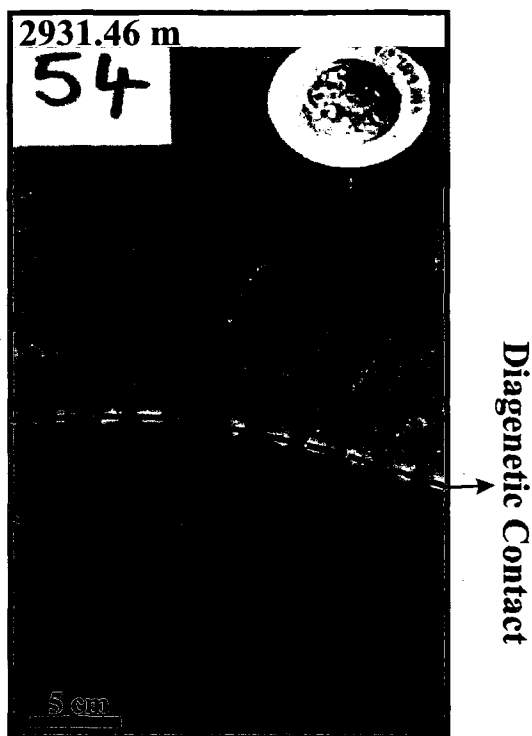


Figure 3.37 (Appx. 3.2 photo 54): Diagenetic contact between grey and beige medium-grained sandstone

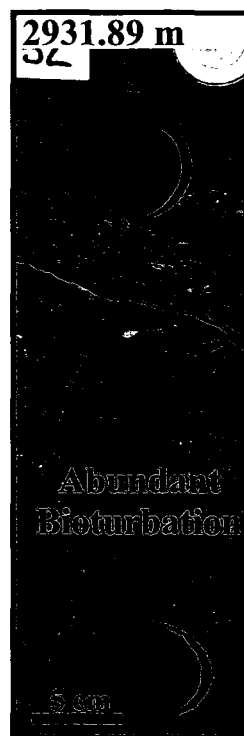


Figure 3.38 (Appx. 3.2 photo 52): Mudstone with interbedded fine-grained sandstone with very patchy siderite cementation.

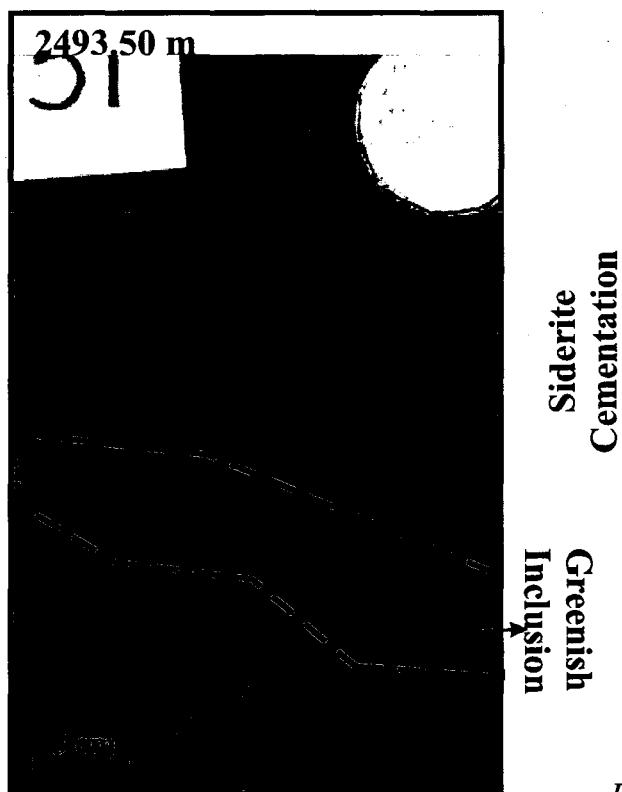


Figure 3.39(Appx. 3.2 photo 51): Bioturbated sandstone with greenish concretions

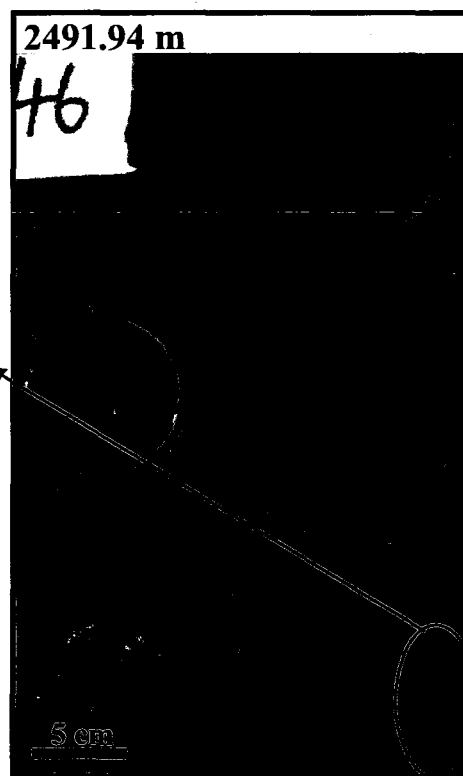


Figure 3.40 (Appx. 3.2 photo 46): Facies 1 shale overlying bioturbated Facies 3 sandstone (sideritic diagenesis).

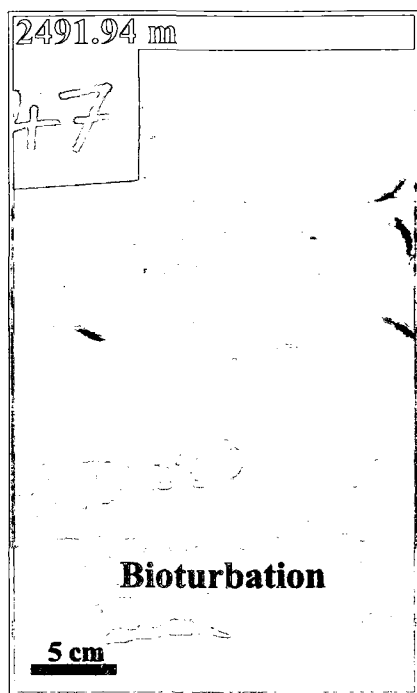


Figure 3.41 (Appx. 3.2 photo 47): Bioturbated sandstone with patchy siderite cementation



Figure 3.42 (Appx. 3.2 photo 48): Bioturbated sandstone with patchy siderite cementation and shelly fragments.

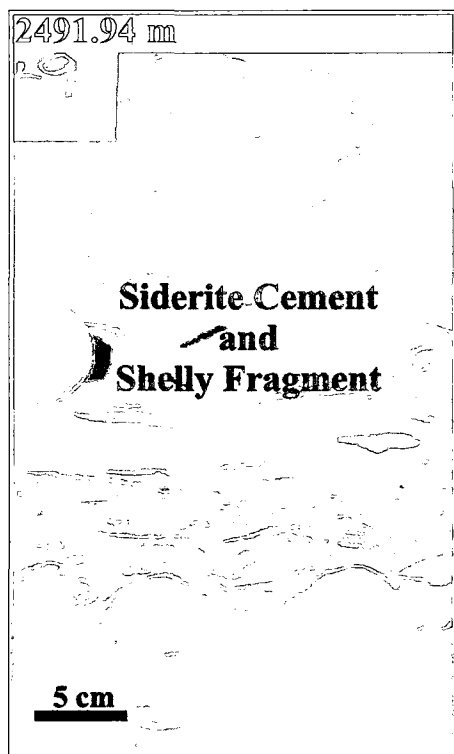


Figure 3.43 (Appx. 3.2 photo 49): Bioturbated sandstone with patchy siderite cementation and abundant shelly fragments that appear undisturbed.

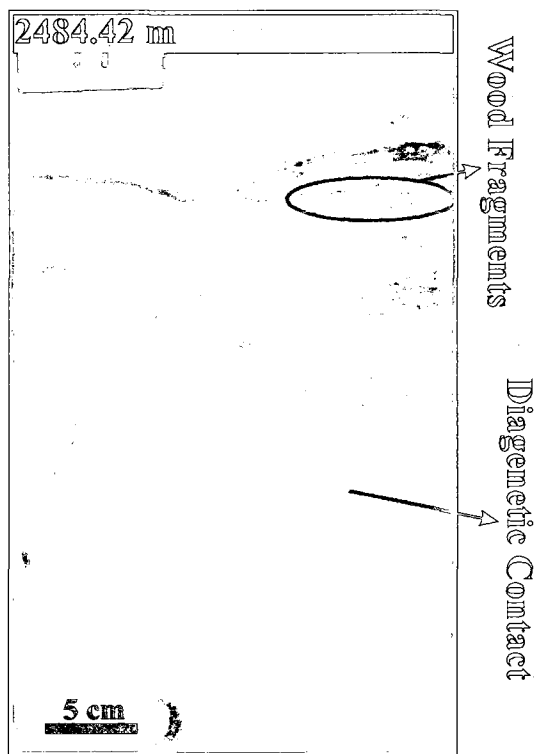


Figure 3.44 (Appx. 3.2 photo 41): Bioturbation on the top of a facies of fine-grained sandstone with some wood fragments.

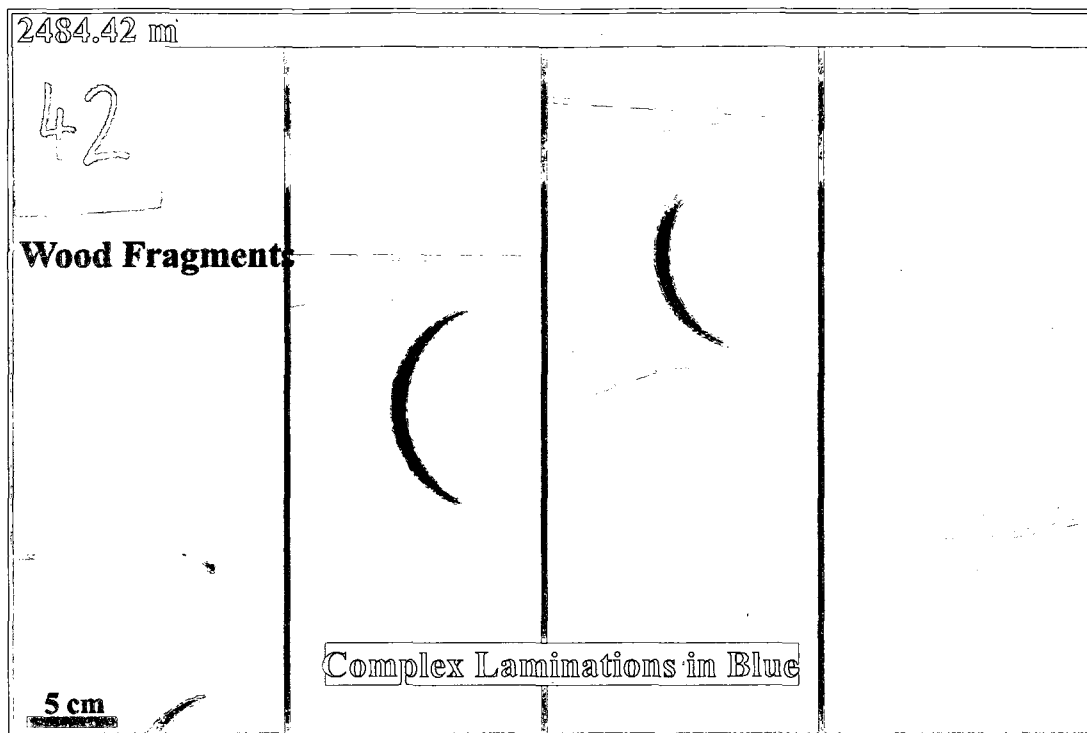


Figure 3.45 (Appx. 3.2 photos 42a-d): Fine grained sandstone with thinner beds showing wood fragments, cross lamination, complex laminations, and erosional surfaces.

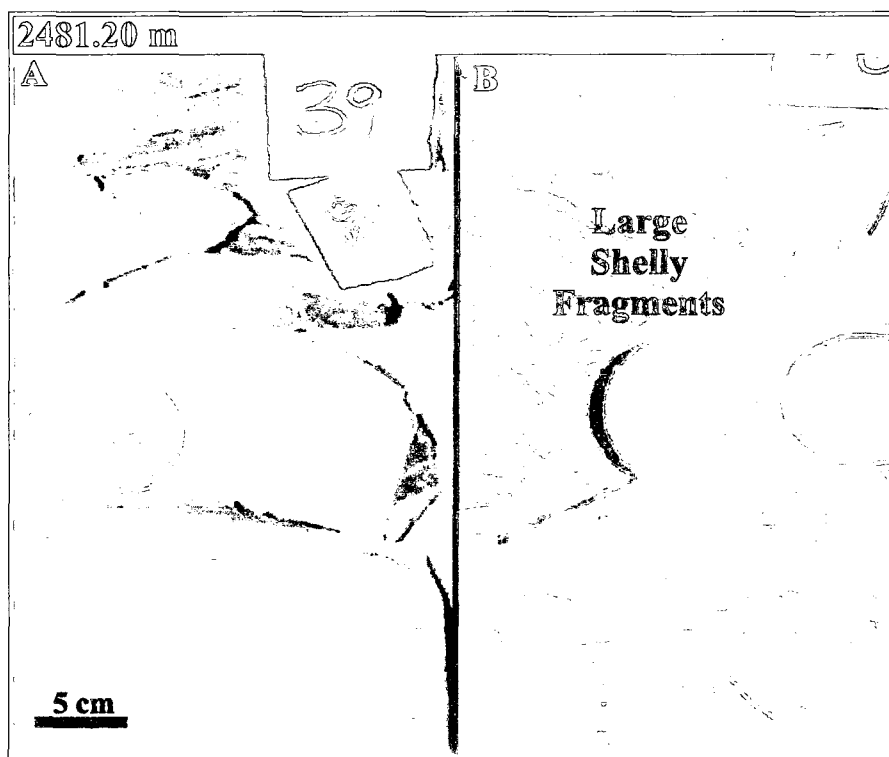


Figure 3.46a (Appx. 3.2 photos 39 & 40): Facies 1 shale overlying facies 3 fine-grained sandstones with some shelly fragments, and 3.46b: Large shell fragments at the base of the unit.

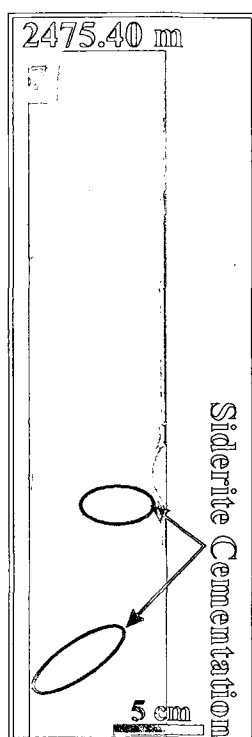


Figure 3.47 (Appx. 3.2 photo 37): Bioturbated fine grained sandstone with considerable siderite cement

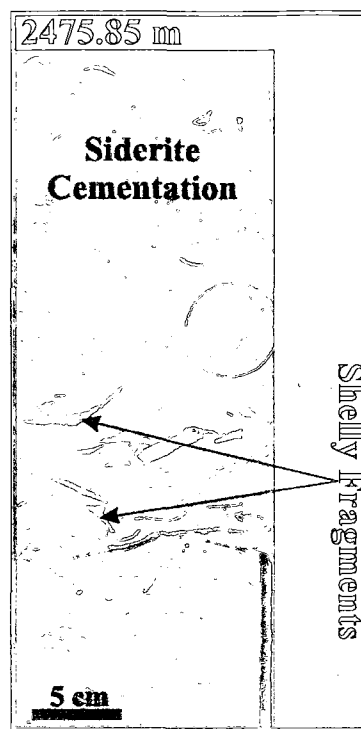


Figure 3.48 (Appx. 3.2 photo 38a): Fine grained sandstone with abundant shells and areas with and without siderite cementation.

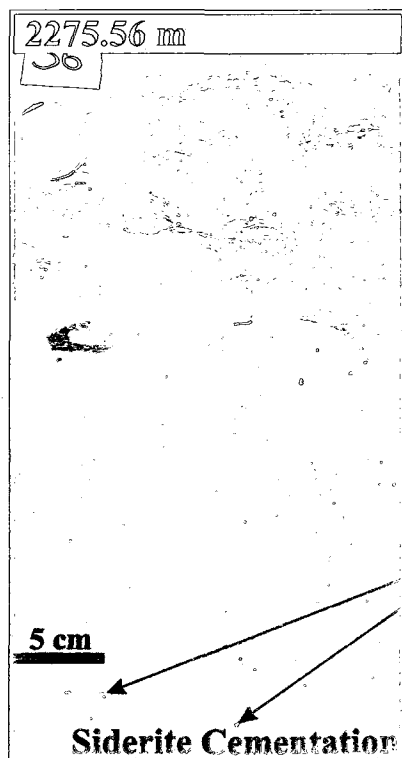


Figure 3.49 (Appx. 3.2 photo 36): Bioturbated medium grained sandstone with siderite cementation and few shelly fragments.

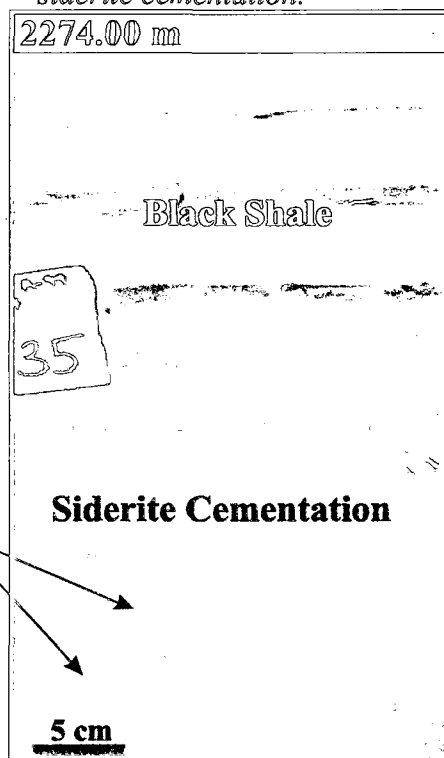


Figure 3.50 (Appx. 3.2 photo 35): Facies 1 black shale with bioclasts overlying sideritic mudstone.

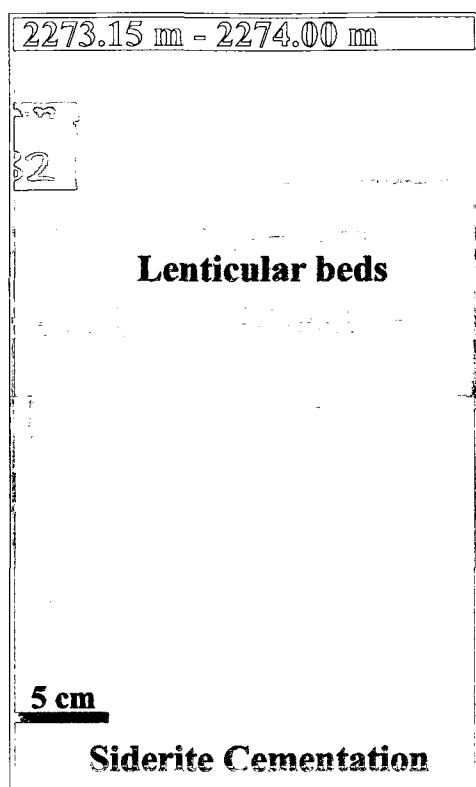


Figure 3.51 (Appx. 3.2 photo 32): Sandstone with lenticular beds and siderite concretions

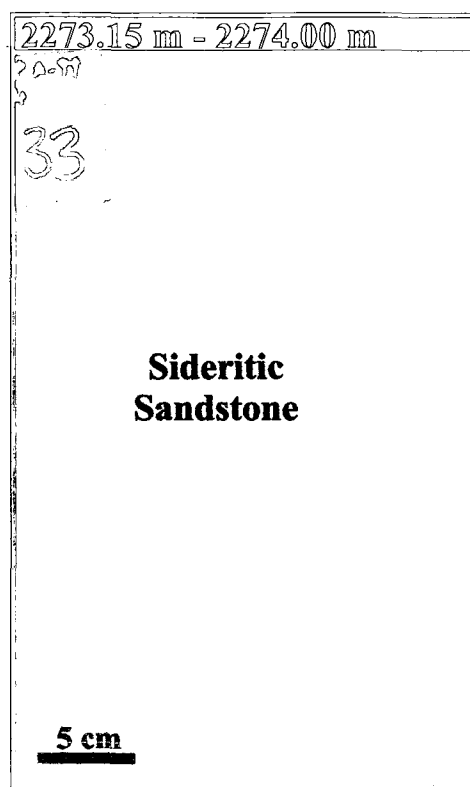


Figure 3.52 (Appx. 3.2 photo 33): Sideritic sandstone with common bioturbation

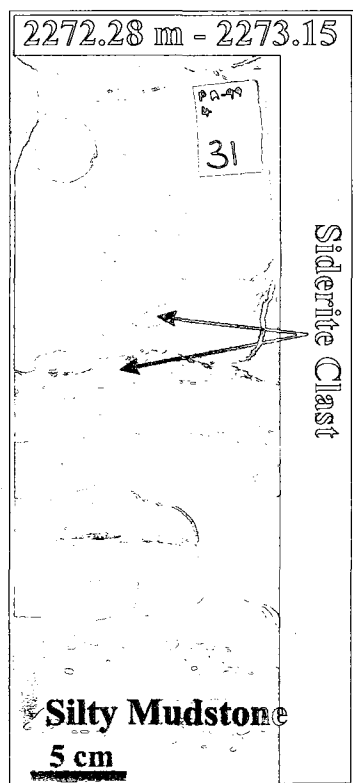


Figure 3.53 (Appx. 3.2 photo 31): Interbedded fine grained sandstone and mudstone with sparse bioturbation at the base.

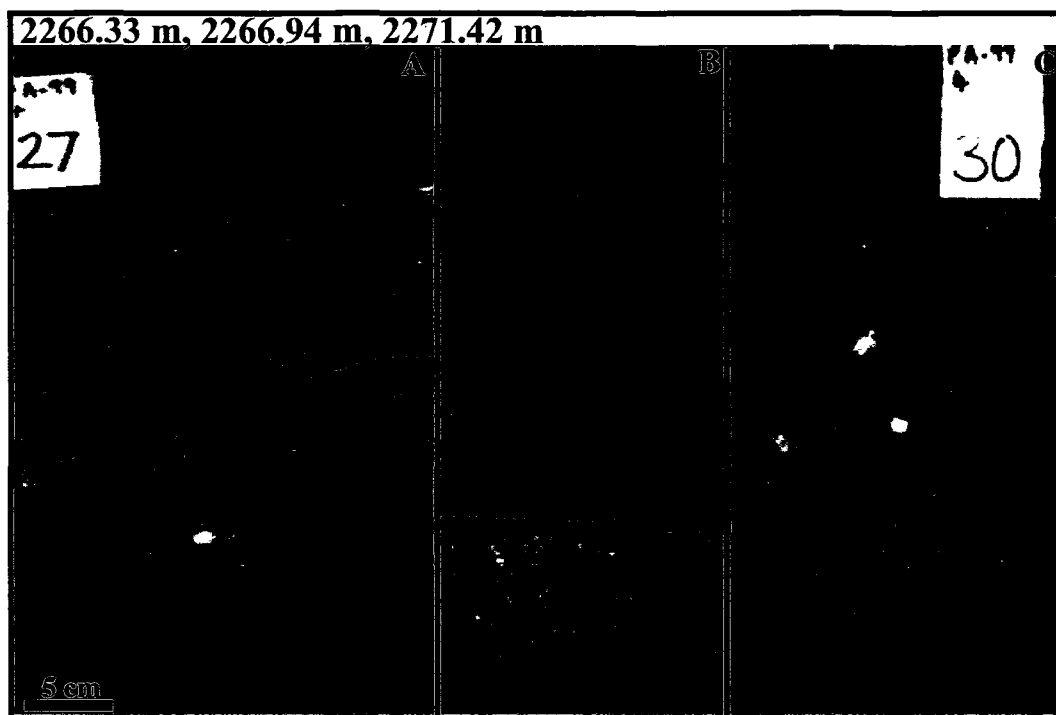


Figure 3.54 (Appx. 3.2 photos 27, 28a, & 30): (A) 2266.33 m: Coarse sandstone with low angle cross-bedding and phytodetritus, ~5 mm lithic granules, a large mud clast and an erosional base. (B) 2266.94 m: coarse sandstone interbedded with sideritic silty mudstone. (C) 2271.42 m: Conglomerate of siderite intraclasts and granules <5 mm.

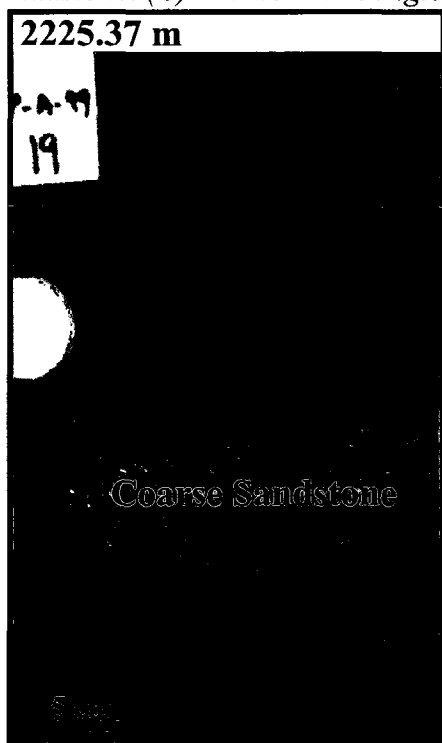


Figure 3.55 (Appx. 3.2 photo 19): Coarse-grained sandstone with erosional base and muddy laminae over sparsely bioturbated brown mudstone and laminated fine grained sandstone beds.

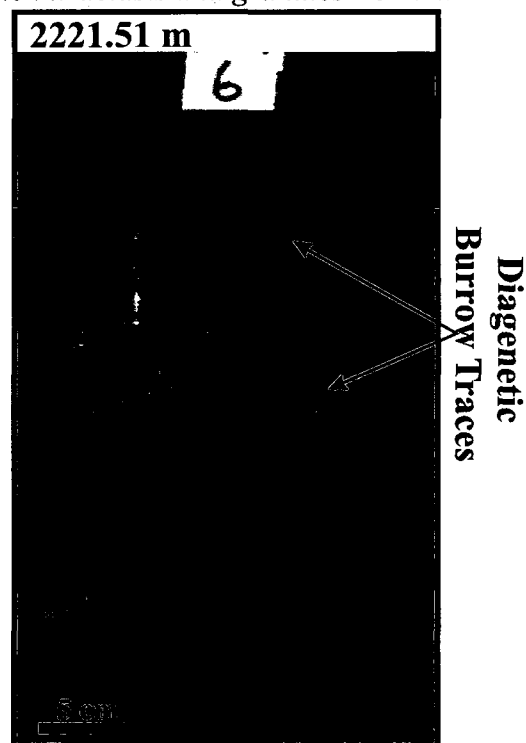


Figure 3.56 (Appx. 3.2 photo 6): Moderately bioturbated mudstone with fine-grained sandstone, mud fragments and brown staining.

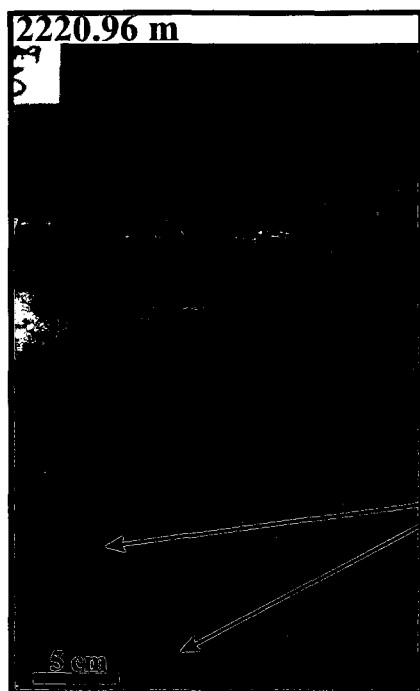


Figure 3.57 (Appx. 3.2 photo 3): Bioturbated mudstone with beds of very fine-grained sandstone to siltstone with some siderite concretions.



Figure 3.58 (Appx. 3.2 photo 18): Abundant phytodetritus and fine siderite intraclasts in fine to medium grained sandstone, with trough cross-bedding in the sandstone.

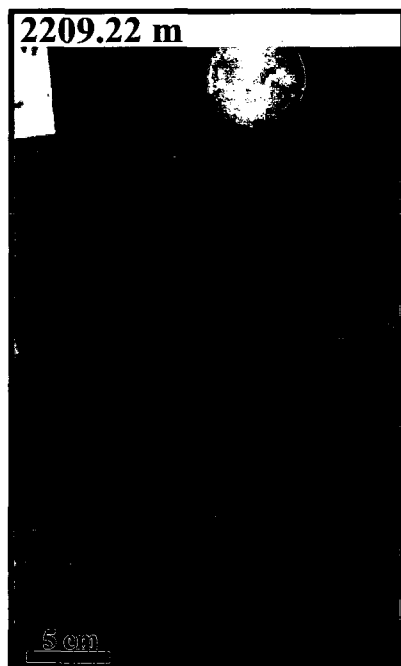


Figure 3.59a (Appx. 3.2 photo 14): Black shale over laminated and bioturbated fine-grained sandstone with coal layers and coarse-grained sandstone. This is interpreted as a possible maximum flooding surface.

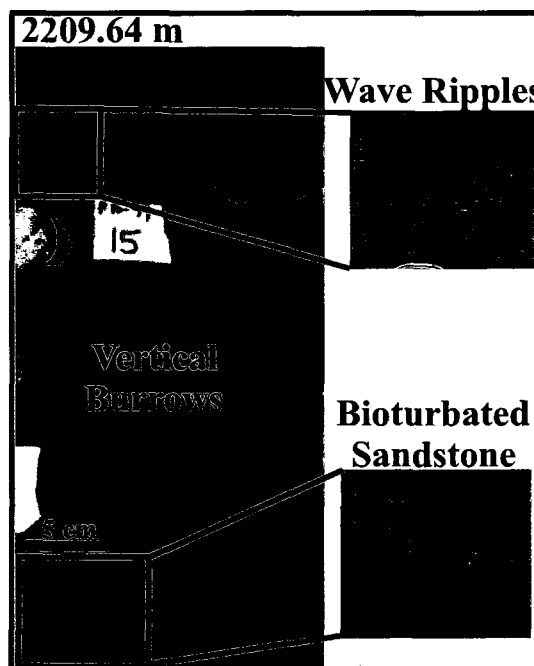


Figure 3.59b (Appx. 3.2 photo 15): Fine-grained sandstone with common bioturbation interbedded with mudstone.

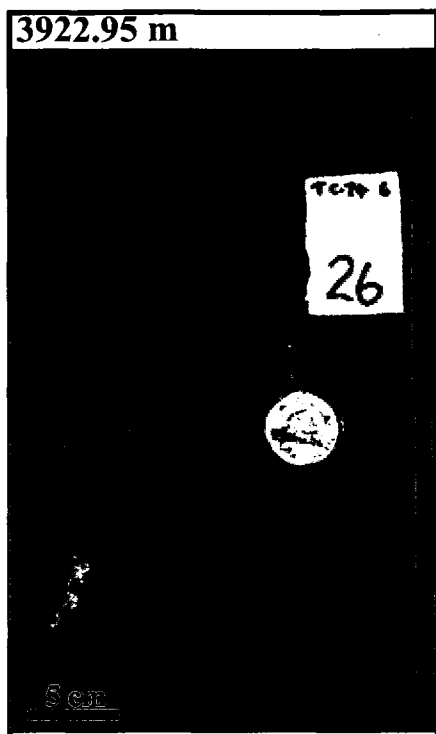


Figure 3.60 (Appx. 3.1 photo 26): Fine to medium grained sandstone in a fining upwards succession.

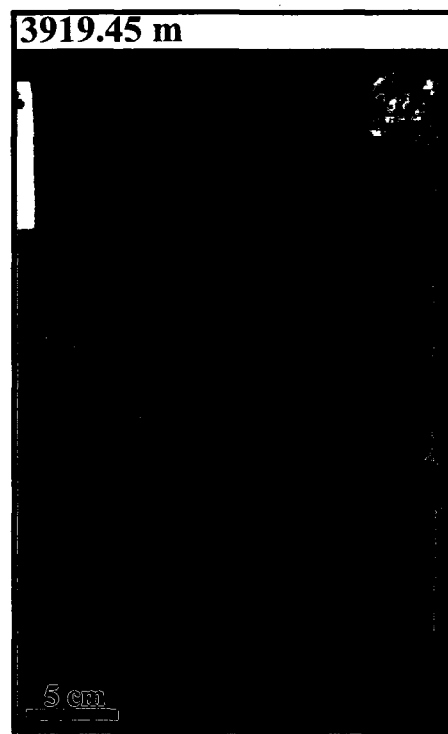


Figure 3.61 (Appx. 3.1 photo 27): Fine-grained sandstone rich in *Ophiomorpha*, mud drapes and the rare horizontal burrows.

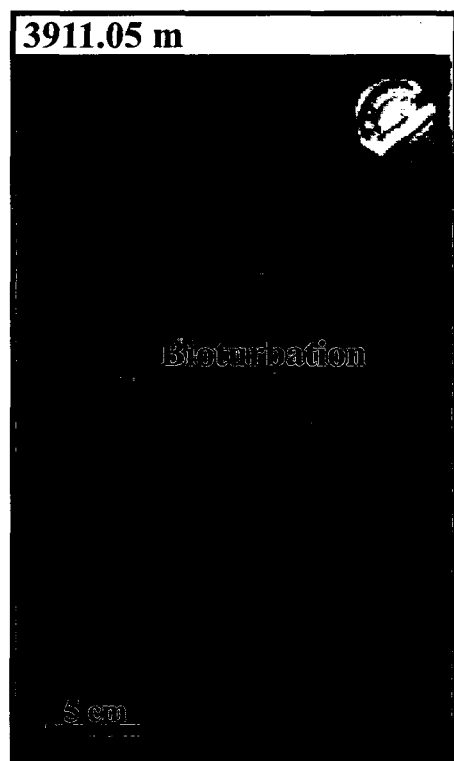


Figure 3.67 (Appx. 3.1 photo 28): Sandy mudstone with *Ophiomorpha*.

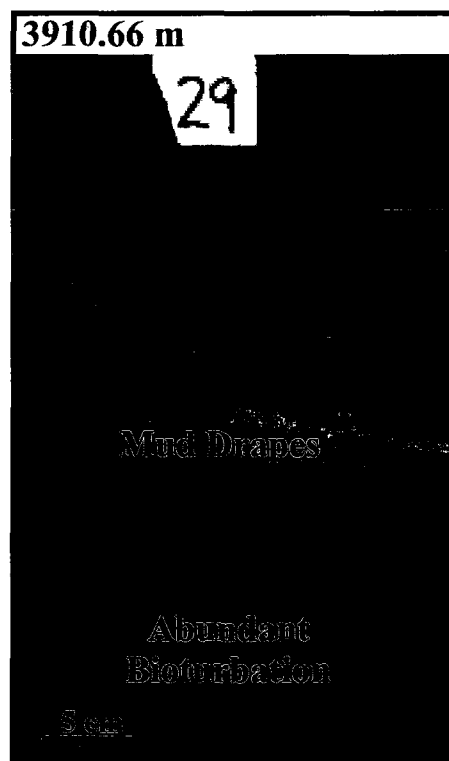


Figure 3.68 (Appx. 3.1 photo 29): Mudstone with fine-grained sandstone laminae with sparsely distributed mud drapes.

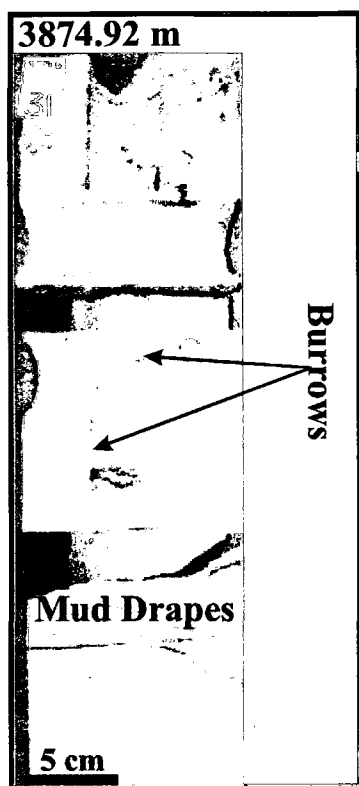


Figure 3.69 (Appx. 3.1 photo 31): Commonly bioturbated fine-grained sandstone with mud drapes, burrows, and *Ophiomorpha*.

3.5 DETAILED CHARACTER OF TRANSGRESSIVE UNITS

3.5.1 Introduction

A packet (Fig. 3.70), as defined in this study, includes the sediments within the transgressive unit and the immediately underlying (regressive/prograded) sediments below the transgressive surface of erosion. The transgressive unit is recognized on the basis of abrupt changes in inferred sedimentation rates. Packets have been identified in both studied wells (Thebaud C-74 and Peskowsk A-99); some with evidence of a major transgression and others with evidence of only minor transgression. The packet interval considered in this study extends up to 20 metres below the TS because Berner (1980) argued that the depth of complete sulphate reduction may be tens of metres deep.

As earlier discussed in section 2.1.1, this study is focused on packets where early diagenetic changes are suspected to have occurred in underlying prograded sediments and such diagenetic changes are now found within and beneath the transgressive unit that often contain facies 3 sediments which are siderite-cemented, reworked, and fine to coarse-grained sandstones. Where facies 3 is present, this implies a major depositional change that is characteristic of environments where transgression has occurred.

Sequence boundaries, some corresponding to a transgressive surface, have been recognized on the basis of an erosional surface separating a more distal facies above from a more shoreline-proximal facies below. Sequence boundaries have been interpreted at the following depths in the Peskowsk well: 3795.24 m, 2273.15 m, 2222.12m, and 2213.12 m (refer to core stratigraphy in section 3.3). However, many of the

progradational successions and the overlying transgressive surfaces are probably parasequences and not sequences.

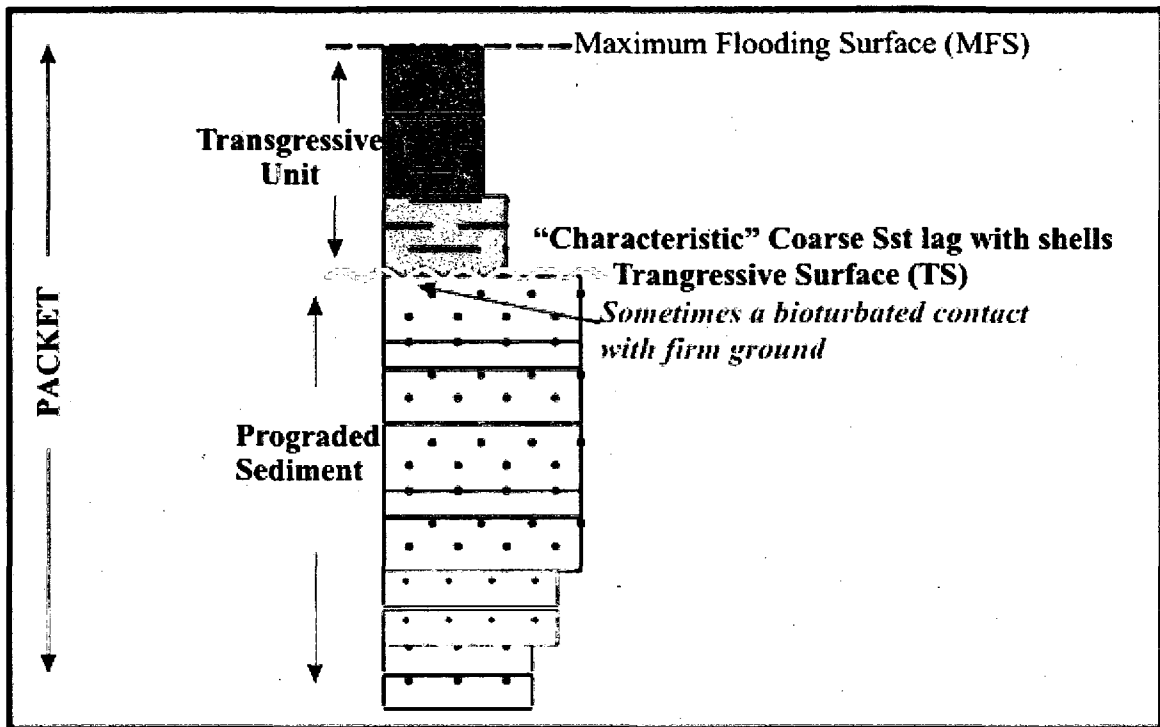


Figure 3.70: A conceptual "packet" as defined in this study.

3.5.2 Identified Packets in Thebaud C-74

The character of sediment packets in the Thebaud C-74 well are alike, with a unit of facies 1 mudstones interpreted as Maximum Flooding Surface (MFS) overlying transgressive facies 3. These facies 3 sediments have distinguishing features that include the presence of siderite cementation, normally graded fine to coarse-grained sandstone beds and abundant shell fragments, and less frequently present characteristics includes: the presence lesser shell fragments, and a mixture of fine-grained sandstone with mudstones. The facies 3 sediments sometimes overlie cross-laminated fine-grained sandstone rich in *Ophiomorpha* with mud drapes (sub-facies 4o). Observations on individual transgressive surfaces are summarized in Table 3.3

Table 3.3: Summary of observations from packets in Thebaud C-74 and Peskowesk A-99

Wells	Packet Depths (m)		Packet Number	TS ¹ Depths (m)	Transgressive Unit Thickness (m)	Lithofacies above the TS	Interpretation of the Packet		TS Change ²
	Top	Bottom					Below the TS	Above the TS and facies 3	
Thebaud C-74	3901.35	3908.11	1	3903.79	1	3b to 1	Tidal estuary deposits	Reworked sediments lacking bioturbation with open shelf shales	A+
	3872.28	3875.32	2	3872.83	0.5	3s to 1	Tidal estuary deposits	MFS muddy sandstone	A
	3862.10	3865.00	3	3862.88	1	3 to 1	Tidal estuary deposits	Reworked sediment to open shelf deposits	A
	3859.40	3861.01	4	3859.92	0.5	3l to 1	Open Shelf Shale	Bioclastic reworked sediment to open shelf deposits	B-
Peskowesk A-99	3800.70	3805.38	1	3802.05	0.4	3m to 0m	Prodeltaic sandstone	Reworked sediments to muddy prodelta	A-
	3795.22	3800.70	2	3798.50	2	3m to 5	Shoreface	Reworked sediments with predominated mudstone and tidal flat deposits	C
	2948.20	2954.34	3	2950.72	2	0m	Fluvial deposits	Muddy prodelta	A-
	2936.02	2942.72	4	2938.20	2	5s	10 meter parasequence, fluvial at the top	Tidal flat plus coastal deposits	C
	2929.95	2935.18	5	2931.89	0.5	3 to 2c	Tidal flat, predominantly sandstones	Reworked sediments and shoreface (60-90% sandstone)	B+
	2493.33	2495.28	6	2494.15	0.5	3 to 0	Lagoon deposits	Reworked sediments to prodelta deposits	A-
	2480.30	2482.72	7	2481.72	5	3a to 1	1 meter of Shoreface (60-90% sandstone) over river mouth	Reworked sediments with mud laminae and open shelf shales	A
	2222.30	2273.17	8	2228.65	4	5	45 metre thick fluvial deposits	Tidal flat deposits	B+
	2208.00	2213.00	9	2210.15	2	5	Fluvial deposits	Tidal flat deposits	B

¹: TS: Transgressive Surface²: TS change considers the inferred magnitude of environmental change while comparing the sediment below the TS with that above

TS Change A+ represents moving from a very shallow water facies into the Transgressive highstand facies association of facies 3, then into open shelf and overlain by a thick progradational succession.

TS change B+ represents moving from a very shallow water facies into shoreface or river mouth facies, then into a progradational sequence.

TS change C represents moving from a fluvial facies into a tidal facies.

Packet 1: 3902.49 m to 3908.11 m

This packet (Fig. 3.71) has a TS at 3903.79 m, and it is made up of a 5 metres thick progradational succession with about 4 metres of sub-facies 4o (rich in *Ophiomorpha* and mud drapes, Fig. 3.16), that abruptly pass up into a 1 metres thick sub-facies 3b (reworked sediments with an erosional base, Fig. 3.9). These sediments then pass gradually up into facies 1 (open shelf shales, Fig. 3.4).

Packet 2: 3872.28 m to 3875.32 m

This packet has a TS at 3872.83 m, and it is made up of a thin progradational succession with about 0.5 metres of sub-facies 4o, which abruptly pass up into a 0.5 metres thick sub-facies 3s (reworked sediments with a sharp base lacking bioturbation, Fig. 3.14). The facies gradually passes up into a sub-facies 2d due to the presence of > 70 % sandstone.

Packet 3: 3862.88 m to 3865.00 m

This packet has a TS at 3862.88 m, a 3 metres thick progradational succession that culminates in 2 metres of sub-facies 4o with *Ophiomorpha* and mud drapes, and abruptly passes up into a 1 meter thick facies 3 (reworked sediments with coarse lithics in siderite cemented medium-grained sandstone). The transgressive unit is capped by a MFS interval with facies 1 shale.

Packet 4: 3859.92 m to 3861.01 m

This packet has a TS at 3859.92 m, and it is made up of a 1.5 metres thick sediment succession with 0.5 metres thick interval of facies 1 that contains the MFS overlying 0.5

metres of bioclastic reworked sediments (sub-facies 3l, Fig. 3.11). These reworked sediments could be part of the Highstand System Tract (HST) overlying sediments of the packet from 3862.88 m to 3865.00 m. There is no change in sediment facies below and above the TS.

3.5.3 Identified Packets in Peskowsk A-99

Packet 1: 3801.58 m to 3805.38 m

This packet has a TS at 3802.05 m. A 4 metres thick progradational succession, made up of sub-facies 0s (cross laminated sandstone with interbedded mudstone, Fig. 3.3) that gradually passes up into a thin (0.4 metres) sub-facies 3m (Fig. 3.12): reworked sediments with abundant shelly fragments and interbedded mudstone. This sub-facies 3m gradually pass up into sub-facies 0m (thin bedded sandstone with a predominance of mudstone).

Packet 2: 3795.22 m to 3800.70 m

This packet has a TS at 3798.50 m, and it is made up of a 6 metres thick progradational succession which culminates in 3 metres of sub-facies 2c (Fig. 3.7): bioturbated sandstone and mudstone with 60 to 90 percent sandstone that gradually pass up into a 1 meter thick sub-facies 3m (reworked sediments with interbedded mudstone), capped by a 2 metres thick tidal flat deposit (facies 5, Fig. 3.18).

Packet 3: 2948.20 m to 2954.34 m

This packet has a TS at 2950.72 m. A 6 metres thick progradational succession culminates in 4 metres of sub-facies 4x (Fig. 3.17) with cross-bedded sandstone lacking mud drapes. It is overlain abruptly by a 2 metres thick facies 0m (thin bedded sandstone with a predominance of mudstone, Fig. 3.2). Characteristic facies 3 sediments are absent, but the TS is interpreted between the fluvial sandstones and the overlying marine prodeltaic sub-facies 0m.

Packet 4: 2936.02 m to 2942.72 m

This packet (Fig. 3.72) has a TS at 2938.20. A 10 metres thick progradational succession culminates in 4 metres of sub-facies 4x with cross-bedded sandstone that abruptly pass up into facies 5 (tidal flat deposits). Characteristic facies 3 sediments are absent.

Packet 5: 2929.95 m to 2935.18 m

This packet has a TS at 2931.89 m, and it is made up of a 6 m thick retrogradational succession which culminates in 4 metres of sub-facies 5s (Fig. 3.19): tidal flat deposits with coarse-grained sandstone beds in places, rare bioclasts, sparse siderite cementation and a predominance of interbedded fine-grained sandstone and mudstone. It is overlain by 0.5 metres of characteristic facies 3 (siderite-cemented fine to coarse-grained reworked sandstone with abundant shelly fragments), which gradually pass up into a 1.5 metres thick sub-facies 2c with abundantly bioturbated sandstone (60-90% sandstone) and interbedded mudstone.

Packet 6: 2491.98m to 2495.28 m

This packet has a TS at 2494.15 m. A 1.8 metres thick retrogradational succession culminates in a 1.3 metres sub-facies 2b (Fig. 3.6) with moderately bioturbated sandstone (< 60% sandstone) that abruptly pass up into a 0.6 metres of facies 8 (Fig. 3.20) with commonly bioturbated, grey-green sandy mudstone with heavy shelly fossils, capped by characteristic facies 3 sediments.

Packet 7: 2480.30 m to 2482.72 m

This packet (Fig. 3.73) has a TS at 2491.72 m. A 1.5 metres thick progradational succession culminates in a 1 meter thick sub-facies 2c with abundantly bioturbated sandstone (60-90% sandstone), overlain by a 0.5 metres thick transgressive sub-facies 3a (reworked sediments with mudstone laminae, Fig. 3.8). This sediment succession is capped by a 0.8 metres thick facies 1 (open shelf deposits).

Packet 8: 2222.30 m to 2273.17 m

This packet has a TS at 2228.65 m. A very thick (45.32 metres) progradational succession culminates in a 0.8 metres of sub-facies 2b with moderately bioturbated sandstone (< 60% sandstone). It is overlain by 44.52 metres of sub-facies 4x with cross-bedded sandstone lacking mud drapes. The progradational fluvial succession gradually passes up into a 4 metres thick facies 5 (tidal flat deposits) with evidence of slumping. Characteristic facies 3 sediments are absent.

Packet 9: 2208.00 m to 2216.00 m

This packet (Fig. 3.74) has a TS at 2210.15 m. A 6 metres thick slightly progradational succession that culminates in 4 metres of sub-facies 4x with cross-bedded sandstone lacking mud drapes, which gradually pass up into 2 metres of facies 5 (tidal flat deposits). Characteristic facies 3 sediments are absent.

3.6 CHAPTER SUMMARY

Conventional cores were interpreted based on lithofacies types and transgressive units. The term "packet" is used in this chapter to group sediments within a transgressive unit above a transgressive surface with the immediately underlying prograded sediments. Such packets are the focus of the study and during core interpretation, sampling was done based on the presence of this packets. Nine packets are identified in this chapter with some showing major evidence of transgression and other very minor evidence of transgression, along with changes in facies types, referred to as the magnitude of environmental change. The characters of the different packets were investigated considering the magnitude of environmental change, which is based on a scheme from A+ to C. The next chapter presents more results, but based on petrographic studies on thin sections using the petrographic microscope, scanning electron microscope, electron microprobe, and powder samples for X-ray diffraction analysis, all in order to produce a detailed paragenetic sequence of early diagenetic minerals.

Packet 1: 3901.35 m - 3908.11 m showing an A type TS change* at Thebaud C-74

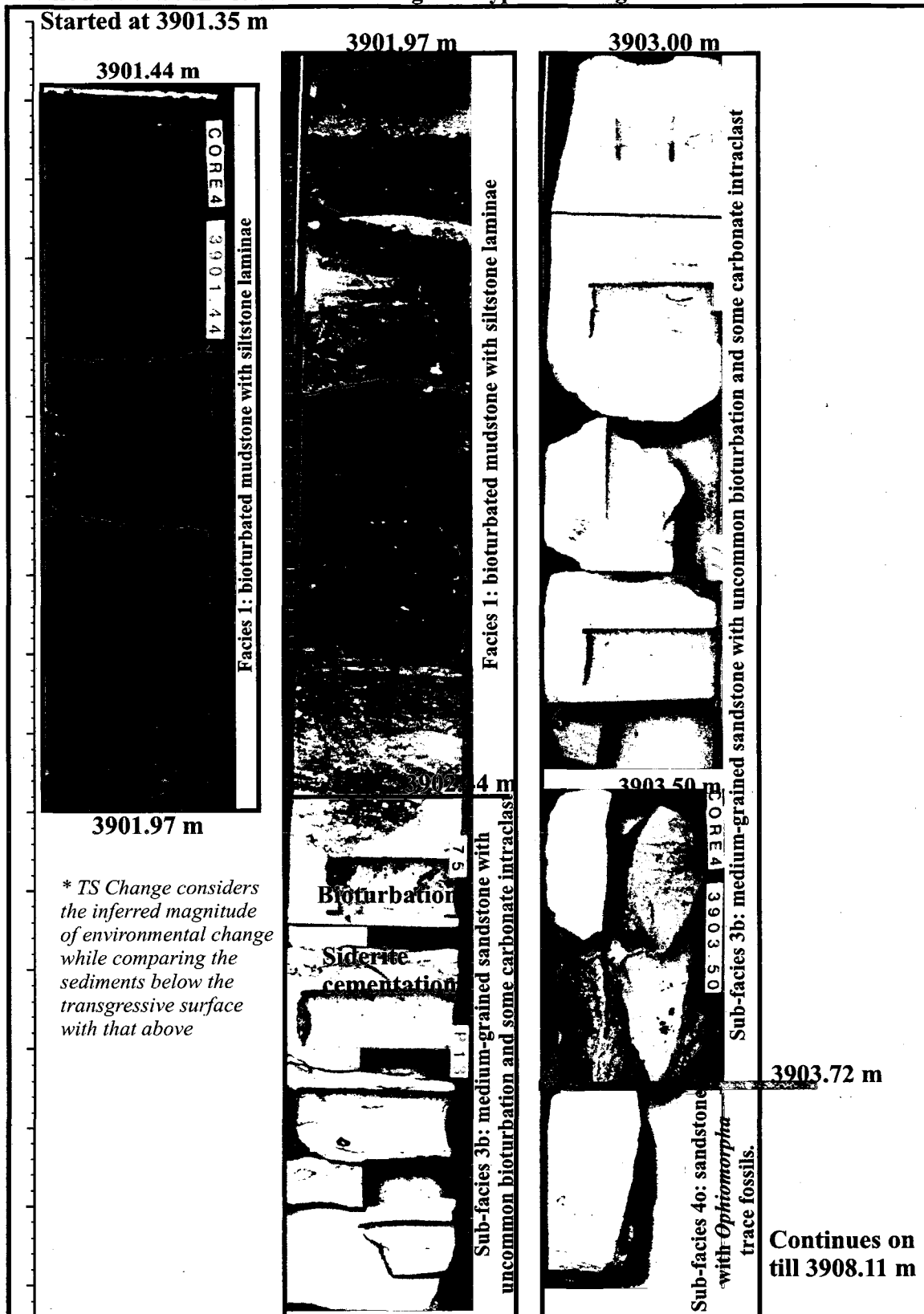
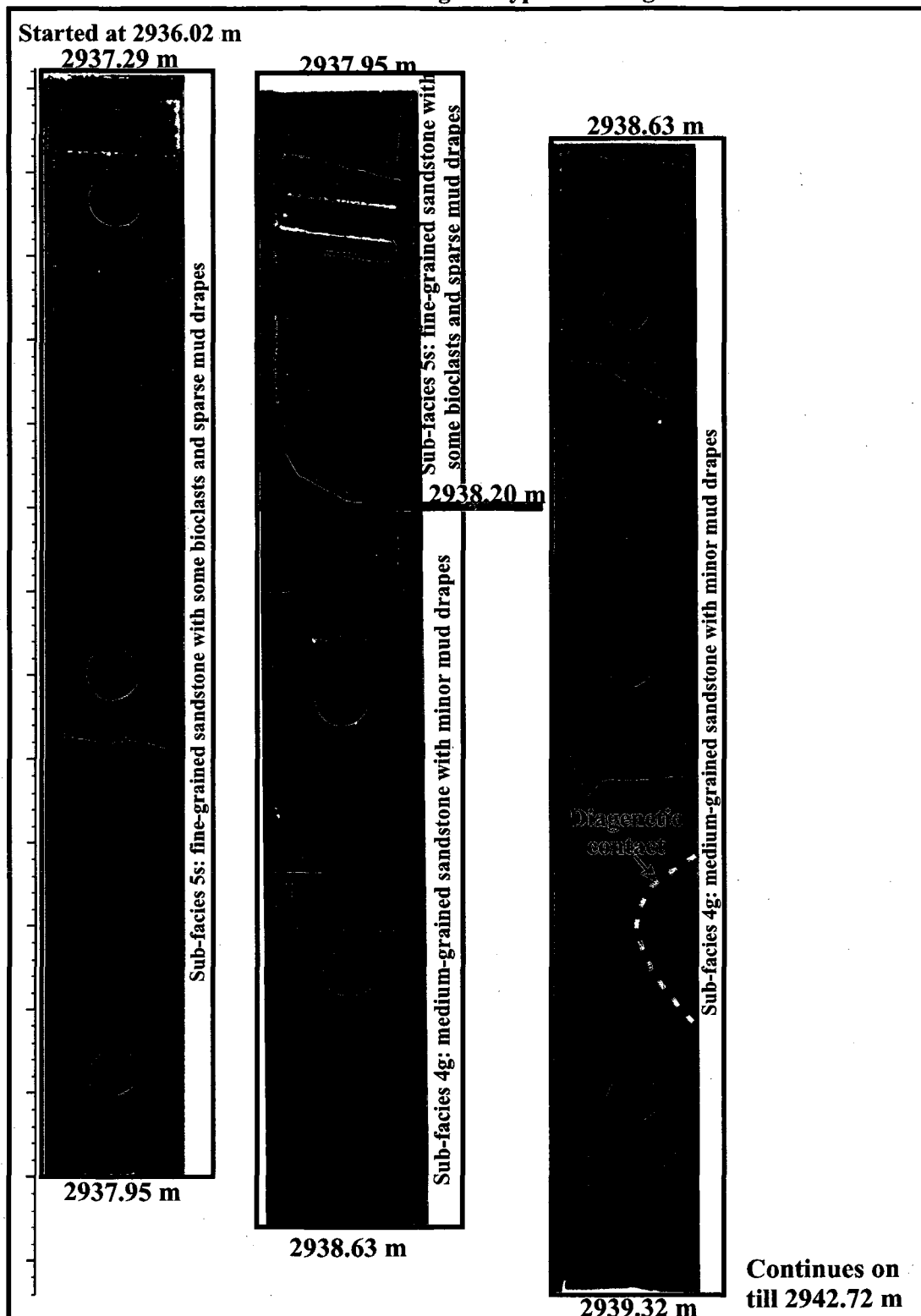


Fig. 3.71: Core photo of packet 1 at Thebaud C-74.

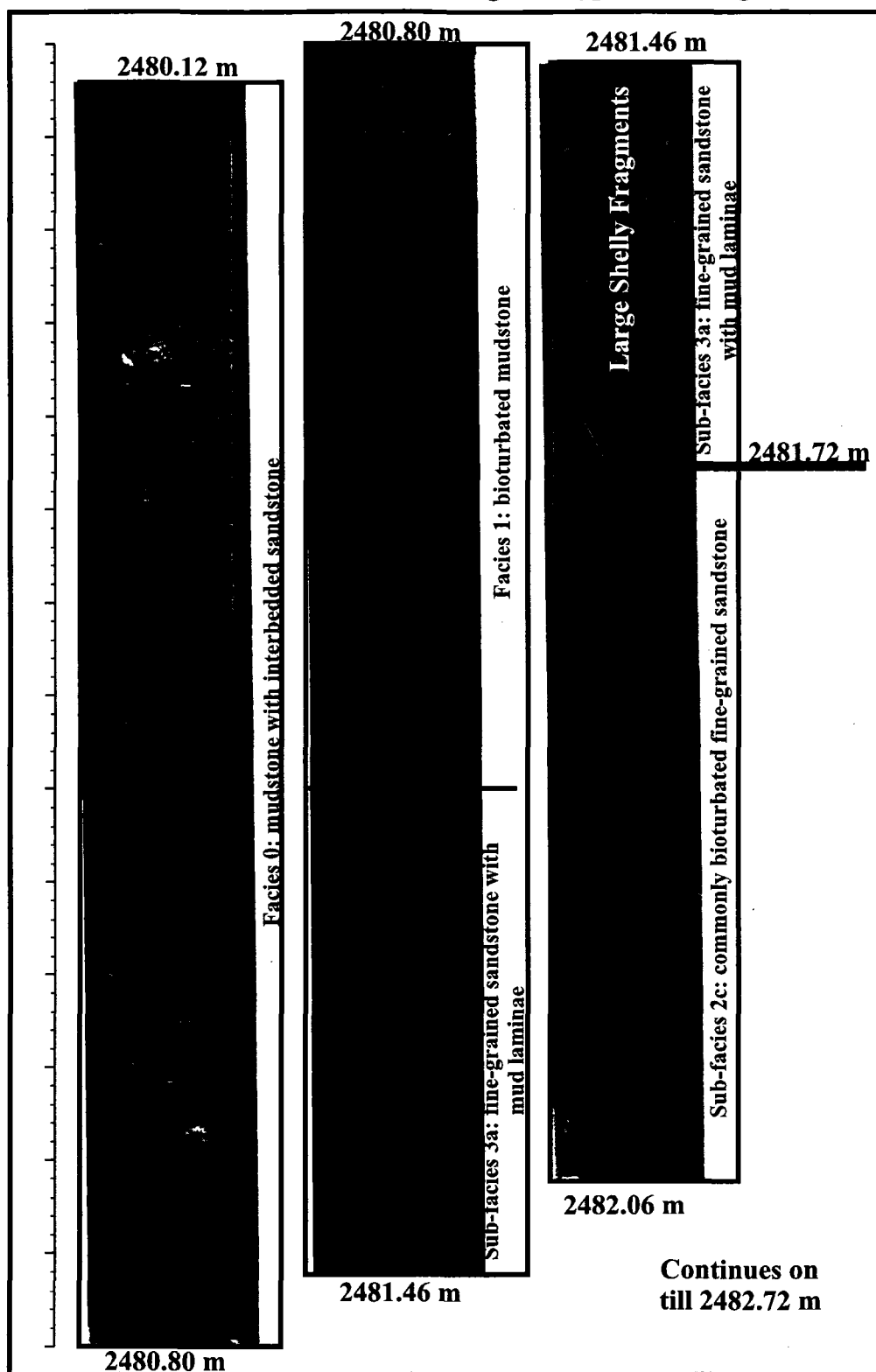
Packet 4: 2936.02 m - 2942.72 m showing a C type TS change* at Peskowesk A-99



* TS Change considers the inferred magnitude of environmental change while comparing the sediments below the transgressive surface with that above

Fig. 3.72: Core photo of packet 4 at Peskowesk A-99.

Packet 7: 2480.30 m - 2482.72 m showing an A types TS change* at Peskowesk A-99.

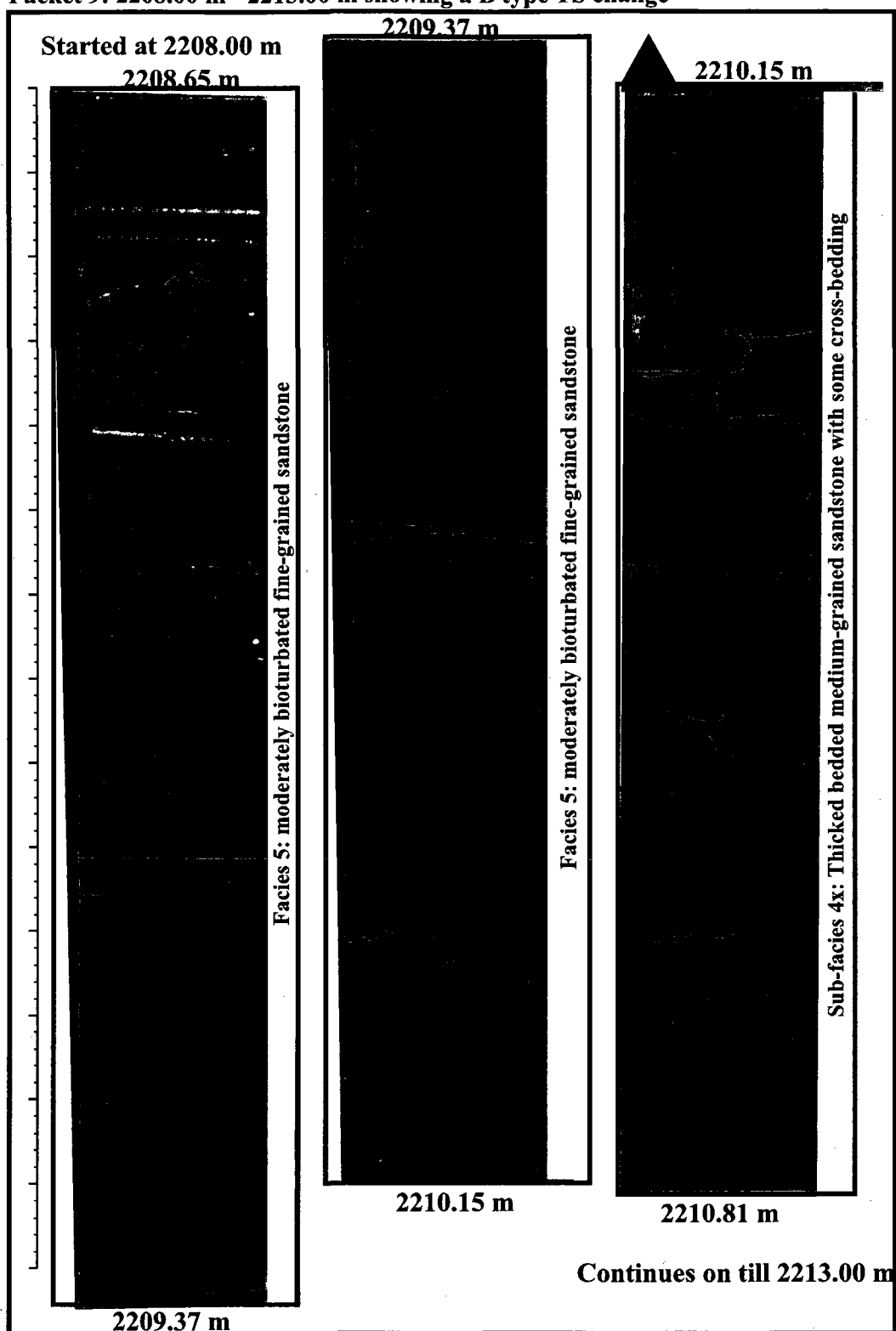


* TS Change considers the inferred magnitude of environmental change while comparing the sediments below the transgressive surface with that above

Fig. 3.73: Core photo of packet 7 at Peskowesk A-99.

Peskowesk A-99

Packet 9: 2208.00 m - 2213.00 m showing a B type TS change*



* TS Change considers the inferred magnitude of environmental change while comparing the sediments below the transgressive surface with that above

Fig. 3.74: Core photo of packet 9 at Peskowesk A-99.

CHAPTER 4: PETROGRAPHY

4.1 LABORATORY METHODS

4.1.1 Electron Microprobe, Scanning Electron and Petrographic Microscopes

Sampling methods have been discussed in detail in chapter 3. Polished thin sections of representative samples (23 for Peskowsk A-99 and 55 for Thebaud C-74) were prepared at Vancouver Petrographics Ltd location. Porosity percentage was estimated using thin sections that were vacuum-impregnated with blue epoxy (Tables 4.1 & 4.2, App. 4.1 & 4.2). Chemical variations were investigated in identified diagenetic minerals, predominantly carbonates, using electron microprobe (EMP) chemical mineral analysis. The paragenetic sequence of the different diagenetic phases was investigated using the petrographic microscope and backscattered electron images obtained from scanning electron microscope (SEM) and EMP (App. 4.3a & 4.4a).

Electron Microprobe (EMP) mineral chemical analyses were carried out at the Dalhousie University Regional Electron Microprobe and Image Analysis facility. Thin sections' X and Y coordinates on spots of interest were obtained using the SEM at the Saint Mary's University Regional Analytical Centre. The equipment used is a JEOL-8200 electron microprobe with five wavelength spectrometers and a Noran 133 eV energy dispersion detector. The beam of the EMP was set at 15kV and 20nA with beam diameter 1-10 microns. The energy dispersive spectrometer (EDS) was used for quick mineral recognition and then a proper quantitative chemical analysis of the identified mineral spot was done (App. 4.3b & 4.4b). The textural relationship between diagenetic phases was determined with the help of backscattered electron (BSE) images.

4.1.2 X-ray Diffraction

In order to get samples into a powder form, the less than or equal to 53.85g samples were washed and then crushed using a hammer on the rock samples while wrapped in thick plastic bags to avoid contamination and loss of sample and then pulverized in an alumina ceramic mill. Powder samples were homogenized, which was necessary because larger samples had to be pulverized in portions. Using a diamond carbide pen, glass slides were cut into a 1-inch square, and cleaned using Kim wipes. The well name and depth was then written on one side of the slide. Less than 1 gram of powder, from each sample, was mixed in a mortar with methanol and smeared on the other side of the slide, and left to air dry. Dried samples were placed in groups into a Siemens Kristaloflex diffractometer at the Geological Survey of Canada (Co K α radiation source) for analysis (Appendix 4.5 and 4.6). The detection limit used for the study is ~5 wt %, hence minerals with abundance less than this detection limit may not appear as a peak on the X-ray diffractogram.

In order mark peaks on the diffractogram, the 2 theta values are first determined by using a table of 2 theta value. The 2 theta quartz peaks is then used to check if the 2 theta calibrations are correct. Therefore, plots of peak minerals from the X-ray diffraction data are normalized to quartz abundance.

Table 4.1: Summary of Petrography with Lithofacies at Thebaud C-74

Well: Thebaud C-74				Cement: listed in chronological order where apparent and indicated by (#); otherwise order is unknown					Porosity
#	Depths (m)	Lithofacies (after Karim et al., 2008)	Rock Types	% of total rock	cement 1: mineral	cement 2: mineral	cement 3: mineral	other cements	remaining porosity as % of total rock
1	3859.95	3l	Mudstone	15	10% Chl	3% Pyrite	2% Carb		1
2	3861.23	0	Very Fine Sandstone	5	3% Carb	2% Pyrite			5
3	3862.56 (a)	1	Mudstone	35	18% Pyrite	10% Chl	5% Carb	2%Qtz overgrowth	5
4	3862.56 (b)	1	Mudstone	20	10% Carb	5% Pyrite	5% Chl		10
5	3862.91	3	Mudstone	20	10% Carb	5% Pyrite	5% Chl		10
6	3862.98 (a)	3	Mudstone	27	20% Carb	5% Chl	2% Pyrite		10
7	3862.98 (b)	3	Mudstone	30	10% Carb	10% Chl	10% Pyrite		20
8	3863.08	3	Medium Sandstone	40	20% Sid	10% Carb	5% Pyrite	5% Chl	5
9	3863.38	4o	Medium Sandstone	12	5% Pyrite	5% Chl	2% Qtz overgrowth		10
10	3863.53	4o	Medium Sandstone	10	Pyrite				10
11	3863.99	4o	Medium Sandstone	20	10% Pyrite	5% Carb	5% Qtz overgrowth		2
12	3864.51	4o	Fine Sandstone	35	15% Pyrite	10% Carb	5% Sid	5% Chl	2
13	3864.52	4o	Fine Sandstone	25	15% Sid	5% Qtz overgrowth	5% Chl		10
14	3864.99	2c	Fine Sandstone	35	15% Sid	5% Qtz overgrowth	5% Chl		10
15	3865.53	2c	Fine Sandstone	35	20% Pyrite	10% Carb	5% Qtz overgrowth		10
16	3865.56	2c	Fine Sandstone	31	15% Sid	10% Carb	5% Chl	1% Qtz overgrowth	10
17	3865.95	2c	Fine Sandstone	36	20% Carb	15% Pyrite	5% Chl	1% Qtz overgrowth	3
18	3866.79	2c	Fine Sandstone	35	10% Carb	10% Pyrite	10% Qtz overgrowth	5% Chl	3
19	3867.39	2c	Fine Sandstone	31	15% Pyrite	10% Carb	5% Chl	1% Qtz overgrowth	2
20	3868.31 (a)	1c	Fine Sandstone	47	30% Carb	10% Pyrite	5% Chl	2% Qtz overgrowth	10
21	3868.31 (b)	1c	Fine Sandstone	52	30% Carb	15% Pyrite	5% Chl	2% Qtz overgrowth	10
22	3868.39	1c	Fine Sandstone	30	20% Pyrite	5% Carb	5% Qtz overgrowth		2
23	3868.77	1c	Fine Sandstone	40	30% Carb	10% Pyrite	5% Chl	5% Qtz overgrowth	1
24	3868.94	1c	Fine Sandstone	32	20% Carb	10% Pyrite	2% Qtz overgrowth		3
25	3869.64	1c	Fine Sandstone	25	15% Pyrite	5% Carb	5% Chl		2
26	3870.01	1c	Fine Sandstone	30	10% Carb	10% Chl	5% Pyrite	5% Qtz overgrowth	10
27	3870.19	1c	Fine Sandstone	35	15% Pyrite	15% Carb	5% Sid		5
28	3870.62 (a)	1c	Fine Sandstone	28	15% Carb	8% Pyrite	5% Chl		10

Table 4.1: Summary of Petrography with Lithofacies at Thebaud C-74

Well: Thebaud C-74				Cement: listed in chronological order where apparent and indicated by (#); otherwise order is unknown					Porosity
#	Depths (m)	Lithofacies (after Karim et al., 2008)	Rock Types	% of total rock	cement 1: mineral	cement 2: mineral	cement 3: mineral	other cements	remaining porosity as % of total rock
29	3870.62 (b)	1c	Fine Sandstone	20	10% Pyrite	5% Carb	5% Chl		20
30	3871.05	1c	Fine Sandstone	45	20% Carb	15% Pyrite	5% Sid	5% Chl	5
31	3871.36	1c	Fine Sandstone	25	20% Carb	3% Pyrite	2% Qtz overgrowth		25
32	3871.47	1c	Fine Sandstone	22	10% Carb	10% Chl	2% Pyrite		20
33	3872.58 (a)	3s	Fine Sandstone	38	20% Carb	10% Sid	8% Pyrite		2
34	3872.58 (b)	3s	Fine-Medium	33	15% Carb	10% Sid	8% Pyrite		2
35	3876.72	0	Fine Sandstone	27	15% Carb	5% Sid	5% Chl	2% Qtz overgrowth	10
36	3879.56	9	Fine-Medium	27	15% Carb	5% Sid	5% Chl	2% Qtz overgrowth	10
37	3881.59	9	Medium Sandstone	27	15% Carb	5% Sid	5% Chl	2% Qtz overgrowth	10
38	3882.96	9	Fine-Medium	27	15% Carb	5% Sid	5% Chl	2% Qtz overgrowth	10
39	3902.65	3b	Fine-Medium	35	20% Carb	10% Chl	5% Qtz overgrowth		10
40	3905.10	4o	Fine-Medium	27	10% Sid	10% Chl	5% Qtz overgrowth	2% Carb	13
41	3906.75	4o	Fine-Medium	27	10% Sid	10% Chl	5% Qtz overgrowth	2% Carb	10
42	3907.93	4o	Fine Sandstone	35	20% Sid	5% Carb	5% Qtz overgrowth	5% Chl	10
43	3908.65	4o	Fine-Medium	30	10% Sid	10% Chl	5% Qtz overgrowth	2% Carb	10
44	3909.92	4o	Fine-Medium	20	15% Sid	5% Chl			5
45	3911.66	4o	Fine-Medium	35	20% Carb	10% Chl	5% Qtz overgrowth		10
46	3912.40	9	Fine-Coarse Sandstone	7	5% Sid	2% Qtz overgrowth			15
47	3913.73	9	Fine-Coarse Sandstone	10	Sid				10
48	3914.34	9	Fine-Coarse Sandstone	40	25% Carb	10% Sid	3% Chl	2% Qtz overgrowth	10
49	3915.74	9	Medium Sandstone	20	15% Sid	5% Qtz overgrowth			10
50	3917.06	9	Fine-Coarse Sandstone	35	20% Carb	10% Chl	5% Qtz overgrowth		10
51	3918.64	4o	Fine Sandstone	10	Sid				10
52	3920.04	4o	Fine Sandstone	15	Sid				0
53	3921.98	9	Fine-Medium	35	20% Carb	10% Chl	5% Qtz overgrowth		10
54	3924.50	9	Fine Sandstone	38	20% Sid	10% Chl	5% Carb	3% Qtz overgrowth	10
55	3926.15	2b	Fine Sandstone	10	5% Qtz overgrowth	4% Carb	1% Sid		10

Abbreviations: Chl = chlorite, Sid = siderite, Carb = carbonates like calcite, Fe-calcite, Mg-calcite, ankerite, or dolomite, pyrite is either framboidal or platy pyrite, Qtz = quartz. Mineral abbreviations after Kretz, 1983.

Table 4.2: Summary of Petrography with Lithofacies at Peskowesk A-99

Well: Peskowesk A-99				Cement: listed in chronological order where apparent and indicated by (#); otherwise order is unknown					Porosity
#	Depths (m)	Lithofacies (after Karim et al., 2008)	Rock Types	% of total rock	cement 1: mineral	cement 2: mineral	cement 3: mineral	other cements	remaining porosity as % of total rock
1	2209.83	5	Fine Sandstone	15	Pyrite				15
2	2221.17 (a)	1	Mudstone	25	20% Pyrite	5% Sid			2
3	2221.17 (b)	1	Mudstone	10	8% Pyrite	1% Carb	1% Qtz overgrowth		1
4	2231.82	4x	Fine Sandstone	20	10% Chl	5% Qtz overgrowth	3% Pyrite	2% Kao	20
5	2245.84	4x	Coarse Sandstone	6	5% Sid	1% Pyrite			30
6	2249.39	4x	Medium Sandstone	16	5% Sid	5% Chl	4% Pyrite	2% Qtz overgrowth	10
7	2275.64	1	Mudstone	40	30% Carb	10% Pyrite			0
8	2275.70	1	Mudstone	25	20% Sid	4% Pyrite	1% Qtz overgrowth		20
9	2481.34 (a)	3a	Fine Sandstone	30	25% Sid	3% Pyrite	2% Qtz overgrowth		0
10	2481.34 (b)	3a	Fine Sandstone	30	25% Sid	5% Pyrite			1
11	2482.68	2c	Fine Sandstone	50	30% Sid	15% Pyrite	4% Qtz overgrowth	1% Chl	3
12	2492.25	3	Fine Sandstone	8	4% Pyrite	2% Qtz overgrowth	2% Carb		10
13	2493.19 (a)	3	Fine Sandstone	20	15% Pyrite	5% Qtz overgrowth			2
14	2493.19 (b)	3	Fine Sandstone	22	20% Pyrite	2% Qtz overgrowth			10
15	2492.02	8	Fine Sandstone	11	10% Pyrite	1% Qtz overgrowth			2
16	2931.91	3	Fine Sandstone	33	15% Qtz overgrowth	15% Carb	3% Pyrite		0
17	2942.03	4x	Fine Sandstone	40	25% Carb	10% Sid	5% Pyrite		2
18	2945.38	0	Fine Sandstone	25	12% Carb	10% Qtz overgrowth	3% Pyrite		25
19	3795.24 (a)	1	Fine Sandstone	47	42% Sid	4% Pyrite	1% Carb		2
20	3795.24 (b)	1	Fine Sandstone	50	40% Sid	5% Pyrite	5% Carb		2
21	3796.50	5	Fine Sandstone	25	20% Pyrite	3% Carb	2% Qtz overgrowth		0
22	3813.15	3o	Muddy Sandstone	25	20% Carb	4% Pyrite	1% Qtz overgrowth		0
23	3813.63	3o	Muddy Sandstone	30	18% Carb	10% Pyrite	2% Qtz overgrowth		0

Abbreviations: Chl = chlorite, Sid = siderite, Carb = carbonates like calcite, Fe-calcite, Mg-calcite, ankerite, or dolomite, pyrite is either framboidal or platy pyrite, Qtz = quartz. Mineral abbreviations after Kretz, 1983.

4.2 PETROGRAPHIC RESULTS

4.2.1 Introduction

Using optical microscopy and back-scattered electron imaging, the textural relationships between diagenetic cements, detrital minerals and layers in identified coated grains were examined at both studied wells. Cements fill pore space as small as 5 μm and as wide as 300 μm . Samples were further investigated using petrography and X-ray diffraction. 55 thin sections from Thebaud C-74 were studied by optical microscopy (Table 4.1). 14 representative probe thin sections were selected for EMP chemical analysis (App. 4.3b). At Peskowsk A-99, 23 thin sections were studied using the optical microscope (Table 4.2), and 17 representative probe thin sections were studied using the EMP for chemical analysis (App. 4.4b). At Thebaud C-74, 23 samples have been newly collected for the purpose of this thesis, and the remaining 32 samples were collected from previous projects. All 23 new samples at Thebaud C-74 plus 52 samples collected for the purpose of this thesis, from Peskowsk A-99 were studied using X-ray diffraction (App. 4.5 and 4.6).

4.2.2 Coated Grains

Coated grains preserve a record of sea-floor diagenesis in their concentric layers. A detailed description of coated grain types from both studied wells are given in Table 4.3 and their stratigraphic locations with lithofacies and Transgressive Surface sediment change is given in Table 4.4b. Using EMP chemical analysis, the minerals of the concentric layers in some coated grains were identified in the Thebaud C-74 samples (Table 4.3b). Two types of coated grains have been identified: (a) coated grains (about 100 μm in

Table 4.3: Detailed Description of Coated Grains Types in Studied Wells

CG ¹ Types	CG Serial #	Descriptions	Concentric Layers Mineralogy Younger → Older				Nucleus Mineralogy	Notes
			CL1	CL2	CL3	CL4		
1	CG1	Dismembered coated grain.	Calcite	NA	NA	NA	Kaolinite	App. 4.4a-13
1	CG2	Composite coated grains	Calcite	NA	NA	NA	Kaolinite	App. 4.4a-14
2	CG3	Coated grain with three concentric layers	Siderite	Glaucinite, Glt + Chl	Kaolinite + FeO	NA	Quartz	App. 4.4a-23
2	CG4	Coated grain with three concentric layers	Siderite	Glaucinite, Chl + Glt	Illite	NA	Quartz	Fig. 4.1C
2	CG5	Coated grain with three concentric layers	Siderite	Kaolinite + TiO ₂	Kaolinite + FeO	NA	K-feldspar	App. 4.4a-25
2	CG6	Dismembered coated grain.	Siderite	Kaolinite	Glaucinite, Glt + Chl	NA	Quartz	App. 4.4a-26
2	CG7	Coated grain with three concentric layers	Siderite	Chlorite	Glaucinite	NA	Quartz	App. 4.4a-27
2	CG8	Superficial coated grain with a single coat	Chlorite + Glaucinite	NA	NA	NA	Quartz	App. 4.4a-28
2	CG9	Coated grain with a single coating	Siderite	NA	NA	NA	Chlorite	App. 4.4a-33
2b	CG10	Coated grain with a single coating	Glaucinite + Chlorite	NA	NA	NA	Kaolinite + Quartz	App. 4.4a-35
3a	CG11	Coated grain with two concentric layers	Fe-calcite	Pyrite + CaO	NA	NA	Pyrite	Fig. 4.1E
2	CG12	Coated grain with two concentric layers	Siderite + Glaucinite	Glaucinite	NA	NA	Fe-calcite	Fig. 4.2B
2	CG13	Superficial coated grain with a single coat	Glaucinite	NA	NA	NA	Sid + Chl intraclast	App. 4.4a-43
2b	CG14	Coated grain with two concentric layers	Chlorite	Chlorite + Glaucinite	NA	NA	Quartz	Fig. 4.1D
3b	CG15	Coated grain with four concentric layers	Mg-calcite	Mg-Fe calcite	Illite	Ankerite	Fe-calcite	Fig. 4.1F
3b	CG16	Asymmetrical coated grain, with single coating.	Mg-calcite	NA	NA	NA	A mixture of carbonates*	* Euhedral Sid App. 4.4a-67
3a	CG17	Asymmetrical coated grain with three coats	Mg-calcite	Pyrite	Ankerite	NA	Fe-calcite	App. 4.4a-70
3b	CG18	Coated grain with three concentric layers	Mg-Fe calcite	Mg-calcite	Ankerite	NA	Chlorite	App. 4.4a-72
3b	CG19	Coated grain with two concentric layers	Mg-calcite	Ankerite	NA	NA	Ankerite + Glaucinite	App. 4.4a-74

Table 4.3: Detailed Description of Coated Grains Types in Studied Wells

CG ¹ Types	CG Serial #	Descriptions	Concentric Layers Mineralogy Younger → Older				Nucleus Mineralogy	Notes
			CL1	CL2	CL3	CL4		
2b	CG20	Superficial coated grain with a single coating	Chlorite	NA	NA	NA	Chlorite + Glauconite	Fig. 4.1A
2b	CG21	Superficial coated grain with concentric layers of 1 mineral	Chlorite	NA	NA	NA	Fe-calcite	App. 4.3a-8
2c	CG22	Coated grain with two concentric layers	Franc. + Glauconite	Franc. + Glauconite	NA	NA	Chlorite + Glauconite	App. 4.3a-13
2e	CG23	Coated grain with three concentric layers	Chlorite + Glauconite	Chlorite + Glauconite	Illite	NA	Quartz	App. 4.3a-15
2e	CG24	Coated grain with a single coating	Illite	NA	NA	NA	Pb contaminated Qtz	App. 4.3a-19
2d	CG25	Coated grain with multiple concentric layers	Pyrite + Ab	Pyrite + Ab	Pyrite + Ab	Chl + Glt + Ab	Berthierine + Na ₂ O	App. 4.3a-29
2	CG26	Coated grain with two concentric layers	Sid + Glt + Na ₂ O	Glauconite	NA	NA	Chlorite	App. 4.3a-30
2e	CG27	Coated grain with a single coating	Glauconite + Chlorite	NA	NA	NA	Quartz	App. 4.3a-37

Type 1: Clay nucleus with carbonate concentric layers

Type 2: Detrital nucleus with concentric layers made up of Fe carbonate (siderite or Fe-calcite), chlorite, glauconite and clay minerals. Variation may include concentric layers of francolite or berthierine (2c and 2d). This type is generally Fe-rich.

Type 3: Ca-Mg carbonate nucleus and concentric layers with or without phosphorite minerals. Variations may include pyrite or glauconite.

Subdivisions with small alphabets (e.g. a, b, or c) indicate a variation in coated grain types from the above general description.

CG¹: coated grains, chl: chlorite, kln: kaolinite, Glt: glauconite, Qtz: quartz, Sid: siderite

Table 4.4: Stratigraphic Distribution of Coated Grains in Studied Wells

Wells	Depths (m)	Facies	Packet ¹	TS Change ²	CG ³ Types	CG Serial #	Descriptions
Peskowesk A-99	2221.17	1	NA	NA	1	CG1	Dismembered coated grain.
	2221.17	1	NA	NA	1	CG2	Composite coated grains
	2275.64	2c	NA	NA	2	CG3	Coated grain with three concentric layers
	2275.64	2c	NA	NA	2	CG4	Coated grain with three concentric layers
	2275.64	2c	NA	NA	2	CG5	Coated grain with three concentric layers
	2275.64	2c	NA	NA	2	CG6	Dismembered coated grain.
	2275.64	2c	NA	NA	2	CG7	Coated grain with three concentric layers
	2481.34	3a	7	A	2	CG8	Superficial coated grain with a single coat
	2481.34	3a	7	A	2	CG9	Coated grain with a single coating
	2482.68	2c	7	A	2b	CG10	Coated grain with a single coating
	2482.68	2c	7	A	3a	CG11	Coated grain with two concentric layers
	2492.25	3	NA	NA	2	CG12	Coated grain with two concentric layers
	2492.25	3	NA	NA	2	CG13	Superficial coated grain with a single coat
	2493.19	3	6	A-	2b	CG14	Coated grain with two concentric layers
	3813.15	3o	NA	NA	3b	CG15	Coated grain with four concentric layers
	3813.15	3o	NA	NA	3b	CG16	Asymmetrical coated grain, with single coating
	3813.15	3o	NA	NA	3a	CG17	Asymmetrical coated grain with three coats
	3813.63	3o	NA	NA	3b	CG18	Coated grain with three concentric layers
	3813.63	3o	NA	NA	3b	CG19	Coated grain with two concentric layers

Table 4.4: Stratigraphic Distribution of Coated Grains in Studied Wells

Wells	Depths (m)	Facies	Packet ¹	TS Change ²	CG ³ Types	CG Serial #	Descriptions
Thebaud C-74	3859.95	3l	4	B-	2b	CG20	Superficial coated grain with a single coat
	3862.91	3	3	A-	2b	CG21	Superficial coated grain with a single coat
	3863.09	3	3	A-	2c	CG22	Coated grain with two concentric layers
	3864.51	4o	3	A-	2e	CG23	Coated grain with three concentric layers
	3866.79	2c	NA	NA	2e	CG24	Coated grain with a single coating
	3902.65	3b	1	A+	2d	CG25	Coated grain with two concentric layers
	3902.65	3b	1	A+	2	CG26	Coated grain with two concentric layers
	3921.98	9	NA	NA	2e	CG27	Coated grain with a single coating

¹: A packet is defined as the sediment above and below a TST. This packets are not available for all depths were coated grains are identified

²: TS change compares the sediments below the TST with that above the TST which is the inferred magnitude of environmental change.

³: Coated grains

Type 1: Clay nucleus with carbonate concentric layers

Type 2: Detrital or Fe-calcite nucleus with concentric layers made up of siderite, chlorite, glauconite and clay minerals. Variation may include concentric layers of francolite or berthierine (2c and 2d). This type is generally Fe-rich.

Type 3: Ca-Mg carbonate pyrite or chlorite nucleus and concentric layers made up principally of Mg-calcite, ankerite or Fe-calcite. Variations may include illite.

Subdivisions with small alphabets (e.g. a, b, or c) indicate a variation in coated grain types from the above general description.

diameter) with chlorite and glauconite as principal minerals (Fig. 4.1A) and (b) coated grains (about 200 μm in diameter) consisting of Fe-calcite and chlorite (Fig. 4.1B).

Calcite (Fe or Mg rich) identified in coated grains is interpreted to be of early generation. Note that calcite usually forms during later recrystallization, perhaps through meteoric water. It is however possible that calcite in the coated grains in this study is of later diagenesis with an aragonite precursor. Aragonite and calcite are polymorphs, and they can only be distinguished by chemical analysis not petrographic studies.

The chlorite and glauconite coated grains at Thebaud C-74 (e.g. Fig. 4.1A) occur in mudstone with siderite replaced burrows and shelly fragments. There are coated grains consisting of a single layer made up of chlorite with the nucleus a mixture of chlorite and glauconite. The Fe-calcite and chlorite coated grains (e.g. Fig. 4.1B) occur in very coarse-grained sandstone with siderite cementation, and consist of concentric layers made up of Fe-calcite and chlorite.

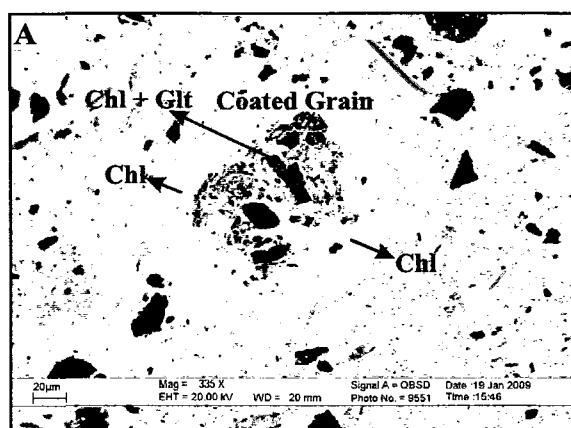
At Peskowsk A-99, coated grains about 240 μm in diameter, have three concentric layers made up of illite, chlorite plus glauconite, and siderite with the siderite being the youngest (outermost) layer (Fig. 4.1C) with detrital quartz nucleus, or have two concentric layers made up of chlorite plus glauconite, and chlorite as the youngest layer also with a detrital quartz nucleus (Fig. 4.1D). Other coated grains (~ 50 μm in diameter) have two concentric layers made up of Fe-calcite in the outer layer and pyrite with a nucleus made up of pyrite crystals (Fig. 4.1E), and some coated grains (~ 240 μm in

Figure 4.1: Various BSE images from both studied wells showing coated grains.

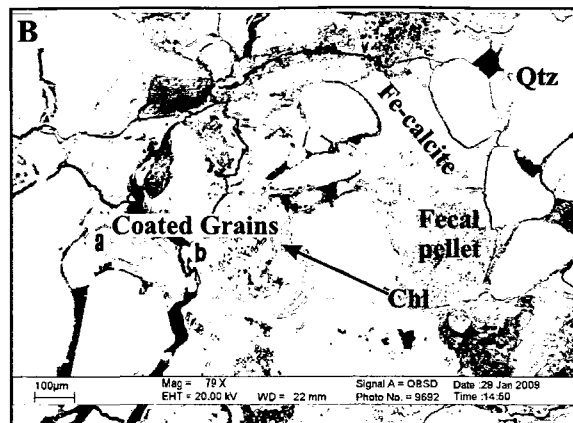
Thebaud C-74 (A) 3859.95 m: mudstone with siderite cementation and few shelly fragments. Coated grain consists of chlorite plus glauconite nucleus and a single layer made up of chlorite. (B) 3862.91 m: very coarse-grained sandstone (pebbles present) with siderite cementation and fecal pellet. Coated grains (a) and (b) with an asymmetric form. Both coated grains have an Fe-calcite nucleus and concentric layers made up of chlorite and Fe-calcite. The Fe-calcite may form as a result of chlorite dissolution due to the presence of chlorite relics within the Fe-calcite. Peskowsk A-99 (C) 2275.64: reddish brown mudstone formed as a result of siderite cementation. Coated grain has a quartz nucleus with three concentric layers. The youngest layer is made up of siderite with glauconite and chlorite as the middle layer, and the oldest layer is made up of illite. (D) 2493.15: sandstone with sparse shelly fragments and siderite cementation. Coated grain is made up of a quartz nucleus with a single layer of chlorite. (E) 2482.68 m: sandstone with 15% shelly fragments (some shale removed from sample). Coated grain made up of a pyrite crystals nucleus and an outer layer of microcrystalline calcite and pyrite. (F) 3813.15 m: muddy TST sandstone with shelly fragments. Coated grain has an Fe-calcite nucleus with four concentric layers made up of a younger Mg-calcite layer, followed by a layer made up of Mg-Fe-calcite, an illite middle layer and an ankerite layer as the oldest layer.

Abbreviations: Chl = chlorite, Sid = siderite, Glt = glauconite, Py = pyrite either as framboidal or platy pyrite, Qtz = quartz. Mineral abbreviations after Kretz, 1983.

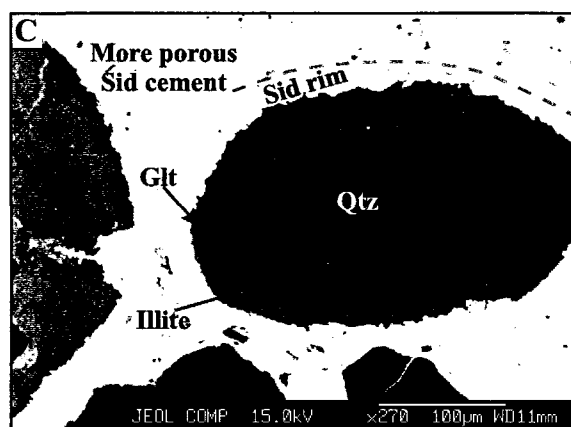
FIGURE 4.1



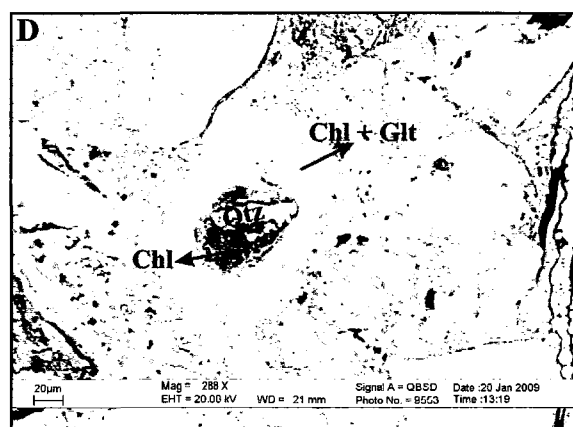
Thebaud C-73 3859.59 m



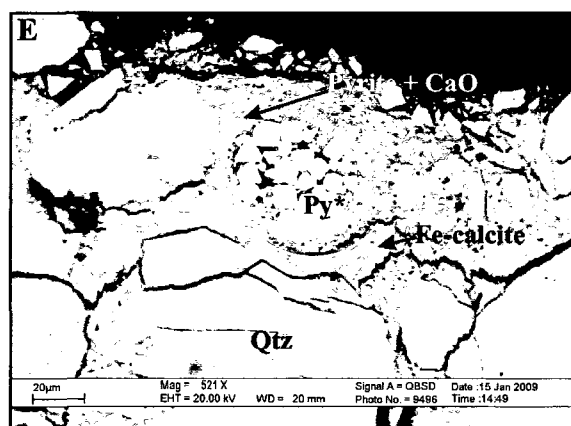
Thebaud C-74 3862.91 m



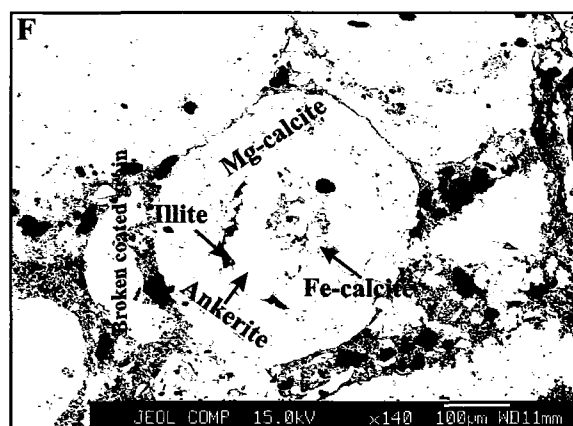
Peskowsk A-99 2275.64 m



Peskowsk A-99 2493.19 m



Peskowsk A-99 2482.68 m



Peskowsk A-99 3813.15 m

*= SEM Identification

diameter) have four concentric layers made of ankerite, illite, Mg-Fe-calcite, and a younger Mg-calcite outermost layer with a Fe-calcite nucleus (Fig. 4.1F).

The siderite, glauconite, and illite coated grains at Peskowsk A-99 (e.g. Fig. 4.1C) occur in siderite-cemented mudstone. The coated grain in Fig. 4.1D occurs in greenish sandstone with shelly and wood fragments. The coated grain with Fe-calcite and pyrite mineralogy (e.g. Fig. 4.1E) occurs in sandstone with 15% shelly fragments. Coated grains with Fe-calcite, illite, ankerite and Mg-calcite (e.g. Fig. 4.1F) occur in reworked sandstones with shelly fragments.

The coated grains at Thebaud C-74 occur in facies 2c, 3, 3b, 3l, and 4o. At Peskowsk A-99, coated grains occur in facies 2c (e.g. Figs. 4.1C and 4.1E) with abundantly bioturbated sandstone (60-90 %), some coated grains occur in facies 3 with abundantly bioturbated reworked sediments (e.g. Fig. 4.1D), and others occur in bioclastic limestone of facies 3o in the Mic Mac Formation (e.g. Fig. 4.1F).

4.2.3 Carbonate Cement

At Thebaud C-74, Fe-calcite is the most common type of carbonate cement. Fe-calcite is identified as cement that fills the intergranular pores between quartz grains (Fig. 4.2A), and sometimes post-dating quartz-overgrowth usually associated with the presence of chlorite grains (Fig. 4.2B). Mg-calcite (or calcite in some samples) was identified with chlorite and/or glauconite in intraclasts (Fig. 4.2C).

Other carbonate cements identified include ankerite grains (Fig. 4.2D) and euhedral crystals of siderite (occurring with chlorite) with low totals (Fig. 4.2E), similar in texture to the early siderite identified by Karim et al. (2008). X-ray diffraction (5 wt % detection limit) studies showed the presence of siderite in only a very few samples, and siderite cement was identified in small amounts at more depths using optical microscopy (Table 4.1).

Fe-calcite, Mg-calcite and siderite cements all occur in both the bioclastic limestone deposits (facies 3l) and open shelf deposits (facies 1) at Thebaud, while late Fe-calcite post-dating quartz-overgrowths occur in tidal estuary sandstones (facies 4o) with abundant *Ophiomorpha* and mud drapes but lacking cross-bedding. The late ankerite is present in thick-bedded graded sandstone (facies 9).

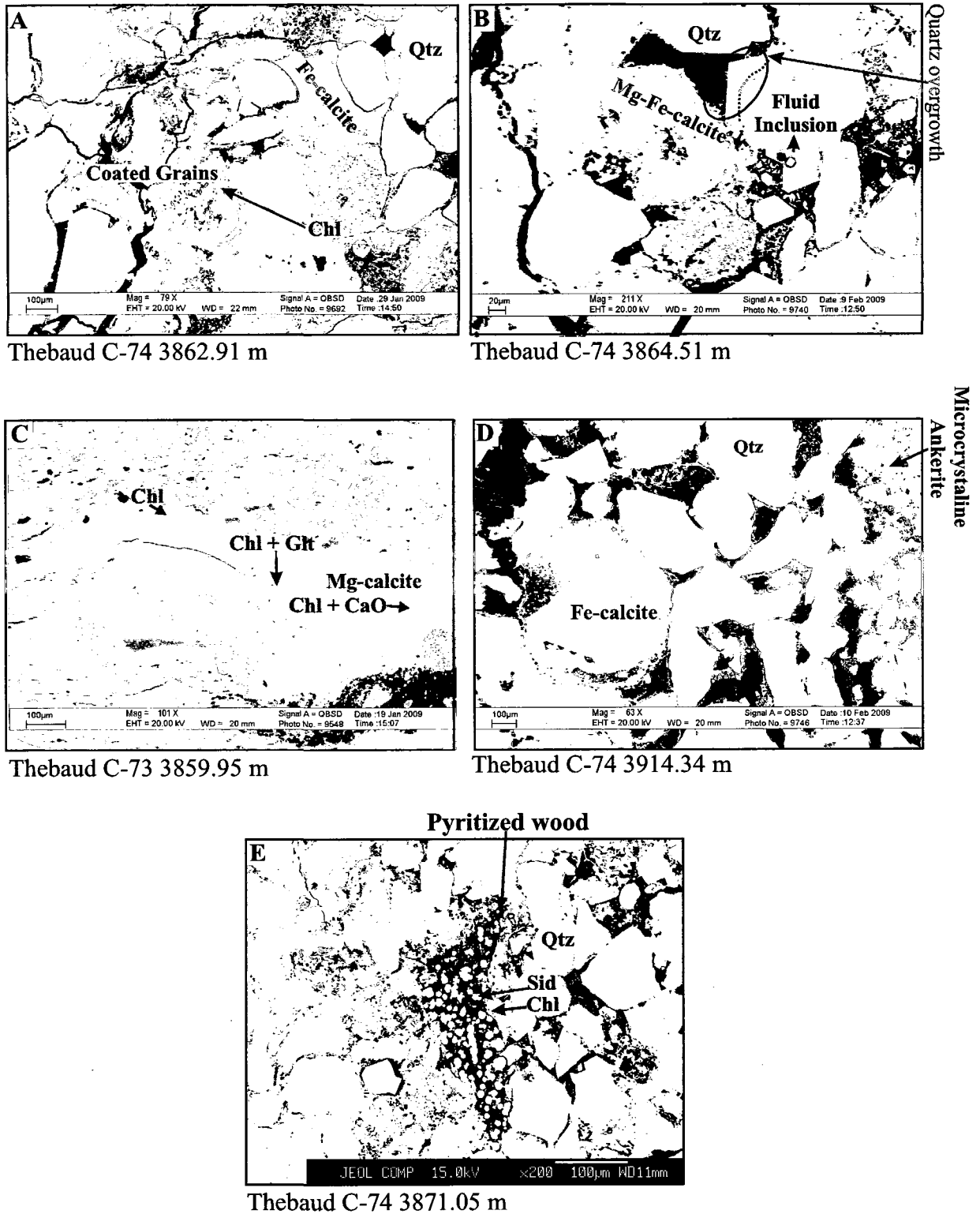
At Peskowsk A-99, the carbonate cements present occur in a variety of forms. In the Logan Canyon sandstones, carbonate cements occur as (i) fine-grained pore-filling siderite cement pre-dating quartz-overgrowth (Fig. 4.3A), (ii) fine-grained pore-filling calcite cement (Fig. 4.3B), (iii) Mg-rich microcrystalline siderite, as euhedral crystals rimming K-feldspar grains (Fig. 4.3C), (iv) calcite layers in a coated grain (Fig. 4.3D), and (v) pore-filling siderite grains rimming coated grains (150 μm and 240 μm) with layers consisting of glauconite, kaolinite and chlorite (Fig. 4.3E) or illite (Fig. 4.3F).

In the Missisauga and Mic Mac Formations sandstones at Peskowsk A-99, carbonate cements occur as (i) microcrystalline Fe-calcite outer layer in coated grains with nucleus

Figure 4.2: Various BSE images from the Thebaud C-74 well. (A) 3862.91 m: very coarse-grained sandstone (pebble sized sand present) with siderite cementation and fecal pellet. Coated grain (a) and (b) with an asymmetric form. Both coated grains have a carbonate nucleus of Fe-calcite mineralogy and concentric layers made up of chlorite and Fe-calcite. The Fe-calcite forms as a result of chlorite dissolution due to the presence of chlorite relics within the Fe-calcite. (B) 3864.51 m: fine grained sandstone with thick beds of mudstone. Fe-calcite and Mg-calcite cements occurring as a result of feldspar dissolution (Fe-Mg-calcite forming on relics of feldspars). Quartz overgrowth also present. (C) 3859.95 m: mudstone with siderite burrows and shelly fragments. Mg-calcite cement coating an intraclast with chlorite and calcite mineralogy. (D) 3914.34 m: fine to coarse-grained sandstone with rare pebbles and siderite-cemented nodules. Fe-calcite cement present in round clusters with microcrystalline ankerite cement. (E) 3871.05 m: fine-grained sandstone with silty mudstone and burrows. Pyritized wood with fine-grained siderite and chlorite cements.

Abbreviations: Chl = chlorite, Sid = siderite, Glt = glauconite, Qtz = quartz.
Mineral abbreviations after Kretz, 1983.

FIGURE 4.2

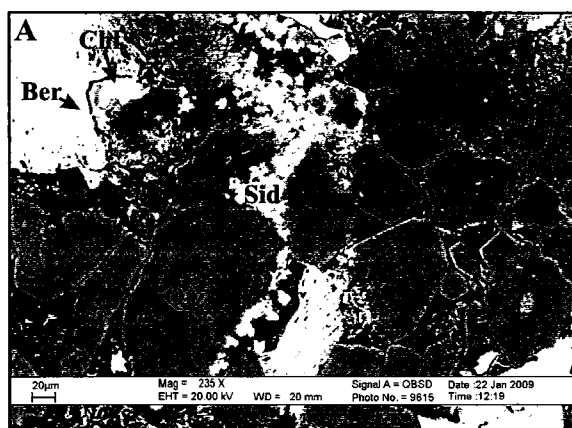


*= SEM Identification

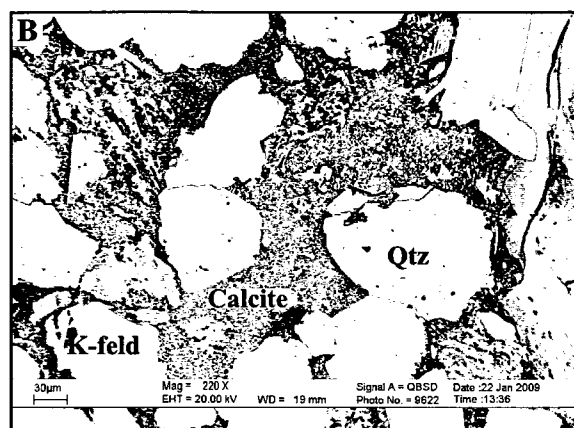
Figure 4.3: Various BSE images from the Peskowsk A -99 well. (A & B) 2209.83 m: homogeneous sandstone with dispersed wood fragments. (A) Microcrystalline siderite filling pores between detrital quartz grains, later formed quartz overgrowths, with the berthierine later forming chlorite cement. (B) Microcrystalline calcite cement filling wide pore spaces between detrital quartz grains. Analyzed K-feldspar is either a zoned detrital grain or a detrital K-feldspar with different composition diagenetic K-feldspar overgrowth. (C & D) 2221.17 m: mudstone with several whitish brown nodules (not shown on both images). (C) Lithic clast of K-feldspar grains rimmed by euhedral crystals of Mg-siderite. (D) A symmetrical (equal layers) coated grain with calcite layers included in a composite, dismembered coated grain, also with calcite layers and chlorite nucleus. (E & F) 2275.64 m: reddish brown mudstone as a result of siderite cementation. (E) Coated grain has a quartz nucleus and three concentric layers. Siderite is the youngest layer, glauconite and chlorite make up the middle layer and kaolinite plus FeO (probably chlorite) make up the oldest layer. (F) Coated grain with a quartz nucleus and three concentric layers made of illite, glauconite plus chlorite, and siderite, respectively in order of growth.

Abbreviations: Chl = chlorite, Sid = siderite, Glt = glauconite, Kln = kaolinite, K-feld = K-feldspar, Mg-Sid = Mg-siderite, Ber = berthierine, Qtz = quartz. Some mineral abbreviations after Kretz, 1983.

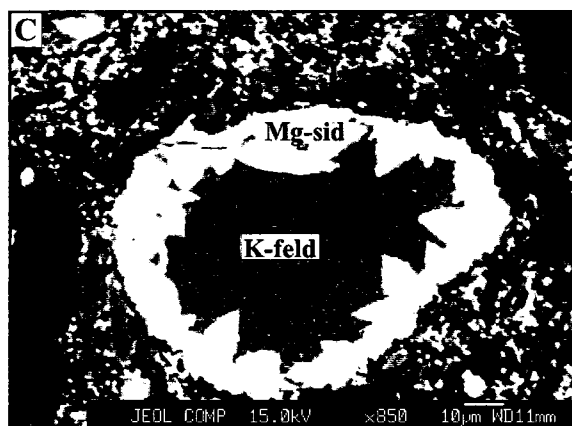
FIGURE 4.3



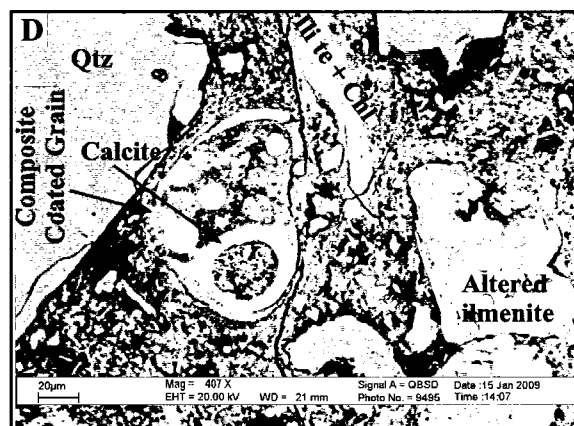
Peskowesk A-99 2209.83 m



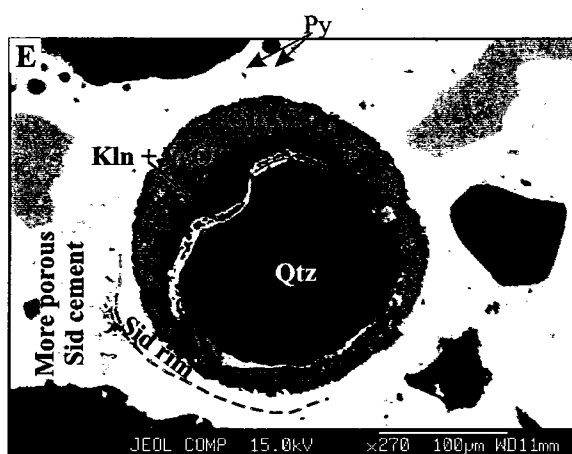
Peskowesk A-99 2209.83 m



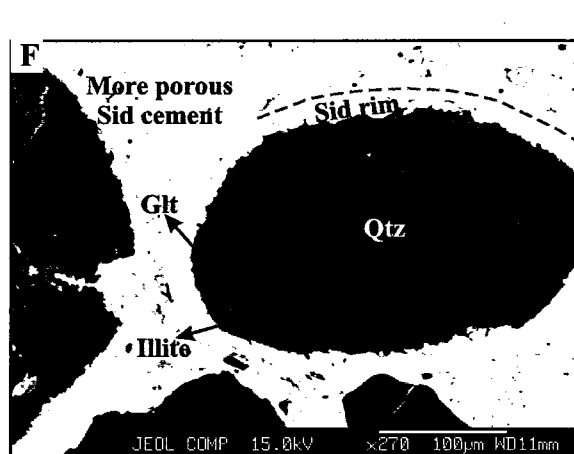
Peskowesk A-99 2221.17 m



Peskowesk A-99 2221.17 m



Peskowesk A-99 2275.64 m



Peskowesk A-99 2275.64 m

*= SEM Identification

made up of pyrite grains (Fig. 4.4A), (ii) pore-filling Fe-calcite post-dating Mg-siderite that appear to be related to K-feldspar dissolution (Fig. 4.4B), (iii) pore-filling calcite post-dating quartz-overgrowth (Fig. 4.4C), (iv) 200 μm foram inifera filled with Fe-calcite (Fig. 4.4D), (v) calcite and Fe-calcite replaced fossils (Fig. 4.4E), and (vi) a 240 μm coated grain (Fig. 4.4F) made up of an Fe-calcite nucleus and four concentric layers of Mg-calcite, Mg-Fe-calcite, illite and ankerite.

The Mg-rich siderite in Fig. 4.3C occurred in open shelf deposits (facies 1), while other identified siderites at Peskowsk A-99 occur in tidal flat deposits (facies 5) and shoreface deposits (facies 2c) with 60-90 % sandstones. The pore-filling calcite occurs in facies 3 sediments with siderite-cemented reworked fine to coarse-grained sandstone with abundant shelly fragments.

4.2.4 Pyrite and Phosphorite Cements

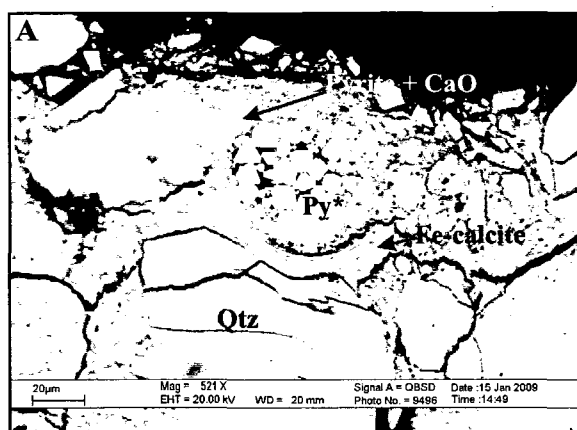
Pyrite is abundant in Thebaud C-74 samples and EMP chemical analyses with optical microscope studies confirm the presence of early framboidal pyrite grains and platy pyrite crystals (Figs. 4.5A and 4.5B). Coated grains (about 100 μm in diameter) in one sample have a nucleus made up of berthierine, albite and pyrite (Fig. 4.5C), and multiple concentric layers made up of chlorite, glauconite and albite as the outermost layers and layers of pyrite plus some albite.

Francolite (carbonate-fluorapatite), a principal mineral of phosphorites, is one of the diagenetic minerals in a coated grain at Thebaud and occurs with pyrite (Fig. 4.5D). Fine-

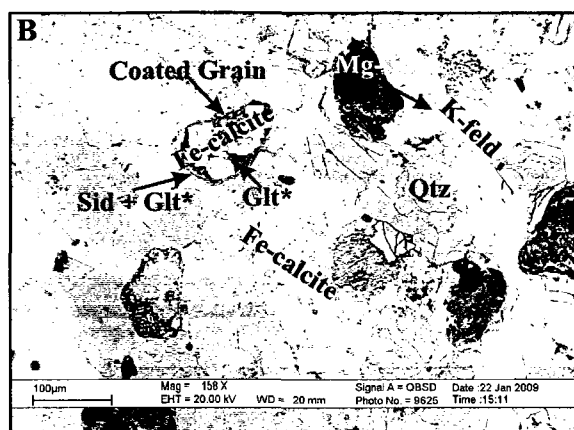
Figure 4.4: Various BSE images from the Peskowsk A-99 well. (A) 2482.68 m: sandstone with 15% shelly fragments (some shale removed from sample). Coated grain made up of a pyrite nucleus and an outer layer of microcrystalline calcite and pyrite. (B) 2492.25 m: sandstone with thin beds of siderite cement and extensive Fe-calcite cementation. Coated grain has an Fe-calcite nucleus with two concentric layers made of siderite and glauconite. (C) 2931.91 m: fine-grained sandstone with prominent greenish burrows. Image of calcite cement in contact with quartz overgrowths. (D & E) 2942.02 m: fine grained sandstone with shelly fragments. (D) Foram filled with calcite, and Fe-calcite. Relics of detrital K-feldspar in a large area of Fe-calcite. (E) Shelly fragment filled with calcite. Extensive calcite cementation. (F) 3813.15 m: muddy TST sandstone with shelly fragments. Coated grain has an Fe-calcite nucleus with four concentric layers made up of a younger Mg-calcite layer, followed by a layer made up of Mg-Fe-calcite, an illite middle layer and an ankerite layer as the oldest layer.

Abbreviations: Ank = ankerite, Sid = siderite, Glt = glauconite, Py = either as framboidal or platy pyrite, K-feld = K-feldspar, Qtz = quartz. Mineral abbreviations after Kretz, 1983.

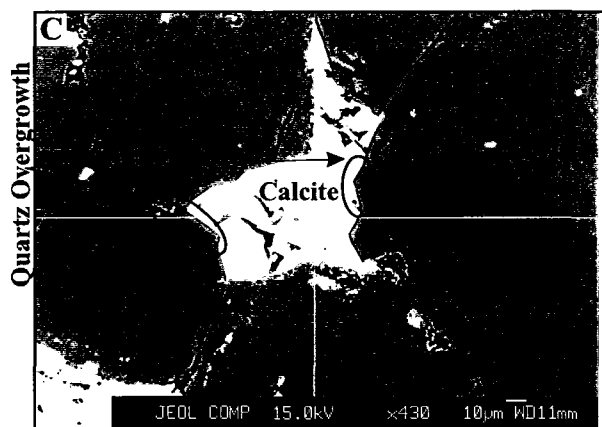
FIGURE 4.4



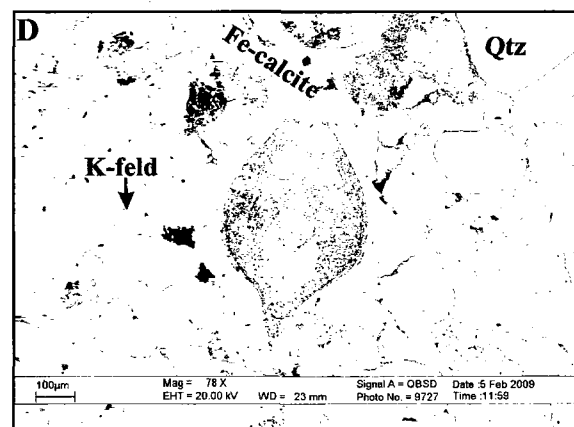
Peskowesk A-99 2482.68 m



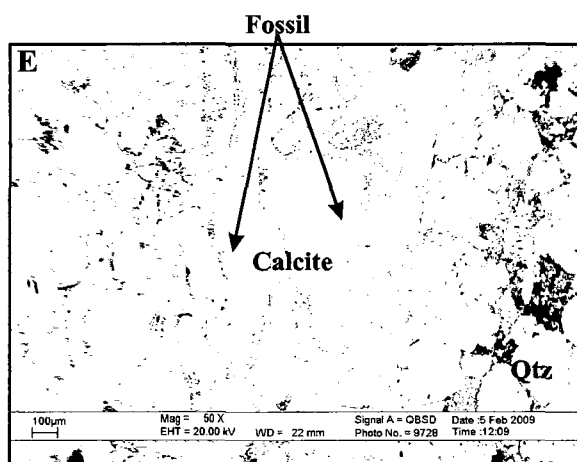
Peskowesk A-99 2492.25 m



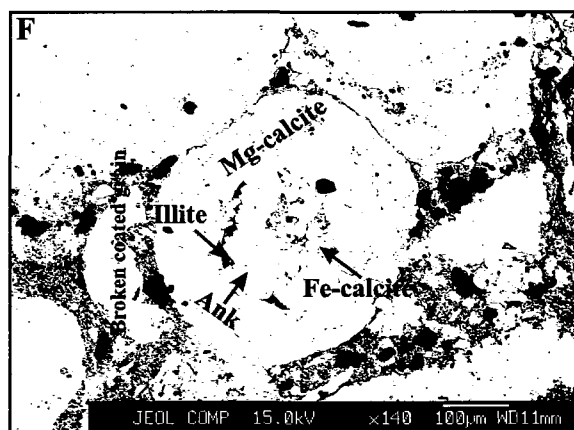
Peskowesk A-99 2931.91 m



Peskowesk A-99 2942.02 m



Peskowesk A-99 2942.02 m



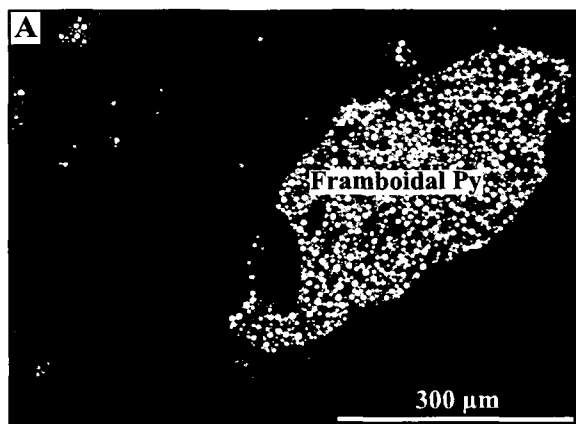
Peskowesk A-99 3813.15 m

*= SEM Identification

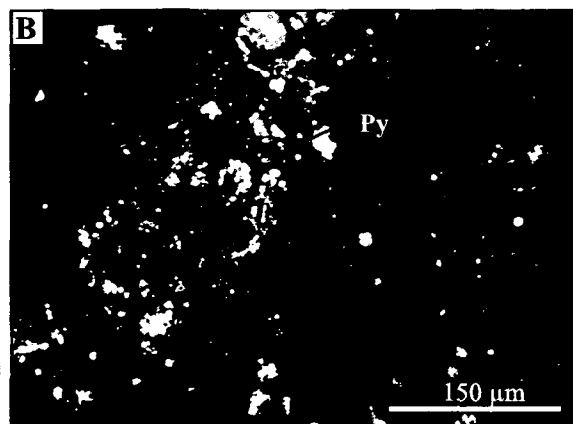
Figure 4.5: microphotographs and BSE images from the Thebaud C-74 well. (A) 3859.95 m (microphotograph): Framboidal pyrite cluster. (B) 3868.39 m (microphotograph): Platy pyrite crystals. (C) 3902.65 m (BSE image): Bioturbated fine to medium-grained sandstone with burrows and siderite cementation. Coated grains in one samples have a nucleus made up of berthierine, albite and pyrite and multiple concentric layers made up of chlorite, glauconite and albite as the outermost layers and layers of pyrite plus some albite. (D) 3863.09 m (BSE image): fine to medium- grained sandstone. Coated grain consist of a nucleus that is a mixture of glauconite, chlorite and pyrite, and an outer layer made up of francolite and glauconite and an outermost layer also made up of francolite and glauconite . (E) 3866.79 m (BSE image): fine grained sandstone with a few coal fragments and burrows. Cements present include calcite, francolite, chlorite and TiO_2 . (F) 3868.38 m (BSE image): bioturbated fine grained sandstone interbedded with silty mudstone with burrows and siderite cementation. Cement present includes Fe-calcite that encloses relics of detrital K-feldspar, francolite and glauconite.

Abbreviations: Chl = chlorite, Glt = glauconite, Py = pyrite, Franc = francolite, Ber = berthierine, Qtz = quartz. Some mineral abbreviations after Kretz, 1983.

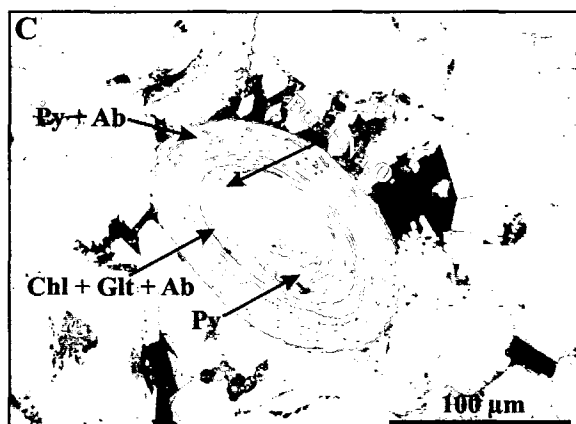
FIGURE 4.5



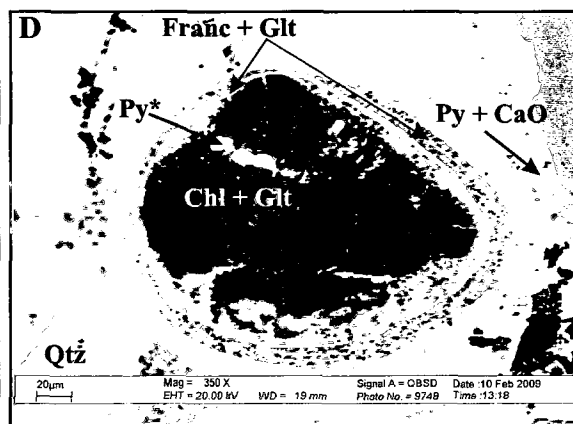
Thebaud C-73 3859.59 m



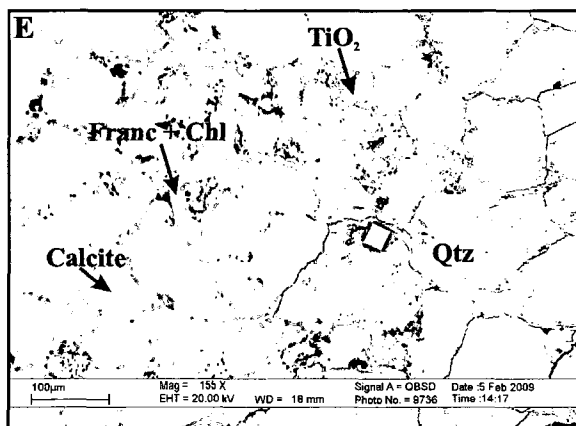
Thebaud C-74 3868.39 m



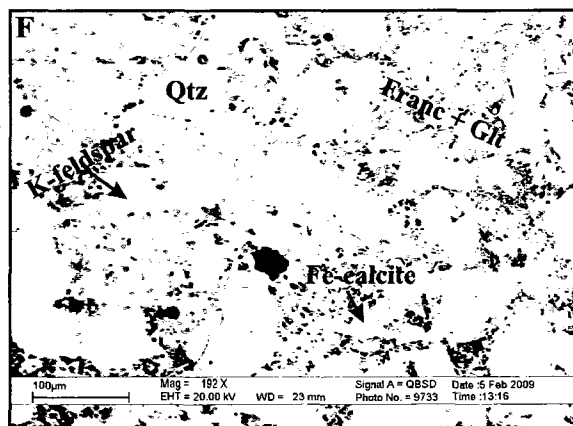
Thebaud C-74 3902.65 m



Thebaud C-74 3863.09 m



Thebaud C-74 3866.79 m



Thebaud C-74 3868.31 m

*= SEM Identification

grained francolite has also been identified occurring with chlorite (Fig. 4.5E) or with glauconite (Fig. 4.5F) as pore-filling cement. The fine-grained francolite in Figs. 4.5E and F occur in samples from facies 2 (shoreface deposits). The occurrences of francolite and pyrite associated with coated grains occur in reworked sediments of facies 3.

Early framboidal pyrite and platy pyrite crystals are abundant in samples from Peskowesk A-99. Framboidal pyrite, identified with EMP chemical analysis and optical microscopy, also occurs within intraclasts (Fig. 4.6A). Pyrite also occurs as pore-filling cement (Fig. 4.6B), and more platy pyrite crystals were found associated with an about 50 μm coated grain (Fig. 4.6C). No francolite or any other phosphate mineral was identified at Peskowesk A-99. However, berthierine as $<5 \mu\text{m}$ grains (Fig. 4.6D) is present in a sandstone with dispersed wood fragments.

The presence of pyrite as both framboids and platy crystals is associated with the reworked sediments of facies 3a and tidal flat deposits (facies 5). Berthierine is associated with tidal flat deposits of facies 5.

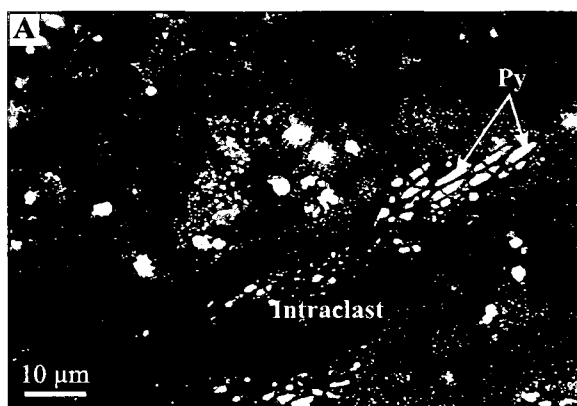
4.2.5 Kaolinite Cement and Concretions

From the X-ray diffraction data, kaolinite is recognized at its highest intensity at 7.08\AA and chlorite at 14\AA . However, chlorite was present at the second level of intensity (002) and is recognized at 7.18\AA (App. 4.5 and 4.6). Because of the close proximity to kaolinite it is difficult to distinguish chlorite from kaolinite and identification of either of these minerals was only possible in samples that had either only a kaolinite peak or only a chlorite peak.

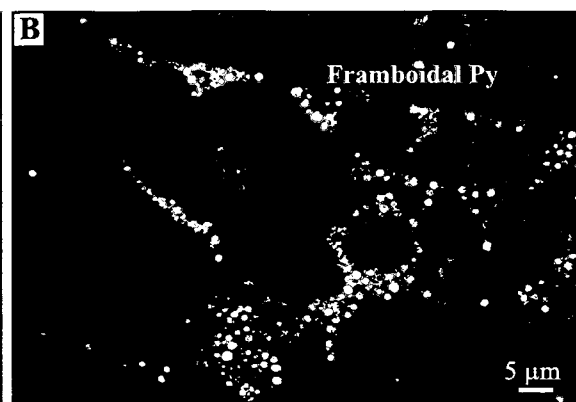
Figure 4.6: *microphotographs and BSE images from the Peskowsk A-99 well. (A) 2942.02 m (microphotograph): Platy and framboidal pyrite grains occurring within an intraclast. (B) 2482.68 m (microphotograph): pore-filing framboidal pyrite. (C) 2482.68 m (BSE image): sandstone with 15% shelly fragments (some shale removed from sample). Coated grain made up of a pyrite crystals nucleus and an outer layer of microcrystalline calcite and pyrite. (D) 2209.83 m (BSE image): sandstone with dispersed wood fragments. Microcrystalline siderite filling some pores between detrital quartz grains. Berthierine fills a pore adjacent to a framework grain with chlorite. Quartz overgrowths have formed where pores are open.*

Abbreviations: Chl = chlorite, Sid = siderite, Ber = berthierine, Qtz = quartz. Mineral abbreviations after Kretz, 1983.

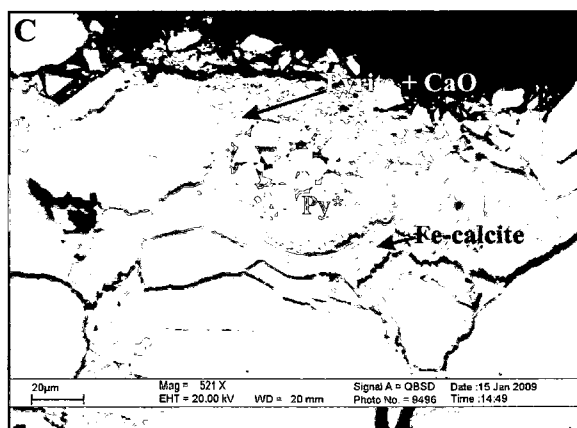
FIGURE 4.6



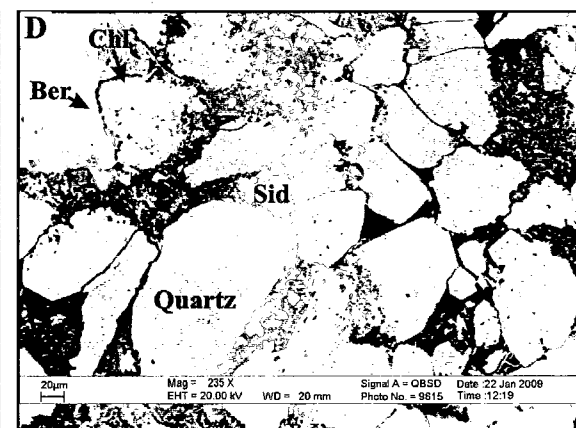
Peskowesk A-99 2942.02 m



Peskowesk A-99 2482.68 m



Peskowesk A-99 2482.68 m



Peskowesk A-99 2209.83 m

*= SEM Identification

Kaolinite is present as pore filling cement at Thebaud C-74 (Fig. 4.7A) in an echinoderm fossil, and as pore- filling cement between detrital quartz grains (Fig. 4.7B). The kaolinite cements were identified in bioclastic limestone deposits of facies 3l and in sediments of facies 9 (river mouth deposits).

Kaolinite is a clay mineral common in sandstones from Peskowsk A-99 as $<5\text{ }\mu\text{m}$ grains (Fig. 4.8A) occurring with calcite. Kaolinite cements identified in a coarsening upward sequence fill empty pore spaces in the sandstones (Fig 4.8B), and this cement is associated with chlorite and calcite. Kaolinite is identified as mixtures with chlorite and glauconite (Fig. 4.8C) and in coated grains together with pyrite (Fig. 4.8D) or with a titania mineral (Fig. 4.8E). Kaolinite mixtures with chlorite were not identified in samples from Thebaud C-74.

Kaolinite cements, and a few mixtures with chlorite occur in tidal flat deposits (facies 5). Other sand sized grains (? intraclasts) made of principally of kaolinite occur in open shelf deposits (facies 1), and the kaolinite in coated grains occur in shoreface deposits (facies 2c) with 60-90 % sandstone and ~10% mudstone and abundant bioturbation.

4.2.6 Chlorite Cement

Petrography studies show that chlorite cement is abundant and widespread throughout Thebaud C-74 (Table 4.1). Chlorite cement occurs with kaolinite in the Thebaud C-74 samples studied using X-ray diffraction (App. 4.5), which is also true for samples from Peskowsk A-99 (App. 4.6). Petrography studies at Peskowsk A-99 identified chlorite

FIGURE 4.7

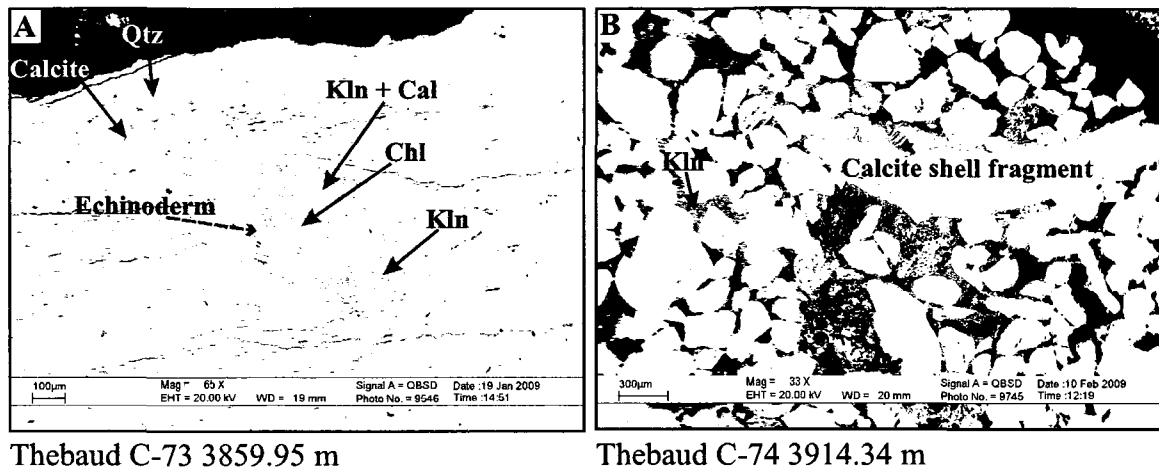


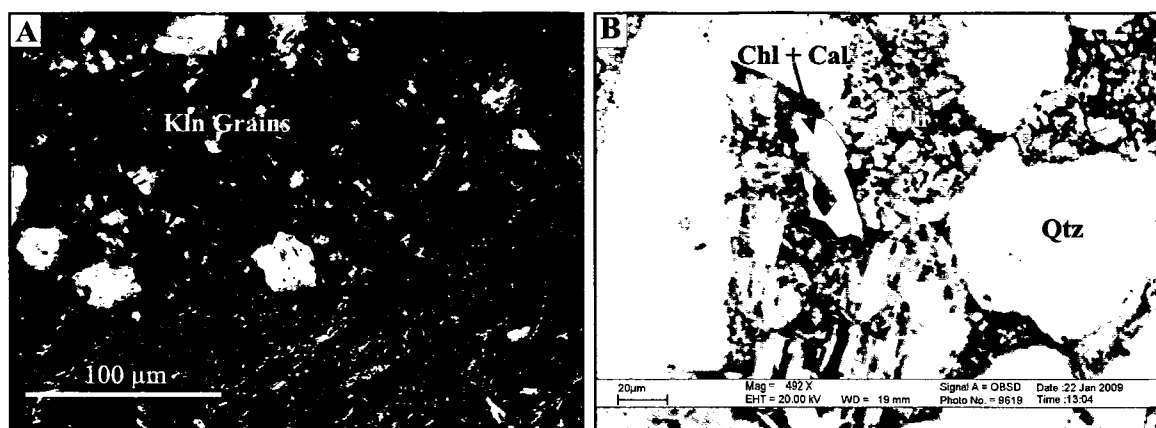
Figure 4.7: Two BSE images from the Thebaud C-74 well. **(A)** 3859.95 m: mudstone with siderite burrows and shelly fragments including echinoderms. Large echinoderm fragment has a glauconite and chlorite coating, and a nucleus made up of kaolinite, calcite and chlorite. **(B)** 3914.34 m: fine to coarse-grained sandstone with rare pebbles and siderite-cemented nodules. Kaolinite cement, occurring with calcite cement, a large calcite shell fragment, and detrital quartz grains.

Abbreviations: Chl = chlorite, Cal = calcite, Kln = kaolinite. Some mineral abbreviations after Kretz, 1983.

Figure 4.8: microphotographs and BSE images from the Peskowsk A-99 well. (A) 2482.68 m (microphotograph: kaolinite grains, and small pieces of lithic clasts. (B & C) 2209.83 m (BSE image): homogeneous sandstone with dispersed wood fragments. (B) Cement present is pore-filling kaolinite cement. (C) kaolinite occurring as a mixture with glauconite and chlorite. (D & E) 2275.64 m (BSE images): reddish brown mudstone as a result of siderite cementation. (D) Coated grain has a quartz nucleus and three concentric layers. Siderite is the youngest layer, glauconite and chlorite make up the middle layer and kaolinite plus FeO (probably chlorite) make up the oldest layer. (E) Coated grain with three concentric layers. The first two layers are made up of kaolinite plus TiO₂ and FeO, and the outermost of siderite and detrital K-feldspar nucleus.

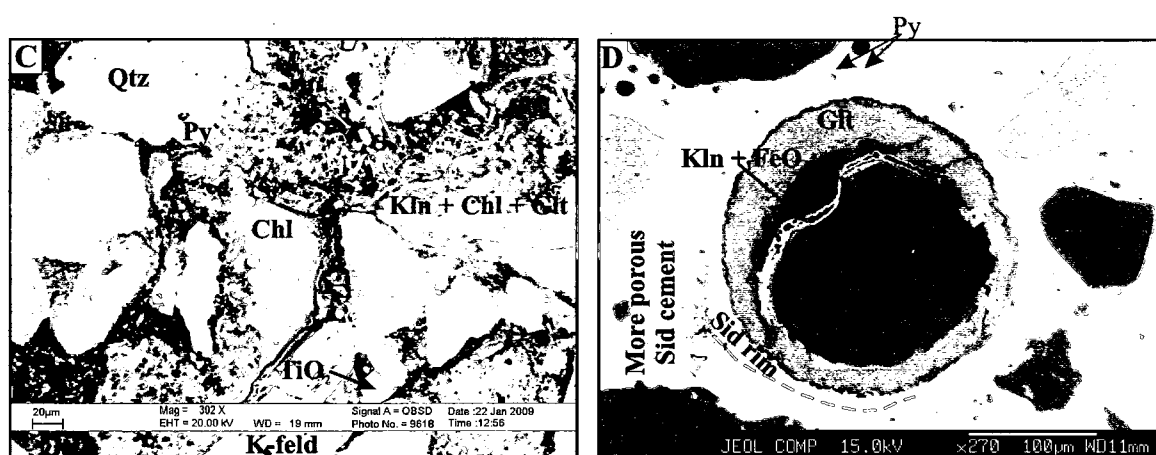
Abbreviations: Chl = chlorite, Sid = siderite, Glt = glauconite, Kln = kaolinite, K-feld = K-feldspar, Cal = calcite, Qtz = quartz. Some mineral abbreviations after Kretz, 1983.

FIGURE 4.8



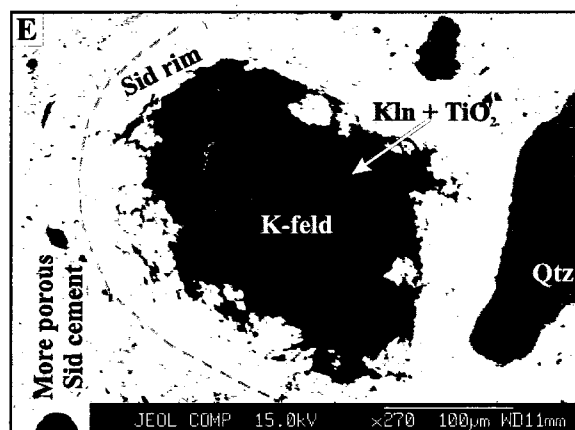
Peskowesk A-99 2482.68 m

Peskowesk A-99 2209.83 m



Peskowesk A-99 2209.83 m

Peskowesk A-99 2275.64 m



Peskowesk A-99 2275.64 m

*= SEM Identification

cements at a few depths (Table 4.2). Intensities for chlorite peaks provide information on chlorite types. Fe-rich chlorite (e.g. berthierine which could later change to chamosite) is associated with odd peaks (001, 003, and 005), while Mg-rich chlorite is associated with even peak intensities (002 and 004).

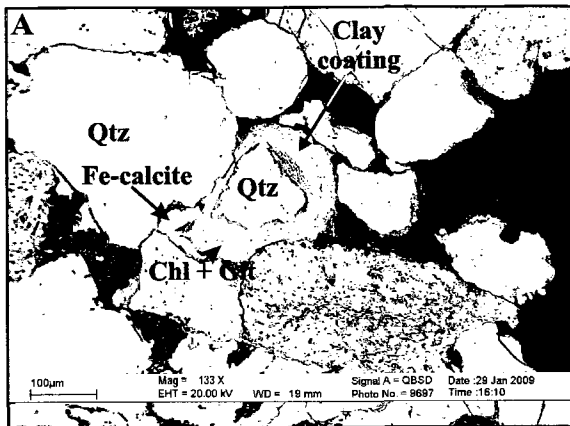
Chlorite is identified in a variety of forms in both studied wells such as: (a) chlorite grains rimming detrital quartz (Fig. 4.9A), (b) pore-filling chlorite occurring in about 50 μm clusters (Fig. 4.9B and C), (c) chlorite replacing framework grains (Fig. 4.9E), (d) chlorite grains mixed with Ti and Ca-minerals rimming a detrital TiO_2 mineral (Fig. 4.9D), and (e) chlorite mixed with glauconite in 100 μm clusters replacing K-feldspar (Fig. 4.9E), or (f) chlorite mixed with Ti and Ca-mineral in a 200 μm detrital lithic clast (Fig. 4.9F). In addition, there are a couple of differences between both wells. The mixture of chlorite with TiO_2 replacing a lithic clast is found only in samples from Peskowsk A-99 (Fig. 4.9F) and the presence of chlorite in coated grain with a single layer, is found only in samples from Thebaud C-74 (Fig. 4.9A).

The chlorite present in this study has a similar mode of occurrence to chlorite studied by Gould (2007) and Karim *et al.* (2008). In addition, the textures are similar e.g. chlorite occurring as thin crystals associated with clay minerals, pore-filling cements, replacing framework grains, in layers in coated grains and in intraclasts. Most chlorite occurrences associated with coated grains and cements replacing framework grains occur in reworked sediments of facies 3, 3a (with mudstone laminae), 3b (lacking bioturbation), and 3l

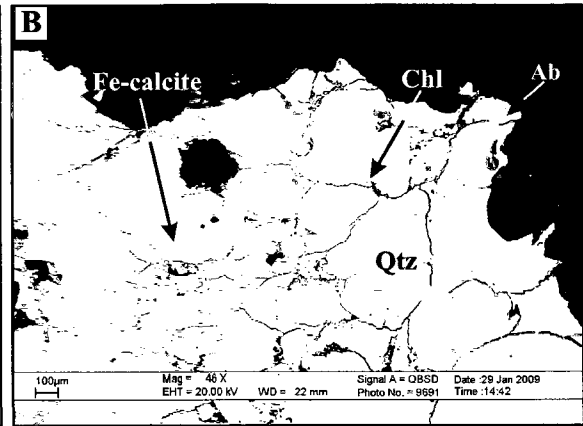
Figure 4.9: Various BSE images from both studied wells. Thebaud C-74 (A) 3921.98 m: fine to medium-grained sandstone with siderite cementation and burrows. Image of detrital quartz with clay (chlorite plus glauconite) coating. (B) 3862.91 m: very coarse-grained sandstone (pebble sized sand present) with siderite cementation. Cement present includes pore-filling calcite and chlorite cements. (C) 3859.95 m: mudstone with siderite burrows and shelly fragments. Echinoderm with Mg-Fe-calcite composition with pores filled with chlorite. Peskowesk A-99 (D) 2481.34 m: sandstone with sparse shelly fragments and siderite cementation. Detrital TiO_2 grain with a single coating of chlorite and calcite. (E) 2221.17 m: mudstone with a whitish brown nodule. Chlorite and glauconite are replacing detrital K-feldspar. (F) 2945.38 m: fine grained sandstone. Chlorite mixed with TiO_2 in a detrital lithic clast.

Abbreviations: Chl = chlorite, Glt = glauconite, K-feld = K-feldspar, Qtz = quartz. Mineral abbreviations after Kretz, 1983.

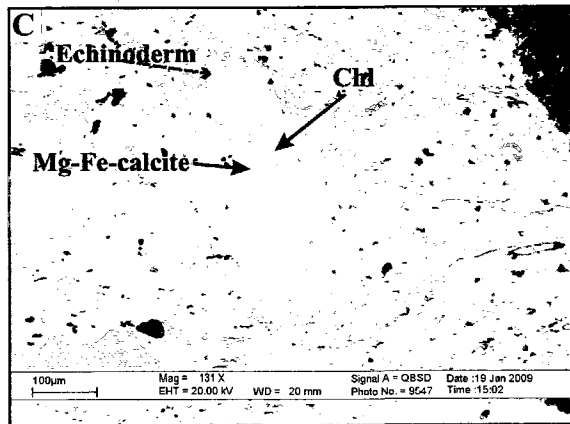
FIGURE 4.9



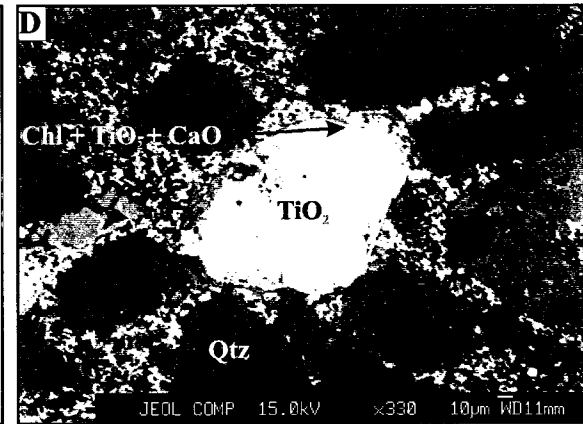
Thebaud C-74 3921.98 m



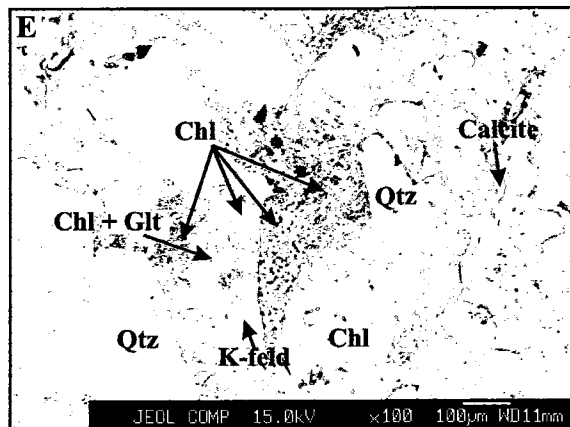
Thebaud C-74 3862.91 m



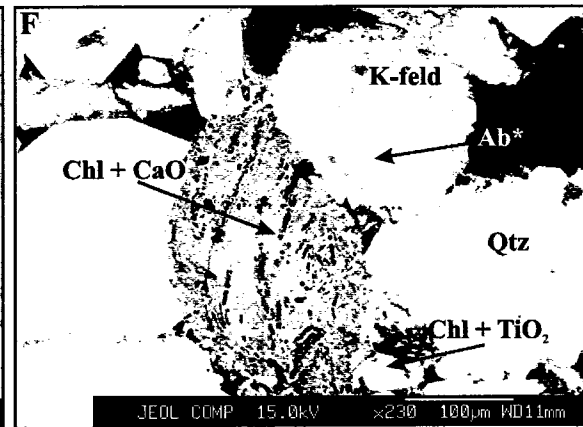
Thebaud C-73 3859.95 m



Peskowesk A-99 2481.34 m



Peskowesk A-99 2221.17 m



Peskowesk A-99 2945.38 m

*= SEM Identification

(bioclastic limestone deposits) at both the Thebaud C-74 and Peskowsk A-99 wells.

Chlorite occurrences in coated grains were found in tidal flat deposits (facies 5).

4.2.7 Quartz Overgrowth

The occurrence of quartz overgrowth is either as a result of early or later diagenesis (30°C to 90°C according to Worden and Burley, 2003). Detailed identification of quartz overgrowth was carried out using optical microscopy and each occurrence is documented as silica cement (Tables 4.1 and 4.2). At Thebaud C-74, the only quartz overgrowth occurrences were associated with fine-grained sandstone with thick beds of mudstone (Fig. 4.10A). The overgrowth for this example occurred on about 150 µm quartz grain identified in facies 4o, fluvial to estuary sandstones rich in *Ophiomopha* and mud drapes.

At Peskowsk A-99, quartz overgrowths are identified on (a) detrital quartz grains in very fine-grained sandstones formed after siderite cementation (Fig. 4.10B), and (b) quartz overgrowth formed after Fe-calcite cementation (Fig. 4.10C). The quartz overgrowth that formed after siderite cement was identified in tidal flat deposits (facies 5), and the quartz overgrowth that formed before Fe-calcite was identified in abundantly bioturbated, siderite-cemented, reworked fine to coarse-grained sandstones of facies 3.

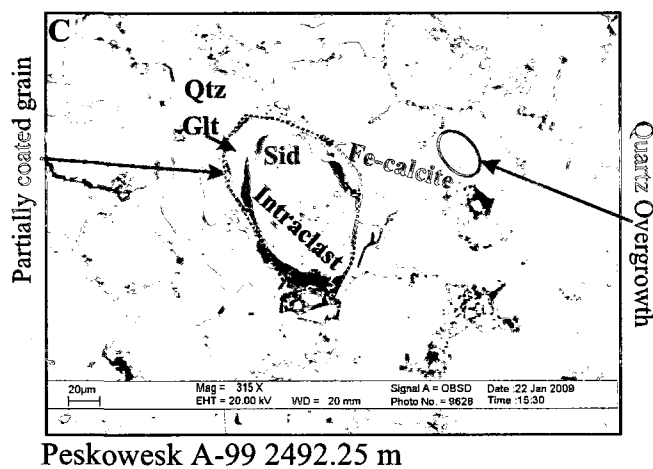
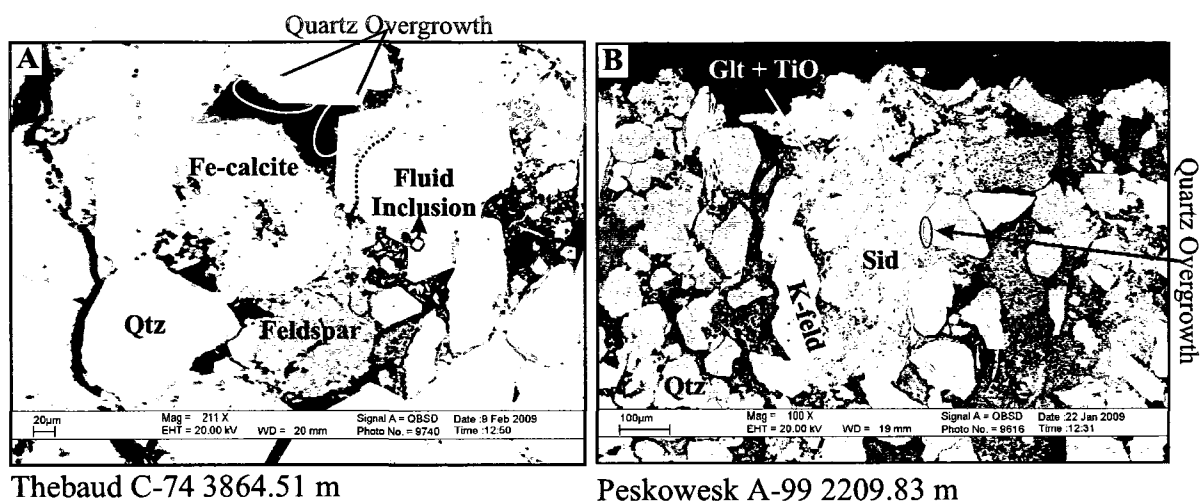
4.2.8 Titanium Minerals

The correlation between Ti and P discussed by Gould (2007) was also investigated in this study by first trying to identify titanium minerals. At Thebaud C-74, EMP chemical analysis revealed the presence of TiO₂ grains with francolite, chlorite and detrital quartz

Figure 4.10: Various BSE images from both studied wells. Thebaud C-74 (A) 3864.51 m: fine-grained sandstone with thick beds of mudstone. Quartz overgrowth on detrital quartz grains. Peskowsk A-99 (B) 2209.83 m: homogeneous sandstone with dispersed wood fragments. Quartz overgrowth forming after early siderite cement. (C) 2492.25 m: sandstone with thin beds of siderite cementation. Partially dismembered coated grain with a nucleus made up of siderite and chlorite intraclast, and a concentric layer made up of glauconite. Cement present is Fe-calcite and the quartz overgrowth formed after the Fe-calcite.

Abbreviations: Chl = chlorite, Sid = siderite, Glt = glauconite, Qtz = quartz. Mineral abbreviations after Kretz, 1983.

FIGURE 4.10



*= SEM Identification

(Fig. 4.11A) in shoreface deposits of sub-facies 2c. Titanium minerals like rutile and anatase were identified using X-ray diffraction (Appendix 4.5), and more detrital TiO_2 minerals, probably rutile were identified by optical microscopy (Table 4.1). A grain of TiO_2 (Fig. 4.11A) was also recognized.

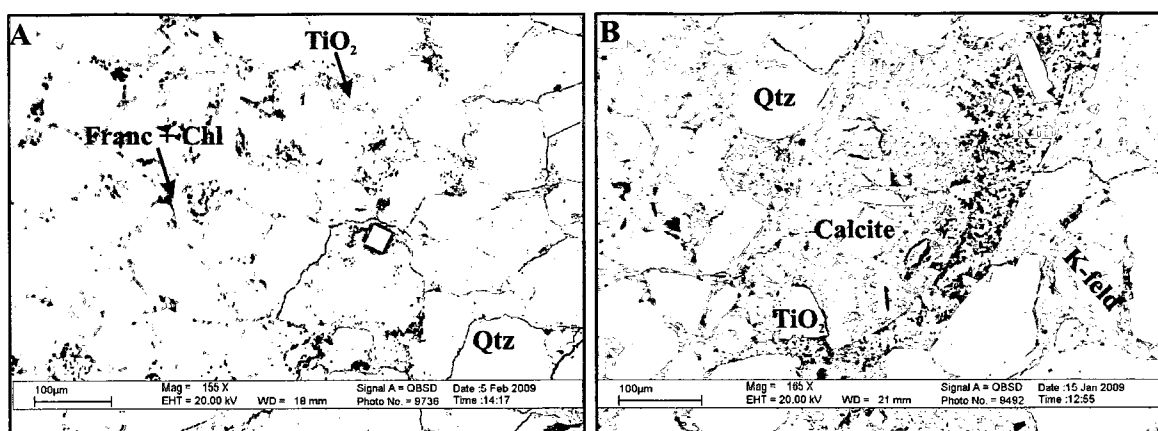
At Peskowsk A-99, a variety of titanium minerals were identified. There was (a) diagenetic TiO_2 (Fig. 4.11B), (b) TiO_2 minerals formed as a result of ilmenite alteration (Fig. 4.11C), and (c) TiO_2 mixed with glauconite with a fine-grained texture in about 2 μm grains (Fig. 4.11D) or with diagenetic chlorite (Fig. 4.11E). Titanium minerals were difficult to identify at Peskowsk A-99 by X-ray diffraction, and available peaks were either weak. Hence, a stacking of XRD diffractograms with TiO_2 minerals peaks (e.g. anatase and rutile) for high versus low TiO_2 levels, from geochemical analysis, was done to confirm a presence or absence of titanium minerals (Fig. 4.12). Based on the stacked peaks, anatase and rutile were present with very weak peaks, and these peaks could not be measured effectively. Anatase occurs at major intensity with 3.52Å and rutile occurs at a major intensity with 3.25Å. The presence of anatase is not systematic and the rutile peak occurs with a feldspar peak.

TiO_2 minerals mixed with glauconite and/or chlorite, and those occurring within coated grains were identified in reworked sediments of facies 3, 3a and bioclastic limestone (sub-facies 3o). Detrital TiO_2 minerals occurs in open shelf deposits (facies 1) and diagenetic TiO_2 minerals occurs in fluvial deposits of sub-facies 4x with cross-bedded sandstone, lacking mud drapes.

Figure 4.11: Various BSE images from both studied wells. Thebaud C-74 (A) 3866.79 m: fine-grained sandstone with a few coal fragments and burrows. TiO_2 grains occurring in pore spaces between detrital quartz grains. Peskowsk A-99 (B) 2221.17 m: mudstone with several whitish brown nodules. Diagenetic TiO_2 grains occurring in contact with kaolinite cement. **(C)** 2249.39 m: medium-grained sandstone. Ilmenite altering to TiO_2 minerals (e.g. rutile, anatase). **(D)** 2493.19 m: greenish sandstone with shelly and wood fragments. Pore-filling diagenetic TiO_2 mixed with glauconite. **(E)** 3813.63 m: muddy TST sandstone with shelly fragments. TiO_2 mixed with diagenetic chlorite.

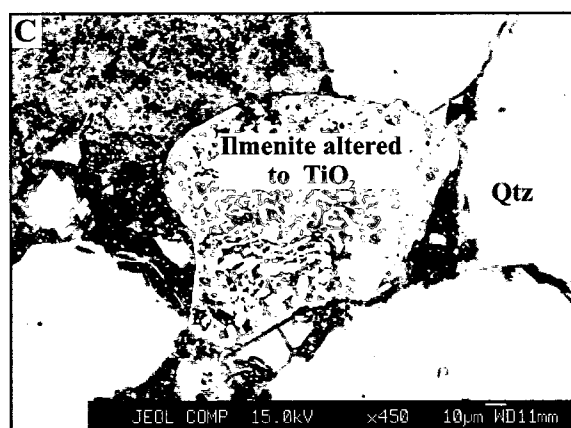
Abbreviations: Chl = chlorite, Sid = siderite, Glt = glauconite, Kln = kaolinite, K-feld = K-feldspar, Ank = ankerite, Franc = francolite, Qtz = quartz. Some mineral abbreviations after Kretz, 1983.

FIGURE 4.11

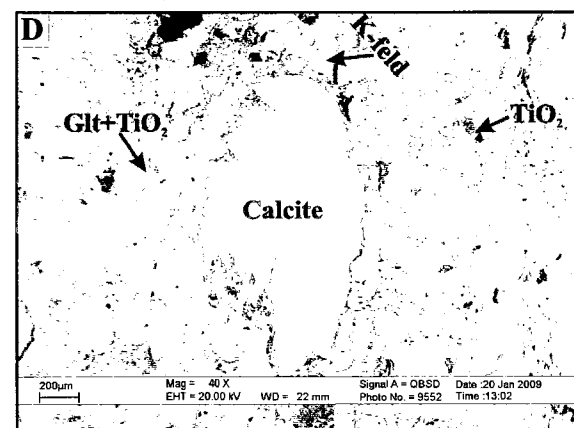


Thebaud C-74 3866.79 m

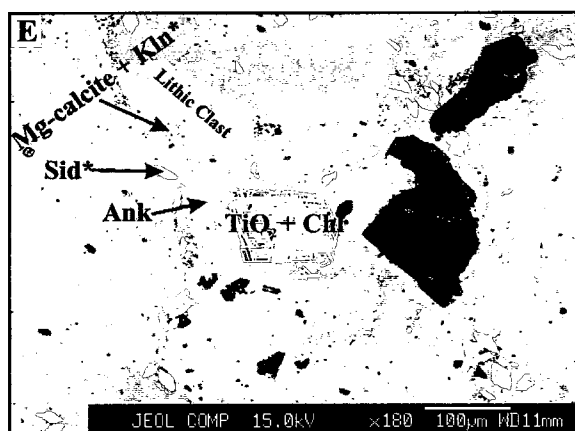
Peskowesk A-99 2221.17 m



Peskowesk A-99 2249.39 m



Peskowesk A-99 2493.19 m



Peskowesk A-99 3813.63 m

*= SEM Identification

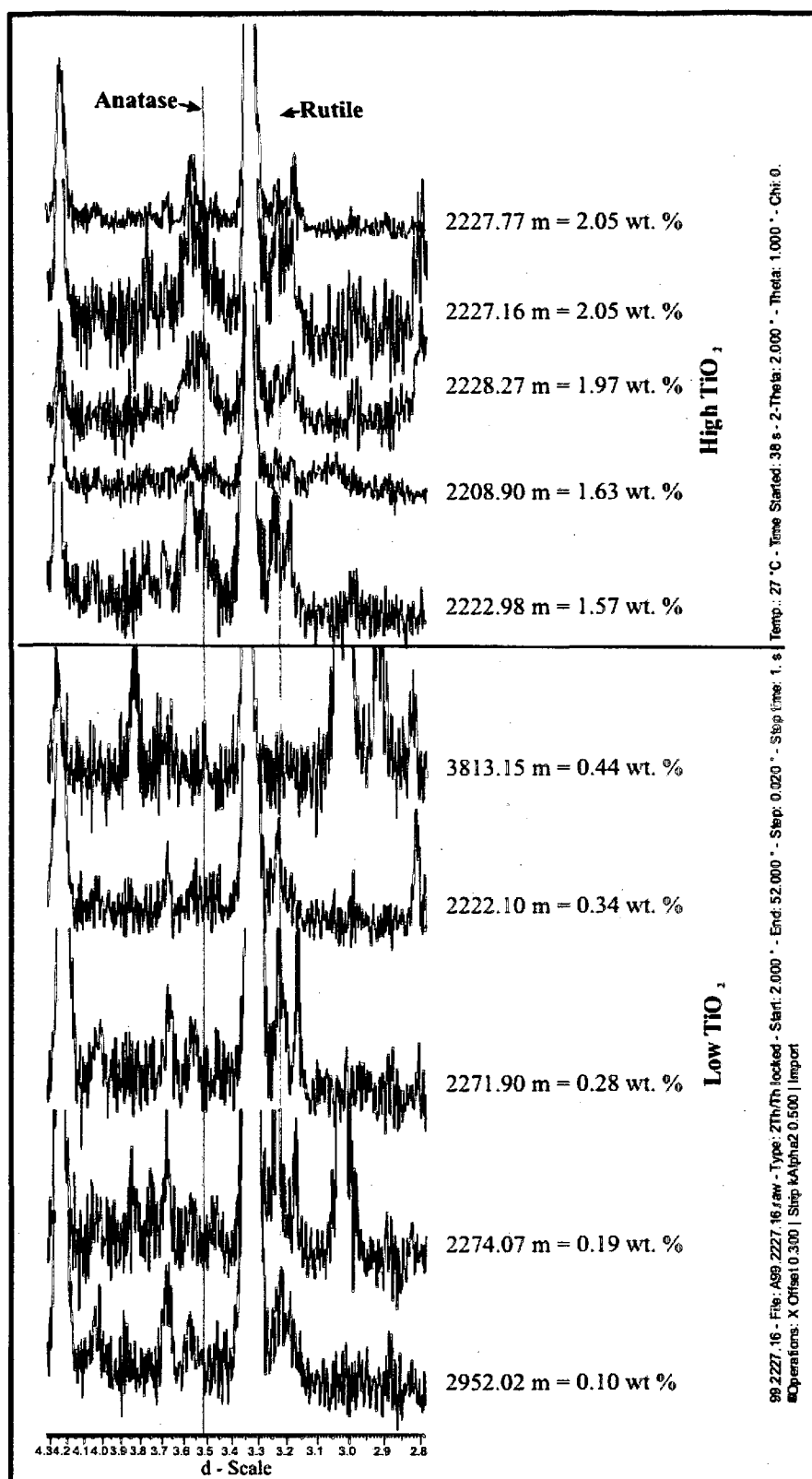


Figure 4.12: Peskowesk A-99; X-ray diffraction plots stacking of high vs. low TiO_2 to identify Anatase and Rutile. Low titanium samples have <1.00 wt. % and high titanium samples have > 1.00 wt. %.

4.3 PARAGENETIC SEQUENCE OF IDENTIFIED MINERALS

4.3.1 Thebaud C-74

The EMP chemical analyses of the carbonate minerals identified in the Mississauga Formation sandstones of the Thebaud C-74 well were plotted on a classification diagram (Fig. 4.13) as siderite, calcite and magnesite (App. 4.7). EMP chemical analysis identified only two siderite occurrences, but with very low totals and also occurring as mixtures with chlorite and/or glauconite, therefore no siderite chemical analyses were available for the classification diagram.

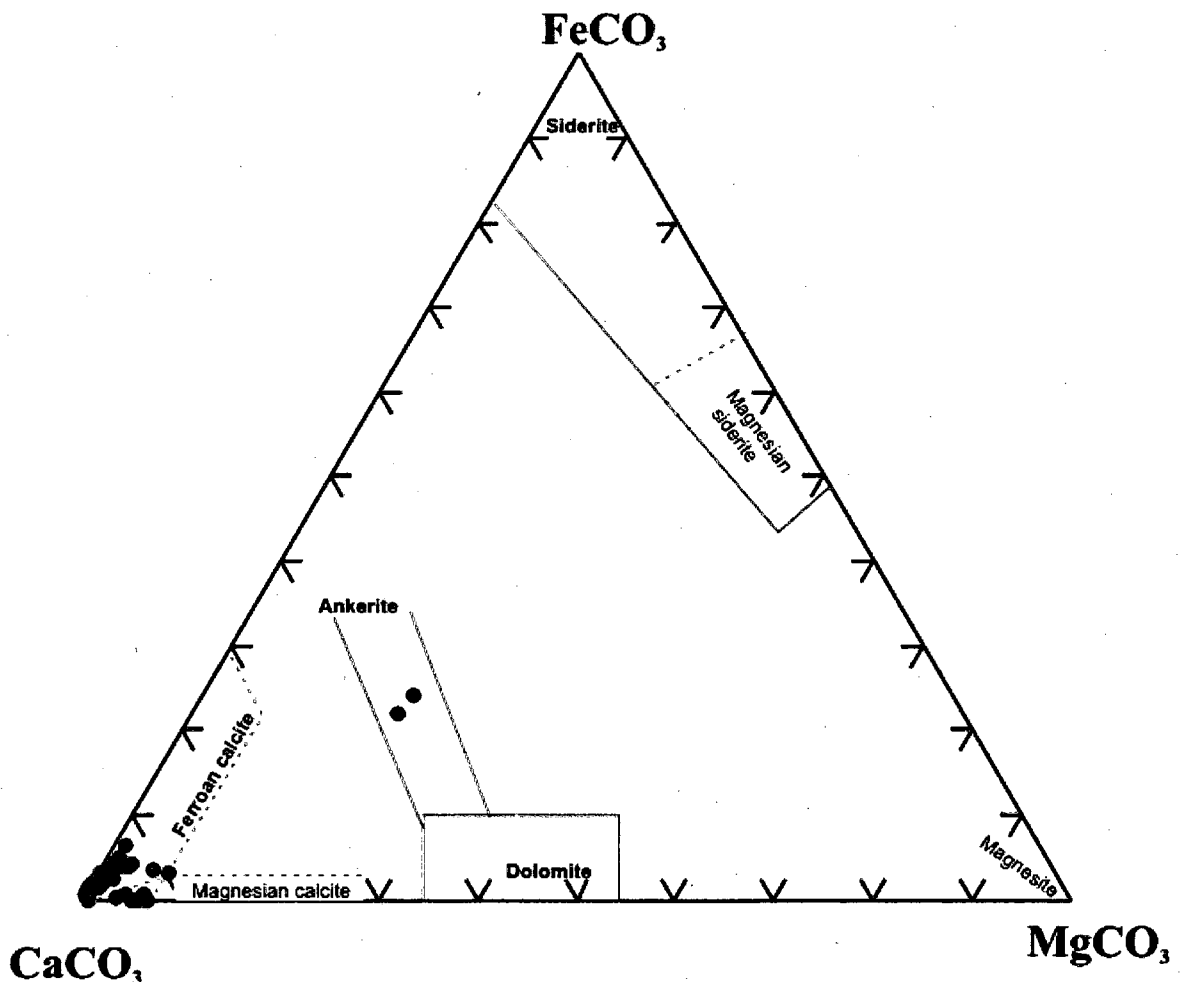


Figure 4.13: Carbonate classification diagram from the Thebaud C-74 well. Fields were created using carbonate analyses from Chang et al. (1996).

Calcite (with 1.48-2.67 wt % Mg and 1.09-1.73 wt % Fe) occurs in echinoderms with a spongy texture (the “Stereom” structure) having pores filled by chlorite (examples are in Appendix 4.3a, Figs. 1, 2, 9 and 36). It is suggested that the echinoderm pores was originally filled with Fe-rich clays, which altered to chlorite during burial diagenesis (Fig. 4.9C). Based on previous studies (Dickson, 2001 and Dickson, 2004) echinoderms have calcite or Mg-calcite mineralogy with variable Mg/Ca ratio in amounts greater than 5 mole %. At Thebaud C-74, the echinoderms mostly have Fe-calcite mineralogy with very little Mg-calcite influence (e.g. Fig. 36 in Appendix 36). Whether the Fe-calcite was secreted by the echinoderm, or Fe entered the structure during later recrystallization is unknown.

Glauconite predates Mg-calcite and/or calcite, chlorite and francolite (Fig. 4.2C, App. 4.3a-5, 13). Kaolinite predates calcite and Fe-calcite (App. 4.3a-33, 35), and some calcite occurrences have textural evidence (relics of K-feldspar below the calcite) that suggests that they precipitated as a result of feldspar dissolution (Fig. 4.2B). Mg-calcite may predate Fe-calcite (App. 4.3a-24). Quartz overgrowth predates Fe-calcite (Fig. 4.2B). Berthierine predates chlorite and pyrite (Fig. 4.5C), and pyrite framboids are identified in contact with detrital quartz grains (Fig. 4.5A) which suggests that they may have formed earlier during diagenesis.

Figure 4.14 summarizes the chronological order of mineral crystallization between diagenetic cements at the Thebaud C-74 well.

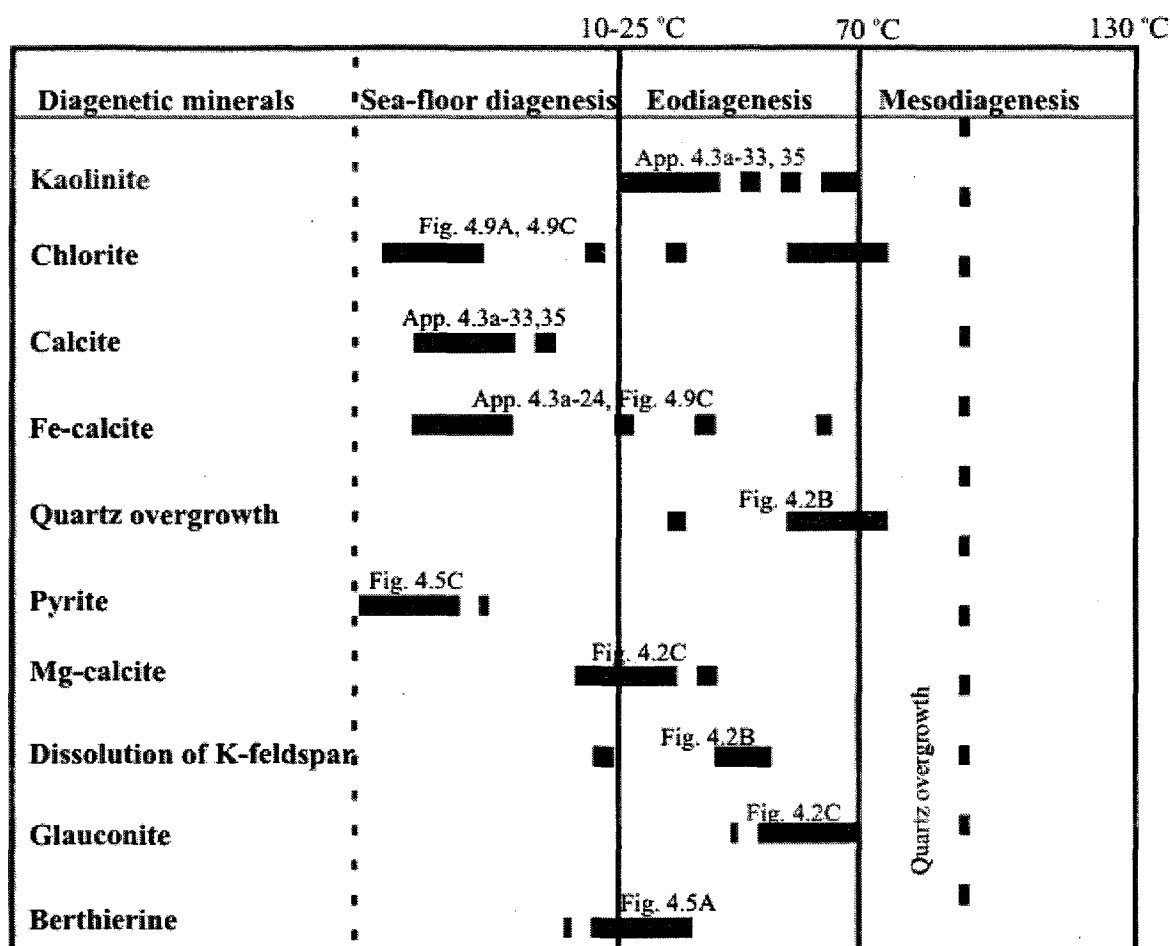


Figure 4.14: Paragenetic sequence deduced from textural relationship in sandstones from the Thebaud C-74 well. The boundary between eodiagenesis and mesodiagenesis is according to Morad et al. (2007) and El Ghali et al. (2006).

4.3.2 Peskowesk A-99

The EMP chemical analyses of the carbonate minerals identified in the Logan Canyon, Missisauga, and Mic Mac Formation sandstones of the Peskowesk A-99 well were plotted on a classification diagram (Fig. 4.15) as siderite, calcite and magnesite (App. 4.8). In the Logan Canyon sandstones, chlorite postdates berthierine and quartz overgrowth postdates early siderite (Fig. 4.6D). Early siderite predates quartz overgrowth but postdates glauconite and kaolinite (Figs. 4.10B, 4.8B, App. 4.4a-25). Kaolinite mixed with FeO predates glauconite (App. 4.4a-23).

In the Missisauga sandstones, Fe-calcite postdates glauconite (Fig. 4.10C, App. 4.4-41). Quartz overgrowth and Fe-calcite postdates kaolinite (App. 4.4-60), and quartz overgrowth predates calcite (Fig. 4.4C). Pyrite predates Fe-calcite (Fig. 4.6C), and pyrite often occurs in contact with detrital quartz grains (App. 4.4-4). In the Mic Mac Formation sandstones, more kaolinite is identified, predating Fe-calcite (App. 4.4a-64). In some coated grains from the Mic Mac Formation sandstone, Fe-calcite, chlorite and kaolinite predates ankerite and Mg-calcite (Fig. 4.1F, App. 4.4a-72, 74) respectively.

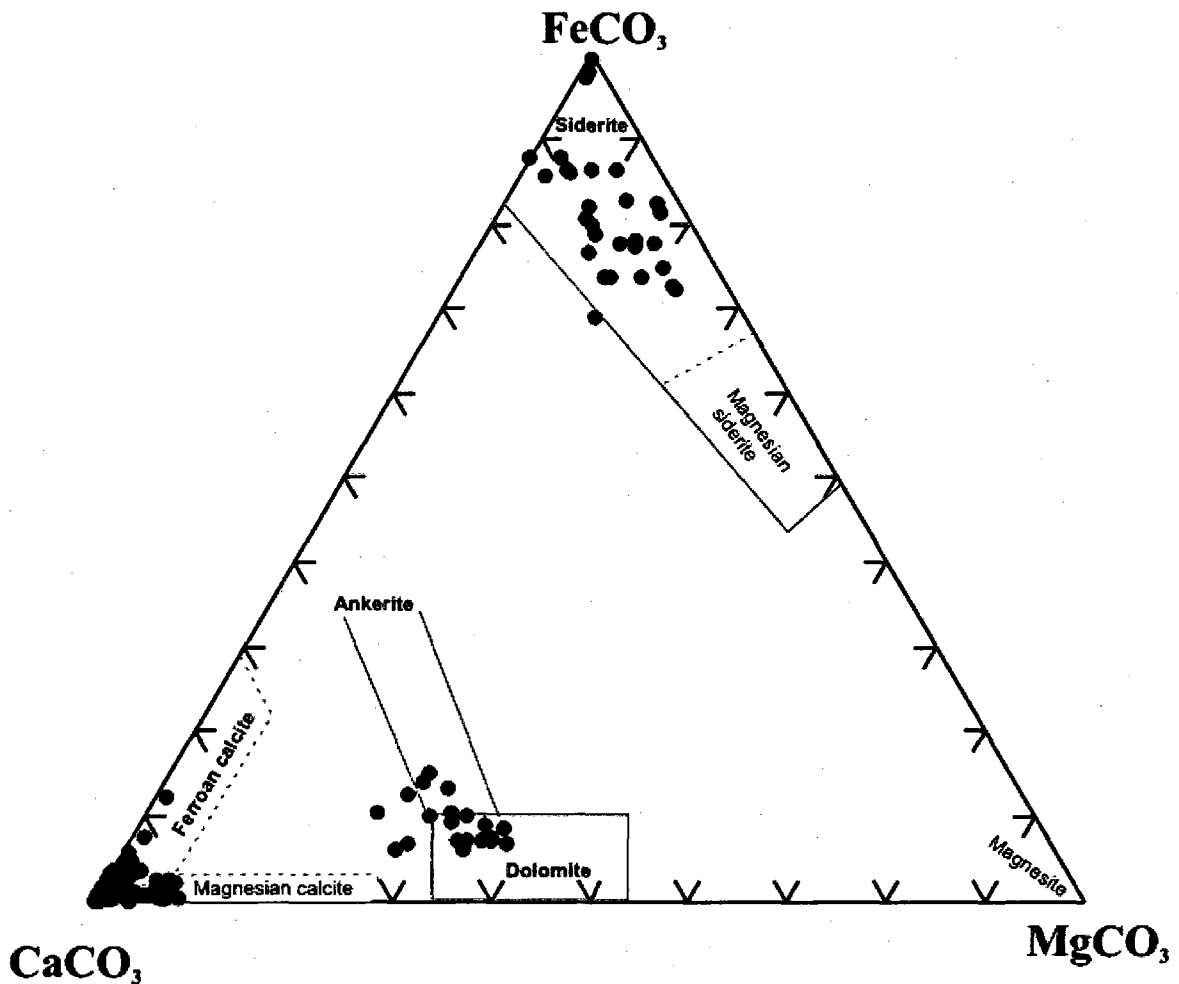
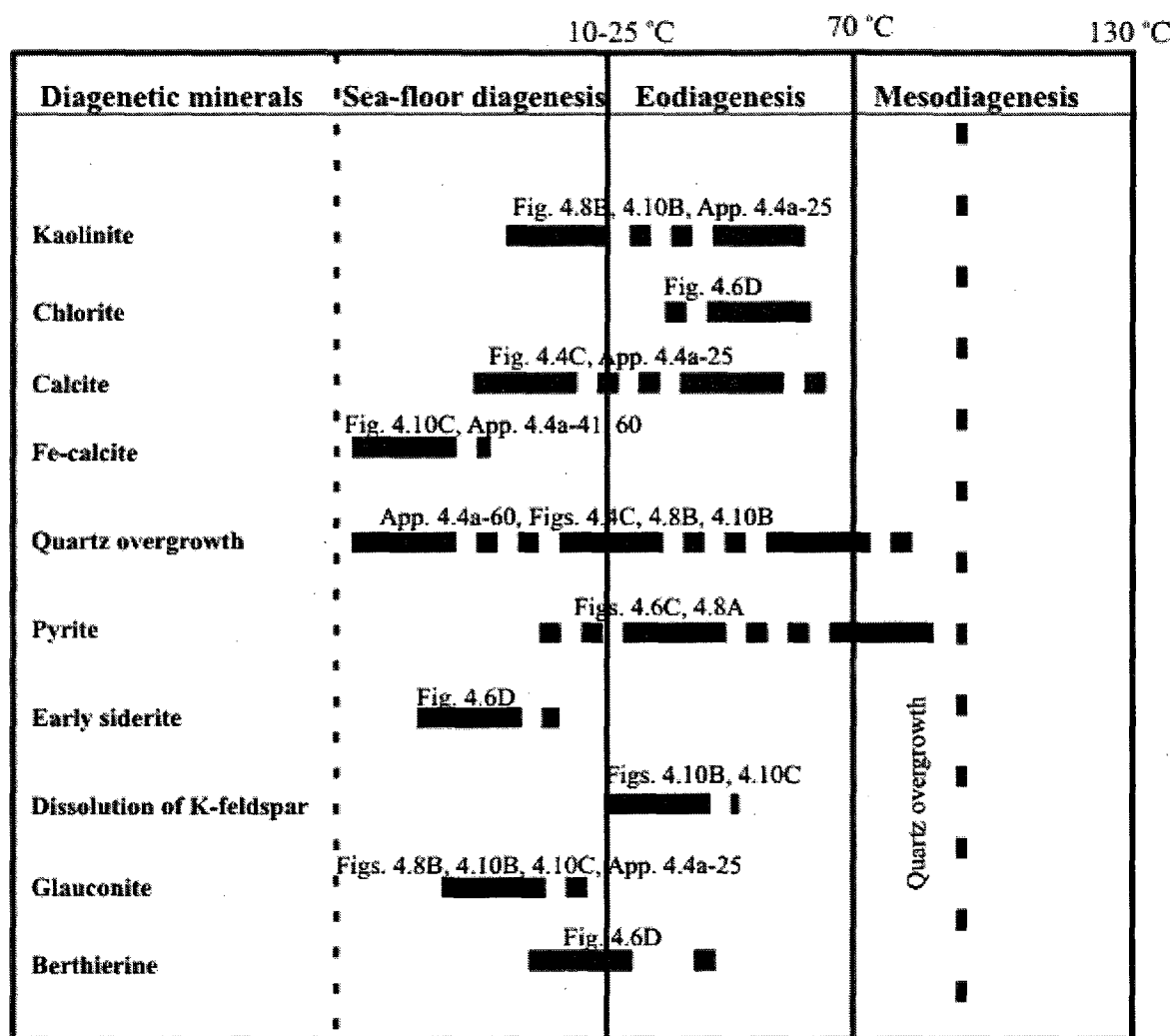


Figure 4.15: Carbonate classification diagram from the Peskowsk A-99 well. Fields were created using carbonate analyses from Chang et al. (1996).

Figure 4.16 summarizes the chronological order of mineral crystallization between diagenetic cements, and detrital grains at the Peskowsk A-99 well.



4.16: Paragenetic sequence deduced from textural relationship in sandstones from the Peskowsk A-99 well. The boundary between eodiagenesis and mesodiagenesis is according to Morad et al. (2007) and El Ghali et al. (2006).

4.4 CHAPTER SUMMARY

The petrographic study in this chapter showed the presence of the following diagenetic minerals: Fe-rich clay, perhaps odinite (a precursor of chlorite), carbonate (calcite, siderite), pyrite (framboids and platy), glauconite, and francolite (carbonate fluorapatite). Most early diagenetic minerals were identified within coated grains, because the coated preserve a record of sea-floor diagenesis in their concentric layers. A paragenetic sequence of sea-floor diagenetic minerals was then produced based on mineral textures used to determine early versus late precipitation. For both wells, Fe-calcite is found in coated grains, suggesting early precipitation. However, it is possible that the calcite and Fe-calcite formed by eodiagenetic replacement of an aragonite precursor. Other early minerals include pyrite and glauconite. The following chapter presents geochemical results using whole rock geochemistry, and carbon analysis.

CHAPTER 5: GEOCHEMICAL RESULTS

5.1 LABORATORY METHODS

After removing an offcut for a thin section (78 samples from studied wells: Tables 5.1a and 5.1b), the individual remaining samples were weighed, washed (using distilled water to remove mud and other contaminants), crushed (first with a small clean hammer with the samples wrapped in thick, clean, clear plastic wraps; then using a micromill equipped with a ceramic bowl) and pulverized similar to the method used for X-ray diffraction powder analysis.

Whole rock geochemical analyses were done by Activation Laboratories Limited, according to their code 4Lithoresearch and code 4B1 packages, which combine lithium metaborate/tetraborate fusion ICP analysis for major elements (SiO_2 , TiO_2 , Al_2O_3 , Fe_2O_3 , MnO , MgO , CaO , Na_2O , K_2O and P_2O_5) and ICP-MS analysis for trace elements using the international rock standards (Activation Laboratories Ltd. 2006) package for Ba, Rb, Sr, Y, Zr, Nb, Pb, Ga, Zn, S, Cu, Ni, V, Cr, La, Ce, Pr, Nd, Sm, Eu, Gd, Tb, Dy, Ho, Er, Tm, Yb, Lu, Co, As, Cs, Hf, Sb, Sc, Ta, Th, and U.

Whole rock geochemical data for Thebaud C-74 is in Table 5.2a and for Peskowsk A-99 in Table 5.2b.

Table 5.1a: Location and other information of analytical samples from Thebaud C-74

Well	Depths (m)	Sample Status ¹	Formation	Facies	Lithology	Dominant Cement ²
Thebaud C-74	3859.95	new ⁺	Missisauga	3l	Mudstone	Chlorite
	3860.38	new	Missisauga	1	Mudstone	Chlorite
	3861.23	new	Missisauga	0	Very Fine Sandstone	Carbonates
	3862.56	new	Missisauga	0	Mudstone	Carbonates and Pyrite
	3862.91	new	Missisauga	3	Mudstone	Carbonates
	3863.08	new	Missisauga	3	Fine-Coarse Sandstone	Siderite
	3863.53	new	Missisauga	4o	Fine-Coarse Sandstone	Pyrite
	3863.99	new	Missisauga	4o	Fine-Coarse Sandstone	Pyrite
	3864.51	new	Missisauga	4o	Fine Sandstone	Pyrite
	3864.52	old ⁺	Missisauga	4o	Fine Sandstone	Siderite
	3864.99	new	Missisauga	4o	Fine Sandstone	Siderite
	3865.53	new	Missisauga	2c	Fine Sandstone	Pyrite
	3865.56	old	Missisauga	2c	Fine Sandstone	Siderite
	3865.95	new	Missisauga	2c	Fine Sandstone	Carbonates
	3866.79	new	Missisauga	2c	Fine Sandstone	Carbonates
	3867.39	new	Missisauga	2c	Fine Sandstone	Pyrite
	3868.39	new	Missisauga	2c	Fine Sandstone	Pyrite
	3868.77	new	Missisauga	1	Fine Sandstone	Carbonates
	3868.94	new	Missisauga	1	Fine Sandstone	Carbonates
	3869.64	new	Missisauga	1	Fine Sandstone	Pyrite
	3870.01	new	Missisauga	1	Fine Sandstone	Carbonates
	3870.19	new	Missisauga	1	Fine Sandstone	Pyrite
	3870.62	new	Missisauga	3	Fine Sandstone	Carbonates
	3871.36	new	Missisauga	3	Fine Sandstone	Carbonates
	3871.47	new	Missisauga	3	Fine Sandstone	Carbonates

Table 5.1a: Location and other information of analytical samples from Thebaud C-74

Well	Depths (m)	Sample Status ¹	Formation	Facies	Lithology	Dominant Cement ²
Thebaud C-74	3872.58	new	Missisauga	3	Fine Sandstone	Carbonates
	3876.72	old	Missisauga	0	Fine Sandstone	Carbonates
	3879.56	old	Missisauga	9	Fine-Medium Sandstone	Carbonates
	3881.59	old	Missisauga	9	Medium Sandstone	Carbonates
	3882.96	old	Missisauga	9	Fine-Medium Sandstone	Carbonates
	3902.65	old	Missisauga	3	Fine-Medium Sandstone	Carbonates
	3905.10	old	Missisauga	4o	Fine-Medium Sandstone	Siderite
	3906.75	old	Missisauga	4o	Fine-Medium Sandstone	Siderite
	3907.93	old	Missisauga	5	Fine Sandstone	Siderite
	3908.65	old	Missisauga	4o	Fine-Medium Sandstone	Siderite
	3909.92	old	Missisauga	4o	Fine-Medium Sandstone	Siderite
	3911.66	old	Missisauga	4o	Fine-Medium Sandstone	Carbonates
	3912.40	old	Missisauga	9	Fine-Coarse Sandstone	Siderite
	3913.73	old	Missisauga	9	Fine-Coarse Sandstone	Siderite
	3915.74	old	Missisauga	9	Medium Sandstone	Siderite
	3917.06	old	Missisauga	9	Fine-Coarse Sandstone	Carbonates
	3918.64	old	Missisauga	9	Fine Sandstone	Siderite
	3920.04	old	Missisauga	9	Fine Sandstone	Siderite
	3921.98	old	Missisauga	9	Fine-Medium Sandstone	Carbonates
	3924.50	old	Missisauga	9	Fine Sandstone	Siderite
	3926.15	old	Missisauga	2b	Fine Sandstone	Quartz Overgrowth

¹ Cement types are identified from thin sections samples only; new⁺ refers to core samples specifically collected for this thesis, whereas old⁺ refers to samples that had already been collected for other projects.

² Dominant cement in thin section from optical microscopy and electron microprobe chemical analysis

Table 5.1b: Location and other information of analytical samples from Peskowesk A-99.

Well	Depths (m)	Sample Status ¹	Formation	Facies	Lithology	Dominant Cement ²
Peskowesk A-99	2208.90	new ⁺	Logan Canyon	9	Shale	NA ³
	2209.25	old ⁺	Logan Canyon	5	Shale	NA
	2209.35	new	Logan Canyon	5	Fine Sandstone	NA
	2209.83	new	Logan Canyon	5	Sandstone	Siderite and Pyrite
	2210.15	new	Logan Canyon	5	Sandstone	NA
	2210.37	old	Logan Canyon	4	Sandstone	NA
	2213.57	old	Logan Canyon	0m	Shale	NA
	2215.78	old	Logan Canyon	0m	Shale	NA
	2219.03	old	Logan Canyon	0	Shale	NA
	2220.70	new	Logan Canyon	0	Shale	NA
	2221.17	new	Logan Canyon	0	Mudstone	Calcite and Pyrite
	2221.69	old	Logan Canyon	3	Shale	NA
	2222.10	new	Logan Canyon	2c	Coarse Sandstone	NA
	2222.98	new	Logan Canyon	5	Mudstone	NA
	2223.37	new	Logan Canyon	5	Sandstone	NA
	2224.26	new	Logan Canyon	5	Sandstone	NA
	2225.67	new	Logan Canyon	5	Shale	NA
	2226.44	new	Logan Canyon	5	Sandstone	NA
	2227.16	new	Logan Canyon	5	Shale	NA
	2227.77	new	Logan Canyon	5	Coarse Sandstone	NA
	2228.16	old	Logan Canyon	5	Shale	NA
	2228.23	new	Logan Canyon	5	Sandstone	NA
	2228.27	new	Logan Canyon	5	Shale	NA
	2230.62	old	Logan Canyon	4x	Sandstone	NA

Table 5.1b: Location and other information of analytical samples from Peskowesk A-99.

Well	Depths (m)	Sample Status ¹	Formation	Facies	Lithology	Dominant Cement ²
Peskowesk A-99	2231.82	new	Logan Canyon	4x	Fine sandstone	Clays and Mg-siderite
	2233.62	old	Logan Canyon	4x	Sandstone	NA
	2234.44	old	Logan Canyon	4x	Sandstone	NA
	2238.65	old	Logan Canyon	4x	Sandstone	NA
	2245.84	new	Logan Canyon	4x	Coarse sandstone	Siderite
	2249.39	new	Logan Canyon	4x	Medium sandstone	Siderite and Kaolinite
	2267.02	new	Logan Canyon	4g	Sandstone	NA
	2269.84	old	Logan Canyon	4g	Sandstone	NA
	2271.90	new	Logan Canyon	4g	Sandstone	NA
	2273.15	new	Logan Canyon	9b	Sandstone	NA
	2273.58	old	Logan Canyon	9b	Sandstone	NA
	2274.07	new	Logan Canyon	9b	Sandstone	NA
	2274.15	new	Logan Canyon	2b	Sandstone	Siderite
	2275.64	new	Logan Canyon	1	Mudstone	Siderite
	2275.70	new	Logan Canyon	1	Sandstone	Siderite
	2479.35	old	Missisauga	0	Shale	NA
	2480.55	new	Missisauga	1	Shale	NA
	2481.14	new	Missisauga	1	Shale	NA
	2481.34	new	Missisauga	3a	Sandstone	Siderite and Chlorite
	2482.42	old	Missisauga	2c	Sandstone	NA
	2482.68	new	Missisauga	2c	Sandstone	Siderite and Calcite
	2483.77	new	Missisauga	9g	Sandstone	NA
	2485.01	new	Missisauga	9g	Sandstone	NA
	2486.53	new	Missisauga	0m	Sandstone	NA

Table 5.1b: Location and other information of analytical samples from Peskowesk A-99.

Well	Depths (m)	Sample Status ¹	Formation	Facies	Lithology	Dominant Cement ²
Peskowesk A-99	2487.76	new	Missisauga	0m	Shale	NA
	2488.85	old	Missisauga	0m	Shale	NA
	2492.25	new	Missisauga	3	Sandstone	Fe-calcite and Pyrite
	2492.62	old	Missisauga	3	Shale	NA
	2493.19	new	Missisauga	3	Fine Sandstone	Calcite and Pyrite
	2494.02	new	Missisauga	2b	Fine Sandstone	Siderite and Pyrite
	2927.36	old	Missisauga	1	Shale	NA
	2931.07	new	Missisauga	2c	Sandstone	NA
	2931.91	new	Missisauga	3	Fine sandstone	Calcite and Quartz overgrowths
	2933.38	new	Missisauga	5s	Fine sandstone	NA
	2934.42	old	Missisauga	5s	Sandstone	NA
	2934.52	new	Missisauga	5s	Fine sandstone	NA
	2935.46	new	Missisauga	9f	Fine sandstone	NA
	2936.85	new	Missisauga	5s	Fine sandstone	NA
	2938.05	new	Missisauga	4g	Fine sandstone	NA
	2939.05	old	Missisauga	4g	Shale	NA
	2939.79	new	Missisauga	4g	Fine sandstone	NA
	2940.05	new	Missisauga	4g	Fine sandstone	NA
	2940.90	old	Missisauga	4g	Shale	NA
	2942.03	new	Missisauga	4g	Fine sandstone	Calcite
	2945.38	new	Missisauga	0m	Fine sandstone	Fe-calcite
	2947.43	old	Missisauga	2c	Shale	NA
	2950.73	new	Missisauga	0m	Sandstone	NA
	2952.02	new	Missisauga	4x	Sandstone	NA

Table 5.1b: Location and other information of analytical samples from Peskowesk A-99.

Well	Depths (m)	Sample Status ¹	Formation	Facies	Lithology	Dominant Cement ²
Peskowesk A-99	2953.20	new	Missisauga	4x	Sandstone	NA
	2954.35	new	Missisauga	4x	Coarse sandstone	NA
	3794.37	new	Mic Mac	4g	Fine sandstone	NA
	3795.24	new	Mic Mac	4g	Sandstone	Siderite
	3795.30	old	Mic Mac	1	Sandstone	NA
	3796.50	new	Mic Mac	0s	Fine Sandstone	Glauconite and Pyrite
	3806.51	old	Mic Mac	3l	Sandstone	NA
	3812.19	new	Mic Mac	3l	Muddy Sandstone	NA
	3812.64	old	Mic Mac	3o	Sandstone	NA
	3813.15	new	Mic Mac	3o	Muddy Sandstone	Mg-calcite
	3813.63	new	Mic Mac	3o	Muddy Sandstone	Mg-calcite

¹ Cement types are identified from thin sections samples only; new⁺ refers to core samples specifically collected for this thesis, whereas old⁺ refers to samples that had already been collected for other projects.

² Dominant cement in thin section from optical microscopy and electron microprobe chemical analysis

³ No Petrographic thin sections were available for these samples

Table 5.2a: Representative whole rock geochemical analyses for Thebaud C-74.

Well	Thebaud C-74									
Formation	Mississauga									
Depth (m)	Detection Limit ³	3860.38	3861.23	3862.56	3862.90	3863.08	3863.53	3863.99	3864.50	3864.52
Lithology ¹		Mudstone	Fine Sst	Med-C Sst	V.Crs Sst	Fine-M Sst	Fine Sst	Fine Sst	Fine Sst	Fine Sst
Major Elements (wt%)										
SiO ₂	0.01	57.58	80.06	80.40	79.45	65.59	90.73	91.40	87.75	82.34
TiO ₂	0.00	1.28	0.68	0.29	0.16	0.29	0.61	0.57	0.56	0.716
Al ₂ O ₃	0.01	17.29	5.54	5.63	3.28	3.95	4.02	3.81	5.04	5.33
Fe ₂ O _{3t}	0.01	17.44	4.72	5.56	5.68	4.87	2.77	2.51	3.87	4.65
MnO	0.00	0.06	0.07	0.07	0.17	0.34	0.01	0.01	0.01	0.011
MgO	0.01	2.19	0.55	0.69	0.65	0.77	0.33	0.31	0.50	0.57
CaO	0.01	1.15	6.73	5.93	9.92	22.66	0.49	0.43	0.88	0.82
Na ₂ O	0.01	0.78	1.19	0.79	0.59	1.11	0.97	0.90	0.82	1.23
K ₂ O	0.01	2.11	0.34	0.59	0.01	0.30	0.27	0.25	0.48	0.48
P ₂ O ₅	0.01	0.11	0.11	0.04	0.04	0.11	0.06	0.06	0.07	0.08
LOI	0.01	8.81	6.12	6.12	8.95	16.83	1.74	1.38	2.07	2.706
Total		100.20	98.54	100.00	99.12	99.55	98.81	98.82	98.75	98.94
Trace Elements (ppm)										
Ba	3.00	265	185	205	354	223	4092	4278	354	275
Rb	1.00	80	21	27	11	8	8	11	18	20
Sr	2.00	192	225	240	258	661	168	173	118	140
Y	0.50	34.3	29.5	18.7	14.6	22.0	15.8	18.8	15.9	18.2
Zr	1.00	544	483	215	131	222	713	669	313	417
Nb	0.20	81.6	41.9	27.2	16.0	27.1	30.1	30.4	21.4	24.8
Pb	5.00	19	13	6	4	4	9	8	5	6
Ga	1.00	23	27	24	19	16	17	17	17	8
Zn	1.00	124	148	116	34	24	44	43	51	57
S (wt %)	1.00	0.46	0.08	0.22	0.11	0.13	0.14	0.14	0.18	0.231
Cu	1.00	14	8	9	11	4	44	25	14	17
Ni	20.00	67	25	28	20	14	19	14	21	26
V	5.00	399	45	79	48	52	35	27	55	56
Cr	0.05	180	110	80	50	70	242	191	80	140
La	0.05	53	36	29	23	28	34	35	30	30.6
Ce	0.01	115	80	66	55	68	77	76	67	72.3
Pr	0.05	10.50	8.83	6.40	5.26	7.00	7.59	7.75	6.75	7.06
Nd	0.01	36.1	33.8	21.5	19.0	26.7	25.3	25.6	22.6	26.2
Sm	0.005	6.73	7.91	4.20	4.09	6.08	5.28	5.42	4.53	4.52
Eu	0.01	1.440	1.890	0.868	0.834	1.370	0.627	0.517	0.844	0.897
Gd	0.01	5.93	7.04	3.61	3.37	5.25	3.81	3.94	3.56	3.51
Tb	0.01	1.15	1.12	0.62	0.58	0.80	0.56	0.64	0.56	0.62
Dy	0.01	7.35	5.83	3.70	3.18	4.35	3.21	3.43	3.07	3.42
Ho	0.01	1.49	1.04	0.72	0.58	0.79	0.62	0.67	0.58	0.67
Er	0.005	4.48	2.88	2.17	1.63	2.11	1.86	1.99	1.71	1.97
Tm	0.01	0.726	0.430	0.342	0.242	0.297	0.291	0.323	0.266	0.291
Yb	0.002	4.73	2.87	2.26	1.60	1.89	1.93	2.21	1.68	1.9
Lu	1.00	0.693	0.415	0.335	0.235	0.282	0.313	0.332	0.242	0.288
Co	1.00	22	9	12	9	9	5	5	6	6
As	0.01	22	8	15	10	14	b.d. ²	b.d.	6	11
Cs	0.10	4.4	0.9	1.4	0.6	0.3	0.3	0.4	0.8	0.9
Hf	0.10	13.3	11.1	5.5	3.2	5.0	15.8	14.3	6.9	9.9
Sb	0.20	3.1	6.6	4.3	4.4	5.0	5.3	5.2	3.7	b.d
Sc	0.10	19	4	5	3	3	4	2	6	5
Ta	0.01	4.55	2.83	2.08	1.21	1.66	2.23	2.10	1.50	1.78
Th	0.05	23	9	9	6	5	6	7	5	4.82
U	0.01	3	2	1	1	2	1	2	1	1.3

¹ sst = sandstone; ² b.d. = below detection limit; ³ detection limits

Table 5.2a: Representative whole rock geochemical analyses for Thebaud C-74.

Well										
Formation	Missisauga									
Depth (m)	3864.99	3865.52	3865.56	3865.94	3866.79	3867.39	3868.38	3868.77	3868.94	3869.64
Lithology ¹	Muddy Sst	Muddy Sst	Fine Sst	Muddy Sst	Fine Sst	Fine Sst	Sandy Mst	V. fine Sst	V. fine Sst	Mudstone
Major Elements (wt%)										
SiO ₂	83.97	83.12	81.18	77.48	85.96	86.64	81.94	77.08	76.58	77.81
TiO ₂	0.76	0.85	0.81	0.74	0.68	0.61	0.72	0.72	0.74	1.17
Al ₂ O ₃	6.90	7.19	6.46	6.30	5.27	5.20	7.09	4.56	4.33	10.20
Fe ₂ O _{3t}	4.64	4.75	4.67	3.88	4.48	3.96	6.27	3.64	3.57	6.93
MnO	0.02	0.02	0.019	0.11	0.02	0.02	0.02	0.17	0.20	0.01
MgO	0.65	0.68	0.61	0.59	0.52	0.49	0.72	0.49	0.47	0.83
CaO	1.23	1.44	1.2	9.16	1.58	1.56	1.36	11.77	12.73	0.43
Na ₂ O	0.84	0.91	0.83	0.88	1.02	1.10	1.11	1.06	0.90	1.02
K ₂ O	0.90	0.92	0.86	0.82	0.38	0.31	0.67	0.40	0.35	1.55
P ₂ O ₅	0.07	0.09	0.09	0.09	0.10	0.08	0.09	0.09	0.08	0.10
LOI	3.60	3.39	3.485	8.11	3.02	2.60	3.53	9.81	10.81	4.90
Total	99.27	98.78	100.2	100.00	100.80	99.11	99.18	99.53	100.50	100.90
Trace Elements (ppm)										
Ba	199	241	175	147	222	219	198	227	176	203
Rb	40	47	33	31	14	17	24	12	12	49
Sr	172	184	169	417	150	132	189	641	645	140
Y	26.0	28.6	20.2	22.3	16.8	20.0	20.2	22.8	19.9	33.8
Zr	726	805	463	639	600	485	436	492	556	678
Nb	38.0	48.3	29.8	32.0	22.3	30.8	28.4	23.2	22.8	40.6
Pb	5	6	7	5	11	6	13	6	5	16
Ga	22	22	10	17	7	14	14	10	9	14
Zn	61	53	60	40	47	40	64	47	45	72
S	0.43	0.35	0.345	0.32	0.40	0.15	0.81	0.09	0.07	0.84
Cu	13	9	16	8	8	8	11	6	7	10
Ni	27	25	26	19	26	25	37	15	13	38
V	70	79	74	62	53	53	67	48	46	89
Cr	190	170	130	140	130	120	90	90	110	120
La	54	60	36.5	45	25	33	34	29	27	54
Ce	117	128	84.3	98	61	73	77	67	62	122
Pr	11.70	12.90	8.1	9.84	6.43	7.72	7.63	7.03	6.54	12.10
Nd	37.8	42.0	29.9	33.2	24.1	27.6	25.8	25.0	23.6	40.9
Sm	7.40	8.04	5.06	6.77	5.38	5.97	5.12	5.54	5.17	8.18
Eu	1.400	1.510	1.04	1.270	1.030	1.190	1.020	1.210	1.040	1.410
Gd	5.77	6.29	3.81	5.36	3.99	4.73	4.22	4.74	4.40	6.04
Tb	0.95	1.04	0.7	0.84	0.61	0.74	0.71	0.79	0.71	1.10
Dy	5.34	5.99	3.88	4.73	3.39	4.01	3.97	4.48	3.89	6.79
Ho	1.03	1.13	0.74	0.88	0.62	0.75	0.77	0.84	0.71	1.34
Er	3.04	3.40	2.27	2.52	1.82	2.17	2.30	2.37	2.04	3.93
Tm	0.469	0.527	0.338	0.387	0.292	0.330	0.354	0.361	0.313	0.597
Yb	2.95	3.36	2.33	2.44	1.94	2.06	2.23	2.20	1.98	3.82
Lu	0.445	0.512	0.351	0.384	0.296	0.329	0.348	0.326	0.299	0.573
Co	13	14	8	9	7	8	15	4	3	16
As	10	10	13	8	5	7	10	b.d.	b.d.	8
Cs	1.8	2.1	1.5	1.4	0.6	0.7	1.0	0.5	0.5	2.4
Hf	16.6	18.2	11.6	14.2	14.8	11.0	10.0	11.0	12.4	16.9
Sb	6.1	6.4	b.d.	3.6	0.6	5.5	3.8	4.2	3.6	0.0
Sc	7	7	7	6	4	4	6	5	5	10
Ta	2.67	3.39	2.17	2.26	1.73	2.18	2.07	1.69	1.80	3.11
Th	9	12	6.84	8	6	7	8	6	6	12
U	2	3	1.71	2	2	2	2	1	1	3

¹ sst = sandstone; ² b.d. = below detection limit; ³ detection limits

Table 5.2a: Representative whole rock geochemical analyses for Thebaud C-74.

Well										
Formation	Missisauga									
Depth (m)	3870.01	3870.19	3870.62	3871.36	3871.47	3872.58	3876.72	3879.56	3881.59	3882.96
Lithology ¹	Fine Sst	Fine-M Sst	V. fine Sst	Fine Sst	V. fine Sst	V. Crs Sst	Fine Sst	Fine-M Sst	Med Sst	Fine-M Sst
Major Elements (wt%)										
SiO ₂	87.91	86.26	85.96	85.72	86.85	79.03	85.05	87.59	85.91	85.38
TiO ₂	0.58	0.71	0.65	0.60	0.72	0.12	0.696	0.707	1.003	0.785
Al ₂ O ₃	4.95	5.86	5.47	5.20	4.90	1.93	5.21	4.74	4.48	4.27
Fe ₂ O _{3t}	3.77	4.11	4.44	3.88	3.79	1.03	3.95	3.21	2.93	2.82
MnO	0.01	0.01	0.02	0.03	0.02	0.22	0.015	0.01	0.011	0.011
MgO	0.49	0.53	0.55	0.49	0.47	0.18	0.44	0.38	0.36	0.36
CaO	0.85	0.69	1.24	2.45	1.82	16.79	0.99	0.43	0.6	0.92
Na ₂ O	1.00	1.10	1.11	1.09	0.95	0.49	1.23	1.13	1.33	1.39
K ₂ O	0.33	0.61	0.45	0.41	0.38	0.14	0.42	0.39	0.42	0.42
P ₂ O ₅	0.09	0.09	0.08	0.09	0.08	0.02	0.09	0.08	0.09	0.1
LOI	2.35	3.01	2.59	2.92	2.40	12.28	2.16	1.665	1.629	2.208
Total	98.92	99.56	99.79	99.78	100.20	100.30	100.2	100.3	98.75	98.66
Trace Elements (ppm)										
Ba	220	185	233	333	286	61	675	739	437	175
Rb	16	23	16	14	14	4	13	13	13	14
Sr	122	126	152	109	88	637	91	73	67	137
Y	16.7	22.7	19.0	18.4	22.8	11.0	18.6	17.2	23.3	22.3
Zr	345	465	390	390	786	83	488	495	1076	878
Nb	21.1	27.4	25.8	26.4	30.5	9.1	30.9	26.9	27.8	24.4
Pb	7	14	5	7	4	b.d.	10	10	9	7
Ga	9	11	10	9	10	5	10	8	7	7
Zn	39	50	55	63	57	14	92	87	72	72
S	0.17	0.38	0.18	0.07	0.08	0.05	0.28	0.13	0.182	0.214
Cu	5	10	19	26	15	6	17	21	16	13
Ni	18	24	21	18	20	2	30	25	21	18
V	45	49	44	48	48	23	38	41	47	34
Cr	60	70	70	70	110	0	120	140	200	140
La	24	36	28	28	34	14	26.6	26.8	30.3	26.9
Ce	52	80	63	61	74	31	55.2	55.2	64.5	56.1
Pr	5.47	8.49	6.71	6.38	7.72	3.14	5.93	5.92	6.87	6.1
Nd	20.0	29.8	23.2	22.4	26.7	11.3	22.2	21.5	25.5	22.9
Sm	4.26	6.21	4.89	4.58	5.51	2.40	3.98	3.71	4.59	4.01
Eu	0.786	1.110	0.917	0.910	1.080	0.531	0.827	0.762	0.871	0.791
Gd	3.38	4.82	3.97	3.80	4.46	2.13	3.39	3.02	3.7	3.52
Tb	0.58	0.78	0.65	0.61	0.75	0.35	0.6	0.51	0.67	0.63
Dy	3.23	4.48	3.73	3.49	4.39	1.97	3.34	3.02	4.09	3.67
Ho	0.59	0.82	0.71	0.65	0.85	0.36	0.67	0.62	0.87	0.77
Er	1.73	2.38	2.04	1.88	2.54	1.06	2.03	1.87	2.76	2.43
Tm	0.273	0.382	0.316	0.285	0.407	0.164	0.31	0.298	0.435	0.393
Yb	1.78	2.47	1.99	1.79	2.69	1.01	2.01	1.97	3.04	2.66
Lu	0.262	0.350	0.296	0.271	0.414	0.137	0.328	0.314	0.516	0.443
Co	4	10	6	5	5	1	7	9	8	6
As	b.d.	7	b.d.	5	b.d.	b.d.	b.d.	b.d.	b.d.	b.d.
Cs	0.6	0.9	0.6	0.5	0.6	0.2	0.5	0.5	0.4	0.5
Hf	8.0	10.7	9.0	8.7	17.5	2.1	12.1	12.2	25.8	19
Sb	3.2	3.4	4.2	4.6	3.5	23.4	b.d.	b.d.	b.d.	b.d.
Sc	4	5	5	4	5	1	4	4	4	2
Ta	1.48	1.96	1.83	1.93	2.03	0.62	2.13	2.08	2.17	1.89
Th	5	7	6	6	8	3	4.78	4.99	6.23	5.59
U	1	2	1	1	2	1	1.5	1.46	2.26	1.97

¹ sst = sandstone; ² b.d. = below detection limit; ³ detection limits

Table 5.2a: Representative whole rock geochemical analyses for Thebaud C-74.

Well									
Formation	Missisauga								
Depth (m)	3902.65	3905.10	3906.75	3907.93	3908.65	3909.92	3911.66	3912.40	3913.73
Lithology ¹	Fine-M Sst	Fine-M Sst	Fine-M Sst	Mudstone	Fine-M Sst	Fine-M Sst	Fine-M Sst	Fine-C Sst	Fine-C Sst
Major Elements (wt%)									
SiO ₂	88.7	90.45	90.43	75.63	86.28	89.45	90.01	90.31	89.29
TiO ₂	0.294	0.337	0.445	0.281	0.354	0.369	0.594	0.34	0.257
Al ₂ O ₃	2.43	2.71	3.81	2.64	2.71	1.95	3.14	3.24	2.29
Fe ₂ O _{3t}	1.55	1.22	1.66	2.85	3.12	2	2.73	2	2.25
MnO	0.021	0.017	0.013	0.096	0.018	0.014	0.004	0.007	0.034
MgO	0.12	0.12	0.13	0.31	0.29	0.17	0.29	0.19	0.21
CaO	1.92	1.22	0.43	9.05	1.7	1.41	0.32	0.32	0.59
Na ₂ O	1.26	1.2	1.12	0.54	1.05	0.99	1.14	1.37	0.94
K ₂ O	0.12	0.21	0.34	0.28	0.19	0.18	0.13	0.25	0.13
P ₂ O ₅	0.06	0.06	0.07	0.04	0.04	0.08	0.06	0.07	0.05
LOI	2.695	1.771	1.881	8.147	2.885	1.935	1.041	1.107	2.013
Total	99.18	99.31	100.3	99.87	98.64	98.56	99.45	99.22	98.09
Trace Elements (ppm)									
Ba	165	468	223	118	201	354	1041	1457	11670
Rb	6	6	10	8	7	5	7	5	4
Sr	73	56	93	396	136	91	72	76	392
Y	7.3	7.4	8.4	14.6	10.8	9.1	13.5	7.9	6.9
Zr	188	178	216	166	367	313	550	137	114
Nb	13	14.6	17	10.5	11.8	9	17.9	18.2	13.9
Pb	18	12	11	5	4	6	4	5	8
Ga	3	3	4	4	4	3	6	4	3
Zn	197	26	28	27	18	19	21	31	31
S	0.435	0.284	0.651	0.432	0.578	0.325	0.083	0.138	0.142
Cu	13	13	16	10	12	13	16	17	17
Ni	23	14	18	13	16	13	19	17	15
V	11	19	30	23	31	21	33	23	18
Cr	90	90	90	70	110	120	160	90	110
La	10.7	10.7	14.6	16.2	15.7	12.4	18	13.2	10.9
Ce	23	23.1	31.3	37.6	35.1	27.9	39	27.5	22.5
Pr	2.56	2.38	3.26	4.03	3.72	3.05	4.1	2.77	2.29
Nd	9.66	8.85	12	16.1	14.3	12	15	10	8.28
Sm	1.98	1.56	1.91	3.23	2.47	2.48	2.59	1.62	1.47
Eu	0.426	0.423	0.466	0.863	0.518	0.587	0.546	0.42	0.291
Gd	1.68	1.28	1.48	2.94	1.97	2.1	2.04	1.24	1.05
Tb	0.26	0.22	0.25	0.51	0.33	0.32	0.38	0.22	0.19
Dy	1.39	1.31	1.47	2.83	1.84	1.68	2.41	1.36	1.16
Ho	0.26	0.27	0.31	0.49	0.35	0.33	0.51	0.28	0.24
Er	0.76	0.81	0.97	1.33	1.02	1	1.56	0.85	0.72
Tm	0.116	0.127	0.146	0.188	0.158	0.153	0.248	0.132	0.112
Yb	0.75	0.85	0.99	1.17	1.05	1.03	1.69	0.85	0.76
Lu	0.11	0.132	0.16	0.166	0.164	0.165	0.27	0.127	0.117
Co	8	6	8	3	4	3	2	3	3
As	13	5	7	8	8	b.d	b.d	b.d	b.d
Cs	0.2	0.2	0.3	0.3	0.3	0.2	0.2	0.2	0.1
Hf	4	4.3	5.3	4	7.2	7.4	12.2	3.3	3.1
Sb	b.d	b.d	b.d	b.d	b.d	b.d	b.d	b.d	b.d
Sc	b.d	2	3	4	3	2	3	3	2
Ta	1.05	1.07	1.38	0.77	0.91	0.78	1.36	1.42	1.14
Th	2	2.26	2.97	2.64	3.69	2.56	4.04	2.62	2.18
U	0.73	0.57	0.75	0.64	0.81	0.92	1.25	0.6	0.51

¹ sst = sandstone; ² b.d. = below detection limit; ³ detection limits

Table 5.2a: Representative whole rock geochemical analyses for Thebaud C-74.

Well							
Formation	Missisauqua						
Depth (m)	3915.74	3917.06	3918.64	3920.04	3921.98	3924.50	3926.15
Lithology ¹	Fine-C Sst	Fine-C Sst	Fine Sst	Fine Sst	Fine-M Sst	Fine Sst	Fine Sst
Major Elements (wt%)							
SiO ₂	91.31	91.83	89.8	84.71	85.07	81.77	78.7
TiO ₂	0.249	0.28	0.257	0.762	0.388	0.605	0.845
Al ₂ O ₃	2.4	2.34	2.55	6	3.48	5.86	7.61
Fe ₂ O _{3t}	2.16	1.84	1.66	4.28	1.7	4.13	3.88
MnO	0.027	0.017	0.014	0.005	0.028	0.021	0.015
MgO	0.18	0.17	0.12	0.46	0.17	0.38	0.41
CaO	0.33	0.42	1.05	0.26	2.93	1.02	0.52
Na ₂ O	0.98	0.95	1.12	1.26	1.3	1.75	1.93
K ₂ O	0.01	0.18	0.12	0.28	0.25	0.23	0.79
P ₂ O ₅	0.05	0.05	0.05	0.11	0.07	0.12	0.14
LOI	1.503	1.204	1.944	2.016	3.291	3.157	3.769
Total	99.21	99.28	98.61	100.2	98.66	99.03	98.59
Trace Elements (ppm)							
Ba	4240	1654	277	91	173	125	223
Rb	4	4	4	11	5	9	25
Sr	154	74	80	107	93	127	140
Y	5.4	5.7	6.2	12.6	12.3	10.9	16
Zr	113	149	166	370	156	260	370
Nb	13.2	14.4	11.4	31.9	20.1	29.5	33.3
Pb	8	5	4	4	< 3	25	20
Ga	3	3	3	12	4	9	11
Zn	34	32	31	46	46	30	141
S	0.143	0.083	0.404	0.063	0.087	0.79	1.08
Cu	18	23	13	10	11	13	15
Ni	19	15	16	28	12	33	30
V	18	16	21	48	25	40	64
Cr	120	110	90	120	110	90	110
La	10.3	10.5	8.41	24.1	13.2	20.8	32.2
Ce	21	21.6	17	49.2	28.6	41.8	64.9
Pr	2.14	2.17	1.83	5.21	3.07	4.46	6.59
Nd	7.44	7.62	6	18.2	11.6	15.3	22.5
Sm	1.19	1.21	0.99	2.87	2.29	2.41	3.51
Eu	0.285	0.277	0.247	0.694	0.853	0.64	0.906
Gd	0.87	0.9	0.85	2.17	2.13	1.93	2.82
Tb	0.15	0.16	0.16	0.39	0.38	0.33	0.49
Dy	0.96	1.03	1.03	2.39	2.31	2.06	2.91
Ho	0.2	0.22	0.22	0.5	0.44	0.42	0.6
Er	0.6	0.68	0.69	1.54	1.25	1.27	1.92
Tm	0.095	0.111	0.114	0.238	0.183	0.191	0.299
Yb	0.63	0.74	0.78	1.6	1.14	1.26	1.96
Lu	0.092	0.114	0.125	0.256	0.163	0.195	0.3
Co	3	3	3	4	2	13	11
As	b.d	b.d	b.d	b.d	b.d	10	6
Cs	0.1	0.1	0.2	0.4	0.2	0.3	0.9
Hf	2.7	3.7	3.5	9.4	3.9	5.8	8.6
Sb	b.d	b.d	b.d	b.d	b.d	b.d	b.d
Sc	b.d	b.d	3	5	2	3	6
Ta	1.04	1.12	0.92	2.6	1.52	2.63	3.11
Th	1.97	2.22	1.76	4.31	2.71	3.96	5.44
U	0.47	0.53	0.41	1.24	0.6	0.98	1.44

¹ sst = sandstone; ² b.d. = below detection limit; ³ detection limits

Table 5.2b: Representative whole rock analyses for Peskowesk A-99.

Well		Peskowesk A-99								
Formation		Logan Canyon								
Depth (m)		2208.90	2209.25	2209.35	2209.83	2210.15	2210.37	2213.57	2215.78	2219.03
Lithology ¹	Detection Limit ³	Shale	Shale	Fine Sst	Sst	Sst	Sst	Sst	Sst	Shale
Major Elements (wt%)										
SiO ₂	0.01	69.28	44.46	79.34	79.25	83.31	82.14	45.32	46.95	49.84
TiO ₂	0.00	1.63	1.38	1.13	1.20	1.05	0.59	1.45	1.41	1.46
Al ₂ O ₃	0.01	13.99	17.80	9.80	9.49	8.26	7.04	17.55	18.28	18.33
Fe ₂ O _{3t}	0.01	9.12	12.64	4.51	4.77	2.25	2.03	11.18	8.65	7.84
MnO	0.00	0.05	0.09	0.03	0.03	0.02	0.02	0.14	0.06	0.08
MgO	0.01	1.19	1.50	0.76	0.71	0.54	0.43	1.90	1.80	1.82
CaO	0.01	0.38	0.39	0.43	0.47	0.42	0.46	1.05	0.94	0.74
Na ₂ O	0.01	1.09	0.93	1.15	1.29	1.43	0.98	1.01	1.10	1.07
K ₂ O	0.01	3.05	2.98	2.56	2.56	2.35	1.95	2.90	2.88	2.76
P ₂ O ₅	0.01	0.18	0.22	0.19	0.18	0.12	0.10	0.35	0.27	0.26
L.O.I	0.01	14.32	17.74	4.22	4.62	3.36	3.55	16.75	16.53	14.97
Total		98.46	100.13	99.83	99.40	100.70	99.29	99.60	98.87	99.17
Trace Elements (ppm)										
Ba	3.00	401	407	676	599	2193	3890	413	406	411
Rb	1.00	79	109	56	51	49	46	108	109	115
Sr	2.00	98	119	86	95	150	164	150	156	143
Y	0.50	27.3	27	20.6	22.8	14.9	11	39	38	38
Zr	1.00	407	172	399	438	422	122	251	217	223
Nb	0.20	32.7	32	23.2	24.8	23.1	13	40	38	36
Pb	5.00	9	28	10	4	11	11	14	14	30
Ga	1.00	16	27	11	10	9	8	27	24	26
Zn	1.00	71	86	165	70	74	62	108	95	97
S (wt %)	1.00	3.91	6.903	1.43	1.53	0.30	0.127	1.129	1.104	0.552
Cu	1.00	19	38	10	10	23	23	23	33	29
Ni	20.00	50	130	47	37	64	24	78	98	76
V	5.00	107	122	67	66	63	37	140	153	142
Cr	0.05	150	131	150	130	220	101	131	143	139
La	0.05	42	55.2	26	24	21	14.7	49.1	62.2	50.5
Ce	0.01	80	109	53	48	40	26.2	93.9	122	94.2
Pr	0.05	8.45	11.9	5.87	5.48	4.40	3.02	10.4	13	10.4
Nd	0.01	28.6	43.8	22.1	20.1	15.4	11.8	41.6	50.9	40.8
Sm	0.005	5.58	7.8	4.48	4.06	2.98	2.2	7.9	9.3	7.6
Eu	0.01	1.290	1.84	1.100	1.030	0.706	0.64	2.12	2.45	2.02
Gd	0.01	4.74	5.7	4.05	3.65	2.60	2	7.3	8	6.9
Tb	0.01	0.78	0.9	0.65	0.61	0.44	0.3	1.1	1.2	1.1
Dy	0.01	4.54	4.9	3.58	3.62	2.59	1.8	6.4	6.9	6.2
Ho	0.01	0.92	0.9	0.69	0.73	0.52	0.4	1.2	1.3	1.2
Er	0.005	2.84	2.7	2.07	2.20	1.58	1.1	3.6	3.8	3.7
Tm	0.01	0.446	0.42	0.309	0.330	0.242	0.15	0.5	0.54	0.53
Yb	0.002	3.03	2.6	1.99	2.18	1.64	1	3.3	3.5	3.5
Lu	1.00	0.470	0.38	0.315	0.337	0.255	0.15	0.49	0.51	0.51
Co	1.00	15	32	14	9	34	9	16	27	21
As	0.01	5	10	b.d. ²	b.d	b.d	b.d	7	32	15
Cs	0.10	3.5	6	1.4	1.1	1.0	0.8	5.2	5.2	6
Hf	0.10	10.1	4.9	10.5	10.9	10.0	3	6.3	5.7	5.9
Sb	0.20	b.d	0.9	b.d	b.d	1.5	b.d	b.d	0.7	0.6
Sc	0.10	12	16	8	8	6	5	20	18	20
Ta	0.01	2.59	2.4	1.62	1.64	1.52	0.9	2.7	2.2	1.9
Th	0.05	9	10	6	5	5	2.9	11.4	11.7	11.6
U	0.01	3	2.8	2	2	2	0.9	2.5	2.5	2.5

¹ sst = sandstone; ² b.d. = below detection limit; ³ detection limits

Table 5.2b: Representative whole rock analyses for Peskowesk A-99.

Well	Peskowesk A-99									
Formation	Logan Canyon									
Depth (m)	2220.70	2221.17	2221.69	2222.10	2222.98	2223.37	2224.26	2225.67	2226.44	2227.16
Lithology ¹	Shale	Mudstone	Shale	Coarse Sst	Mudstone	Sst	Sst	Shale	Sst	Shale
Major Elements (wt%)										
SiO ₂	56.25	72.13	48.99	86.82	72.83	78.04	82.14	64.09	79.02	60.39
TiO ₂	1.54	1.32	1.37	0.34	1.57	1.16	0.98	1.91	1.46	2.05
Al ₂ O ₃	22.75	12.01	19.30	5.77	14.61	11.61	9.52	21.06	10.84	19.12
Fe ₂ O _{3t}	11.42	9.27	8.00	2.95	5.23	4.15	2.32	6.03	2.79	10.13
MnO	0.12	0.07	0.09	0.02	0.06	0.07	0.02	0.12	0.03	0.25
MgO	2.08	1.18	1.76	0.31	1.23	0.87	0.72	1.64	0.66	1.93
CaO	1.11	0.79	0.89	0.55	0.34	0.32	0.30	0.37	0.37	0.79
Na ₂ O	1.15	0.79	0.98	1.45	1.12	0.95	1.16	1.12	1.54	1.33
K ₂ O	3.21	2.18	2.75	1.98	2.83	2.60	2.62	3.47	3.07	3.67
P ₂ O ₅	0.34	0.16	0.31	0.03	0.12	0.11	0.11	0.18	0.16	0.29
L.O.I	14.53	7.35	14.38	3.91	8.22	5.14	4.63	13.35	3.00	10.91
Total	98.99	100.40	98.82	98.63	98.97	100.80	100.70	100.10	99.68	98.27
Trace Elements (ppm)										
Ba	350	341	368	3547	402	517	817	418	479	435
Rb	122	71	114	40	87	59	56	114	56	119
Sr	150	117	140	178	106	82	94	135	112	131
Y	39.6	28.4	38	10.5	35.3	21.2	15.2	35.3	27.3	39.8
Zr	225	738	215	182	609	438	301	347	1060	399
Nb	36.6	31.3	37	10.0	39.4	30.7	24.4	46.4	43.3	50.7
Pb	11	6	12	15	12	10	23	9	17	5
Ga	28	17	25	6	20	13	10	28	12	29
Zn	91	97	97	67	89	102	93	103	111	101
S	0.62	0.85	0.539	0.52	0.80	0.49	0.12	0.11	0.49	0.04
Cu	30	16	31	28	11	13	7	20	18	28
Ni	79	54	79	20	48	43	29	66	62	58
V	184	130	167	46	114	78	56	151	71	186
Cr	150	500	143	60	300	170	150	150	300	320
La	68	43	51.7	13	50	31	24	54	37	67
Ce	135	87	108	27	95	60	49	102	76	125
Pr	14.30	8.74	13.2	2.66	9.96	6.48	5.65	11.70	8.37	13.30
Nd	52.2	30.8	43.5	9.9	35.1	23.4	19.6	38.2	29.6	46.5
Sm	10.50	6.14	8.2	2.13	7.09	4.54	3.91	7.28	6.04	9.17
Eu	2.390	1.250	2.01	0.492	1.600	1.050	0.906	1.650	1.410	2.030
Gd	9.22	5.55	7.5	1.87	6.24	4.02	3.32	6.54	5.21	7.31
Tb	1.38	0.85	1.1	0.32	1.02	0.65	0.48	1.04	0.83	1.23
Dy	7.44	5.01	6.4	1.94	5.94	3.60	2.54	5.88	4.64	7.30
Ho	1.39	1.01	1.3	0.39	1.20	0.71	0.48	1.15	0.93	1.46
Er	4.00	3.06	3.7	1.15	3.63	2.12	1.41	3.32	2.83	4.26
Tm	0.580	0.481	0.51	0.175	0.548	0.320	0.215	0.493	0.433	0.628
Yb	3.64	3.28	3.4	1.19	3.60	2.11	1.43	3.19	2.91	4.04
Lu	0.545	0.508	0.47	0.184	0.547	0.318	0.224	0.496	0.456	0.622
Co	26	20	21	8	18	15	10	21	17	17
As	29	16	25	5	b.d	b.d	b.d	5	8	b.d
Cs	6.1	2.7	5.8	0.8	3.5	1.8	1.3	7.6	1.0	6.2
Hf	6.6	19.6	5.1	4.5	14.2	10.6	7.3	8.9	22.6	9.8
Sb	3.2	1.7	0.9	b.d	2.1	b.d	10.9	3.2	2.2	0.8
Sc	21	13	20	4	12	8	7	18	8	19
Ta	2.80	2.05	1.9	0.81	2.70	2.05	1.67	3.66	2.80	3.67
Th	13	12	15.8	3	10	6	5	13	8	13
U	3	3	3.5	1	3	2	2	3	3	3

¹ sst = sandstone; ² b.d. = below detection limit; ³ detection limits

Table 5.2b: Representative whole rock analyses for Peskowesk A-99.

Well	Peskowesk A-99									
Formation	Logan Canyon									
Depth (m)	2227.77	2228.16	2228.23	2228.27	2230.62	2233.62	2234.44	2238.65	2267.02	2269.84
Lithology ¹	Coarse Sst	Shale	Sst	Shale	Sst	Sst	Sst	Sst	Sst	Sst
Major Elements (wt%)										
SiO ₂	83.97	43.95	81.65	52.70	87.04	87.10	86.83	85.99	89.38	87.52
TiO ₂	2.05	1.59	1.09	1.97	0.28	0.53	0.16	0.52	0.14	0.10
Al ₂ O ₃	8.46	17.67	10.50	20.87	4.76	5.21	5.35	5.66	4.42	4.06
Fe ₂ O _{3t}	1.55	12.13	2.71	14.28	0.86	0.99	1.11	1.18	0.38	1.17
MnO	0.03	0.24	0.04	0.28	0.01	0.01	0.01	0.02	0.00	0.02
MgO	0.35	3.53	0.50	3.95	0.12	0.14	0.10	0.17	0.07	0.10
CaO	0.34	0.66	0.30	0.81	0.62	0.49	0.54	0.45	0.46	0.68
Na ₂ O	0.96	1.10	0.79	1.22	0.84	0.74	0.79	0.87	3.83	0.50
K ₂ O	2.01	2.90	2.19	3.64	1.78	1.80	2.21	2.02	1.57	1.59
P ₂ O ₅	0.14	0.18	0.14	0.22	0.05	0.06	0.04	0.06	0.00	0.03
L.O.I	3.30	14.89	4.59	13.99	3.03	2.73	2.41	2.67	2.04	3.22
Total	101.00	98.84	99.97	98.96	99.39	99.80	99.55	99.61	98.07	98.99
Trace Elements (ppm)										
Ba	1082	372	801	392	6700	5700	6120	5020	3578	7810
Rb	36	129	46	120	39	39	49	43	36	35
Sr	89	124	79	141	230	194	215	186	141	246
Y	23.8	43	16.5	44.2	7	11	6	10	7.4	5
Zr	1420	294	252	299	113	223	72	245	93	64
Nb	51.4	40	29.6	37.9	11	19	10	19	5.8	6
Pb	73	18	15	7	23	21	22	23	22	21
Ga	8	45	13	43	6	6	6	7	5	4
Zn	120	125	99	127	54	51	50	72	43	51
S	0.26	0.038	0.52	0.18	0.146	0.141	0.148	0.171	0.13	0.197
Cu	78	32	27	26	12	13	12	14	74	15
Ni	29	100	50	112	16	11	12	28	29	13
V	63	227	58	227	18	29	14	25	24	8
Cr	400	242	120	210	56	93	53	115	0	55
La	24	65.8	23	79	10	12.4	8.4	13.5	9	6.9
Ce	50	130	46	152	17.2	21.3	13.9	23.3	18	12.5
Pr	5.57	15.5	5.00	16.40	1.98	2.47	1.6	2.71	1.84	1.44
Nd	19.5	48.8	17.4	54.3	7.7	9.5	5.9	10.4	6.8	5.7
Sm	4.07	8.5	3.56	10.40	1.3	1.8	1.1	1.9	1.46	1.1
Eu	0.922	2.16	0.877	2.520	0.42	0.57	0.36	0.56	0.448	0.38
Gd	3.62	7.5	3.13	8.43	1.2	1.7	1	1.7	1.35	1
Tb	0.63	1.1	0.52	1.41	0.2	0.3	0.2	0.3	0.22	0.2
Dy	3.81	6.6	3.03	8.45	1.2	1.7	0.9	1.7	1.32	0.9
Ho	0.78	1.4	0.60	1.70	0.2	0.4	0.2	0.3	0.26	0.2
Er	2.39	4.3	1.76	4.95	0.7	1.1	0.6	1.1	0.80	0.5
Tm	0.377	0.6	0.258	0.716	0.11	0.17	0.09	0.17	0.121	0.08
Yb	2.65	4	1.63	4.51	0.8	1.1	0.6	1.1	0.77	0.5
Lu	0.439	0.57	0.241	0.652	0.12	0.17	0.08	0.17	0.110	0.07
Co	9	19	14	21	6	2	2	7	10	2
As	b.d	b.d	b.d	b.d	b.d	b.d	b.d	b.d	b.d	b.d
Cs	0.6	7.2	1.3	7.2	b.d	b.d	b.d	b.d	0.5	b.d
Hf	26.1	6.8	5.9	8.3	2.8	4.9	1.8	5.7	2.4	1.7
Sb	b.d	b.d	0.0	0.8	b.d	b.d	b.d	b.d	0.0	b.d
Sc	7	26	7	25	2	3	b.d	4	5	b.d
Ta	3.43	1.9	2.06	2.71	0.7	1	0.6	1	0.48	0.3
Th	6	18.5	5	13	2.1	2.7	2.1	2.7	2	1.5
U	3	4.7	2	3	0.6	0.8	0.5	0.9	1	0.4

¹ sst = sandstone; ² b.d. = below detection limit; ³ detection limits

Table 5.2b: Representative whole rock analyses for Peskowesk A-99.

Well	Peskowesk A-99							Mississauga		
Formation	Logan Canyon									
Depth (m)	2271.90	2273.15	2273.58	2274.07	2274.15	2275.64	2275.70	2479.35	2480.55	2481.14
Lithology ¹	Sst	Sst	Sst	Sst	Sst	Mudstone	Sst	Shale	Shale	Shale
Major Elements (wt%)										
SiO ₂	91.85	87.47	81.80	75.53	77.25	34.35	77.23	53.39	60.00	59.25
TiO ₂	0.28	1.02	0.39	0.19	0.31	0.28	0.84	1.21	1.50	1.39
Al ₂ O ₃	4.72	4.47	4.07	5.16	4.52	3.45	10.58	22.55	23.71	25.21
Fe ₂ O _{3t}	0.57	1.34	5.15	2.58	2.61	47.47	6.65	6.28	8.32	7.81
MnO	0.01	0.00	0.07	0.17	0.15	0.67	0.01	0.04	0.06	0.04
MgO	0.09	0.18	0.39	0.30	0.31	2.25	0.90	1.57	1.66	1.72
CaO	0.42	0.39	0.44	12.80	12.16	7.44	0.32	0.19	0.33	0.25
Na ₂ O	0.71	3.65	0.61	0.68	0.63	0.43	0.70	0.82	1.09	0.97
K ₂ O	1.54	1.69	1.65	2.46	2.02	0.76	2.54	2.76	3.13	3.19
P ₂ O ₅	0.04	0.00	0.08	0.03	0.03	2.88	0.14	0.09	0.16	0.11
L.O.I	2.50	2.34	4.50	10.01	10.34	22.18	7.31	10.97	10.30	9.92
Total	100.80	98.34	99.15	100.20	100.60	98.50	101.00	99.87	99.35	99.18
Trace Elements (ppm)										
Ba	4598	3200	1190	490	453	230	344	361	385	379
Rb	35	37	44	56	43	23	87	146	141	156
Sr	162	136	89	286	230	225	97	121	123	130
Y	7.0	29.0	12	9.8	9.7	58.4	25.1	33	38.7	36.0
Zr	135	1910	300	109	210	150	516	217	242	240
Nb	13.0	25.9	15	9.2	10.5	10.1	31.7	32	32.1	31.4
Pb	15	12	9	6	8	14	6	25	16	16
Ga	5	6	6	6	5	5	16	27	29	30
Zn	55	52	36	26	26	46	38	86	88	83
S	0.23	0.24	0.386	0.30	0.29	0.26	1.08	0.488	0.95	0.64
Cu	48	11	13	2	2	0	24	37	33	32
Ni	11	17	21	17	12	11	36	82	93	83
V	12	37	51	33	30	82	111	170	164	177
Cr	30	352	116	30	60	50	140	147	140	150
La	13	35	14.9	14	17	88	67	50.5	60	65
Ce	25	76	33	34	39	178	143	102	121	133
Pr	2.74	7.31	3.01	2.67	3.26	17.00	13.10	12.3	12.10	13.10
Nd	9.9	23.8	11.4	10.1	11.5	65.3	42.5	39.6	44.0	45.7
Sm	2.02	4.66	2.1	2.04	2.36	14.50	8.31	7.3	9.31	9.49
Eu	0.672	0.780	0.58	0.592	0.558	3.740	1.770	1.65	2.140	2.130
Gd	1.73	3.91	1.9	1.70	1.90	14.30	6.29	6.5	8.05	7.76
Tb	0.25	0.71	0.3	0.27	0.31	2.01	0.92	0.9	1.28	1.19
Dy	1.36	4.64	1.9	1.60	1.79	10.20	4.81	5.3	6.98	6.53
Ho	0.26	1.04	0.4	0.31	0.35	1.71	0.94	1.1	1.35	1.25
Er	0.74	3.37	1.3	0.86	1.00	4.14	2.79	3.3	3.99	3.70
Tm	0.107	0.562	0.2	0.125	0.147	0.494	0.420	0.47	0.588	0.542
Yb	0.69	3.93	1.4	0.79	0.97	2.58	2.75	3	3.61	3.44
Lu	0.102	0.653	0.22	0.120	0.151	0.338	0.417	0.42	0.522	0.504
Co	2	6	8	7	4	6	21	29	32	30
As	b.d	7	11	12	6	8	17	15	12	18
Cs	0.5	0.6	0.7	0.7	0.6	0.6	2.5	7.7	8.3	9.3
Hf	3.3	47.6	7.1	2.5	4.8	3.2	12.9	5	6.4	6.1
Sb	2.0	0.4	b.d.	b.d.	b.d.	0.8	b.d.	b.d.	b.d.	b.d.
Sc	2	3	5	3	3	10	11	23	22	22
Ta	1.06	1.87	0.7	0.49	0.55	0.50	1.66	1.8	2.26	2.13
Th	2	11	3.8	2	3	3	10	21.4	15	15
U	1	3	1	1	1	2	2	4.5	3	3

¹ sst = sandstone; ² b.d. = below detection limit; ³ detection limits

Table 5.2b: Representative whole rock analyses for Peskowesk A-99.

Well	Peskowesk A-99									
Formation	Missisauqua									
Depth (m)	2481.34	2482.42	2482.68	2483.77	2485.01	2486.53	2486.53	2487.76	2488.85	2492.62
Lithology ¹	Sst	Sst	Sst	Sst	Sst	Sst	Sst	Shale	Shale	Shale
Major Elements (wt%)										
SiO ₂	80.28	84.86	49.24	91.69	88.28	83.50	83.98	55.31	53.62	59.44
TiO ₂	0.75	0.83	0.85	0.38	1.08	1.15	1.30	1.46	1.35	1.30
Al ₂ O ₃	8.63	5.75	12.05	4.36	5.83	8.05	7.78	26.54	21.74	16.86
Fe ₂ O _{3t}	6.28	2.83	25.07	1.04	2.12	4.14	3.73	9.63	6.12	6.78
MnO	0.09	0.01	0.35	0.01	0.01	0.02	0.02	0.13	0.05	0.03
MgO	0.82	0.37	2.98	0.14	0.34	0.52	0.50	2.02	1.52	1.18
CaO	0.47	0.13	6.93	0.52	0.17	0.22	0.25	0.56	0.40	0.32
Na ₂ O	0.73	0.87	0.76	0.60	0.71	0.86	0.87	1.00	0.88	0.89
K ₂ O	1.78	1.32	1.50	1.52	1.37	1.43	1.41	3.17	2.70	2.26
P ₂ O ₅	0.14	0.06	0.24	0.03	0.07	0.08	0.08	0.13	0.17	0.17
L.O.I	4.55	3.16	16.80	1.75	1.96	3.04	3.09	13.63	11.45	10.01
Total	98.44	100.19	98.60	99.03	100.30	99.70	98.54	99.35	100.00	99.24
Trace Elements (ppm)										
Ba	353	353	247	4893	391	370	556	363	359	357
Rb	63	39	60	37	38	42	37	146	144	104
Sr	77	68	164	173	60	63	67	145	139	114
Y	22.3	18	30.5	10.0	23.8	28.6	30.8	31.9	36	38
Zr	442	316	264	241	768	670	804	243	237	359
Nb	17.8	18	18.9	8.8	20.7	23.8	23.3	33.5	37	49
Pb	10	5	10	34	12	14	12	12	19	11
Ga	12	8	14	4	7	10	8	31	30	23
Zn	48	39	34	77	47	98	92	86	81	84
S	0.17	0.095	0.36	0.15	0.04	0.40	0.37	0.13	0.22	2.078
Cu	9	14	12	9	8	9	10	43	34	33
Ni	30	20	24	10	29	28	28	73	69	60
V	78	38	105	19	44	63	62	201	170	139
Cr	110	128	90	50	160	120	110	150	152	222
La	33	20.8	28	12	30	32	35	58	47	45.5
Ce	78	39.5	58	23	63	67	72	108	97.7	93.3
Pr	7.83	4.3	6.24	2.56	6.44	6.66	7.75	10.50	11.9	11.2
Nd	30.3	16.6	25.5	9.5	22.8	24.5	27.4	35.8	38.9	36.8
Sm	6.66	3.1	6.35	1.99	4.67	5.13	5.59	7.09	7.2	7
Eu	1.440	0.85	1.520	0.520	0.982	0.989	1.110	1.590	1.7	1.57
Gd	5.52	2.9	6.01	1.76	4.11	4.58	4.86	5.76	6.9	6.4
Tb	0.78	0.4	0.89	0.29	0.67	0.76	0.83	0.96	1	1
Dy	4.09	2.7	5.09	1.71	4.01	4.51	5.02	5.61	5.5	5.8
Ho	0.79	0.5	1.04	0.34	0.82	0.92	1.04	1.15	1.2	1.2
Er	2.30	1.7	3.12	1.02	2.52	2.81	3.21	3.50	3.3	3.7
Tm	0.351	0.25	0.470	0.154	0.392	0.442	0.497	0.536	0.45	0.52
Yb	2.30	1.7	3.02	1.03	2.64	3.01	3.33	3.51	3.1	3.5
Lu	0.348	0.26	0.477	0.165	0.416	0.479	0.551	0.522	0.43	0.5
Co	6	7	9	2	15	7	5	18	23	15
As	6	b.d	11	b.d	b.d	b.d	b.d	11	14	12
Cs	2.4	1	3.1	0.6	0.9	1.2	1.2	9.0	8.3	5.3
Hf	11.0	7.3	6.6	6.0	18.5	17.0	20.5	6.4	5.3	8
Sb	b.d	0.9	4.5	8.2	2.4	b.d	6.8	b.d	0.6	0.7
Sc	9	5	16	2	5	7	8	20	21	16
Ta	1.10	1	1.24	0.69	1.37	1.53	1.77	2.45	2.1	2.7
Th	7	4.7	7	3	8	8	9	15	19.5	15.3
U	2	1.3	2	1	2	3	3	3	3.9	4.1

¹ sst = sandstone; ² b.d. = below detection limit; ³ detection limits

Table 5.2b: Representative whole rock analyses for Peskowesk A-99.

Well	Peskowesk A-99									
Formation	Missisauga									
Depth (m)	2927.36	2931.07	2931.91	2933.38	2934.42	2934.52	2935.46	2936.85	2938.05	2939.05
Lithology ¹	Shale	Sst	Fine Sst	Fine Sst	Sst	Fine Sst	Fine Sst	Fine Sst	Fine sst	Shale
Major Elements (wt%)										
SiO ₂	60.15	82.39	79.50	79.20	86.89	69.34	91.51	66.19	70.20	50.28
TiO ₂	1.03	0.88	0.11	0.11	0.13	0.19	0.23	0.15	0.28	0.11
Al ₂ O ₃	16.65	8.32	2.44	2.50	2.55	1.81	3.49	2.09	2.60	2.59
Fe ₂ O _{3t}	6.42	4.54	1.34	1.17	2.30	1.70	1.94	1.55	1.15	1.54
MnO	0.02	0.01	0.16	0.12	0.04	0.10	0.01	0.08	0.10	0.13
MgO	1.81	1.01	0.27	0.25	0.47	0.35	0.38	0.32	0.24	0.30
CaO	0.63	0.47	15.21	15.48	2.44	25.75	0.89	28.67	24.25	24.23
Na ₂ O	0.89	0.67	0.31	0.40	0.50	0.28	0.57	0.33	0.50	0.34
K ₂ O	3.01	1.65	0.61	0.77	0.82	0.45	0.88	0.57	0.61	0.92
P ₂ O ₅	0.08	0.06	0.02	0.02	0.03	0.04	0.04	0.04	0.04	0.04
L.O.I	8.65	3.50	10.50	10.90	3.60	16.44	1.89	17.78	16.83	19.76
Total	99.34	100.60	100.90	100.60	99.77	99.51	99.57	99.95	100.60	100.24
Trace Elements (ppm)										
Ba	306	217	114	149	1040	108	494	133	116	187
Rb	136	58	19	19	22	14	25	15	17	23
Sr	109	77	185	191	80	257	54	254	219	311
Y	31	22.5	11.6	10.5	9	7.9	6.4	9.1	16.4	11
Zr	283	557	51	77	95	106	111	108	93	56
Nb	42	24.7	4.5	5.3	8	5.8	7.8	6.8	8.2	8
Pb	23	13	7	7	17	4	12	3	5	b.d.
Ga	22	11	3	3	3	2	5	3	3	3
Zn	83	38	10	16	30	9	31	12	17	b.d.
S	1.013	0.11	0.08	0.05	0.283	0.04	0.16	0.05	0.03	0.074
Cu	30	11	3	2	13	2	5	2	2	8
Ni	63	2	2	3	11	4	9	3	4	7
V	112	74	18	15	17	15	31	15	20	16
Cr	118	160	0	20	67	30	30	30	30	134
La	44.9	40	12	12	11.8	11	15	11	16	12.3
Ce	93.8	83	27	24	23.5	22	33	23	29	23.8
Pr	11.2	8.26	2.67	2.46	2.72	2.31	3.32	2.42	3.31	2.74
Nd	36.8	28.3	10.4	9.1	11.2	8.8	12.4	9.2	13.4	11.4
Sm	6.7	5.56	2.26	1.94	2.3	1.94	2.62	2.09	3.19	2.1
Eu	1.47	1.160	0.563	0.472	0.58	0.437	0.586	0.515	0.830	0.58
Gd	5.8	4.50	2.20	1.77	2	1.71	2.18	1.95	3.15	2.1
Tb	0.9	0.70	0.35	0.29	0.3	0.26	0.34	0.29	0.49	0.3
Dy	5.3	3.99	1.93	1.62	1.7	1.43	1.95	1.58	2.64	1.7
Ho	1.1	0.81	0.37	0.32	0.3	0.27	0.39	0.30	0.48	0.3
Er	3.2	2.45	1.01	0.88	0.9	0.77	1.13	0.85	1.31	0.9
Tm	0.46	0.371	0.138	0.124	0.13	0.109	0.166	0.117	0.176	0.12
Yb	3	2.43	0.81	0.75	0.8	0.67	1.05	0.70	1.02	0.8
Lu	0.42	0.374	0.115	0.110	0.13	0.101	0.159	0.101	0.141	0.11
Co	18	12	2	b.d.	2	20	4	b.d.	b.d.	b.d.
As	12	8	6	b.d.	9	b.d.	10	b.d.	b.d.	9
Cs	6.1	2.3	0.4	0.3	b.d.	0.3	0.6	0.2	0.4	b.d.
Hf	7	14.0	1.2	1.8	2.2	2.5	2.7	2.4	2.6	1.4
Sb	b.d.	2.7	6.4	2.5	b.d.	5.0	4.1	2.4	1.8	b.d.
Sc	17	8	2	b.d.	2	b.d.	2	1	1	2
Ta	2.7	1.75	0.28	0.41	0.4	0.88	0.59	0.38	0.59	0.4
Th	14.2	8	2	2	3	2	3	2	2	2.4
U	2.7	2	b.d.	b.d.	0.5	b.d.	1	b.d.	1	0.4

¹ sst = sandstone; ² b.d. = below detection limit; ³ detection limits

Table 5.2b: Representative whole rock analyses for Peskowesk A-99:

Well	Peskowesk A-99									
Formation	Missisauga									
Depth (m)	2939.79	2940.05	2940.90	2942.03	2945.38	2947.43	2950.73	2952.02	2953.20	2954.35
Lithology ¹	Fine Sst	Fine Sst	Shale	Fine Sst	Fine Sst	Shale	Sst	Sst	Sst	Coarse Sst
Major Elements (wt%)										
SiO ₂	73.83	63.29	51.07	67.98	88.41	56.27	87.52	92.20	90.07	94.61
TiO ₂	0.15	0.12	1.37	0.11	0.36	1.36	0.26	0.10	0.12	0.08
Al ₂ O ₃	2.70	2.73	24.81	2.53	4.99	17.56	5.52	4.18	3.36	2.59
Fe ₂ O _{3t}	0.90	1.79	4.64	1.24	1.62	6.38	3.90	0.98	0.64	0.82
MnO	0.14	0.14	0.03	0.24	0.05	0.13	0.01	0.01	0.00	0.01
MgO	0.21	0.36	2.07	0.32	0.35	1.64	0.51	0.18	0.09	0.15
CaO	20.96	30.31	0.18	26.52	2.49	0.39	0.29	0.37	0.76	0.38
Na ₂ O	0.34	0.36	0.75	0.32	0.55	1.03	0.79	0.59	3.71	0.43
K ₂ O	0.74	0.82	4.12	0.67	1.11	3.12	1.02	1.14	1.41	0.67
P ₂ O ₅	0.04	0.05	0.12	0.04	0.03	0.17	0.04	0.04	0.03	0.03
L.O.I	13.66	19.07	10.64	16.96	2.75	11.30	2.81	1.67	1.84	1.38
Total	98.83	99.59	99.80	99.08	101.00	99.35	100.60	100.60	98.90	99.20
Trace Elements (ppm)										
Ba	118	155	440	241	276	345	1268	2411	3119	2089
Rb	18	20	185	17	26	124	28	29	22	20
Sr	330	327	151	428	52	119	70	99	115	81
Y	12.3	11.4	40	15.5	17.3	42	9.2	7.1	5.5	4.8
Zr	108	53	229	79	216	359	173	90	87	60
Nb	6.6	5.8	37	5.5	12.6	56	19.3	12.1	10.2	7.9
Pb	4	7	b.d.	7	6	27	21	17	18	9
Ga	3	3	34	3	6	26	9	5	4	4
Zn	6	11	93	25	36	123	52	42	44	30
S	0.07	0.07	0.026	0.12	0.06	0.473	1.30	0.16	0.12	0.09
Cu	1	3	49	2	3	28	14	15	12	25
Ni	3	2	73	2	8	65	34	9	7	7
V	15	19	181	19	22	123	24	13	15	9
Cr	40	0	150	0	70	124	40	0	20	0
La	17	15	60.5	18	14	58.4	19	15	10	9
Ce	35	32	121	37	31	122	36	30	21	19
Pr	3.79	3.47	15	4.09	3.37	14.7	3.70	2.96	2.01	1.84
Nd	14.3	13.0	49.2	15.9	13.1	48	13.3	10.1	7.0	6.1
Sm	3.09	2.91	9.2	3.57	2.99	8.8	2.60	1.95	1.33	1.15
Eu	0.711	0.685	2.1	0.836	0.710	1.79	0.578	0.406	0.335	0.245
Gd	2.87	2.62	8.1	3.37	3.07	8	2.09	1.47	1.12	0.92
Tb	0.42	0.38	1.2	0.51	0.50	1.2	0.31	0.23	0.17	0.15
Dy	2.24	2.06	6.9	2.70	2.99	7.1	1.72	1.29	0.97	0.84
Ho	0.42	0.38	1.4	0.49	0.59	1.5	0.34	0.25	0.19	0.17
Er	1.15	1.07	4.3	1.34	1.69	4.5	0.99	0.74	0.59	0.51
Tm	0.157	0.147	0.61	0.180	0.238	0.6	0.151	0.110	0.088	0.077
Yb	0.93	0.85	4	1.04	1.46	4	1.00	0.71	0.56	0.50
Lu	0.130	0.113	0.56	0.147	0.199	0.56	0.141	0.105	0.085	0.074
Co	b.d.	b.d.	21	b.d.	2	27	6	2	3	2
As	7	11	b.d.	9	b.d.	9	5	b.d.	b.d.	b.d.
Cs	0.3	0.4	9.6	0.3	0.5	5.4	0.5	0.4	0.3	0.3
Hf	2.4	1.3	5.7	1.8	5.2	8.9	4.0	2.3	2.1	1.5
Sb	6.7	6.0	b.d.	2.2	4.4	0.5	1.3	b.d.	5.7	2.5
Sc	1	b.d.	26	2	3	18	3	1	6	1
Ta	0.37	0.35	2.4	0.32	0.96	3.6	1.33	1.05	0.80	0.71
Th	2	2	19.3	2	3	14.2	4	3	2	2
U	b.d.	b.d.	4.4	b.d.	1	3.9	1	1	1	b.d.

¹ sst = sandstone; ² b.d. = below detection limit; ³ detection limits

Table 5.2b: Representative whole rock analyses for Peskowsk A-99.

Well	Peskowsk A-99							
Formation	Mic Mac							
Depth (m)	3794.37	3795.24	3795.30	3806.51	3812.19	3812.64	3813.15	3813.63
Lithology ¹	Fine Sst	Sst	Sst	Sst	Sst	Muddy Sst	Muddy Sst	Muddy Sst
Major Elements (wt%)								
SiO ₂	92.24	42.08	87.23	23.89	44.52	34.17	29.10	26.84
TiO ₂	0.34	0.49	0.33	0.49	0.84	0.63	0.44	0.20
Al ₂ O ₃	2.78	5.95	2.26	9.80	13.26	9.15	7.03	3.49
Fe ₂ O _{3t}	2.09	34.22	2.97	2.64	7.78	2.65	4.56	6.54
MnO	0.04	0.58	0.06	0.06	0.09	0.05	0.14	0.26
MgO	0.51	4.22	0.69	2.37	2.90	2.37	4.62	5.29
CaO	1.20	7.40	2.11	29.38	27.51	23.75	52.23	56.25
Na ₂ O	0.54	0.54	0.47	0.44	0.57	0.48	0.40	0.32
K ₂ O	0.16	1.08	0.22	1.96	2.41	1.65	1.30	0.61
P ₂ O ₅	0.06	3.43	0.06	0.24	0.11	0.10	0.18	0.18
L.O.I	2.12	19.52	3.86	28.12	21.60	24.02	31.51	32.87
Total	99.64	99.46	100.26	99.39	97.01	99.02	98.54	98.47
Trace Elements (ppm)								
Ba	370	141	1360	151	188	145	74	55
Rb	8	36	5	94	87	78	37	17
Sr	86	244	115	689	549	552	733	710
Y	6.9	65.6	7	20	21.5	18	12.1	13.6
Zr	203	209	117	107	178	196	109	70
Nb	10.1	13.4	11	19	20.9	19	9.7	5.4
Pb	4	14	b.d.	7	8	6	10	12
Ga	4	8	3	13	13	13	6	3
Zn	20	20	40	14	50	20	24	15
S	0.04	0.32	0.072	0.321	0.56	0.389	0.48	0.45
Cu	3	7	14	53	14	12	4	3
Ni	14	17	16	28	39	24	19	20
V	22	73	21	85	106	82	77	50
Cr	100	70	171	66	90	86	50	40
La	13	52	10.3	24.2	37	24.1	18	17
Ce	28	128	20.3	48.5	71	47.1	35	32
Pr	2.82	15.20	2.18	6.28	7.67	5.89	3.76	3.42
Nd	10.1	66.0	8.1	21.24	28.2	19.2	13.7	13.4
Sm	2.07	17.20	1.4	4.3	6.07	3.5	2.93	3.11
Eu	0.496	5.200	0.35	1.01	1.270	0.82	0.683	0.820
Gd	1.64	17.50	1.1	4.1	5.08	3.2	2.45	2.70
Tb	0.24	2.45	0.2	0.6	0.78	0.5	0.39	0.43
Dy	1.28	11.70	1.1	3.3	4.25	3	2.21	2.40
Ho	0.25	1.98	0.2	0.7	0.80	0.7	0.43	0.45
Er	0.73	4.80	0.7	2	2.23	2	1.20	1.24
Tm	0.111	0.572	0.1	0.27	0.323	0.28	0.174	0.172
Yb	0.73	3.01	0.6	1.7	2.05	1.9	1.11	1.03
Lu	0.115	0.402	0.1	0.25	0.316	0.28	0.163	0.148
Co	2	5	2	1	15	3	5	7
As	b.d.	17	b.d.	7	14	8	18	27
Cs	0.3	1.5	b.d.	4.8	4.9	4.1	1.8	0.7
Hf	5.2	5.1	2.8	2.8	5.2	5.1	2.6	1.6
Sb	1.5	4.3	b.d.	b.d.	2.7	b.d.	1.3	4.4
Sc	2	8	2	10	11	8	4	3
Ta	0.76	0.75	0.7	0.8	1.39	1.1	0.65	0.16
Th	2	5	2.2	7.1	9	7.3	4	3
U	1	2	0.6	1.4	2	1.6	1	1

¹ sst = sandstone; ² b.d. = below detection limit; ³ detection limits

5.1.1 Carbon Analysis

Carbon is an important element in understanding diagenesis and due to the sufficiently low atomic number of carbon it is not easily determined using ICPMS. Hence, a different method was used to measure carbon. In addition, the volatiles that are part of the laws on ignition (LOI) reported in Table 5.2 are probably due to carbon.

Carbon analysis was conducted using a LECO analyzer. Two sets of 0.25 grams of the powder samples were prepared for total carbon and organic carbon analyses. For total carbon, samples were treated with water over a 2-day period, and for the organic carbon samples they were treated first with water, then with dilute (10 percent) hydrochloric acid to remove organics, and again with water over a 3-day period. A steel ring (with a few percentage of carbon) and Aluminum standard chips ~ 0.05 grams (used as catalysts) had to be added to samples before the samples were analyzed. Values of respective carbon percentages were measured from analysis and used in the calculation of the inorganic carbon content [inorganic carbon = total carbon – organic carbon with all inorganic carbon assumed to be CaCO_3] as in Table 5.3a and 5.3b.

Table 5.3a: Carbon analysis results for Thebaud C-74

Thebaud C-74				Carbon Analysis (wt %)		
Depths (m)	Core #	Sample #	Lithologies	Total	Organic	Inorganic
3861.23	1	1	Very Fine Sandstone	1.40	0.08	1.32
3862.56	1	2	Mudstone	1.40	0.22	1.19
3862.91	1	3	Mudstone	2.41	0.11	2.30
3863.08	1	4V	Fine-Coarse Sandstone	2.05	0.13	1.92
3863.53	1	6	Fine-Coarse Sandstone	0.19	0.07	0.12
3863.99	1	8H	Fine-Coarse Sandstone	0.15	0.06	0.09
3864.51	1	P2	Fine Sandstone	0.26	0.10	0.16
3864.99	1	12H	Fine Sandstone	0.54	0.33	0.21
3865.53	1	P3	Fine Sandstone	0.52	0.26	0.26
3865.95	1	15H	Fine Sandstone	1.89	0.19	1.70
3866.79	1	16	Fine Sandstone	0.36	0.07	0.29
3867.39	1	19V	Fine Sandstone	0.38	0.08	0.30
3868.39	1	20	Fine Sandstone	0.41	0.23	0.17
3868.77	1	P4	Fine Sandstone	2.35	0.04	2.31
3868.94	1	23	Fine Sandstone	2.38	0.04	2.34
3869.64	1	25V	Fine Sandstone	0.51	0.53	-0.02
3870.01	1	27	Fine Sandstone	0.22	0.08	0.14
3870.19	1	28H	Fine Sandstone	0.32	0.24	0.07
3870.62	1	29H	Fine Sandstone	0.31	0.07	0.23
3871.36	1	32H	Fine Sandstone	0.55	0.07	0.48

Table 5.3a: Carbon analysis results for Thebaud C-74

Depths (m)	Core #	Sample #	Lithologies	Total	Organic	Inorganic
3871.47	1	P5	Fine Sandstone	0.42	0.06	0.35
3872.58	1	36V	Fine Sandstone	3.28	0.13	3.15
3860.38	1	3860.38	Limestone	1.15	0.65	0.50


 Average to high Inorganic Carbon Content (1.01 wt % to 3.15 wt %) based on the presented data.

Table 5.3b: Carbon analysis results for Peskowesk A-99

Peskowesk A-99				Carbon Analysis (wt %)		
Depths (m)	Core #	Sample #	Lithologies	Total	Organic	Inorganic
2224.26	1	1	Sandstone	0.48	0.35	0.13
2223.37	1	2	Sandstone	0.89	0.74	0.15
2222.98	1	3	Mudstone	2.03	1.87	0.16
2222.10	1	4	Coarse Sandstone	0.41	0.38	0.02
2221.17	1	5	Mudstone with nodule	1.45	1.00	0.45
2220.70	1	6	Shale rubble	4.50	4.21	0.29
2210.15	1	7	Sandstone	0.39	0.30	0.08
2209.83	1	8	Sandstone	0.14	0.11	0.03
2209.35	1	9	Fine Sandstone	0.24	0.25	-0.01
2208.90	1	10	Black shale	2.55	2.52	0.03
2225.67	2	11	Shale rubble	2.88	4.91	-2.03
2226.44	2	12	Sandstone	0.22	0.11	0.11
2227.16	2	13	Shale rubble	2.41	2.13	0.28
2227.77	2	14	Sandstone, coarse grained	0.31	0.16	0.16
2228.23	2	15	Sandstone	0.43	0.34	0.09
2228.27	2	16	Shale rubble	3.05	3.28	-0.23
2271.90	4	17	More sandy, sandstone	0.36	0.19	0.17
2273.15	4	18	Sandstone	0.33	0.25	0.09
2274.07	4	19	Sandstone	2.71	0.06	2.65
2274.15	4	20	Sandstone	2.62	0.09	2.53

Table 5.3b: Carbon analysis results for Peskowsk A-99

Depths (m)	Core #	Sample #	Lithologies	Total	Organic	Inorganic
2275.64	4	21	Reddish brown mudstone	6.66	0.39	6.27
2275.70	4	22	Dark gray sandstone	0.69	0.66	0.03
2267.02	4	23	Rubbles of granules	0.39	0.39	-0.01
2480.55	5	24	Shale rubble	1.45	1.40	0.05
2481.14	5	25	Shale rubble	1.19	1.19	0.00
2481.34	5	26	Sandstone	0.63	0.30	0.34
2482.68	5	27	Sandstone	4.23	0.60	3.63
2483.77	5	28	Sandstone	0.22	0.17	0.05
2485.01	5	29	Sandstone	0.11	0.07	0.05
2486.53	5	30	Sandstone (laminated)	0.16	0.12	0.03
2486.53	5	30B	Sandstone (laminated)	0.18	0.14	0.04
2487.76	5	31	Shale rubble	3.10	2.70	0.40
2950.73	6	35	Sandstone	0.16	0.14	0.03
2952.02	6	36	Sandstone	0.20	0.13	0.08
2953.20	6	37	Sandstone	0.25	0.14	0.11
2954.35	6	38	Sandstone, coarse grained	0.18	0.11	0.06
2931.07	6	39	Bioturbated sandstone	0.45	0.34	0.11
2931.91	6	40	Fine sandstone	3.15	0.04	3.11
2933.38	6	41	Fine sandstone	3.04	0.03	3.01
2934.52	6	42	Fine sandstone	4.75	0.03	4.72
2935.46	6	43	Fine sandstone	0.29	0.06	0.22

Table 5.3b: Carbon analysis results for Peskowsk A-99

Depths (m)	Core #	Sample #	Lithologies	Total	Organic	Inorganic
2936.85	6	44	Fine sandstone	4.94	0.02	4.92
2938.05	6	45	Fine sandstone	4.89	0.05	4.84
2939.79	6	46	Fine sandstone	4.04	0.03	4.01
2940.05	6	47	Fine sandstone	5.28	0.03	5.25
2942.03	6	48	Fine sandstone	4.91	0.08	4.83
2945.38	6	49	Fine sandstone	0.56	0.04	0.52
3794.37	7	50	Fine sandstone	0.44	0.04	0.40
3795.24	7	51	Sandstone	5.76	0.29	5.47
3812.19	7	53	Muddy sandstone	5.55	0.47	5.08
3813.15	7	54	Muddy sandstone	8.43	0.22	8.21
3813.63	7	55	Muddy sandstone	10.40	0.07	10.33

Average to high Inorganic Carbon Content (1.01 wt % to 10.33 wt %) based on the presented data.

5.2 RESULTS: STATISTICAL ANALYSIS

5.2.1 Introduction

The trends recognized in the geochemical data from both studied wells can be the result of (a) similar geochemical behavior of elements and (b) correlations of unrelated elements. Elements with similar geochemical behaviors tend to enter lattices of the same minerals. Examples of such geochemical behavior include correlation between Zr and Hf, rare earth elements (REE) and Y, Ga and Al, Ga and Rb, Rb and K, Nb with Ta and Ti, P and REE, LOI with Fe, Mg and Ca, which may all be present in detrital or diagenetic minerals. Thus such elemental correlations can be used to infer the presence of specific detrital and diagenetic minerals in the studied wells.

Correlations of unrelated elements may be the result of the: (i) accumulations of stable detrital minerals present e.g. chromite (Cr), zircon (Zr), and ilmenite (Ti). Thus accumulation of chromite, zircon and ilmenite or any combination of these minerals may result in positive correlation of the elements Cr, Zr, and Ti, and such positive correlations help to evaluate the presence of first sediments versus polycyclic sediments; (ii) development of certain cements. Such an example is the development of carbonate minerals and this will produce correlations between the elements Ca, Fe, Mg, Mn, and Sr.

5.2.2 Correlation Coefficient Correlations at Peskowsk A-99

Using the geochemical data, a correlation coefficient matrix table was developed using the data analysis package on Microsoft Excel, for each well studied (Tables 5.4a & 5.4b). This matrix shows a two-dimensional element variation. Correlations among elements in

Table 5.4b: Correlation coefficient matrix, Thebaud C-74

[illegible]

Shale samples removed

Total number of samples removed	42
---------------------------------	----

1

Higher than +/- 0.70 but less than 0.90

Higher than ± 0.90

the whole rock geochemical analysis at Peskowsk A-99 have been divided into three categories: (a) correlations between variables that are high (greater than 0.90), (b) correlations of variables between 0.70 and 0.90, and (c) poorer correlation. Note that these correlations involve both positive and negative coefficient values.

Elemental correlations among elements identified at Peskowsk A-99 with > 0.90 included correlations between Hf and Zr; REE amongst themselves; REE with Y; Nb, Ta and Ti; Ga and Al. There were also non-obvious correlations, such as between Mn with Si (-0.90), and V with Ga (0.93).

Hf and Zr correlate well because Hf readily substitutes for zirconium in a continuous solid solution in the mineral zircon. REE tends to show consistent geochemical behavior e.g. positive correlation between REE and Y found in monazite. Such correlations have been identified in monazites from the Lower Cretaceous deltaic sandstone of the Scotian Basin by Pe-Piper and Mackay (2006). The correlation between Nb, Ta, and Ti has also been identified by Gould (2007), and interpreted as due to Ti oxides. Ga and Al may correlate in any mineral containing Al often feldspars and micas.

Correlations at Peskowsk A-99 with variables correlating between 0.70 and 0.90 include correlation between P and REE, heavy REE, U and Th, and LOI with Ca, Mg and Fe. The correlation between P and REE is probably due to apatite, monazite and other phosphates; the correlation involving heavy REE, U and Th is common in monazite (Pe-

Piper and Mackay, 2006); and the correlations of LOI, Ca, Mg (and Fe) are due to the development of various carbonate cements.

Poorer correlations are identified between Cr with Zr and Ti, which is probably due to concentration of unrelated heavy minerals such as detrital chromite and zircon, and diagenetic TiO_2 minerals. In addition, there is a negative correlation of LOI, Ca, Fe and Mg with SiO_2 . This is probably due to the 100% problem (constant sum effect in major elements) as these elements are abundant in carbonates. No correlation was identified between Ti and P, although Gould (2007) recognized such a correlation at Venture and Thebaud wells.

5.2.3 Correlation Coefficient Correlations at Thebaud C-74

The element correlation at Thebaud (positive and negative variables greater than 0.90, and between 0.70 and 0.90) has many similar features when compared to Peskowsk, but there were a few differences identified. The correlation between Ti and P identified from fewer data by Gould (2007) has been identified at Thebaud ($R^2 = 0.89$), however with additional data the elements showed a very weak correlation coefficient ($R^2 = 0.30$).

There is also a correlation between Mg and LOI, even though such elements are already common in carbonate cements, however Mg may also be abundant in chlorite. Zr shows no correlation with Ti and weaker correlations were found between Zr and Cr than at Peskowsk A-99. Na correlates with Al, which could be due to the presence of plagioclase feldspar.

5.2.4 Principal Component Analysis (PCA)

Principal component analysis (PCA) is synonymous with factor analysis, a statistical method for identifying patterns that may be present in a large set of data. In PCA, sets of correlated variables are transformed into smaller sets of uncorrelated variables referred to as principal components. The following are used in PCA: (a) data screening and reduction, (b) discriminant analysis, (c) regression analysis, and (d) cluster analysis (Smith, 2002). A major objective of performing PCA is to interpret the principal component.

PCA is used at Thebaud C-74 and Peskowsk A-99 as an exploratory tool to investigate unknown trends that may be present in the data, and the PCA method is appropriate as it reduces dimensionality by performing a covariance analysis between factors. Hence, the first principal component in any analysis is the linear combination of maximum variances.

For this study and in order to eliminate the constant sum constraints on geochemical data, the PCA method proposed by Ohta and Arai (2007) was used. For this method, the original geochemical data was subjected to centered logratio transformation (clr-transformation) and calculations were done using singular value decomposition (svd) identical to that used by Pe-Piper *et al.* (2008). The correlations between components and the variables (e.g. major or trace elements), known as the component loadings are able to express the influences of each original variable within a given vector. PCA plots are shown in Figs. 5.3 to 5.6.

In Figs. 5.1A and B, the variances of major elements (Table 5.5a and b) are plotted to show the measure of spread within the data, and the figures display a rapid decrease of variances for both studied wells, as contributions of variables are low after the first principal component (PC1), suggesting that only PC1 provides a reasonable summary (about 90% of the total variance) of the data at Thebaud, and that PC1 and PC2 provide a reasonable summary of the data at Peskowsk. PC1 explains about 80% of the total variance, and PC2 explains about 10% of the total variance.

During preliminary PCA, a few trace elements that are present in abundances near their detection limit appeared to show quite different variations from all other elements. In the case of elements such as P_2O_5 and Cr, all samples with values lower than the detection limit were given a value 0.1 (wt % or ppm) lower than the lowest value. The remaining trace elements with values below detection limit were not included in final PCA.

Figs. 5.2A and B displays the variances of a more general data set with major and selected trace elements, facies and grain sizes (Table 5.6a and b). For this purpose, facies were re-numbered as in Table 5.7 so that similar facies had closer numbers than disparate facies, for labeling purposes. Fig. 5.2A shows that PC1 through to PC3 provide reasonable summary of the data at Thebaud C-74. PC1 explains about 70% of the total variance, PC2 explains about 10% of the total variance and PC3 explains about 5% of the total variance. Fig 5.2B shows that only PC1 and PC2 provide a reasonable summary of the data at Peskowsk A-99. PC1 explains the largest part of the total loadings, about 75%, while PC2 explain about 10% of the total variance.

Table 5.5a: Major elements PCA data with variables loadings for Thebaud C-74

Major Element (wt %)											
# ¹	SiO ₂	TiO ₂	Al ₂ O ₃	FeO	MnO	MgO	CaO	NaO	K ₂ O	P ₂ O ₅	LOI
1	80.06	0.68	5.54	4.72	0.07	0.55	6.73	1.19	0.34	0.11	6.120
2	80.40	0.29	5.63	5.56	0.07	0.69	5.93	0.79	0.59	0.04	6.120
3	79.45	0.16	3.28	5.68	0.17	0.65	9.92	0.59	0.01	0.04	8.950
4	65.59	0.29	3.95	4.87	0.34	0.77	22.66	1.11	0.30	0.11	16.830
5	90.73	0.61	4.02	2.77	0.01	0.33	0.49	0.97	0.27	0.06	1.740
6	91.40	0.57	3.81	2.51	0.01	0.31	0.43	0.90	0.25	0.06	1.380
7	87.75	0.56	5.04	3.87	0.01	0.50	0.88	0.82	0.48	0.07	2.070
8	82.34	0.72	5.33	4.65	0.01	0.57	0.82	1.23	0.48	0.08	2.706
9	81.18	0.81	6.46	4.67	0.02	0.61	1.20	0.83	0.86	0.09	3.485
10	85.96	0.68	5.27	4.48	0.02	0.52	1.58	1.02	0.38	0.10	3.020
11	86.64	0.61	5.20	3.96	0.02	0.49	1.56	1.10	0.31	0.08	2.600
12	77.08	0.72	4.56	3.64	0.17	0.49	11.77	1.06	0.40	0.09	9.810
13	76.58	0.74	4.33	3.57	0.20	0.47	12.73	0.90	0.35	0.08	10.810
14	87.91	0.58	4.95	3.77	0.01	0.49	0.85	1.00	0.33	0.09	2.350
15	86.26	0.71	5.86	4.11	0.01	0.53	0.69	1.10	0.61	0.09	3.010
16	85.96	0.65	5.47	4.44	0.02	0.55	1.24	1.11	0.45	0.08	2.590
17	85.72	0.60	5.20	3.88	0.03	0.49	2.45	1.09	0.41	0.09	2.920
18	86.85	0.72	4.90	3.79	0.02	0.47	1.82	0.95	0.38	0.08	2.400
19	79.03	0.12	1.93	1.03	0.22	0.18	16.79	0.49	0.14	0.02	12.280
20	85.05	0.70	5.21	3.95	0.02	0.44	0.99	1.23	0.42	0.09	2.160
21	87.59	0.71	4.74	3.21	0.01	0.38	0.43	1.13	0.39	0.08	1.665
22	85.91	1.00	4.48	2.93	0.01	0.36	0.60	1.33	0.42	0.09	1.629
23	85.38	0.79	4.27	2.82	0.01	0.36	0.92	1.39	0.42	0.10	2.208
24	88.70	0.29	2.43	1.55	0.02	0.12	1.92	1.26	0.12	0.06	2.695
25	90.45	0.34	2.71	1.22	0.02	0.12	1.22	1.20	0.21	0.06	1.771
26	90.43	0.45	3.81	1.66	0.01	0.13	0.43	1.12	0.34	0.07	1.881
27	86.28	0.35	2.71	3.12	0.02	0.29	1.70	1.05	0.19	0.04	2.885
28	89.45	0.37	1.95	2.00	0.01	0.17	1.41	0.99	0.18	0.08	1.935
29	90.01	0.59	3.14	2.73	0.00	0.29	0.32	1.14	0.13	0.06	1.041
30	90.31	0.34	3.24	2.00	0.01	0.19	0.32	1.37	0.25	0.07	1.107
31	89.29	0.26	2.29	2.25	0.03	0.21	0.59	0.94	0.13	0.05	2.013
32	91.31	0.25	2.40	2.16	0.03	0.18	0.33	0.98	0.01	0.05	1.503
33	91.83	0.28	2.34	1.84	0.02	0.17	0.42	0.95	0.18	0.05	1.204
34	89.80	0.26	2.55	1.66	0.01	0.12	1.05	1.12	0.12	0.05	1.944
35	84.71	0.76	6.00	4.28	0.01	0.46	0.26	1.26	0.28	0.11	2.016
36	85.07	0.39	3.48	1.70	0.03	0.17	2.93	1.30	0.25	0.07	3.291
37	81.77	0.61	5.86	4.13	0.02	0.38	1.02	1.75	0.23	0.12	3.157
38	78.70	0.85	7.61	3.88	0.02	0.41	0.52	1.93	0.79	0.14	3.769
PCA Loadings expressing the influences of each original variable within a given vector											
PC1	0.11	0.28	0.17	0.10	-0.54	0.06	-0.59	0.18	0.31	0.18	-0.27
PC2	0.33	0.01	0.07	0.17	0.10	0.04	-0.27	0.27	-0.83	0.14	-0.03

1: These numbers represents samples plotted on the PCA (Fig. 5.3) and the conversion to depth can be found in table 5.2a

Table 5.5b: Major elements PCA data with variables loadings for Peskowsk A-99

Major Element (wt %)											
# ¹	SiO ₂	TiO ₂	Al ₂ O ₃	FeO	MnO	MgO	CaO	NaO	K ₂ O	P ₂ O ₅	LOI
1	79.34	1.13	9.80	4.51	0.03	0.76	0.43	1.15	2.56	0.19	4.220
2	79.25	1.20	9.49	4.77	0.03	0.71	0.47	1.29	2.56	0.18	4.620
3	83.31	1.05	8.26	2.25	0.02	0.54	0.42	1.43	2.35	0.12	3.360
4	82.14	0.59	7.04	2.03	0.02	0.43	0.46	0.98	1.95	0.10	3.550
5	86.82	0.34	5.77	2.95	0.02	0.31	0.55	1.45	1.98	0.03	3.910
6	78.04	1.16	11.61	4.15	0.07	0.87	0.32	0.95	2.60	0.11	5.140
7	82.14	0.98	9.52	2.32	0.02	0.72	0.30	1.16	2.62	0.11	4.630
8	79.02	1.46	10.84	2.79	0.03	0.66	0.37	1.54	3.07	0.16	3.000
9	83.97	2.05	8.46	1.55	0.03	0.35	0.34	0.96	2.01	0.14	3.300
10	87.04	0.28	4.76	0.86	0.01	0.12	0.62	0.84	1.78	0.05	3.030
11	87.10	0.53	5.21	0.99	0.01	0.14	0.49	0.74	1.80	0.06	2.730
12	86.83	0.16	5.35	1.11	0.01	0.10	0.54	0.79	2.21	0.04	2.410
13	85.99	0.52	5.66	1.18	0.02	0.17	0.45	0.87	2.02	0.06	2.670
14	89.38	0.14	4.42	0.38	0.00	0.07	0.46	3.83	1.57	0.00	2.040
15	87.52	0.10	4.06	1.17	0.02	0.10	0.68	0.50	1.59	0.03	3.220
16	91.85	0.28	4.72	0.57	0.01	0.09	0.42	0.71	1.54	0.04	2.500
17	87.47	1.02	4.47	1.34	0.00	0.18	0.39	3.65	1.69	0.00	2.340
18	81.80	0.39	4.07	5.15	0.07	0.39	0.44	0.61	1.65	0.08	4.500
19	75.53	0.19	5.16	2.58	0.17	0.30	12.80	0.68	2.46	0.03	10.010
20	77.25	0.31	4.52	2.61	0.15	0.31	12.16	0.63	2.02	0.03	10.340
21	80.28	0.75	8.63	6.28	0.09	0.82	0.47	0.73	1.78	0.14	4.550
22	84.86	0.83	5.75	2.83	0.01	0.37	0.13	0.87	1.32	0.06	3.160
23	49.24	0.85	12.05	25.07	0.35	2.98	6.93	0.76	1.50	0.24	16.800
24	91.69	0.38	4.36	1.04	0.01	0.14	0.52	0.60	1.52	0.03	1.750
25	88.28	1.08	5.83	2.12	0.01	0.34	0.17	0.71	1.37	0.07	1.960
26	83.50	1.15	8.05	4.14	0.02	0.52	0.22	0.86	1.43	0.08	3.040
27	79.50	0.11	2.44	1.34	0.16	0.27	15.21	0.31	0.61	0.02	10.500
28	79.20	0.11	2.50	1.17	0.12	0.25	15.48	0.40	0.77	0.02	10.900
29	86.89	0.13	2.55	2.30	0.04	0.47	2.44	0.50	0.82	0.03	3.600
30	69.34	0.19	1.81	1.70	0.10	0.35	25.75	0.28	0.45	0.04	16.440
31	91.51	0.23	3.49	1.94	0.01	0.38	0.89	0.57	0.88	0.04	1.890
32	66.19	0.15	2.09	1.55	0.08	0.32	28.67	0.33	0.57	0.04	17.780
33	70.20	0.28	2.60	1.15	0.10	0.24	24.25	0.50	0.61	0.04	16.830
34	73.83	0.15	2.70	0.90	0.14	0.21	20.96	0.34	0.74	0.04	13.660
35	63.29	0.12	2.73	1.79	0.14	0.36	30.31	0.36	0.82	0.05	19.070
36	67.98	0.11	2.53	1.24	0.24	0.32	26.52	0.32	0.67	0.04	16.960
37	88.41	0.36	4.99	1.62	0.05	0.35	2.49	0.55	1.11	0.03	2.750
38	92.20	0.10	4.18	0.98	0.01	0.18	0.37	0.59	1.14	0.04	1.670
39	90.07	0.12	3.36	0.64	0.00	0.09	0.76	3.71	1.41	0.03	1.840
40	94.61	0.08	2.59	0.82	0.01	0.15	0.38	0.43	0.67	0.03	1.380
41	92.24	0.34	2.78	2.09	0.04	0.51	1.20	0.54	0.16	0.06	2.120
PCA Loadings expressing the influences of each original variable within a given vector											
PC1	0.10	0.31	0.21	0.08	-0.42	0.04	-0.69	0.27	0.22	0.11	-0.23
PC2	-0.27	0.10	-0.07	0.20	0.44	0.21	-0.35	-0.43	-0.21	0.52	-0.12

1: These numbers represents samples plotted on the PCA (Fig. 5.5) and the conversion to depth can be found in table 5.2b

Table 5.6a: Major and Trace Element, Facies and Grain Size PCA Data with variable loadings for Thebaud C-74

Major Elements (wt %)																Trace Elements (ppm)																Others									
# ¹	SiO ₂	TiO ₂	Al ₂ O ₃	FeO	MnO	MgO	CaO	NaO	K ₂ O	P ₂ O ₅	S (wt %)	Ba	Rb	Sr	Y	Zr	Nb	Ni	V	Cr	La	Ce	Yb	Co	Sc	Ta	Th	U	Facies	MGS											
1	80.06	0.68	5.54	4.72	0.07	0.55	6.73	1.19	0.34	0.11	0.08	185	21	225	29.50	483	41.90	25.00	45	110	35.60	79.50	2.87	9.00	4.00	2.83	8.90	2	11	250											
2	80.40	0.29	5.63	5.56	0.07	0.69	5.93	0.79	0.59	0.04	0.22	205	27	240	18.70	215	27.20	28.00	79	80	29.30	66.30	2.26	12.00	5.00	2.08	9.11	1	20	850											
3	79.45	0.16	3.28	5.68	0.17	0.65	9.92	0.59	0.01	0.04	0.11	354	11	258	14.60	131	16.00	20.00	48	50	23.40	54.50	1.60	9.00	3.00	1.21	5.76	1	26	1500											
4	65.59	0.29	3.95	4.87	0.34	0.77	22.66	1.11	0.30	0.11	0.13	223	8	661	22.00	222	27.10	14.00	52	70	27.50	67.60	1.89	9.00	3.00	1.66	5.42	2	26	400											
5	90.73	0.61	4.02	2.77	0.01	0.33	0.49	0.97	0.27	0.06	0.14	4092	8	168	15.81	713	30.11	19.13	35	242	33.83	76.53	1.93	5.03	4.03	2.23	5.90	1	4	250											
6	91.40	0.57	3.81	2.51	0.01	0.31	0.43	0.90	0.25	0.06	0.14	4278	11	173	18.84	669	30.42	14.10	27	191	35.15	76.35	2.21	5.04	2.01	2.10	6.68	2	4	250											
7	87.75	0.56	5.04	3.87	0.01	0.50	0.88	0.82	0.48	0.07	0.18	354	18	118	15.90	313	21.40	21.00	55	80	30.10	67.30	1.68	6.00	6.00	1.50	5.02	1	4	250											
8	82.34	0.72	5.33	4.65	0.01	0.57	0.82	1.23	0.48	0.08	0.23	275	20	140	18.20	417	24.80	26.00	56	140	30.60	72.30	1.90	6.00	5.00	1.78	4.82	1.3	4	250											
9	81.18	0.81	6.46	4.67	0.02	0.61	1.20	0.83	0.86	0.09	0.35	175	33	169	20.20	463	29.80	26.00	74	130	36.50	84.30	2.33	8.00	7.00	2.17	6.84	1.71	24	250											
10	85.96	0.68	5.27	4.48	0.02	0.52	1.58	1.02	0.38	0.10	0.40	222	14	150	16.80	600	22.30	26.00	53	130	25.00	61.00	1.94	7.00	4.00	1.73	6.23	2	24	250											
11	86.64	0.61	5.20	3.96	0.02	0.49	1.56	1.10	0.31	0.08	0.15	219	17	132	20.00	485	30.80	25.00	53	120	32.50	73.10	2.06	8.00	4.00	2.18	7.23	2	24	250											
12	77.08	0.72	4.56	3.64	0.17	0.49	11.77	1.06	0.40	0.09	0.09	227	12	641	22.80	492	23.20	15.00	48	90	29.10	67.00	2.20	4.00	5.00	1.69	5.94	1	24	200											
13	76.58	0.74	4.33	3.57	0.20	0.47	12.73	0.90	0.35	0.08	0.07	176	12	645	19.90	556	22.80	13.00	46	110	27.20	62.30	1.98	3.00	5.00	1.80	5.95	1	20	200											
14	87.91	0.58	4.95	3.77	0.01	0.49	0.85	1.00	0.33	0.09	0.17	220	16	122	16.70	345	21.10	18.00	45	60	24.10	51.80	1.78	4.00	4.00	1.48	5.29	1	20	250											
15	86.26	0.71	5.86	4.11	0.01	0.53	0.69	1.10	0.61	0.09	0.38	185	23	126	22.70	465	27.40	24.00	49	70	35.80	79.60	2.47	10.00	5.00	1.96	6.94	2	20	400											
16	85.96	0.65	5.47	4.44	0.02	0.55	1.24	1.11	0.45	0.08	0.18	233	16	152	19.00	390	25.80	21.00	44	70	28.40	63.10	1.99	6.00	5.00	1.83	6.17	1	20	200											
17	85.72	0.60	5.20	3.88	0.03	0.49	2.45	1.09	0.41	0.09	0.07	333	14	109	18.40	390	26.40	18.00	48	70	27.80	61.10	1.79	5.00	4.00	1.93	5.87	1	20	250											
18	86.85	0.72	4.90	3.79	0.02	0.47	1.82	0.95	0.38	0.08	0.08	286	14	88	22.80	786	30.50	20.00	48	110	34.30	74.20	2.69	5.00	5.00	2.03	7.95	2	20	200											
19	79.03	0.12	1.93	1.03	0.22	0.18	16.79	0.49	0.14	0.02	0.05	61	4	637	11.00	83	9.10	2.00	23	0	13.60	30.60	1.01	1.00	1.00	0.62	2.65	1	32	1500											
20	85.05	0.70	5.21	3.95	0.02	0.44	0.99	1.23	0.42	0.09	0.28	675	13	91	18.60	488	30.90	30.00	38	120	26.60	55.20	2.01	7.00	4.00	2.13	4.78	1.5	11	250											
21	87.59	0.71	4.74	3.21	0.01	0.38	0.43	1.13	0.39	0.08	0.13	739	13	73	17.20	495	26.90	25.00	41	140	26.80	55.20	1.97	9.00	4.00	2.08	4.99	1.46	7	400											
22	85.91	1.00	4.48	2.93	0.01	0.36	0.60	1.33	0.42	0.09	0.18	437	13	67	23.30	1076	27.80	21.00	47	200	30.30	64.50	3.04	8.00	4.00	2.17	6.23	2.26	7	750											
23	85.38	0.79	4.27	2.82	0.01	0.36	0.92	1.39	0.42	0.10	0.21	175	14	137	22.30	878	24.40	18.00	34	140	26.90	56.10	2.66	6.00	2.00	1.89	5.59	1.97	7	400											
24	88.70	0.29	2.43	1.55	0.02	0.12	1.92	1.26	0.12	0.06	0.44	165	6	73	7.30	188	13.00	23.00	11	90	10.70	23.00	0.75	8.00	0.00	1.05	2.00	0.73	28	400											
25	90.45	0.34	2.71	1.22	0.02	0.12	1.22	1.20	0.21	0.06	0.28	468	6	56	7.40	178	14.60	14.00	19	90	10.70	23.10	0.85	6.00	2.00	1.07	2.26	0.57	4	400											
26	90.43	0.45	3.81	1.66	0.01	0.13	0.43	1.12	0.34	0.07	0.65	223	10	93	8.40	216	17.00	18.00	30	90	14.60	31.30	0.99	8.00	3.00	1.38	2.97	0.75	4	400											
27	86.28	0.35	2.71	3.12	0.02	0.29	1.70	1.05	0.19	0.04	0.58	201	7	136	10.80	367	11.80	16.00	31	110	15.70	35.10	1.05	4.00	3.00	0.91	3.69	0.81	4	400											
28	89.45	0.37	1.95	2.00	0.01	0.17	1.41	0.99	0.18	0.08	0.33	354	5	91	9.10	313	9.00	13.00	21	120	12.40	27.90	1.03	3.00	2.00	0.78	2.56	0.92	4	400											
29	90.01	0.59	3.14	2.73	0.00	0.29	0.32	1.14	0.13	0.06	0.08	1041	7	72	13.50	550	17.90	19.00	33	160	18.00	39.00	1.69	2.00	3.00	1.36	4.04	1.25	4	400											
30	90.31	0.34	3.24	2.00	0.01	0.19	0.32	1.37	0.25	0.07	0.14	1457	5	76	7.90	137	18.20	17.00	23	90	13.20	27.50	0.85	3.00	3.00	1.42	2.62	0.6	7	800											
31	89.29	0.26	2.29	2.25	0.03	0.21	0.59	0.94	0.13	0.05	0.14	11670	4	392	6.90	114	13.90	15.00	18	110	10.90	22.50	0.76	3.00	2.00	1.14	2.18	0.51	7	800											
32	91.31	0.25	2.40	2.16	0.03	0.18	0.33	0.98	0.01	0.05	0.14	4240	4	154	5.40	113	13.20	19.00	18	120	10.30	21.00	0.63	3.00	0.00	1.04	1.97	0.47	7	800											
33	91.83	0.28	2.34	1.84	0.02	0.17	0.42	0.95	0.18	0.05	0.08	1654	4	74	5.70	149	14.40	15.00	16	110	10.50	21.60	0.74	3.00	0.00	1.12	2.22	0.53	7	800											
34	89.80	0.26	2.55	1.66	0.01	0.12	1.05	1.12	0.12	0.05	0.40	277	4	80	6.20	166	11.40	16.00	21	90	8.41	17.00	0.78	3.00	3.00	0.92	1.76	0.41	4	250											
35	84.71	0.76	6.00	4.28	0.01	0.46	0.26	1.26	0.28	0.11	0.06	91	11	107	12.60	370	31.90	28.00	48	120	24.10	49.20	1.60	4.00	5.00	2.60	4.31	1.24	7	250											
36	85.07	0.39	3.48	1.70	0.03	0.17	2.93	1.30	0.25	0.07	0.09	173	5	93	12.30	156	20.10	12.00	25	110	13.20	28.60	1.14	2.00	2.00	1.52	2.71	0.6	7	400											
37	81.77	0.61	5.86	4.13	0.02	0.38	1.02	1.75	0.23	0.12	0.79	125	9	127	10.90	260	29.50	33.00	40	90	20.80	41.80	1.26	13.00	3.00	2.63	3.96	0.98	7	250											
38	78.70	0.85	7.61	3.88	0.02	0.41	0.52	1.93	0.79	0.14	1.08	223	25	140	16.00	370	33.30	30.00	64	110	32.20	64.90	1.96	11.00	6.00	3.11	5.44	1.44	23	250											
PCA Loadings																																									
PC1	0.04	0.14	0.04	0.00	-0.51	-0.04	-0.58	0.08	0.11	0.08	0.15	0.29	0.03	-0.25	-0.03	0.14	0.05	0.14	-0.01	0.25	0.01	0.00	0.01	0.06	0.05	0.07	-0.01	0.01	-0.24	-0.07											
PC2	0.14	-0.10	-0.06	-0.03	0.21	-0.09	0.00	0.08	-0.34	-0.02	0.03	0.71	-0.1																												

¹ These number represent samples plotted on PCA (Fig. 5.4) and the depth conversion are on table 5.2b

² Facies use numbers listed in Table 5.7

³ Mean grain size in μm

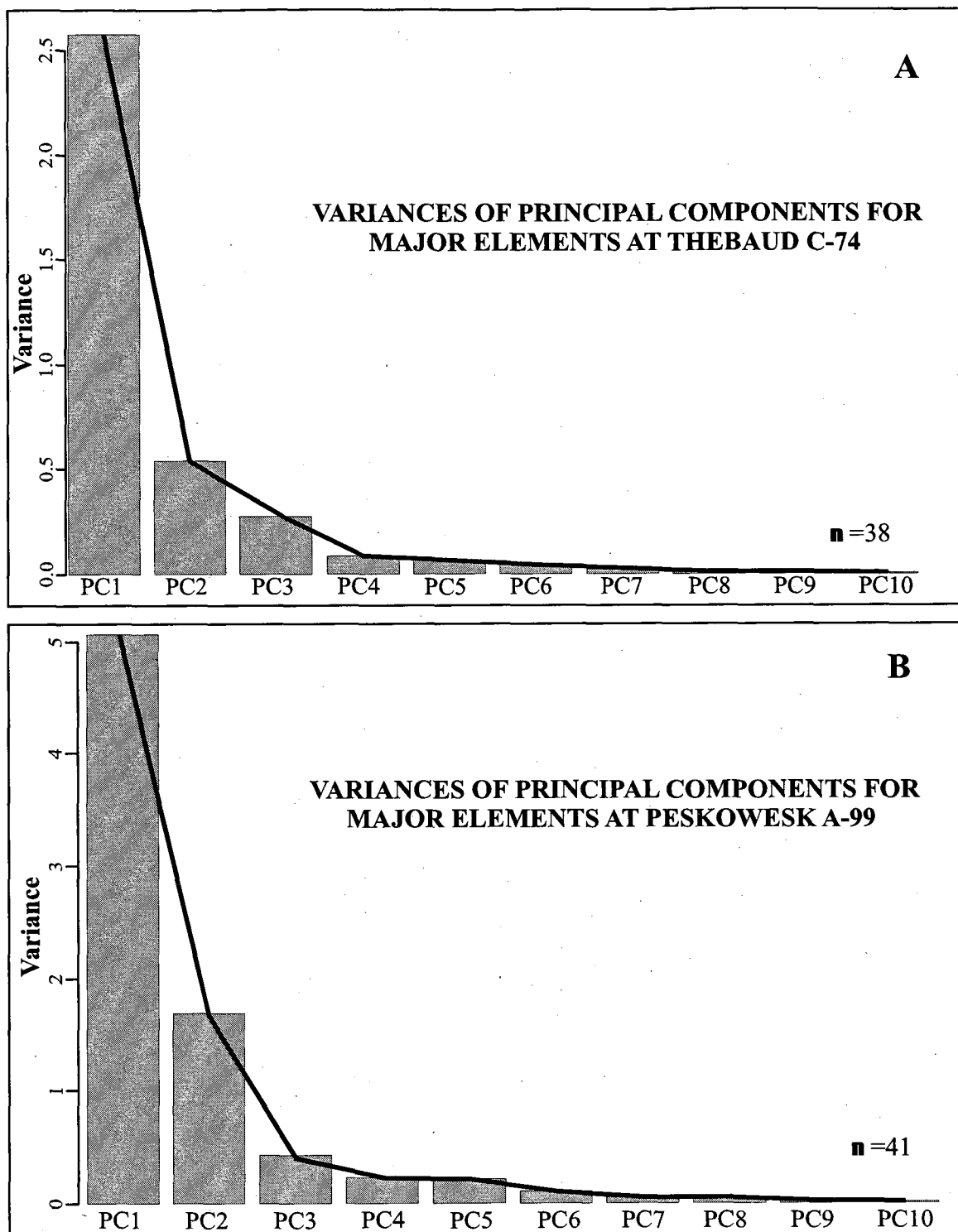
Table 5.6b: Major and Trace Element, Facies and Grain Size PCA Data with variable loadings for Peskovesk A-99

Major Elements (wt %)											Trace Elements (ppm)											Others										
# ¹	SiO ₂	TiO ₂	Al ₂ O ₃	FeO	MnO	MgO	CaO	NaO	K ₂ O	P ₂ O ₅	S (wt %)	Ba	Rb	Sr	Y	Zr	Nb	Ni	V	Cr ⁺ *	La	Ce	Yb	Co	Sc	Ta	Th	U	Facies ²	MGS ³		
1	79.34	1.13	9.80	4.51	0.03	0.76	0.43	1.15	2.56	0.19	1.43	676	56	86	20.6	399	23	47.00	67	150	26.00	53.00	1.99	14.00	8.00	1.62	5.53	2	5	250		
2	79.25	1.20	9.49	4.77	0.03	0.71	0.47	1.29	2.56	0.18	1.53	599	51	95	22.8	438	25	37.00	66	130	24.00	47.70	2.18	9.00	8.00	1.64	4.94	2	5	250		
3	83.31	1.05	8.26	2.25	0.02	0.54	0.42	1.43	2.35	0.12	0.30	2193	49	150	14.9	422	23	64.00	63	220	21.10	40.30	1.64	34.00	6.00	1.52	4.96	2	5	250		
4	82.14	0.59	7.04	2.03	0.02	0.43	0.46	0.98	1.95	0.10	0.13	3890	46	164	11	122	13	24.00	37	101	14.70	26.20	1.00	9.00	5.00	0.90	2.90	0.9	1	750		
5	86.82	0.34	5.77	2.95	0.02	0.31	0.55	1.45	1.98	0.03	0.52	3547	40	178	10	182	10	20.12	46	60	12.88	26.76	1.19	8.05	4.02	0.81	3.49	1	24	1000		
6	78.04	1.16	11.61	4.15	0.07	0.87	0.32	0.95	2.60	0.11	0.49	517	59	82	21.2	438	31	43.00	78	170	30.70	59.90	2.11	15.00	8.00	2.05	6.44	2	5	250		
7	82.14	0.98	9.52	2.32	0.02	0.72	0.30	1.16	2.62	0.11	0.12	817	56	94	15.2	301	24	29.00	56	150	23.80	48.70	1.43	10.00	7.00	1.67	5.31	2	5	250		
8	79.02	1.46	10.84	2.79	0.03	0.66	0.37	1.54	3.07	0.16	0.49	479	56	112	27.3	1060	43	62.00	71	300	37.20	76.20	2.91	17.00	8.00	2.80	7.62	3	5	250		
9	83.97	2.05	8.46	1.55	0.03	0.35	0.34	0.96	2.01	0.14	0.26	1082	36	89	23.8	1420	51	29.00	63	400	23.80	50.30	2.65	9.00	7.00	3.43	6.23	3	6	1000		
10	87.04	0.28	4.76	0.86	0.01	0.12	0.62	0.84	1.78	0.05	0.15	6700	39	230	7	113	11	16.00	18	56	10.00	17.20	0.80	6.00	2.00	0.70	2.10	0.6	1	750		
11	87.10	0.53	5.21	0.99	0.01	0.14	0.49	0.74	1.80	0.06	0.14	5700	39	194	11	223	19	11.00	29	93	12.40	21.30	1.10	2.00	3.00	1.00	2.70	0.8	1	750		
12	86.83	0.16	5.35	1.11	0.01	0.10	0.54	0.79	2.21	0.04	0.15	6120	49	215	6	72	10	12.00	14	53	8.40	13.90	0.60	2.00	0.00	0.60	2.10	0.5	1	750		
13	85.99	0.52	5.66	1.18	0.02	0.17	0.45	0.87	2.02	0.06	0.17	5020	43	186	10	245	19	28.00	25	115	13.50	23.30	1.10	7.00	4.00	1.00	2.70	0.9	1	750		
14	89.38	0.14	4.42	0.38	0.00	0.07	0.46	3.83	1.57	0.00	0.13	3578	36	141	7	93	6	29.18	24	19.99	8.79	17.61	0.77	10.06	5.03	0.48	1.91	1	2	1000		
15	87.52	0.10	4.06	1.17	0.02	0.10	0.68	0.50	1.59	0.03	0.20	7810	35	246	5	64	6	13.00	8	55	6.90	12.50	0.50	2.00	0.00	0.30	1.50	0.4	2	750		
16	91.85	0.28	4.72	0.57	0.01	0.09	0.42	0.71	1.54	0.04	0.23	4598	35	162	7	135	13	11.09	12	30	13.10	25.40	0.69	2.02	2.02	1.06	2.40	1	2	1000		
17	87.47	1.02	4.47	1.34	0.00	0.18	0.39	3.65	1.69	0.00	0.24	3200	37	136	29	1910	26	17.09	37	352	34.89	75.61	3.93	6.03	3.02	1.87	11.36	3	23	250		
18	81.80	0.39	4.07	5.15	0.07	0.39	0.44	0.61	1.65	0.08	0.39	1190	44	89	12	300	15	21.00	51	116	14.90	33.00	1.40	8.00	5.00	0.70	3.80	1	8	250		
19	75.53	0.19	5.16	2.58	0.17	0.30	12.80	0.68	2.46	0.03	0.30	490	56	286	9.8	109	9	17.00	33	30	14.40	33.90	0.79	7.00	3.00	0.49	2.45	1	8	250		
20	77.25	0.31	4.52	2.61	0.15	0.31	12.16	0.63	2.02	0.03	0.29	453	43	230	9.7	210	11	12.00	30	60	17.20	39.20	0.97	4.00	3.00	0.55	2.85	1	8	250		
21	80.28	0.75	8.63	6.28	0.09	0.82	0.47	0.73	1.78	0.14	0.17	353	63	77	22.3	442	18	30.00	78	110	33.30	77.70	2.30	6.00	9.00	1.10	7.29	2	27	250		
22	84.86	0.83	5.75	2.83	0.01	0.37	0.13	0.87	1.32	0.06	0.10	353	39	68	18	316	18	20.00	38	128	20.80	39.50	1.70	7.00	5.00	1.00	4.70	1.3	24	250		
23	49.24	0.85	12.05	25.07	0.35	2.98	6.93	0.76	1.50	0.24	0.36	247	60	164	30.5	264	19	24.00	105	90	27.70	57.80	3.02	9.00	16.00	1.24	6.79	2	24	250		
24	91.69	0.38	4.36	1.04	0.01	0.14	0.52	0.60	1.52	0.03	0.15	4893	37	173	10	241	9	10.08	19	50	11.80	23.29	1.03	2.02	2.02	0.69	2.83	1	10	250		
25	88.28	1.08	5.83	2.12	0.01	0.34	0.17	0.71	1.37	0.07	0.04	391	38	60	23.8	768	21	29.00	44	160	30.40	62.70	2.64	15.00	5.00	1.37	7.57	2	10	250		
26	83.50	1.15	8.05	4.14	0.02	0.52	0.22	0.86	1.43	0.08	0.40	370	42	63	28.6	670	24	28.00	63	120	31.90	67.10	3.01	7.00	7.00	1.53	8.31	3	16	250		
27	79.50	0.11	2.44	1.34	0.16	0.27	15.21	0.31	0.61	0.02	0.08	114	19	185	11.6	51	5	2.00	18	19.99	12.10	27.00	0.81	2.00	2.00	0.28	1.65	0.5	26	250		
28	79.20	0.11	2.50	1.17	0.12	0.25	15.48	0.40	0.77	0.02	0.05	149	19	191	10.5	77	5	3.00	15	20	12.20	24.40	0.75	0.00	0.00	0.41	1.90	0.5	6	250		
29	86.89	0.13	2.55	2.30	0.04	0.47	2.44	0.50	0.82	0.03	0.28	1040	22	80	9	95	8	11.00	17	67	11.80	23.50	0.80	2.00	2.00	0.40	3.00	0.5	6	250		
30	69.34	0.19	1.81	1.70	0.10	0.35	25.75	0.28	0.45	0.04	0.04	108	14	257	7.9	106	6	4.00	15	30	11.40	22.30	0.67	20.00	0.00	0.88	2.02	0.5	6	250		
31	91.51	0.23	3.49	1.94	0.01	0.38	0.89	0.57	0.88	0.04	0.16	494	25	54	6.4	111	8	9.00	31	30	15.10	32.60	1.05	4.00	2.00	0.59	3.27	1	9	250		
32	66.19	0.15	2.09	1.55	0.08	0.32	28.67	0.33	0.57	0.04	0.05	133	15	254	9.1	108	7	3.00	15	30	11.40	22.70	0.70	0.00	1.00	0.38	1.92	0.5	6	250		
33	70.20	0.28	2.60	1.15	0.10	0.24	24.25	0.50	0.61	0.04	0.03	116	17	219	16.4	93	8	4.00	20	30	16.00	28.90	1.02	0.00	1.00	0.59	2.48	1	6	250		
34	73.83	0.15	2.70	0.90	0.14	0.21	20.96	0.34	0.74	0.04	0.07	118	18	330	12.3	108	7	3.00	15	40	17.10	35.00	0.93	0.00	1.00	0.37	2.27	0.5	1	250		
35	63.29	0.12	2.73	1.79	0.14	0.36	30.31	0.36	0.82	0.05	0.07	155	20	327	11.4	53	6	2.00	19	19.99	15.00	31.60	0.85	0.00	0.00	0.35	2.04	0.5	1	250		
36	67.98	0.11	2.53	1.24	0.24	0.32	26.52	0.32	0.67	0.04	0.12	241	17	428	15.5	79	6	2.00	19	19.99	17.50	37.20	1.04	0.00	2.00	0.32	2.34	0.5	1	250		
37	88.41	0.36	4.99	1.62	0.05	0.35	2.49	0.55	1.11	0.03	0.06	276	26	52	17.3	216	13	8.00	22	70	13.80	31.40	1.46	2.00	3.00	0.96	2.89	1	11	250		
38	92.20	0.10	4.18	0.98	0.01	0.18	0.37	0.59	1.14	0.04	0.16	2411	29	99	7.1	90	12	9.00	13	19.99	15.20	30.40	0.71	2.00	1.00	1.05	2.67	1	1	750		
39	90.07	0.12	3.36	0.64	0.00	0.09	0.76	3.71	1.41	0.03	0.12	3119	22	115	6	87</																

Table 5.7: Facies re-numbering chart for both studied wells.

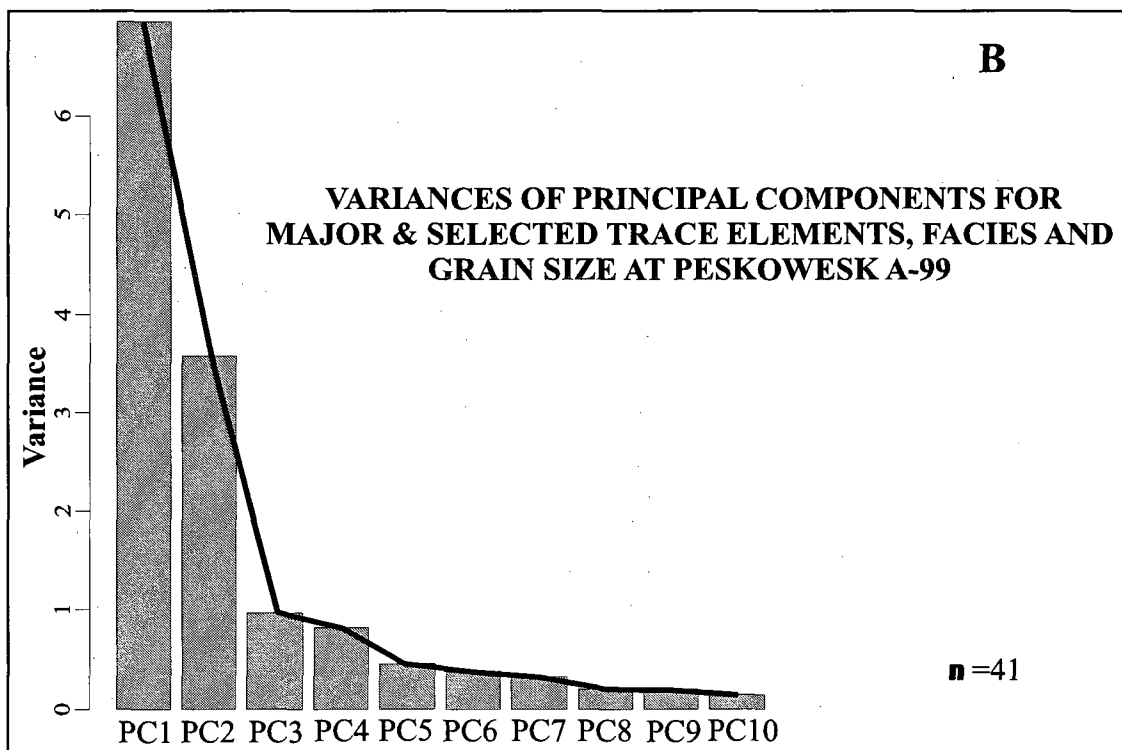
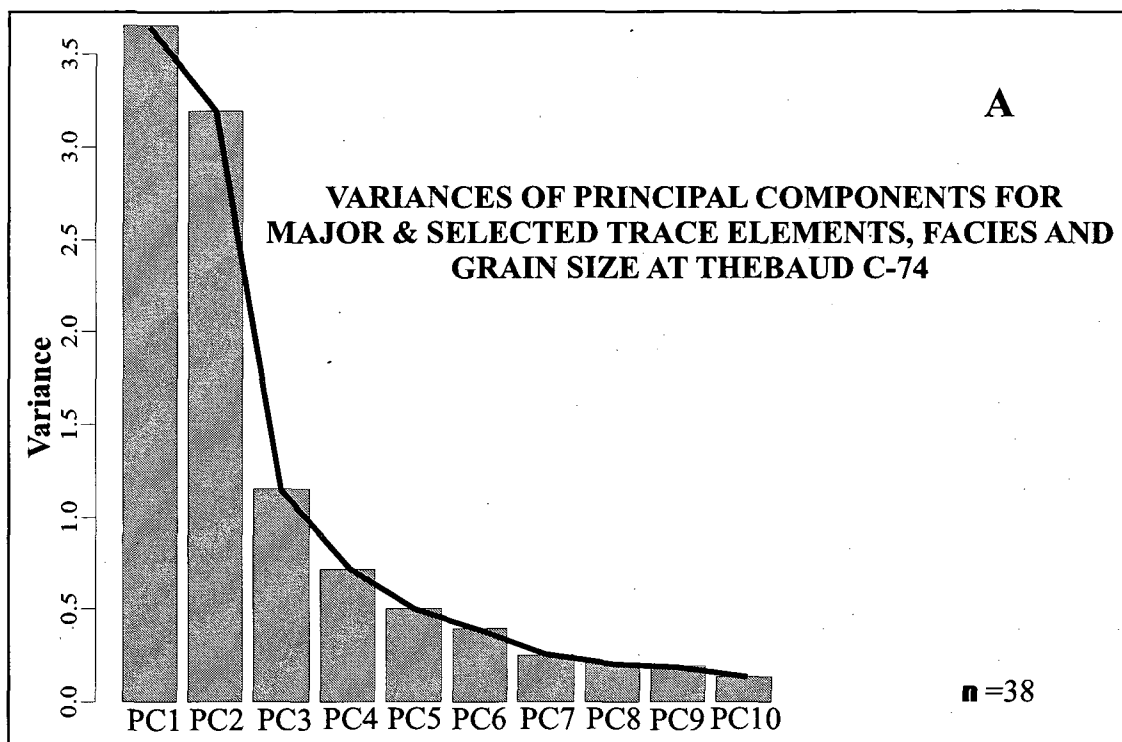
	General Descriptions	Sub facies	Facies # for PCA
Facies 0	Mudstone with sandstone and siltstone beds (< 25 cm) and laminae, absent to moderate bioturbation	0	11
		0a	12
		0c	13
		0g	14
		0l	15
		0m	16
		0n	17
		0o	18
		0s	19
Facies 1	Bioturbated mudstone	1	20
		1c	21
		1d	22
Facies 2	Generally fine-grained sandstone with mudstone	2b	23
		2c	24
		2d	25
Facies 3	Conglomerate formed with bioturbated shelly sandy mudstone to muddy sandstone generally with some coarse sand or granule sized intraclasts and/or lithic clasts. Commonly sideritic diagenesis. In other wells, bioclastic and oolitic limestones	3	26
		3a	27
		3b	28
		3l	29
		3m	30
		3o	31
		3s	32
Facies 4	Fine to coarse sandstone (general medium to coarse), interbedded mudstone with siltstone laminae, and cross-bedding are characteristic	4g	2
		4o	4
		4s	3
		4x	1
Facies 5	Bioturbated fine-grained sandstone	5	5
		5s	6
Facies 9	Thick (> 25 cm) bedded sandstones in "graded" beds, moderate bioturbation at top, plant debris, minor interbedded facies 0	9	7
		9b	8
		9f	9
		9g	10

¹: A re-numbering of facies and sub-facies was required for PCA. Facies numbers do not relate to individual facies distances or interpretations because these numbers are arbitrary. The new scheme suggests inferred relationships between facies.



'n' represents sample numbers

Figure 5.1: Histogram showing the variance of principal components for major elements at Thebaud C-74 (A) and Peskowesk A-99 (B).



'n' represents sample numbers

Figure 5.2: Histogram showing the variance of principal components for major and trace elements, facies and grain size at Thebaud C-74 (A) and Peskowsk A-99 (B).

A few trends are apparent with the application of PCA on major elements (Figs. 5.3 and 5.5) and on combinations of major and trace elements with facies and grain size (Fig. 5.4 and 5.6). These biplots show vectors that correspond to a particular variable (e.g. an element), which is proportional to its component loading. Note that numbers on these figures correspond to the sample numbers on Tables 5.6a and 5.6b.

At Thebaud in the major element PCA (Fig. 5.3), CaO and MnO show strong negative loading on PC1, whereas TiO₂ and P₂O₅ show positive loadings. K₂O loads equally on PC2 and PC1. The remaining major elements show a small positive loading on PC1. The remaining major elements correlate in the center of the plot. Some sub-facies 2c samples load heavily with K₂O (e.g. sample 9). In addition, two samples (samples 3 and 32) have very low K₂O and plot together however one of these samples is a facies 3 and the other is facies 9.

When facies, grain size and major and trace elements are plotted for Thebaud C-74, most variables concentrate in the centre of the plot (Fig. 5.4) with low negative loadings on both PC1 and PC2. As with the major elements PCA (Fig. 5.3), MnO and CaO load strongly together (and MnO with Sr), and load negatively on PC1 but slightly positive on PC2, and K₂O (going with Rb) shows a low positive loading on PC2. Ba shows a strong loading on PC1. Fe₂O_{3T} goes with MgO and both show low positive loadings on PC2. Some facies 3 samples load heavily with CaO and MnO (cluster a), but cluster b does not correspond to any particular facies.

Considering major elements at Peskowsk (Fig. 5.5), the behavior of CaO and MnO is similar to that at Thebaud C-74, showing strong negative loading on PC1. In addition, MgO, Fe₂O_{3T}, and P₂O₅ load positively on PC2 and K₂O, SiO₂, TiO₂, Al₂O₃, and Na₂O load positively on PC1 and negatively on PC2.

When the major and trace elements are considered at Peskowsk, the element loadings are different from those at Thebaud C-74. Fe₂O_{3T} goes with MgO and both show moderate positive loadings on PC2. TiO₂, Zr, Cr, and S go together with low positive loading on PC2. K₂O and Na₂O go together with low negative loading on PC2. SiO₂ and Sr go together with low negative loading on PC2, and Ba shows a strong negative loading on PC1. As with the major elements PCA (Fig. 5.5), MnO and CaO load strongly together, in this case showing low positive loading on PC2. All other major and trace elements concentrate in the centre of the plot with low loading on both PC1 and PC2.

Clusters (a, b, and c) recognized at Peskowsk A-99 (Fig. 5.6), do not correspond to any particular facies. However, cluster b show strong correlation to Ba.

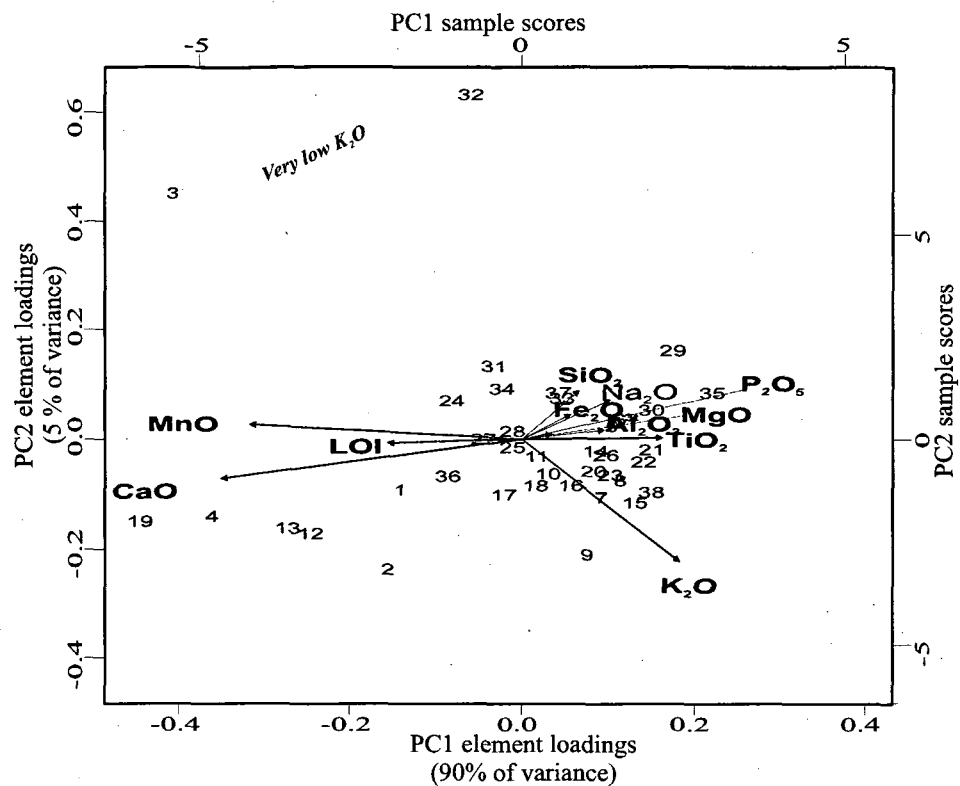


Figure 5.3: PCA biplot of major elements loading at the Thebaud C-74 well.

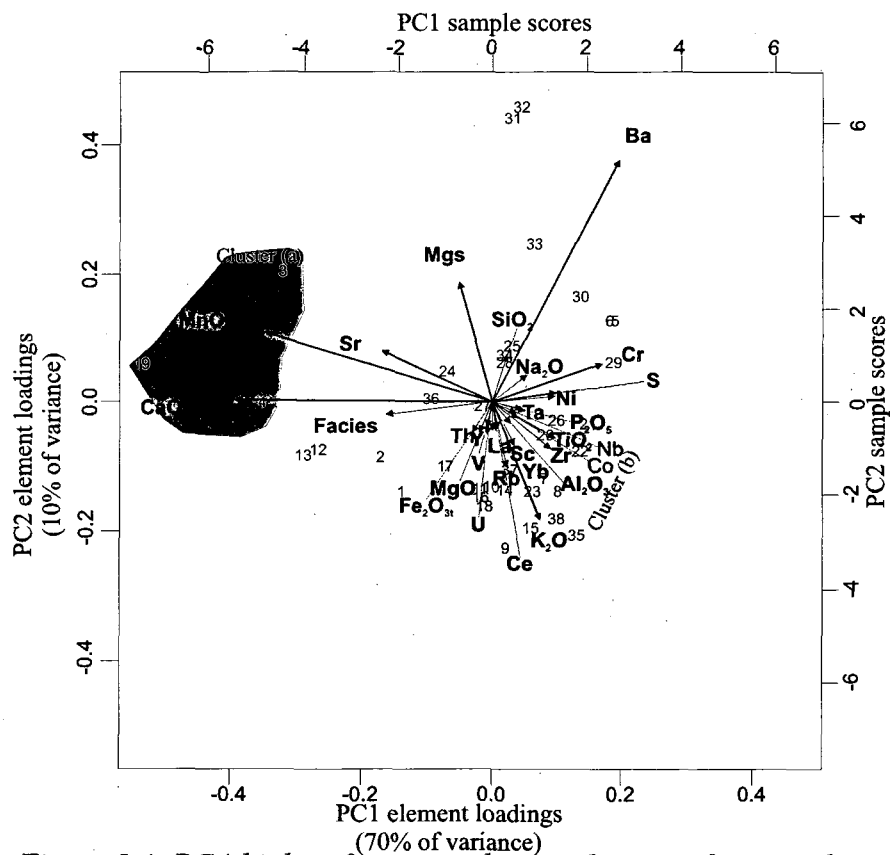


Figure 5.4: PCA biplot of major and trace elements, facies and grain size loading at the Thebaud C-74 well.

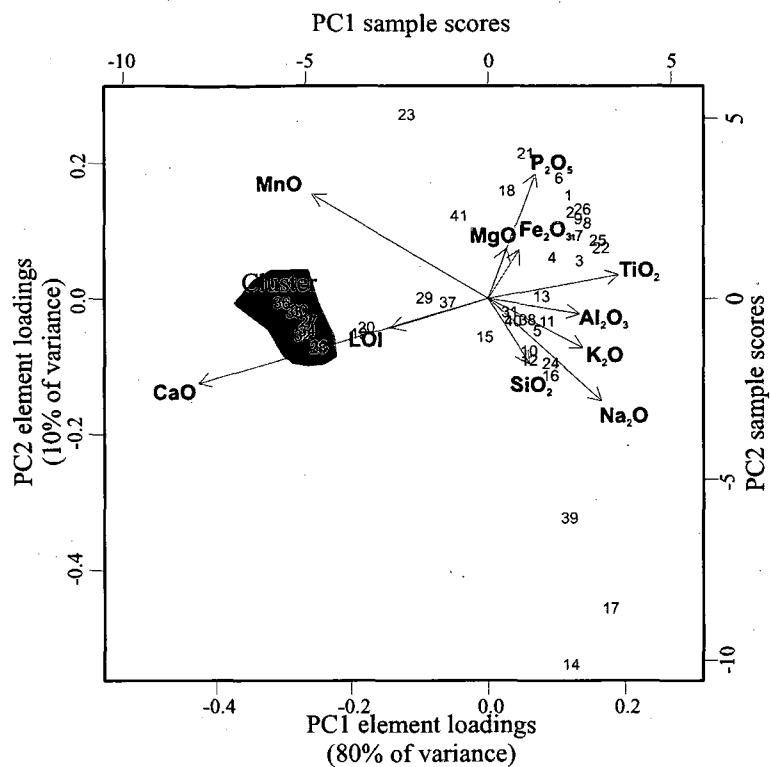


Figure 5.5: PCA biplot of major elements loading at the Peskowsk A-99 well.

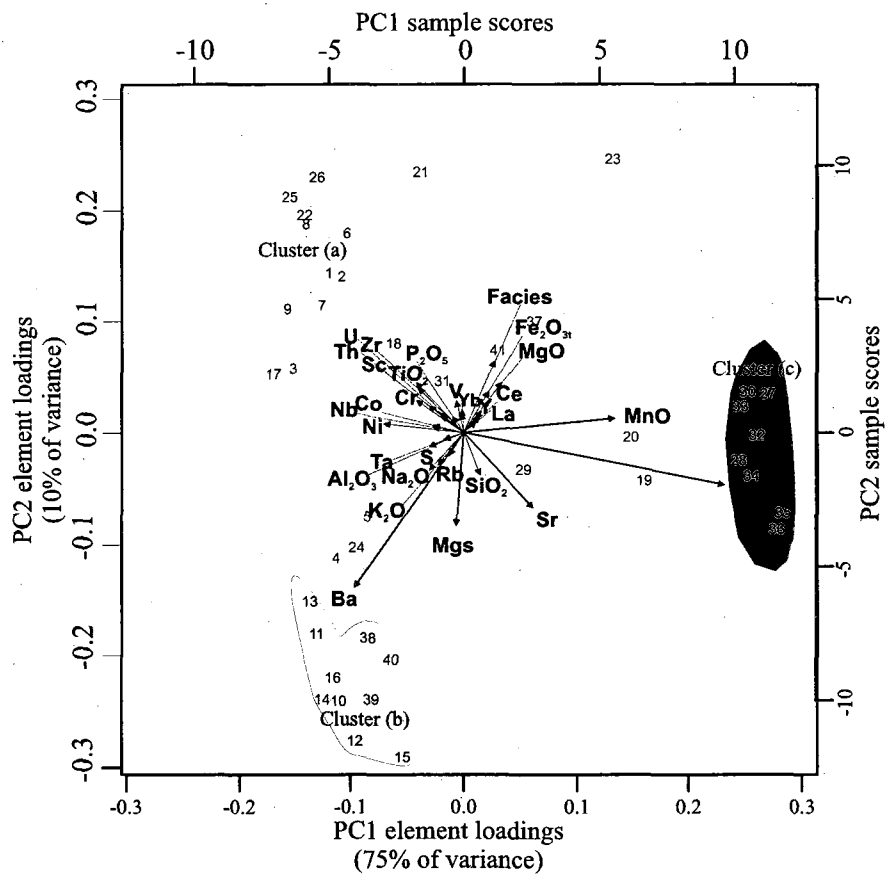


Figure 5.6: PCA biplot of major and trace elements, facies and grain size loading at the Peskowsk A-99 well.

5.3 RESULTS: VARIATION OF ELEMENTS WITH MINERALS AND FACIES

Binary plots are used to show the variation of elements with respect to other elements, selected minerals (e.g. carbonates), and with identified facies (Figs. 5.7 to 5.30). Oxides are plotted on a volatile-free basis. Such plots show important correlations that are not apparent from simple correlation matrices and principal component analysis. In this study, binary plots show the following general features.

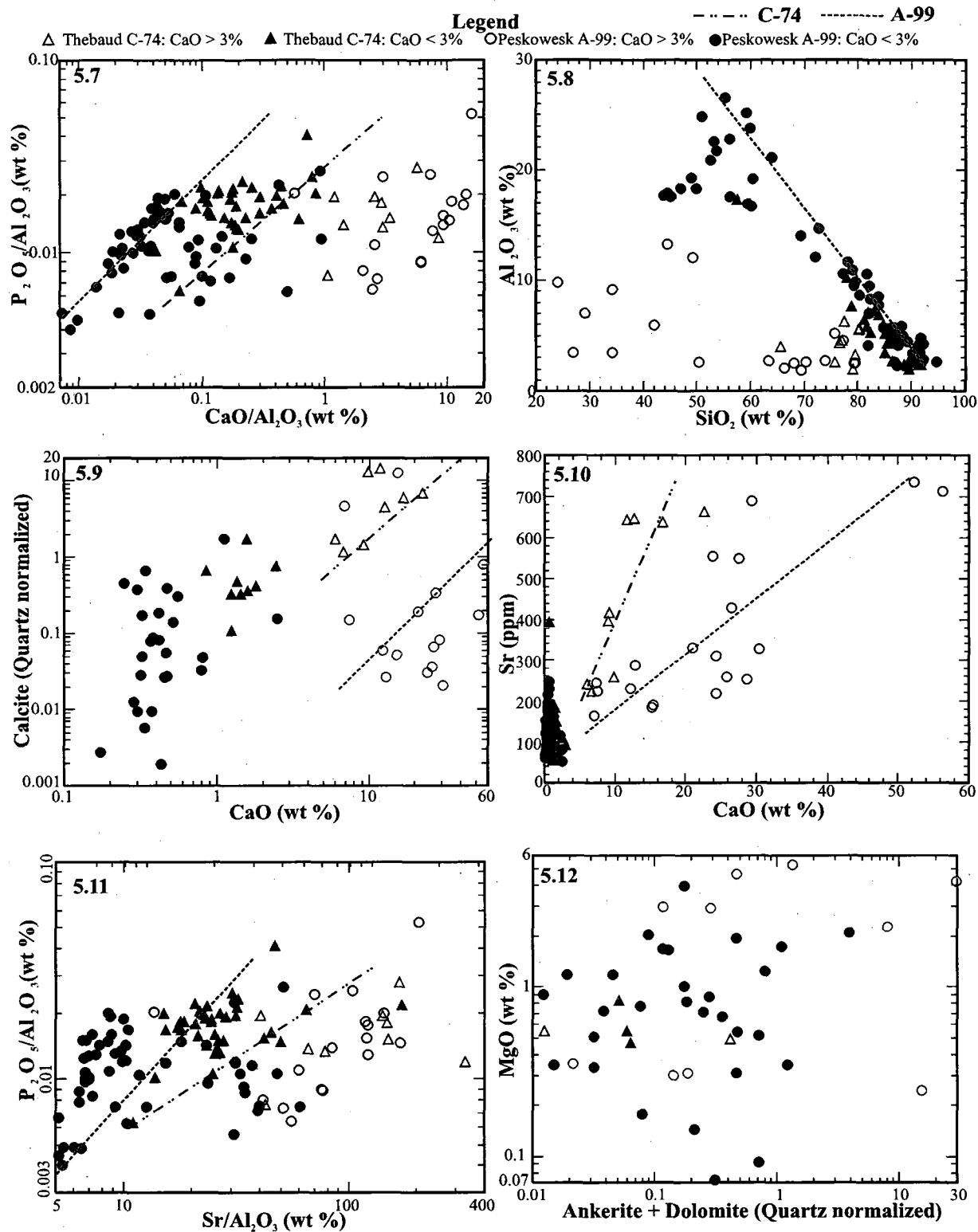
5.3.1 Effect of diagenetic cements: The effect of carbonate cements was investigated by assuming that samples with $\text{CaO} > 3\%$ are carbonate rich: such samples are shown by open symbols in Figs. 5.7 – 5.18. High CaO correlates with high LOI in the PCA plots (Figs. 5.3, 5.5). There is also a good correlation of calcite peak height from X-ray diffraction (normalized to quartz peak height) with CaO (Fig. 5.9). All these observations suggest that high CaO is an indicator of high carbonate. A plot of SiO_2 vs. Al_2O_3 (Fig. 5.8) shows a generally linear trend for samples with low CaO, but those with high CaO fall well off this trend. This is interpreted to result from the constant sum effect, with CaO, LOI, Al_2O_3 , and SiO_2 being the four principal oxides in carbonate-rich samples. The constant sum effect refers to concentrations that are expressed in percentages in oxides that are not independent because they all add up to a constant sum of 100%.

Samples with high Sr tend to have high CaO, although the regression line is different for the two wells studied (Fig. 5.10). There is also a correlation between inorganic carbon (calculated as all C in calcite) and Sr (Fig. 5.25). These several observations suggest that Sr may act as a proxy for high calcium carbonate.

Ankerite and siderite are other carbonate minerals present in some rocks. A plot of MgO vs. ankerite + dolomite determined by X-ray diffraction (Fig. 5.12) shows that there is no simple elemental proxy for these other carbonate minerals, but FeO_T shows a scattered correlation with siderite determined by X-ray diffraction (Fig. 5.23). However, the variation of MgO correlates well with FeO_T (Fig. 5.13), suggesting that MgO variation is predominantly controlled by chlorite, most of which is likely diagenetic.

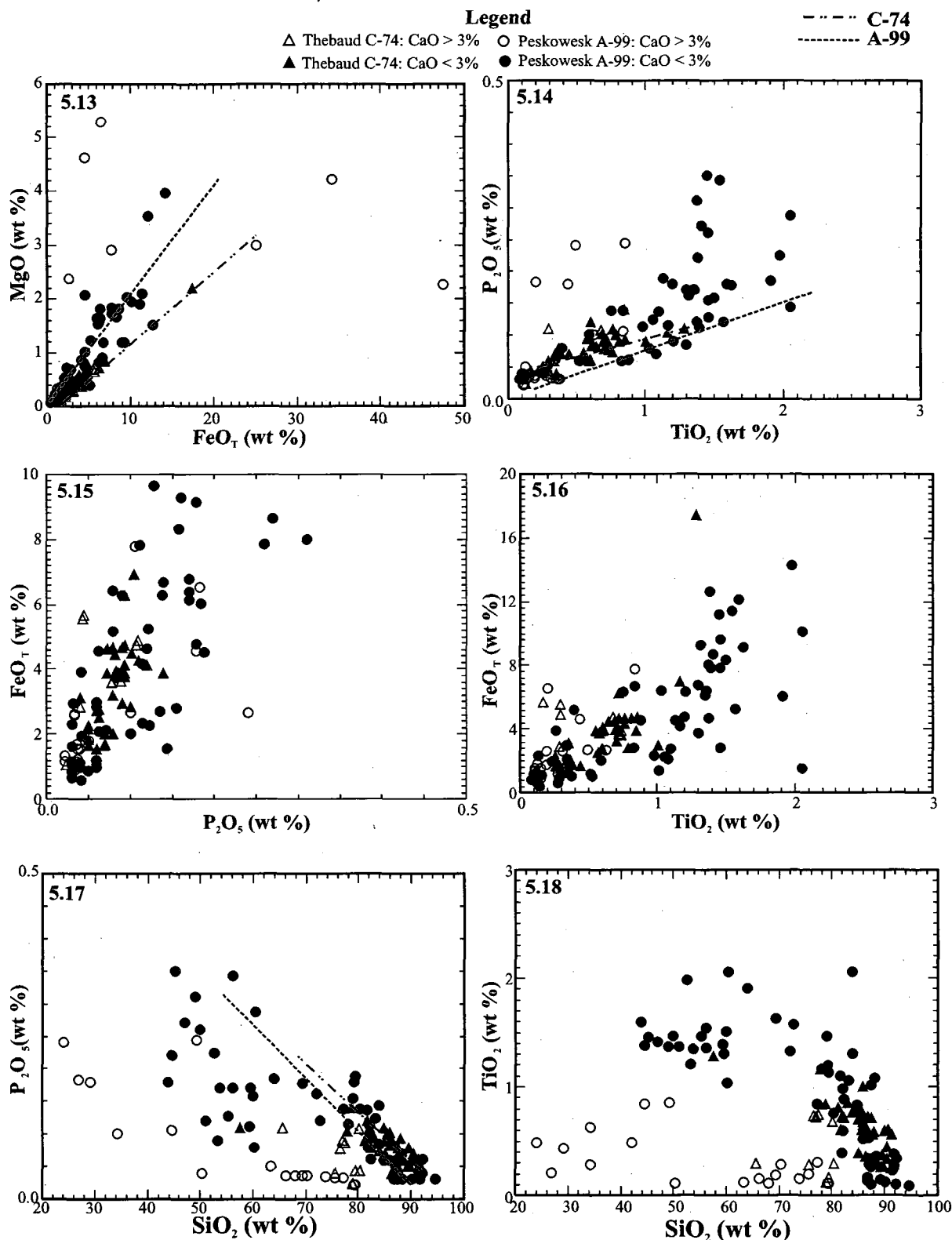
5.3.2 Variations in Geochemistry with Facies: Element variation with facies and sediment type (as proxied by SiO_2 content) has also been investigated. High CaO (> 20%) is restricted to mostly facies 2, 3, and 5. From this study, CaO is largely present in diagenetic calcite. Fig. 5.20 shows that most facies 3 rocks have higher FeO_T than rocks from other facies with similar SiO_2 content, although single samples from facies 4x, 2c and 0 also have $\text{FeO}_T > 5.5\%$. Figs 5.21 and 5.22 show that a few facies 3 rocks have more TiO_2 and P_2O_5 than all other facies with the exception of most of facies 5 rocks, which tend to have more TiO_2 and P_2O_5 than other facies.

5.3.3 Behavior of P and Ti: investigating P and Ti is an objective for this study and both elements show good correlation as in a previous study by Gould (2007). When P is plotted against Ca as oxides normalized to alumina (Fig. 5.7), much of the data falls along different trends for Peskowesk A-99 and Thebaud C-74. Ca co-varies with P at Peskowesk A-99 suggesting the presence of francolite. There is no such variation at Thebaud C-74, suggesting that P is in another mineral e.g. aluminophosphates (Pe-Piper and Dolansky, 2005). Fig. 5.11 shows a relationship between P and Sr (normalized to



Various binary plots for both studied wells divided into high and low CaO. (Fig. 5.7) Ratio plot of P_2O_5/Al_2O_3 versus CaO/Al_2O_3 presented on a logarithmic scale. (Fig. 5.8) Aluminum plots versus silica. (Fig. 5.9) A plot of CaO versus calcite (normalized to quartz). (Fig. 5.10) A plot of Strontium versus CaO. (Fig. 5.11) Ratio plot with P_2O_5/Al_2O_3 versus Ce/Al_2O_3 . (Fig. 5.12) A plot of MgO versus ankerite plus dolomite (normalized to quartz).

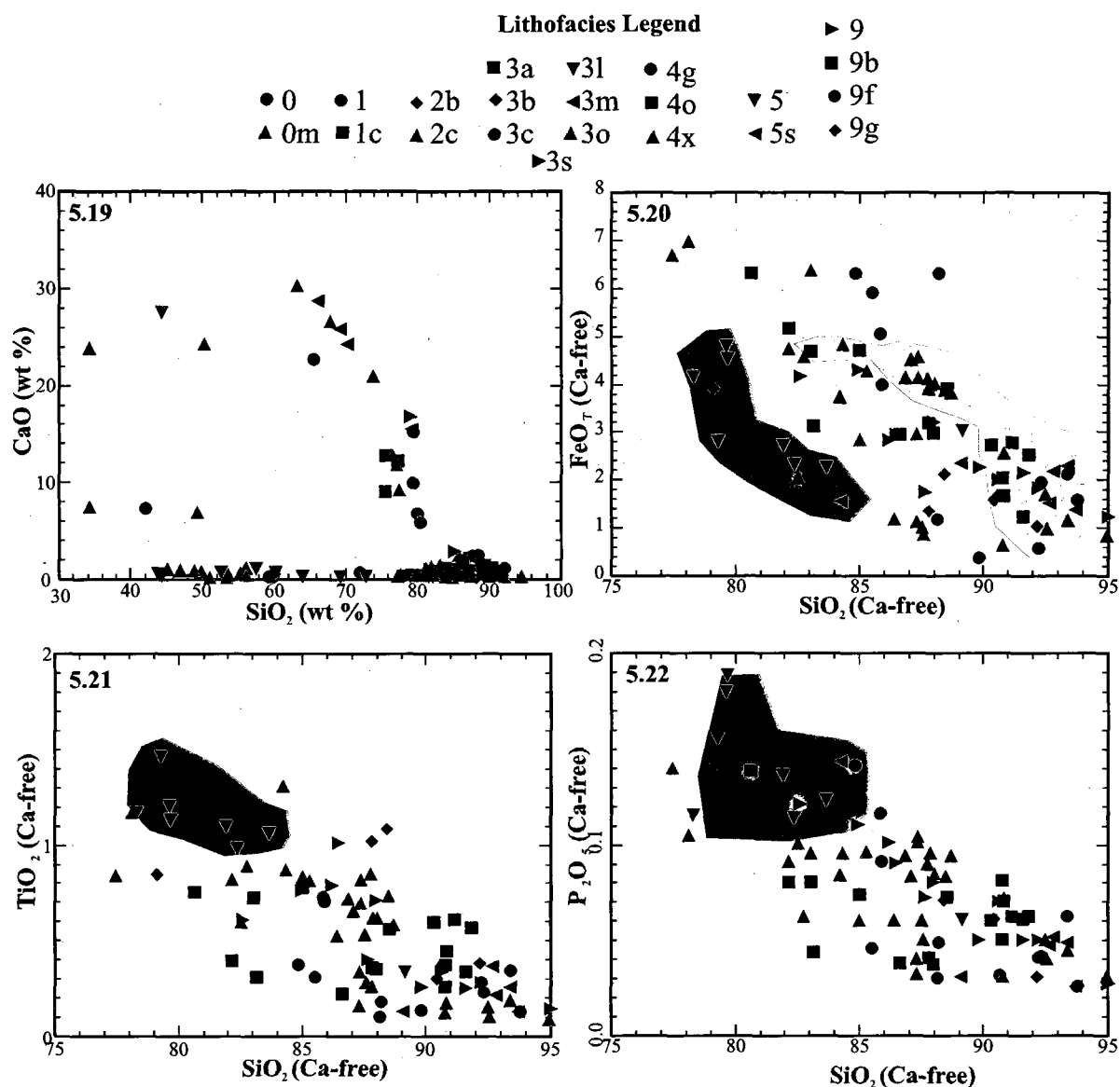
alumina) suggesting P at Thebaud is probably in Al-phosphates that also contain Sr or that Ca is replacing Sr in a phosphate-bearing mineral. The correlation of TiO_2 with P_2O_5 , particularly at Thebaud is good (Fig. 5.14), as also noticed by Gould (2007). At Peskowsk, values of $\text{P}_2\text{O}_5 > 0.2 \%$ shows no correlation with TiO_2 . In addition, high P_2O_5 is associated with high FeO_T (Fig. 5.15). FeO_T also co-varies with TiO_2 for both wells (Fig. 5.16), suggesting that TiO_2 is supplied in ilmenite and its weathering products (Pe-Piper *et al.*, 2005). In addition, high P_2O_5 and TiO_2 both appear to be associated with mudstone or muddy sandstones (Figs. 5.17 and 5.18).



Various binary plots for both studied wells divided into high and low CaO. (Fig. 5.13) A plot of MgO versus total FeO_T. (Fig. 5.14) A plot of Phosphorus versus TiO₂. (Fig. 5.15) A plot of FeO_T versus P₂O₅. (Fig. 5.16) A plot of FeO_T versus TiO₂. (Fig. 5.17) A plot of P₂O₅ versus SiO₂. (Fig. 5.18) A plot of TiO₂ versus SiO₂.

5.3.4 Mineralogical Control of Key Elements: SiO_2 is principally in quartz but can be found in many rock-forming minerals including clays and feldspars. High SiO_2 usually indicates sandstone. SiO_2 has an inverse relationship with Al_2O_3 (Fig. 5.8). High Al_2O_3 is found in shales, but Al can be present in other minerals. The inverse relationship between Al and Si is as a result of the constant sum effect. Fe is an important element that helps show variations with facies (Fig. 5.20), and it is present in iron hydroxides, chlorite (Fig. 5.13), and siderite (Fig. 5.23). Two elements that are the objectives of this study are P and Ti. In Fig. 5.14, P appears to co-vary with Ti. The element S is the product of sulphate reduction during early diagenesis (Fig. 1.4a) and it is mostly present in pyrite (Fig. 5.24), and in aluminophosphates (Fig. 5.11). Inorganic carbon (calculated assuming the C is all in CaCO_3) is the product of remineralization of organic carbon during early diagenesis, but may also be produced during late diagenetic cementation (e.g. calcite cementation after quartz overgrowth in Fig. 4.4C).

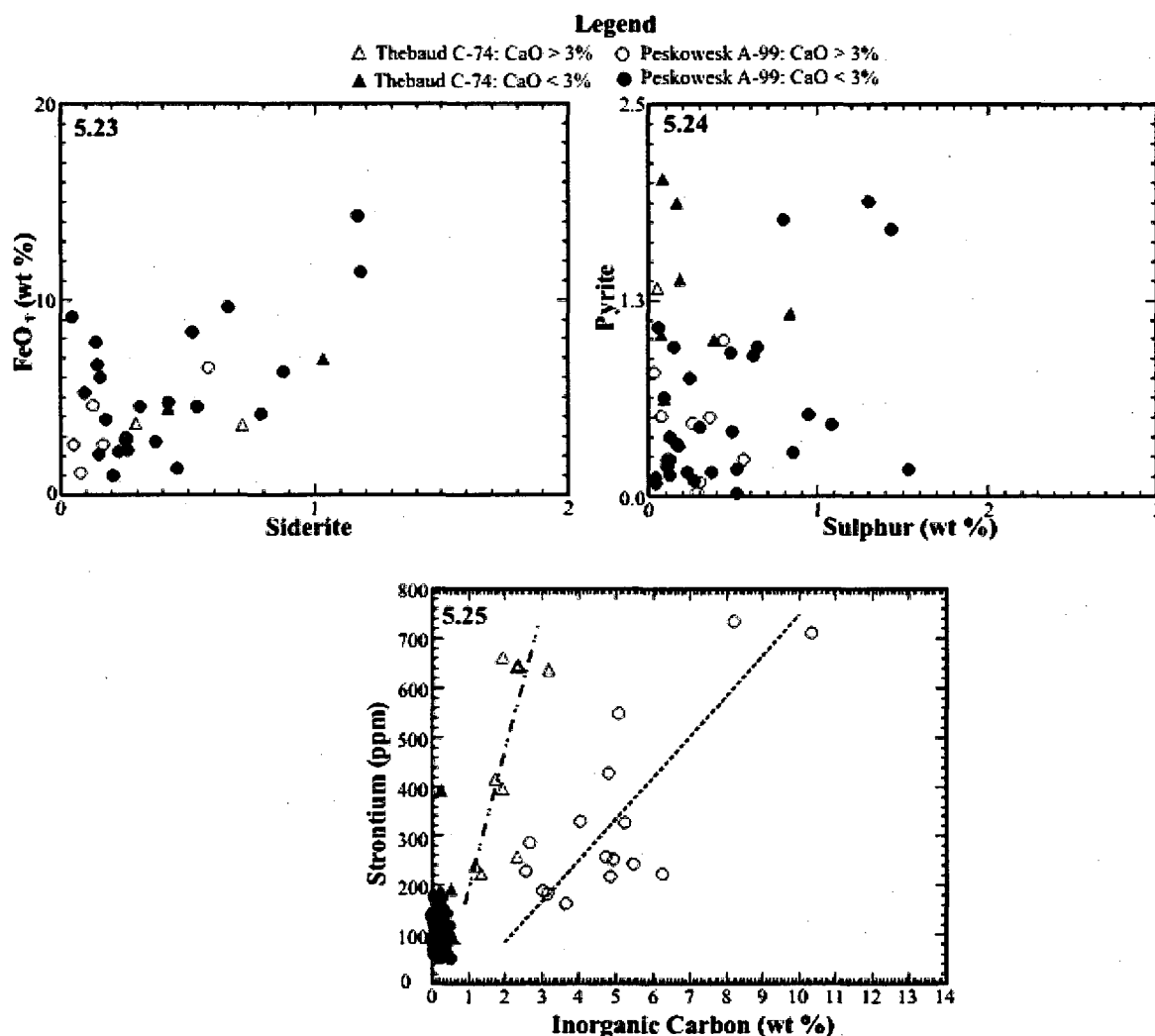
5.3.5 Stratigraphic Variation in Ca, Fe, Mg, Ti, P, Rb and K_2O : The stratigraphic variability of Ca, Fe, Ti and P is important for this study, given the evidence linking the abundances of Ca, P, Fe and Ti (Figs. 5.10, 5.14 – 5.16). In Peskowsk A-99, higher Fe, Mg, Ti, and P are found at shallow depths, and lower Fe, Mg, Ti, and P at greater depths (Fig. 5.26-5.28), while Ca (Fig. 5.29) is higher at greater depths, and lower at shallow depths. The depth range of samples from Thebaud C-74 is small, but they are at the same stratigraphic age (Upper Jurassic) as the deepest samples in Peskowsk A-99 and otherwise show lower Fe, Mg, Ti and P, but higher Ca than the shallow Peskowsk



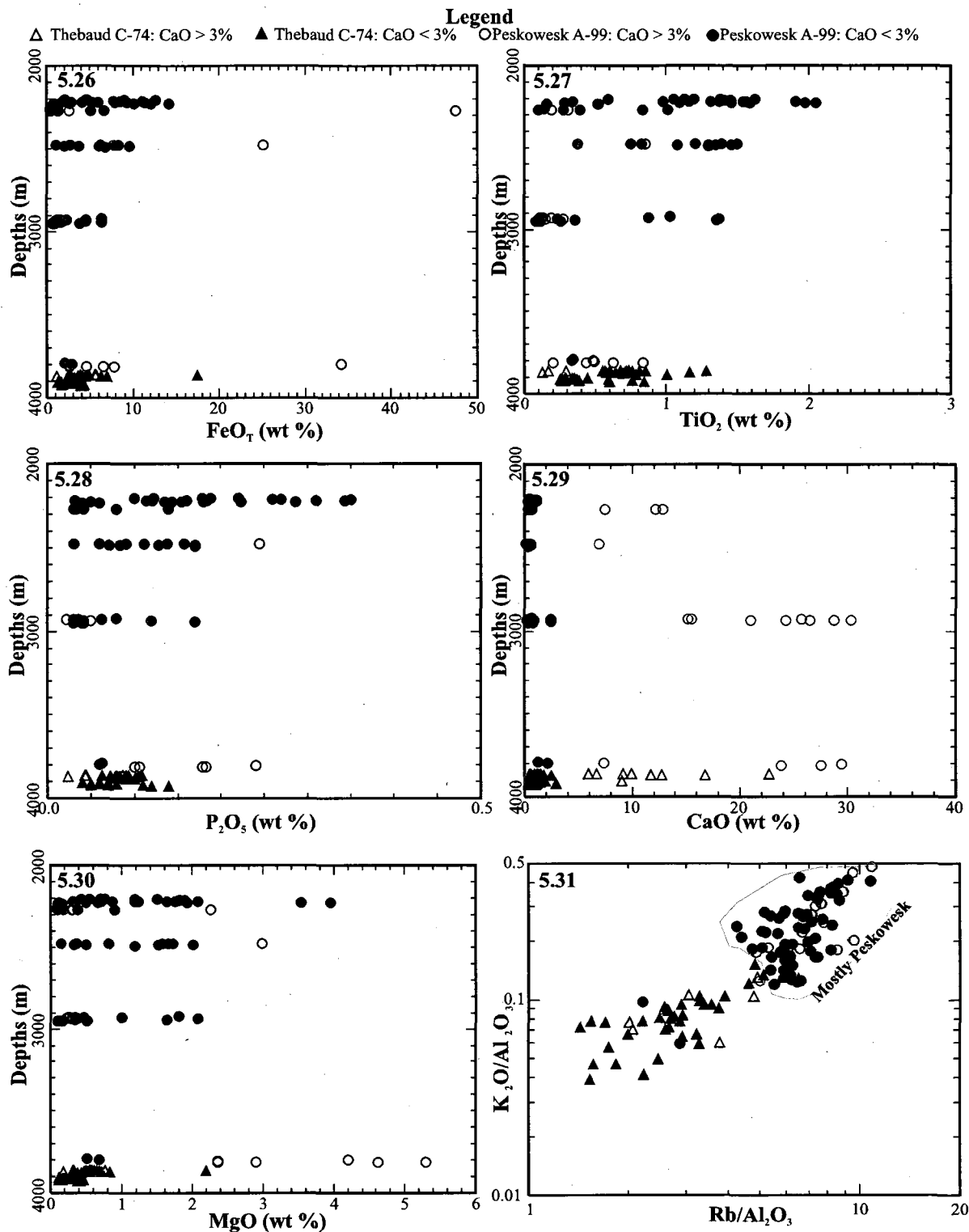
Shaded areas help show correlations between facies types.

Various binary plots for both studied wells with types of facies. (**Fig. 5.19**) A plot of CaO versus silica. FeO_T, TiO₂ and P₂O₅ with SiO₂ have been recalculated on a calcite-free basis assuming CaO was all calcite, using the formula $X * 100 / (100 - \text{CaO})$, where X represents FeO_T, TiO₂ and P₂O₅ or SiO₂ and is indicated by symbols for the following figures. (**Fig. 5.20**) Calcite free FeO_T versus calcite free silica. (**Fig. 5.21**) Calcite free TiO₂ versus calcite free silica. (**Fig. 5.22**) Calcite free P₂O₅ versus calcite free silica.

samples. Fig. 5.30 shows elevated K_2O to Rb ratio at Peskowsk compared to Thebaud (Pe-Piper *et al.*, 2008)



Various binary plots for both studied wells divided into high and low CaO. (Fig. 5.23) Plot of Fe versus siderite from XRD analysis. (Fig. 5.24) Plot of pyrite from XRD analysis versus sulphur. (Fig. 5.25) Strontium versus inorganic carbon (assuming $CaCO_3$).



Various binary plots for both studied wells. (Fig. 5.26) Stratigraphic plot of total FeO versus depths for both studied wells. (Fig. 5.27) Stratigraphic plot of TiO_2 versus depths for both studied wells. (Fig. 5.28) Stratigraphic plot of P_2O_5 versus depths for both studied wells. (Fig. 5.29) Stratigraphic plot of CaO versus depths for both studied wells. (Fig. 5.30) Stratigraphic plot of MgO versus depths for both studied wells. (Fig. 5.31) K_2O plotted versus Rb (alumina normalized).

5.4 RESULTS: DOWNCORE VARIATION OF ELEMENTS

The stratigraphic variations of selected major and trace elements with depth in core, in relation to transgressive surfaces and the inferred magnitude of environmental change across a Transgressive Surface (TS) is shown in a series of downcore plots (Figs. 5.34 - 5.38).

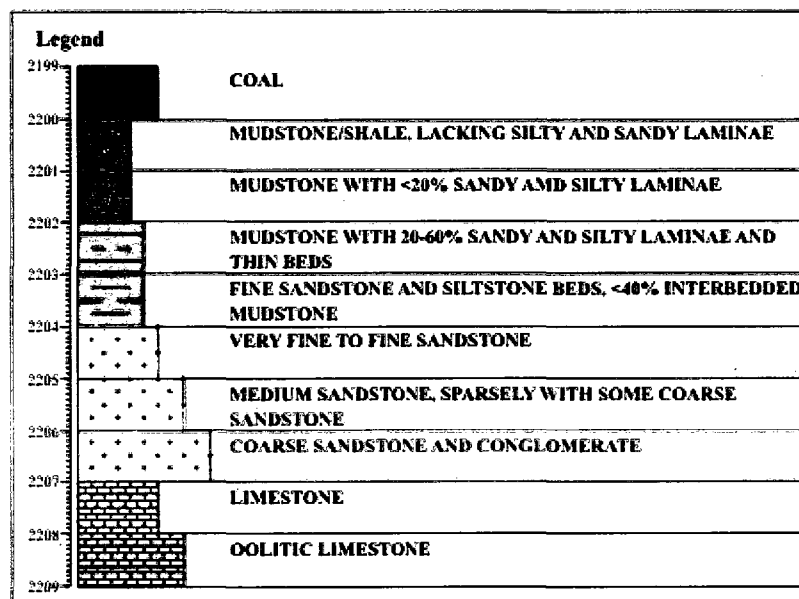


Figure 5.32: Lithology legend for figures 5.34 to 5.38

5.4.1 Geochemical Differences

Geochemical differences between different transgressive surfaces and their underlying sediments may result from rapid change in pore-water profiles following transgression, as proposed by Gould *et al.* (2010). However, such effects may be masked by geochemical variations resulting from different grain sizes of sediments and primary sediment composition, since many elements including Ti, Al, Fe and P show important variations with silica content (Figs. 5.8, 5.17-5.19). Furthermore, the abundance of Ti, Fe and P appear to vary stratigraphically (Figs. 5.26-5.28).

At Thebaud C-74, transgressive surfaces 1, 2, and 3 all involve large inferred rises in relative sea level and are underlain by sediments with relatively uniform SiO_2 and Al_2O_3 contents (Fig. 5.33). No systematic variation in either Fe or Ti is visible below these transgressive surfaces. Data is sparse below transgressive surface 2, but more is available below surfaces 1 and 3. High levels of S are found to 8 m below surface 1 and to 7 m below surface 3. In the same interval, there are few peaks in inorganic carbon and Sr. in addition, S co-varies with SiO_2 (Fig. 5.34).

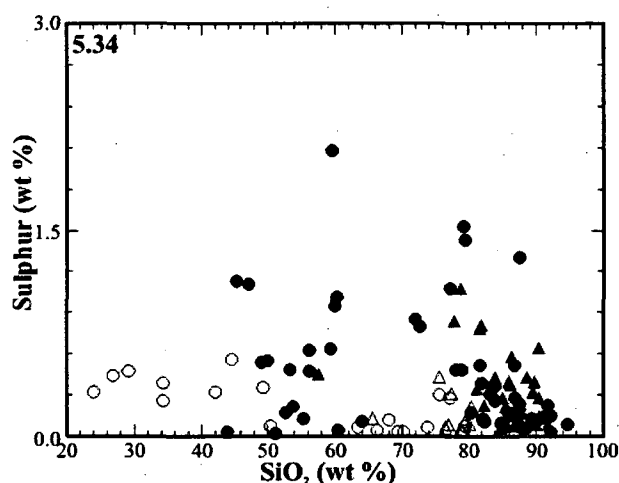


Figure 5.33: Binary plot of sulphur plotted against SiO_2 in weight percentage.

At Peskowsk A-99, transgressive surface 9 (Fig. 5.35) has the best underlying data.

High levels of S are found to 14 m below the surface, with a small inorganic carbon peak at 11 m. Variation in P and Fe follows variation in SiO_2 (i.e. grain size). Most of the other transgressive surfaces at Peskowsk overlie only thin sediment successions and do not show systematic variations in inorganic carbon (e.g. below transgressive surface 4 in Fig. 5.36).

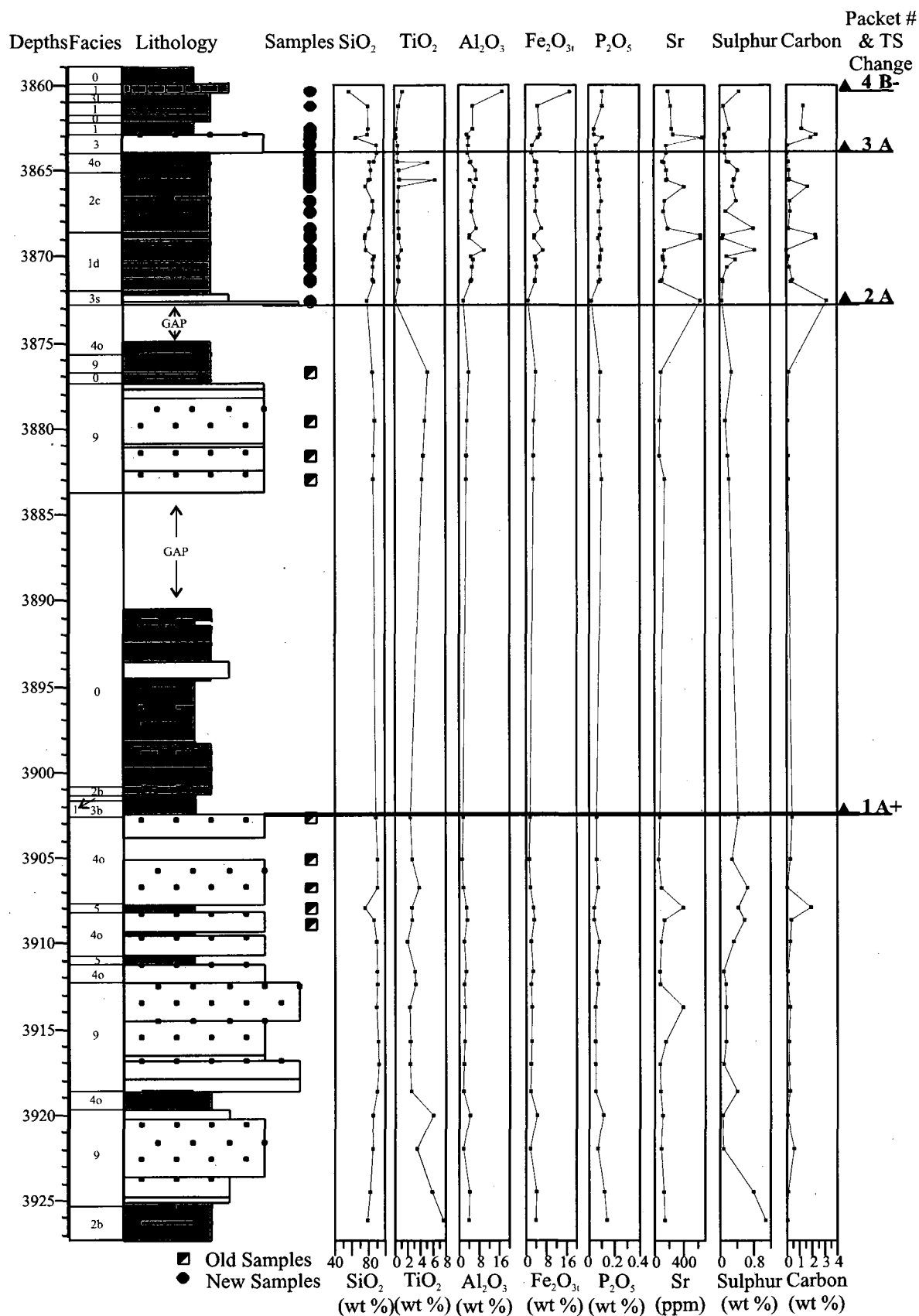
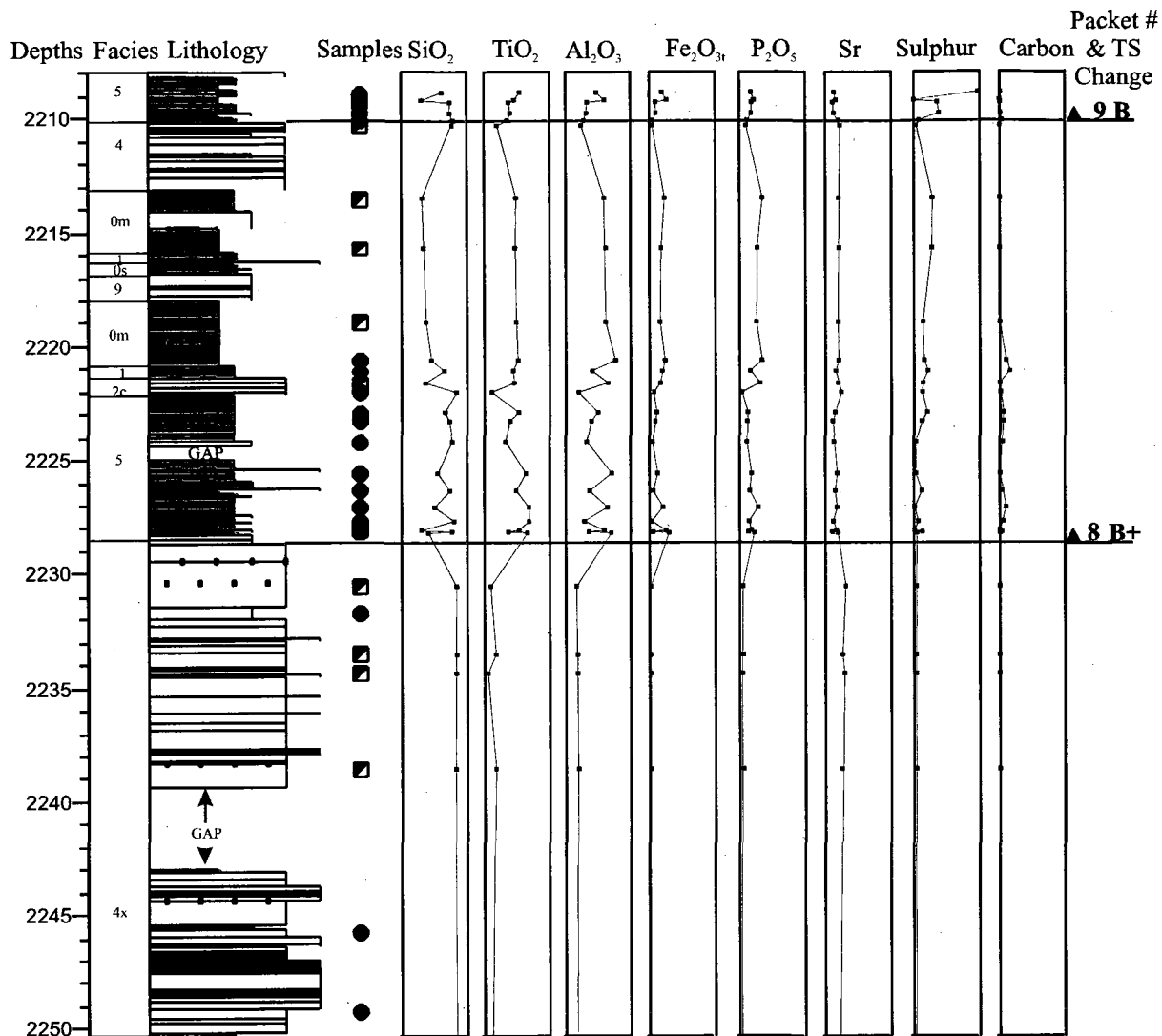


Figure 5.33: Cores 1 to 6 at Thebaud C-74. Stratigraphic variation of selected major and trace elements and inorganic carbon (assuming CaCO_3).



GAP

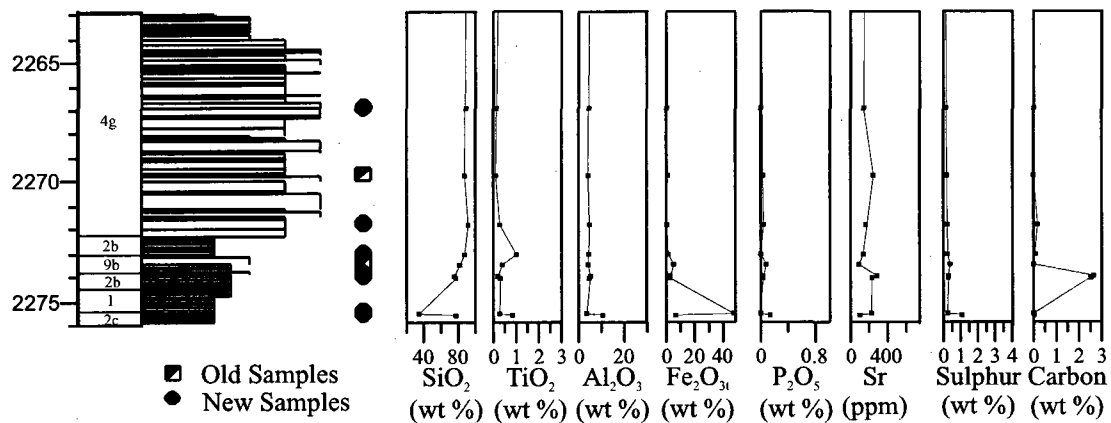


Figure 5.35: Cores 1 to 4 at Peskowsk A-99. Stratigraphic variation of selected major and trace elements and inorganic carbon (assuming CaCO₃).

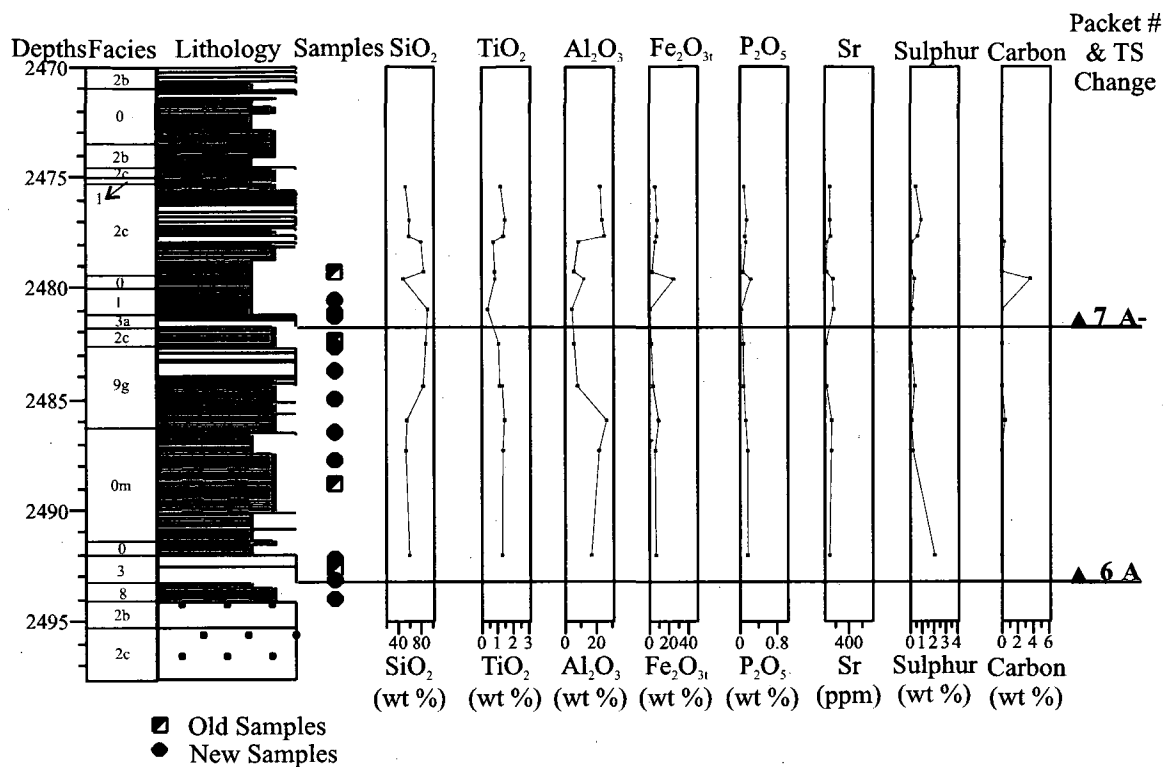


Figure 5.36: Core 5 at Peskowsk A-99. Stratigraphic variation of selected major and trace elements and inorganic carbon (assuming CaCO₃).

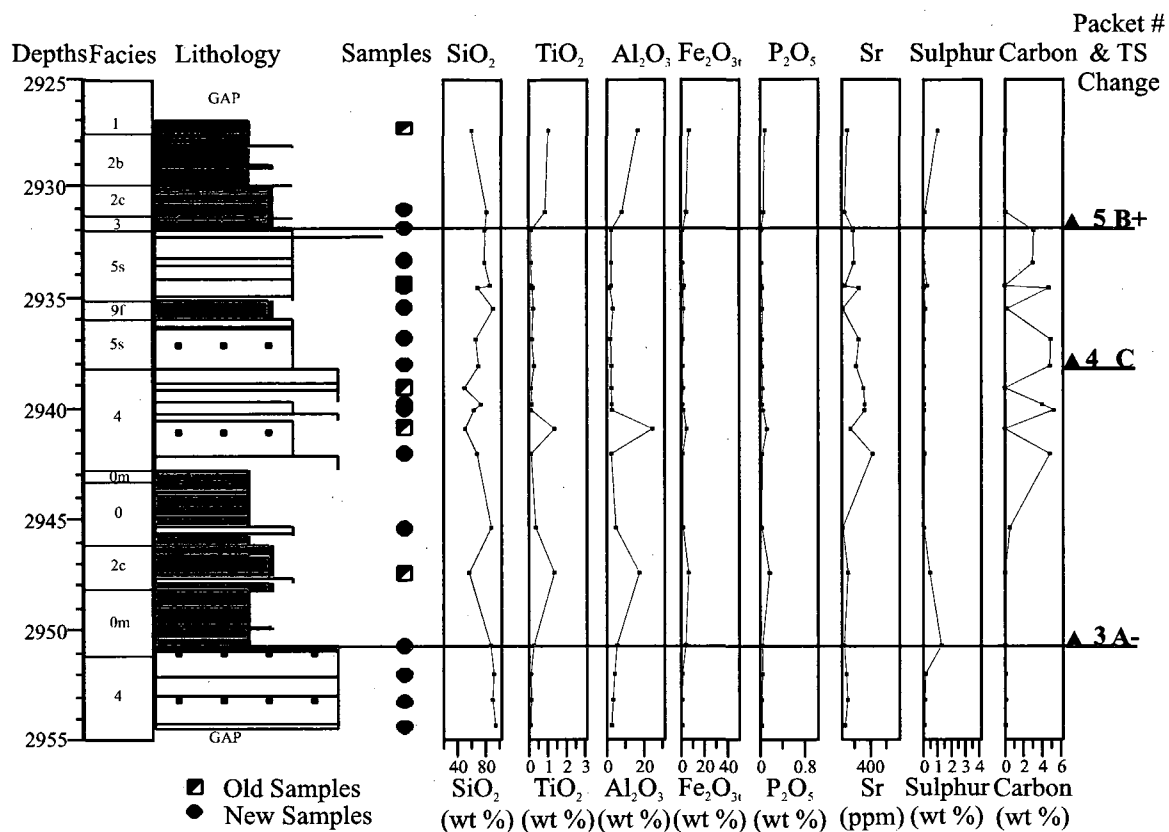


Figure 5.37: Core 6 at Peskowsk A-99. Stratigraphic variation of selected major and trace elements and inorganic carbon (assuming CaCO_3).

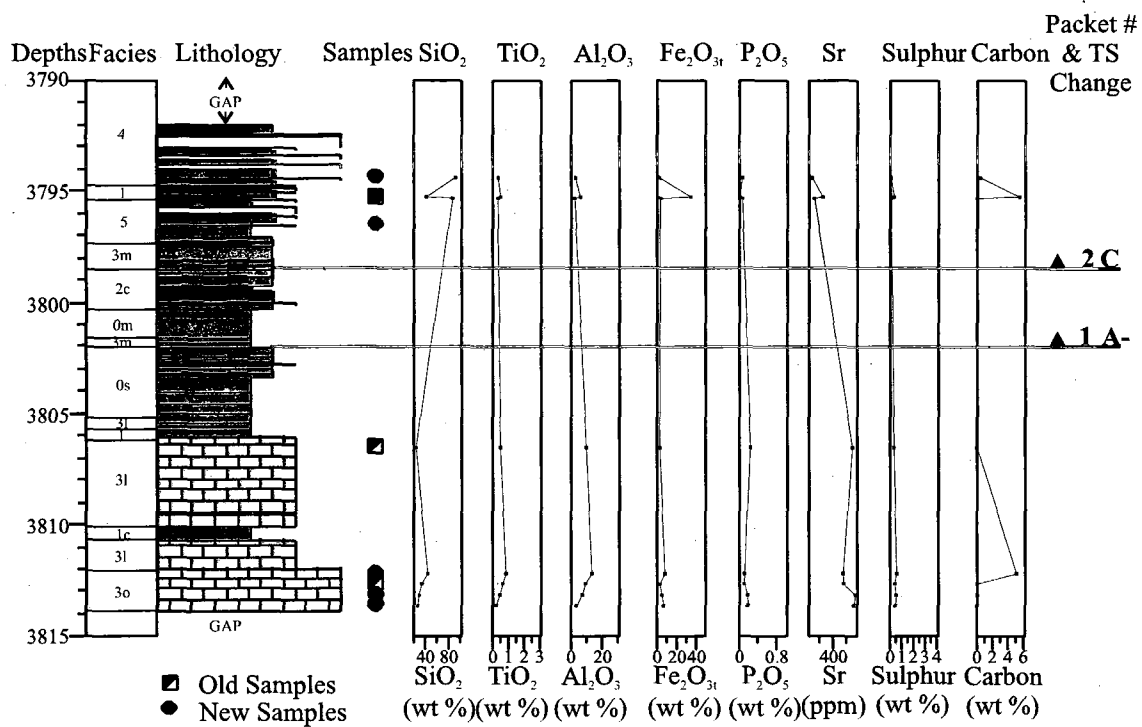


Figure 5.38: Core 7 at Peskowsk A-99. Stratigraphic variation of selected major and trace elements and inorganic carbon (assuming CaCO_3).

Two of the three packets below transgressive surfaces at Thebaud C-74 have inorganic carbon > 0.2 wt % and Ti abundance seems to vary inversely with inorganic carbon abundance. In contrast, cores 1-5 of Peskowsk A-99 rarely have inorganic carbon > 0.2 wt %, whereas overall Ti abundance is locally high (Fig. 5.28).

5.5 CHAPTER SUMMARY

Statistical interpretation of bulk geochemical data was done first by correlation coefficient analysis to view a two dimensional variation of elements, and then by principal component analysis. The principal component helped to distinguish detrital from diagenetic effects. Element plots (binary and downcore) were then used to further investigate the detrital versus diagenetic effects present within the samples. An issue from previous work by Gould (2007), stated in the research objectives, that the abundance of Ti and P is due to abrupt changes in sedimentation rates was also addressed in this chapter. The following chapter is a discussion of the introduction, background and results. This discussion leads to a conclusion for this study.

CHAPTER 6: DISCUSSION AND CONCLUSIONS

6.1 INTRODUCTION AND REVIEW OF OBJECTIVES

Gould *et al.* (2010) observed that early diagenetic processes play an important role in the distribution of diagenetic minerals in the deltaic Lower Cretaceous of the Scotian Basin. They also hypothesized that sea-floor mineralization was controlled by rapid changes in sedimentation rates from progradational deltaic successions to a Transgressive System Tract (TST). This study addresses the issue of reservoir effectiveness as a result of diagenesis and follows up from Gould *et al.* (2010) by examining the influence of sea-floor diagenesis on the later diagenetic history and reservoir quality in the Scotian Basin.

Five objectives were developed for this study based on the working hypothesis that due to abrupt changes caused by transgression, mineralization in various parts of the sediment-water redox profile is interrupted and the sequence of mineral types is fossilized (Fig.

1.3). These objectives are:

1. To determine whether there is a general relationship between P and Ti below the transgressive surface (TS), as suggested by Gould (2007). In addition, to determine whether the distribution of P is an indicator of chlorite rims.
2. To infer sea-floor diagenetic processes from coated grains that occurs in sediments immediately above the TS.
3. To determine why the sediments immediately above the TS are often siderite-rich, and to evaluate the role of bioturbation.
4. To compare the sequence of early diagenetic minerals in the TST and underlying deltaic sediments with literature on modern sea-floor diagenesis.

5. To determine the nature of the early diagenetic system in the overall diagenesis of sandstone reservoirs in the Scotian Basin.

Mineralogical and geochemical investigations were carried out based on these objectives and the hypothesis. The results showed that early diagenetic processes are more complex than hypothesized by Gould *et al.* (2010).

6.1.1 Paleogeographic Setting:

The paleogeographic settings at Thebaud C-74 and Peskowsk A-99 result overall from the progradation of a set of deltas. The most seaward deltas at any one time are shelf-edge deltas (Cummings and Arnott, 2005) that prograded into deep waters of several hundred metres (Piper *et al.*, 2010). Most of the accommodation at this time was provided by the deep waters. The distribution of shelf edge deltas has been mapped by several authors (Cummings and Arnott, 2005 and Piper *et al.*, 2010). The seaward limit of shelf-edge deltas is marked by limestone units that are transitional into shale seaward, as evident in the O-marker. Other deltaic parasequences deposit in a delta-top environment and sediment accommodation was provided mainly by sea-level rise and subsidence.

In the cored intervals, the Lower Mississauga Formation at Thebaud C-74 was deposited in shelf edge deltas but at Peskowsk A-99 the Mississauga and Logan Canyon Formations are a delta-top succession. The Mic Mac Formation at Peskowsk A-99 is associated with outer shelf limestones. In the lithostratigraphy of studied wells (section 2.4), the same units at Peskowsk are thinner than at Thebaud, emphasizing the differences in accommodation.

6.2 DIAGENETIC MINERALS AND PARAGENETIC SEQUENCE

The chronological order of the crystallization of diagenetic minerals is illustrated in Figs. 4.14 and 4.16, and their evolution and occurrence are discussed in detail in chapter 4. The following summarizes the diagenetic minerals identified with their paragenetic sequences.

Ferroan-calcite (Fe-calcite) is a variety of calcite present (Fig. 4.1E), accounting for about two percent of iron (Fe) in the carbonate chemistry of the samples from Thebaud C-74 and Peskowsk A-99. Fe-calcite is a product of either early or late diagenesis (Figs. 4.14 and 4.16). Early Fe-calcite cement is present in some coated grains and forms before kaolinite cements (Fig. 4.16), Fe-calcite may have precipitated from an aragonite precursor because it does not form at the sea floor. Late Fe-calcite precipitates within a temperature range of 65°C to 110°C (El-ghali *et al.*, 2006). Fe-calcite is the most abundant non-clay cement present in Thebaud C-74, where it is mostly of late origin (Karim *et al.*, 2010).

Another mode of occurrence of Fe-calcite is as bioclasts of echinoderms, occurring with Mg-calcite (section 4.3.1). Dickson (2004) found Fe^{2+} concentrations close to or less than the detection limit of 1200 ppm in Upper Jurassic echinoderm stereom. In contrast, the Thebaud C-74 echinoderms (Fig. 4.9C) have an average of 1.9 mole % MgCO_3 and 2.6 mole % FeCO_3 (Appendix 4.7). Dickson (2001) showed that recrystallisation of echinoderm stereoms in his study was isochemical and reported Fe-calcite only as pore filling. There is no evidence that the Fe-calcite making up the Thebaud C-74 echinoderm

stereom is of primary biogenic origin. It is therefore likely of diagenetic origin and implies that isochemical recrystallisation of stereom cannot be assumed. The timing of recrystallisation is unknown. Elsewhere in the Thebaud field, Fe-calcite is found in coated grains (Karim *et al.*, 2010, their Fig. 9B) and is thus likely of sea-floor diagenetic origin; the low porosity of the host sediment makes significant chemical changes during burial diagenesis unlikely. However, ankerite is a common late diagenetic mineral and implies that late basinal fluids had abundant Fe^{2+} .

Magnesium rich calcite (Mg-calcite) is another variety of the calcite present in the wells studied, and its presence accounts for about two percent of Mg content. Mg-calcite occurs either as early pore-filling or infill in fractures (Figs. 4.14 and 4.16) similar to Fe-calcite. In addition, high Mg-calcite can be as a result of an aragonite precursor. In some samples, a mixture of both Mg-calcite and Fe-calcite are found (based on percentages higher than 3 wt %). Mg enrichment is usually as a result of marine water influence and this also increases the amount of Ca.

Three analyses of Mg content of Upper Jurassic echinoderm stereom are reported by Dickson (2004). They show a mean composition of 5 mole % MgCO_3 , with spot analysis ranging from 3-8 mole %. Dickson (2004) argued that this concentration is a consequence of the Mg/Ca ratio in Late Jurassic sea-water and the ambient temperature, and that the Mg-calcite is of a later origin. However, as with the Fe-calcite, there is no evidence that the Mg-calcite making up the Thebaud C-74 echinoderm stereom is of primary biogenic origin. It may be of diagenetic origin.

Ankerite is a carbonate mineral of an isomorphic series of $\text{CaMg}(\text{CO}_3)_2 - \text{Ca}(\text{Fe, Mn})(\text{CO}_3)_2$. Dolomite and Fe-dolomite are the other two carbonates within this isomorphic series. The formation of ankerite can be associated with the dolomitization of calcite during late diagenesis (Kozłowska, 2003). However, ankerite is also identified in cores 5 and 6 of Peskowesk A-99 (Fig. 4.2C) and at Thebaud (Fig. 4.1F) in coated grains suggesting early generation. Ankerite has not been previously recognized as early diagenetic in studies of the Scotian Basin by Pe-Piper and Weir-Murphy (2008) and Karim *et al.* (2010).

Siderite: Like most carbonate cements, siderite can occur as a result of either early or late diagenesis. The amounts of FeCO_3 and MgCO_3 vary in siderite, however in fluvial sandstone MgCO_3 is of a lower content; and this indicates early diagenetic stage for siderite precipitation. Early siderite precipitation has been estimated to occur between 15 °C and 45 °C, while late siderite precipitates between 60°C and 80 °C (Karim *et al.*, 2010). In Peskowesk A-99 (Fig. 4.15), the siderite present is identified to be of early diagenesis generation on the account of low MgCO_3 (Fig. 4.3A). In Thebaud C-74 however, siderite present is identified as a late diagenetic type, and where present, it occurs as a mixture with other silicate minerals and in very low amounts.

Chlorite and Berthierine have been identified in literature to be late diagenetic minerals (Gould *et al.*, 2010). However these minerals can occur as a result of early diagenetic processes (Essene and Peacor, 1997). Chlorite is present in the studied wells as (a) part of the layers in a coated grain, (b) mixtures usually with glauconite, and (c) grains

surrounding carbonate cements or detrital grains, i.e. chlorite rims (Figs. 4.9A and B). Gould (2007) has identified chlorite rims on detrital quartz grains in the Scotian basin. These chlorite rims were found to preserve porosity by preventing the formation of secondary, pore-filling quartz overgrowth in wells.

Berthierine is a Fe-silicate that is in a diagenetic state at low temperatures in the presence of reducing conditions (Essene and Peacor, 1997), common under early sea-floor diagenesis. The presence of berthierine (Fig. 4.3A) suggests that the temperature at formation was less than 70°C, because berthierine transforms to chamosite at about 70°C and to Fe-chlorite at about 100°C (Pe-Piper and Weir-Murphy, 2008). Gould *et al.*, 2010 and Pe-Piper and Weir-Murphy (2008) have both proposed odinite as a precursor of berthierine.

Pyrite (FeS₂) occurs in two forms in the Scotian Basin sandstones: as framboids (Fig. 4.5A) and in platy forms (Fig. 4.6A). Disseminated framboidal pyrite (rounded) is common in offshore environments as an early diagenetic mineral (Burley and Worden, 1988), however, pyrite can precipitate either during early or late diagenesis and is known to form before siderite, except in inner shelf sandstone (Pe-Piper and Weir-Murphy, 2008). Early pyrite can be found in early calcite cement, siderite nodules or in fossil fragments, while late pyrite is associated with pores and fractures (Fig. 4.6B). The presence of pyrite in pores in the presence of Fe-calcite (Fig. 4.6C) suggests that the pyrite formed before late Fe-calcite.

Francolite (Carbonate-fluorapatite), a principal mineral of phosphorites, is one of the diagenetic minerals in the coated grains identified in the Lower Mississauga rocks (Figs. 4.5D), and it occurs as a mixture with glauconite. It has been suggested by Pe-Piper and Weir-Murphy (2008) that the phosphorites in the Lower Cretaceous in the Orpheus Graben are formed on transgressive surfaces. A number of processes can be involved in the formation of phosphorites: these include replacement of carbonates (McArthur *et al.*, 1984 in Pe-Piper and Weir-Murphy, 2008) and inorganic precipitation of phosphorites from pore waters (Froelich *et al.*, 1988). The precipitation of francolite can be indicated by an increase, with depth, in the amount of phosphorus in authigenetic minerals (Cha *et al.*, 2005).

Glauconite is a clay mineral that forms close to the sediment-marine water interface in the oxic to sub-oxic zone, typically in slightly alkaline waters (El-ghali *et al.*, 2009). When it forms in-situ, by the alteration of illite or muscovite, glauconite retains the mica elongated shape but can become rounded if transported. In both studied wells, glauconite with a rounded shape occurs abundantly but as mixtures with chlorite (Fig. 4.9E) and also with francolite at Thebaud (Fig. 4.5C).

Kaolinite forms as K is removed from feldspars and clays and is characteristic of diagenesis by meteoric water (Karim *et al.*, 2010). At Thebaud C-74, kaolinite occurs as cements (Fig. 4.7A), and as pore filling grains at Peskowsk A-99 (Fig. 4.8A).

6.3 PARAGENETIC SEQUENCE AT AND NEAR THE SEA-FLOOR

In coated grains from both studied wells, there is an abundance of diagenetic Fe-rich minerals (e.g. pyrite, siderite, and chlorite) identified during petrographic studies (Figs. 4.1 A-E). In addition, coated grains preserve a record of sea-floor diagenesis in their concentric layers because they form at or near the sea-floor. Hence, the paragenetic sequence of diagenetic minerals at or near the sea-floor is best investigated within coated grains.

In the Thebaud C-74 well, the coated grains in the Lower Mississauga samples are made up of a detrital nucleus with concentric layers made up of Fe-carbonates (siderite or Fe-calcite), chlorite, glauconite and clay minerals (Tables 4.3 and 4.4) and are assigned to type 2. These coated grain types are generally more Fe-rich and may include concentric layers made of francolite or berthierine. In most coated grains, chlorite and glauconite are usually in contact with each other. From Table 4.3, two coated grains show evidence of sequence erosion, where an abrasion surface shows that presence of minerals e.g. CG 22 in Table 4.3 with glauconite forming over francolite.

In the Peskowesk A-99 well, the Logan Canyon samples have coated grains that consist of clay nucleus and concentric layers made of carbonates assigned to type 1. These samples also have type 2 coated grains that are similar to those in the Lower Mississauga samples, but they lack any francolite or berthierine. The Upper Mississauga samples have coated grains that consist of Ca-Mg carbonate nucleus and concentric layers made up principally of Mg-calcite, ankerite or Fe-calcite with minor pyrite or chlorite, assigned to

type 3. The samples also have type 2 coated grains that are similar to that in the Logan Canyon samples. Similar to parts of the Upper Mississauga samples, the Mic Mac Formation samples are also made up of type 3 coated grains.

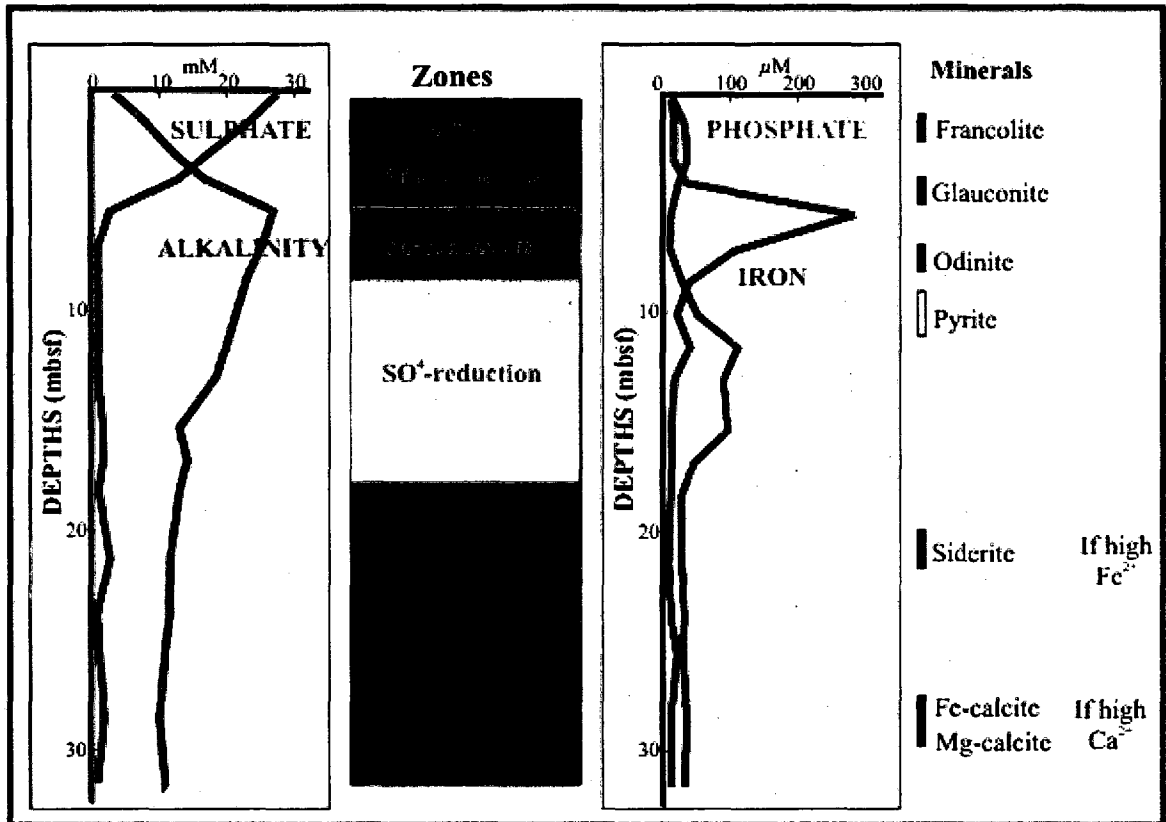


Figure 6.1: Pore-water profile for a high sedimentation rate environment (Burns, 1997) with zones showing expected mineral precipitation for coated grains forming in a low sedimentation rate environment over a few cm.

The fossilization of the diagenetic sea-floor minerals in the Scotian Basin illustrated in Fig. 1.3 is incorporated with Fig. 6.1 to determine the specific evolution of the types of coated grains as the diagenetic minerals in the coated grains will apply to different origins.

Type 1 coated grains are different from types 2 and 3 due to the presence of pure calcite concentric layers. They are similar to ooids from oolitic limestones that form primarily in

agitated shallow marine, warm environments (Tucker *et al.* 1990). These coated grains form above the oxic zone in Fig. 6.1.

Type 2 coated grains are largely controlled by a higher input of Fe^{2+} . The diagenetic minerals in this type forms in different reduction zones (Fig. 6.1). Fe-calcite (due to high Ca^{2+}) and siderite (due to high Fe^{2+}) both formed in the zone of methanogenesis.

Berthierine or odinite, a precursor of chlorite, formed in the Fe reduction zone, while glauconite formed in the oxic zone. The presence of francolite also suggests high Fe^{2+} (Pe-Piper and Weir-Murphy, 2008) and the francolite probably formed within the Mn reduction zone.

As with the type 2 coated grains, the type 3 coated grains appear to have diagenetic minerals that have formed with different zones (Fig. 6.1). Carbonates formed with the zone of methanogenesis, pyrite formed in the sulphate reduction zone, and the precursor of chlorite formed in the Fe reduction zone. The most common carbonates are Mg-calcite and ankerite and this suggests lower Fe^{2+} input with higher Ca^{2+} input.

The low sedimentation rate environments where coated grains formed are similar environments to the early diagenetic cements (i.e. Fe-calcite and siderite) identified in this study in facies 3 sandstones (Chapters 3 and 4). The location of these diagenetic cements on Fig. 6.1 suggests that the diagenetic zones where such minerals are found have been compressed to only a few centimetres.

6.4 THE ROLE OF BURIAL DIAGENESIS IN BULK CHEMISTRY

The focus of this study is largely on early diagenetic processes. However, the possible effect of burial diagenesis (mesogenesis) requires further investigation.

6.4.1 Effects of Early Meteoric Waters

Effects of meteoric water is supported in the studies involving the variability found within early diagenetic minerals (e.g. kaolinite) by Karim *et al.* (2010), where early kaolinite is found to be abundant in fluvial river mouth facies (facies 4 and 9). The influx of meteoric waters is suggested to occur during a sea-level lowstand. In addition, when Mg is high in siderite (like at Peskowsk), these could be the result of a mixing of meteoric and marine water (Karim *et al.*, 2010).

6.4.2 Deeper or Later Diagenesis

The later aspects of diagenesis involve mass transfer reaction of basinal fluids including hydrocarbons (Worden and Burley, 2003), which may lead to (a) the loss of elements like K⁺ from dissolved K-feldspar causing the albitization of K-feldspars, or (b) the enrichment of element species such as Ca, Mg, Fe, Na, and Cl. At temperatures greater than 70°C, the clay mineral smectite changes to illite, leading to the take-up of K⁺ (ultimately derived from dissolved K-feldspars) and this causes some diagenetic effects in sandstone pore-waters. The albitization of K-feldspars is common at the Peskowsk A-99 well. Thebaud C-74 is deeper than Peskowsk A-99 (Fig. 2.5), which suggests that the lack of K-feldspars at Thebaud may be due to burial diagenetic effects.

6.5 STRATIGRAPHIC AND GEOGRAPHIC VARIATIONS IN CHEMISTRY AND MINERALOGY

6.5.1 Detrital Mineralogy and Geochemistry: Geochemically, the Lower Cretaceous sedimentary rocks of the Scotian Basin are unusual in having high Ti and Fe and very low Ca (Pe-Piper *et al.*, 2008). Differences in detrital mineralogy between the studied well are investigated in this section using principal component analysis (PCA) of geochemical data and down core plots of elements dominated by detrital supply (e.g. Fe and Ti).

The principal component analysis (PCA) of bulk geochemical data was helpful because it was possible to discriminate between detrital and diagenetic effects (Figs. 5.3 to 5.6). The first principal component at Thebaud C-74 and Peskowesk A-99 that provides a reasonable summary (about 85% of the total variance) of the data is a result of detrital effects indicated by positive loading of Ti and Fe. K₂O and Rb both have strong PCA loadings at Peskowesk A-99 (Fig. 5.6). No such correlation is identified at Thebaud C-74 (Fig. 5.4). The abundance of K₂O and Rb (Fig. 5.31) is suggested to be a result of abundant K-feldspar at the Peskowesk A-99 well, as sandstones show elevated K₂O to Rb ratio (Fig. 5.31), which is absent at the Thebaud C-74 well, perhaps due to the dissolution.

6.5.2 Bulk Geochemistry of Major Elements involved in Early Diagenesis: Elements abundant in diagenetic minerals include: Fe, P, Ca, Mg and possibly Ti. The bulk geochemistry for the stratigraphic divisions on Table 6.1 was based on data in Table 5.2.

Table 6.1: Stratigraphic and geographic variations in abundance of early diagenetic minerals

Wells	Early Diagenetic Minerals Present	Cores 1-4	Core 5	Core 6	Core 7
		Logan Canyon Formation	Upper Mississauga Formation	Middle Mississauga Formation	Mic Mac Formation
Peskowesk A-99	Calcite, Fe-and/or Mg-calcite	Medium	High	High	High
	Siderite	High	Medium	Medium	Medium
	Fe-rich silicate	Very Low	Very Low	Very Low	Very Low
	Pyrite	Medium	Medium	Medium	Medium
		Cores 1-6			
		Lower Mississauga Formation			
Thebaud C-74	Calcite, Fe-and/or Mg-calcite	High			
	Siderite	Low*			
	Fe-rich silicate	Low			
	Pyrite	Medium			

* siderite is only recognized with very low analytical totals (Chapter 4)

Logan Canyon Formation samples generally have low P and Ca (Figs. 5.28, 5.29), medium Mg (Fig. 5.30) and high amounts of Fe and Ti (Figs. 5.26, 5.27). Upper Missisauga Formation samples have higher Mg concentrations than other samples but Mg is overall low. Core 5 at the Peskowsk A-99 well has medium Fe and Ti with low Ca and P, while in core 6 (middle Missisauga Formation) Fe and Mg are low, P is very low and Ca is high. Lower Missisauga Formation has high Ti (especially at the bottom, Fig. 5.33), with medium Fe and Ca and low Mg and P. The Mic Mac Formation has low Ti and P, medium Fe and high Mg and Ca (Figs. 5.26-5.30).

Sulphur (as pyrite) and carbon (as carbonates) are important diagenetic elements present in samples from the Lower Missisauga sandstones in Thebaud C-74 (Fig. 6.2). They are, however, absent (or have very low analytical values) in sandstones from the Logan Canyon Formation (Fig. 6.3) in Peskowsk A-99.

6.5.3 Variation in Abundance of Early Diagenetic Minerals by stratigraphic units is shown in Table 6.1 which is based on data in Appendices 4.1 and 4.2 and X-ray diffraction data in Fig. 6.4. Logan Canyon Formation samples, which includes cores 1 to 4 at Peskowsk A-99, have more siderite, chlorite, pyrite and kaolinite (Fig. 6.4 C-F) compared to amounts of calcite, and ankerite plus dolomite (Figs. 6.4 A, B). The presence of more siderite seems to correlate with abundant tidal lithofacies.

Upper and Middle Missisauga Formation samples, which includes cores 5 and 6 at Peskowsk A-99, have more calcite (as Mg-calcite and Fe-calcite, Fig. 6.4A), pyrite, and

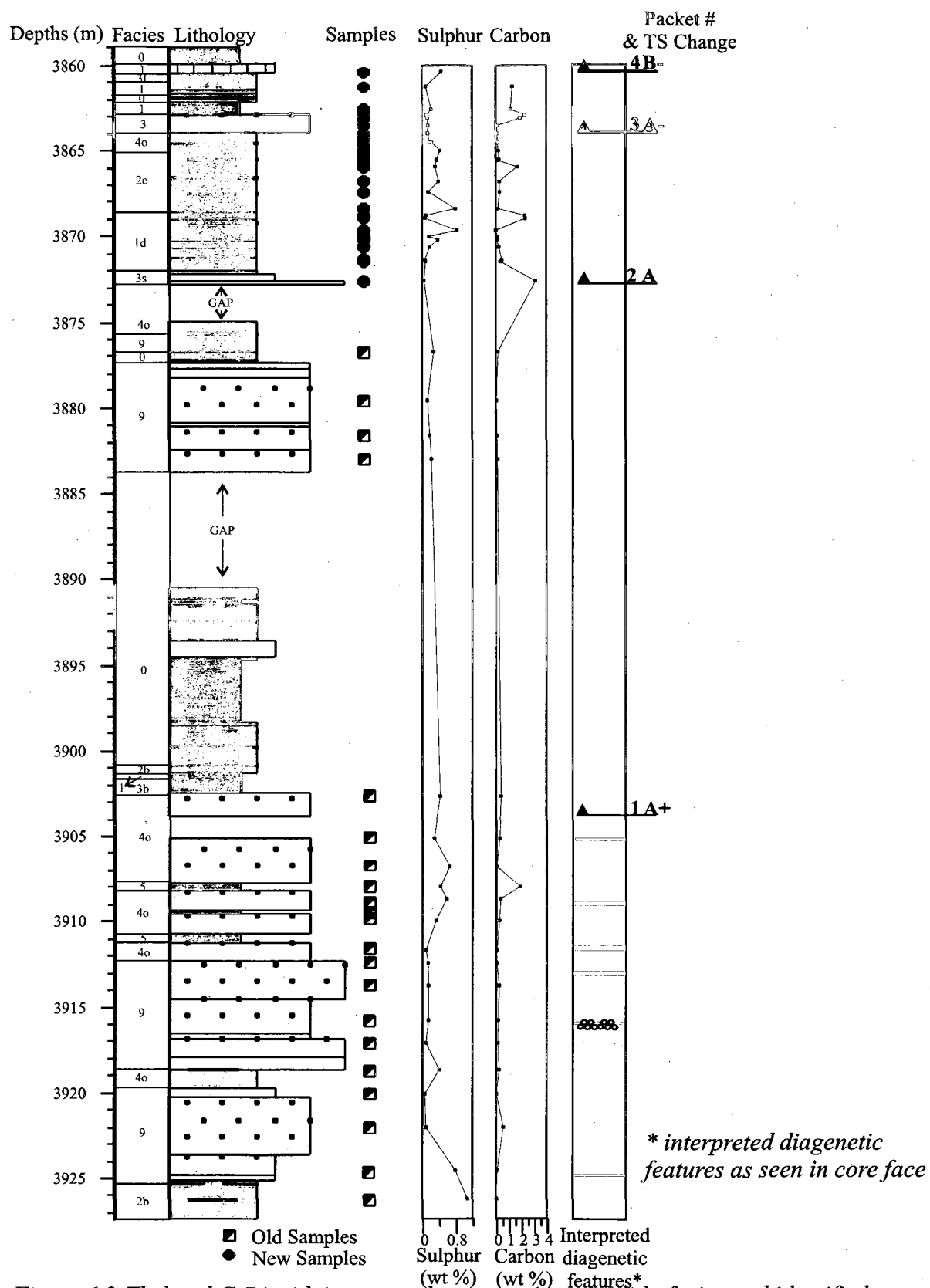


Figure 6.2: Thebaud C-74 with interpreted core stratigraphy, lithofacies and identified diagenetic features, showing geochemical variations in carbon and sulphur.

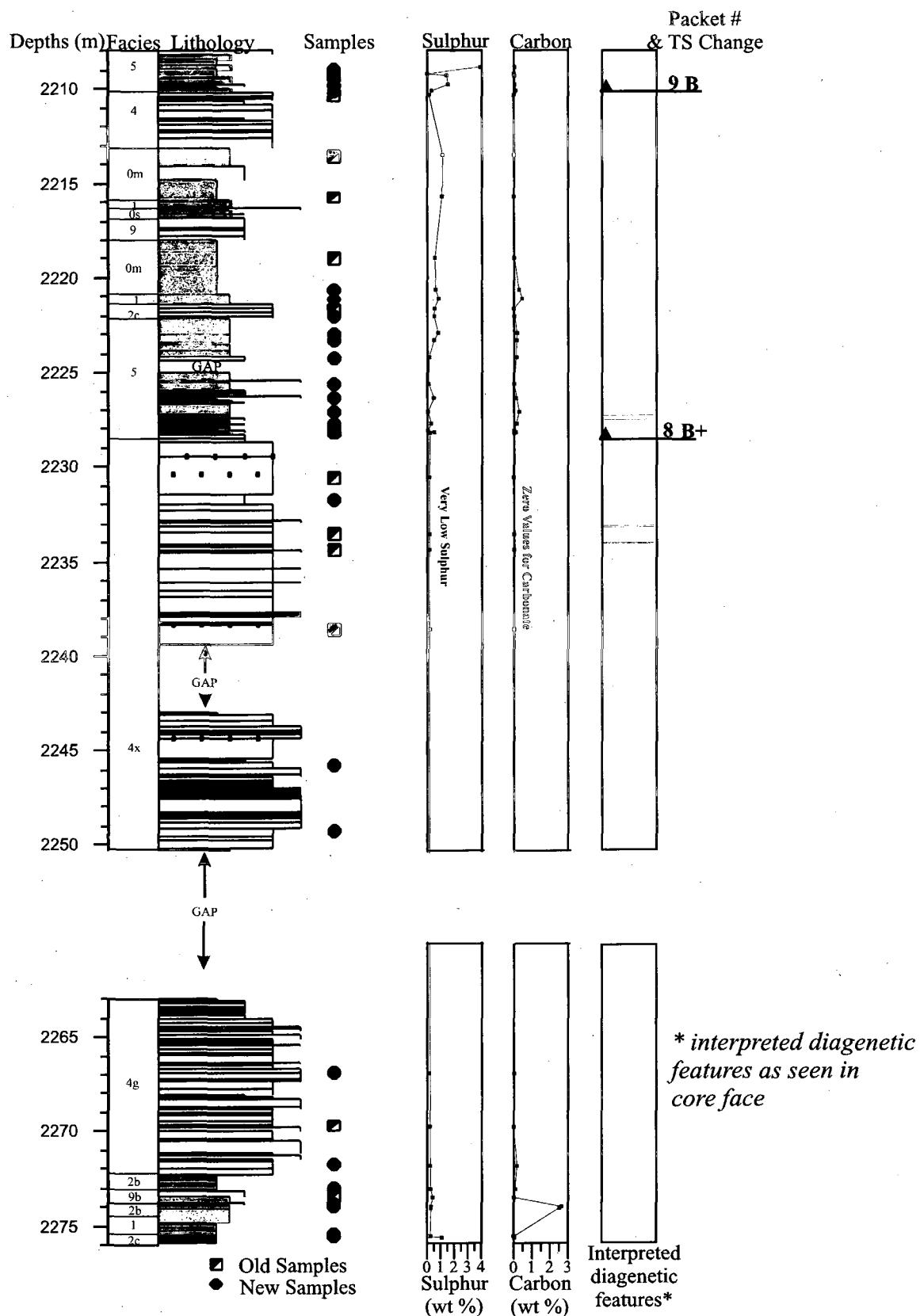


Figure 6.3: Peskowesk A-99 (core 2) with interpreted core stratigraphy, lithofacies and identified diagenetic features, showing geochemical variations in carbon and sulphur.

kaolinite (Figs. 6.4 E, F) compared to the amounts of ankerite plus dolomite, siderite and chlorite (Figs. 6.4 B, C, D). The abundance of calcite is consistent with the presence of common transgressive and shoreface facies.

Lower Mississauga Formation, which includes all Thebaud C-74 samples, and the Mic Mac Formation samples in core 7 at Peskowsk A-99, both have high concentrations of calcite with varying concentrations of pyrite and kaolinite (Figs. 6.4 A, E, F) compared with low concentration of ankerite plus dolomite, siderite and chlorite (Fig. 6.4 B,C,D). Facies 1 with bioturbated mudstone and the fluvial facies 4 (sub-facies 4x) are generally more abundant at these stratigraphic intervals (Fig. 6.4).

b.d. = below detection

Lithofacies Legend

• 0 • 1 ♦ 2b ■ 3a • 3c ◀ 3m ▶ 3s ■ 4o ▼ 5 ▶ 9 • 9f
 ▲ 0m ■ 1c ▲ 2c ♦ 3b ▼ 3l ▲ 3o • 4g ▲ 4x ◀ 5s ■ 9b ♦ 9g

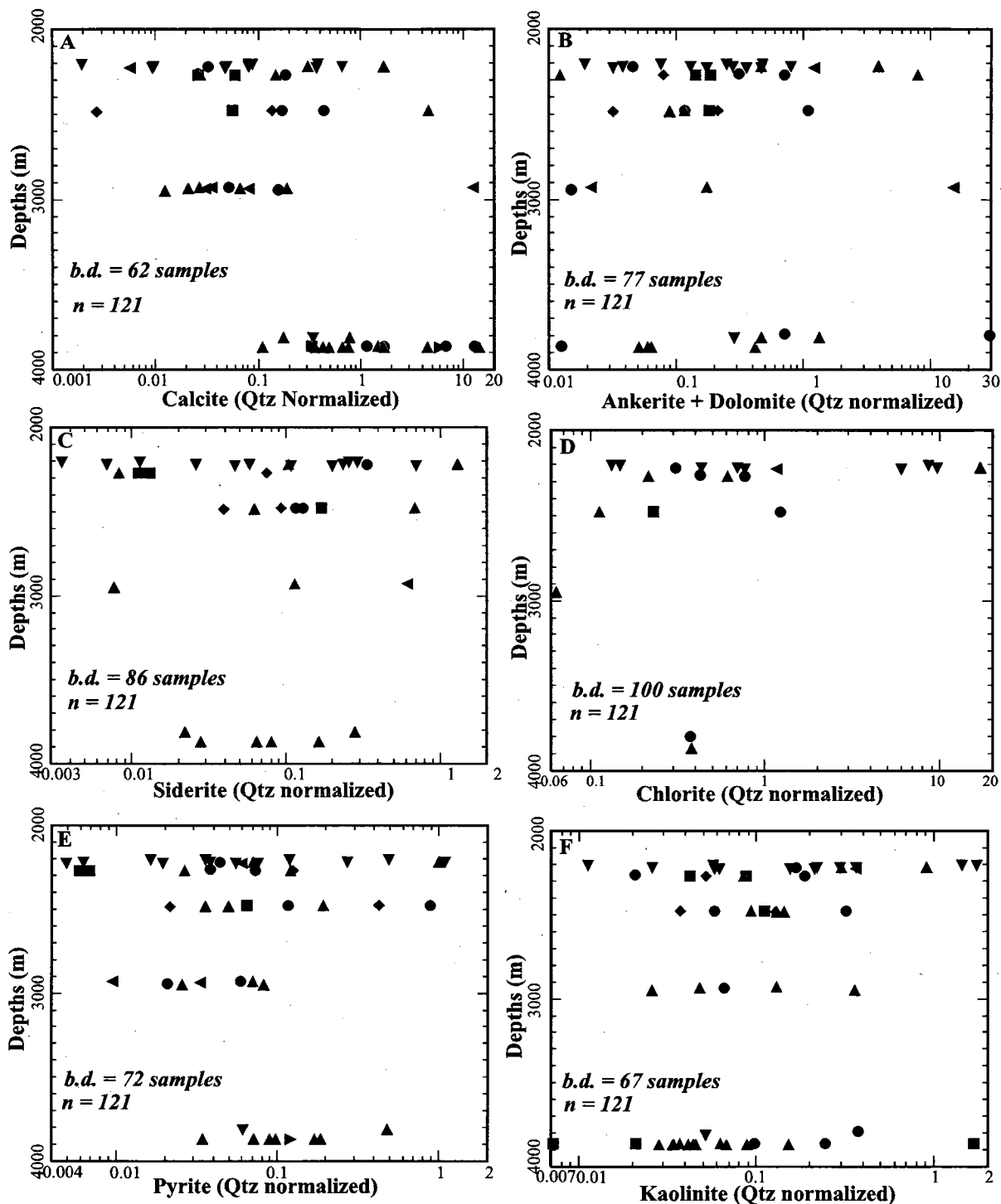


Figure 6.4: Various binary plots for selected diagenetic mineral(Quartz normalized) for both studied wells showing facies variation. (A) Calcite plotted against depth (B) Ankerite + Dolomite plotted against depth (C) Siderite plotted against depth (D) Chlorite plotted against depth (E) Pyrite plotted against depth (F) Kaolinite plotted against depth

6.6 COMPARISON OF TRANSGRESSIVE UNITS

The observations within the transgressive units and underlying prograded sediments (defined as a packet in this study, e.g. Fig. 3.71) for both studied wells are investigated in this section, with reference to minerals observed in coated grains (sea-floor diagenesis) and the geochemical variations within these units. The magnitude of environmental change across a Transgressive Surface (TS) is estimated on a scale of A+ to C (referred to as TS change, Table 3.3), based on the facies changes and inferred changes in sedimentation rates. These differences are likely driven principally by the magnitude of sea-level rise, but paleographic effects such as proximity to a river distributary may be equally important. All TS changes recognized are shown in Table 3.3; examples are discussed here.

6.6.1 Facies and the Sedimentation rates

The most common facies in a given sediment succession probably controls the sedimentation rates. Transgressive deposits that developed while the progradational part of a parasequence formed elsewhere have low net sedimentation rates. By comparison, the presence of facies 9 with a single event bed in the Lower Mississauga samples implies high sedimentation rates (Fig. 5.33). Rapid sediment deposition is also interpreted within the Logan Canyon samples based on the presence of tidal facies 5 (Fig. 5.34).

6.6.2 Thebaud C-74

Packet 1 from 3901.35 m to 3908.11 m, is made up of 5 metre thick progradational succession with about 4 metres of sub-facies 4o (sandstones rich in *Ophiomorpha* and

mud drapes, Fig. 3.71), which abruptly passes up into a one metre of reworked sediments (sub-facies 3b) with an erosional base (Fig. 3.71), which then gradually passes up into bioturbated mudstone. The abrupt contact, and the overlying black mudstones suggests a major change in sedimentation rate, with the thick facies 9 below the facies 4o, the inferred magnitude of environmental change is categorized as an 'A+' type change. Within this packet, type two (Fe-rich) coated grains were identified with diagenetic minerals that include Fe-calcite, glauconite, chlorite, and siderite (Chapter 4). Geochemically, carbonate cementation occurs at the base of the progradational succession (Fig. 5.33), recognized by an increase of S and carbonates (measured as carbon) below the TS.

Packet 3 from 3862.88 m to 3865.00 m, consists of a 3 meters thick progradational succession that culminates in 2 meters of sub-facies 4o (sandstones rich in *Ophiomorpha* and mud drapes Fig. 3.16), which abruptly passes up into one meter of reworked sediments with coarse lithic granules in siderite-cemented medium-grained sandstone, and overlain by black mudstones. The inferred magnitude of environmental change is categorized as an 'A-' type change, as it lacks facies 9 below the TS. The coated grains are similar to those in packet 1 and diagenetic minerals include francolite, chlorite, glauconite, and calcite (Chapter 4). Below the TS, S and carbon (assuming CaCO_3) increases suggesting the presence of carbonate cementation like in packet 1.

Packet 4 from 3859.92 m to 3861.01 m, is made up of a 0.5 meters thick bioturbated mudstone unit that gradually passes up into a 0.5 meters unit with bioclastic reworked

sediments (sub-facies 3l), which is overlain by more bioturbated black mudstone. There is no change in sediment facies below and above the TS, hence the inferred magnitude of environmental change is categorized a 'B-' type. In addition, the coated grain type is also similar to that in packet 1 (Fe-rich), and the diagenetic minerals include chlorite and glauconite (Fig. 4.1A). Below the TS, S and carbon (assuming CaCO_3) increases suggesting the presence of carbonate cementation like in packet 1.

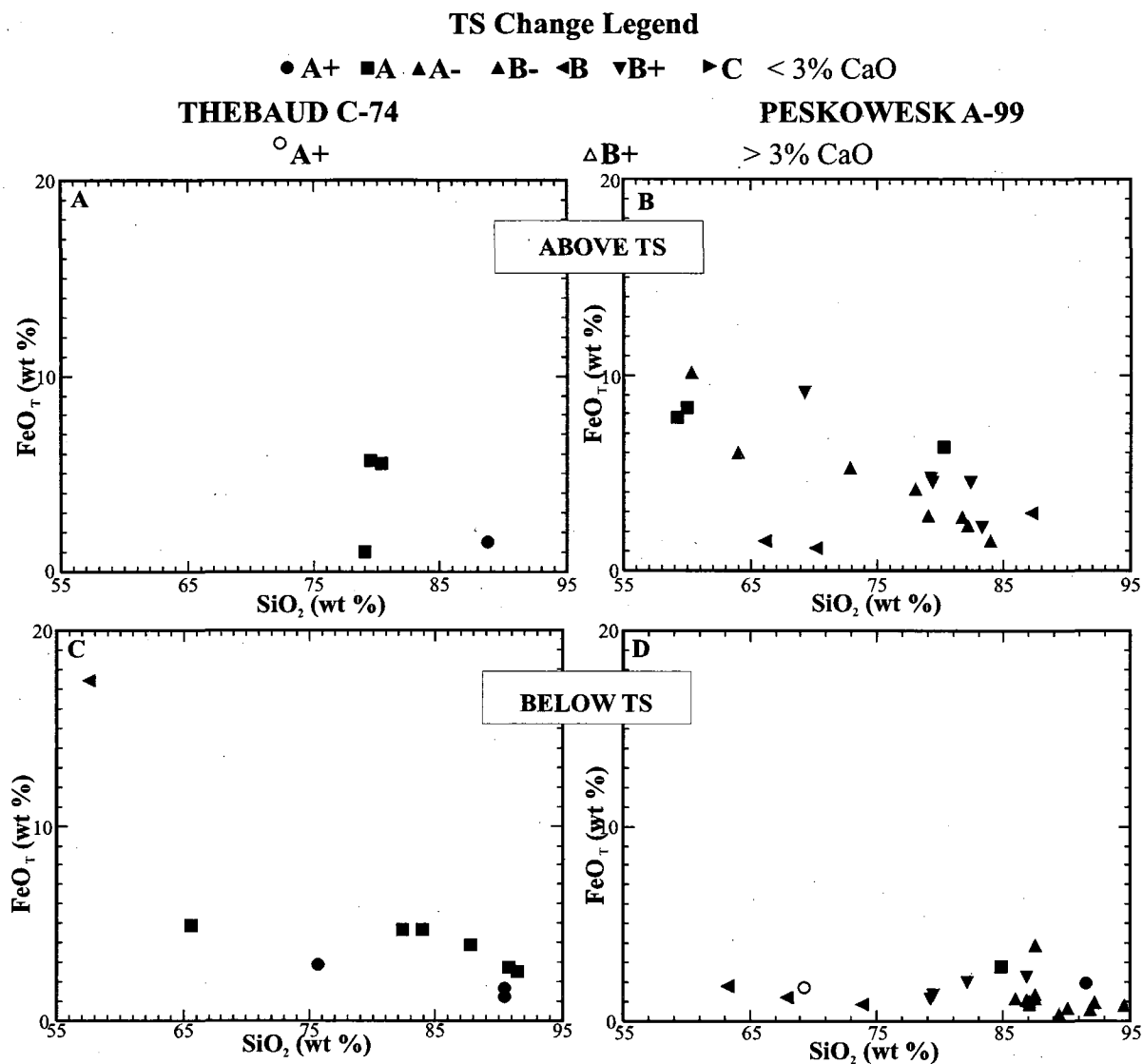
6.6.3 Peskowsk A-99

Packet 6 from 2491.98 m to 2495.28 m, is a 1.8 meters thick retrogradational succession that culminates in 1.3 meters of moderately bioturbated sandstone, with 60% sandstone (sub-facies 2c Fig. 3.6), which abruptly passes up into 0.6 meters of commonly bioturbated, grey-green sandy mudstone with heavy shelly fossils (facies 8, Fig. 3.20), which then passes up into reworked sediments with lithic granules in siderite-cemented medium-grained sandstone capped by a unit of black mudstone with interbedded sandstone (Facies 0). Fig. 4.1D shows the minerals present within this packet that include glauconite suggested to be within the lagoonal facies 8, plus chlorite. The inferred magnitude of environmental change is categorized as an 'A-' type change. Coated grains are similar to those at Thebaud C-74 (type 2: Fe-rich). No geochemical data are available for this packet.

Packet 7 from 2480.30 m to 2482.68 m, a 1.5 meters thick progradational succession that culminates in a 1 meter thick, abundantly bioturbated sandstone (60-90%) with about 10% mudstone (sub-facies 2c Fig. 3.73), which abruptly passes up into a 0.5 meters thick

reworked sediments with mudstone laminae (sub-facies 3a Fig. 3.73), capped by 1 meter of black, bioturbated mudstone. The inferred magnitude of environmental change is categorized as an 'A' type change. Coated grains are classified as type 3 (carbonate rich), and diagenetic minerals include Fe-calcite and pyrite (Fig. 4.1E). Below the TS, S and carbon (assuming CaCO_3) increases, suggesting the presence of carbonate cementation like in packet 1 of Thebaud C-74 (Fig. 5.35).

With respect to the types of inferred environmental change across a TS, binary plots of FeO_T vs. SiO_2 were made for each studied well to test whether a major environmental change resulted in a different amount of precipitation of Fe minerals compared to a smaller environmental change (Fig. 6.5), above and below the TS. The figures (Figs. 6.5A, B, and C) show that there is a weak tendency for higher FeO_T in more abrupt environmental change. Above the TS, there is generally more FeO_T than below the TS. Thus the more abrupt the environmental change and hence the inferred magnitude of sea-level rise (e.g. TS change A) across the TS, the higher the FeO_T content in sediments, suggesting that the precipitation of carbonate cements, largely present in samples with an abrupt TS change and in facies 3 sediments, also increases FeO_T content, perhaps in siderite.



TS Change A+ represents moving from a very shallow water facies into the Transgressive highstand facies association of facies 3, then into open shelf and overlain by a thick progradational succession.

TS change B+ represents moving from a very shallow water facies into shoreface or river mouth facies, then into a progradational sequence.

TS change C represents moving from a fluvial facies into a tidal facies.

Figure 6.5: Various binary plots above and below the TS. (A) Plot of FeO_T against SiO_2 showing TS change variations at Thebaud C-74 above the TS. (B) Plot of FeO_T against SiO_2 showing TS change variations at Peskowesk A-99 above the TS. (C) Plot of FeO_T against SiO_2 showing TS change variations at Thebaud C-74 below the TS. (D) Plot of FeO_T against SiO_2 showing TS change variations at Peskowesk A-99 below the TS.

6.7 FOSSILIZATION OF THE SEA-FLOOR DIAGENETIC SEQUENCE

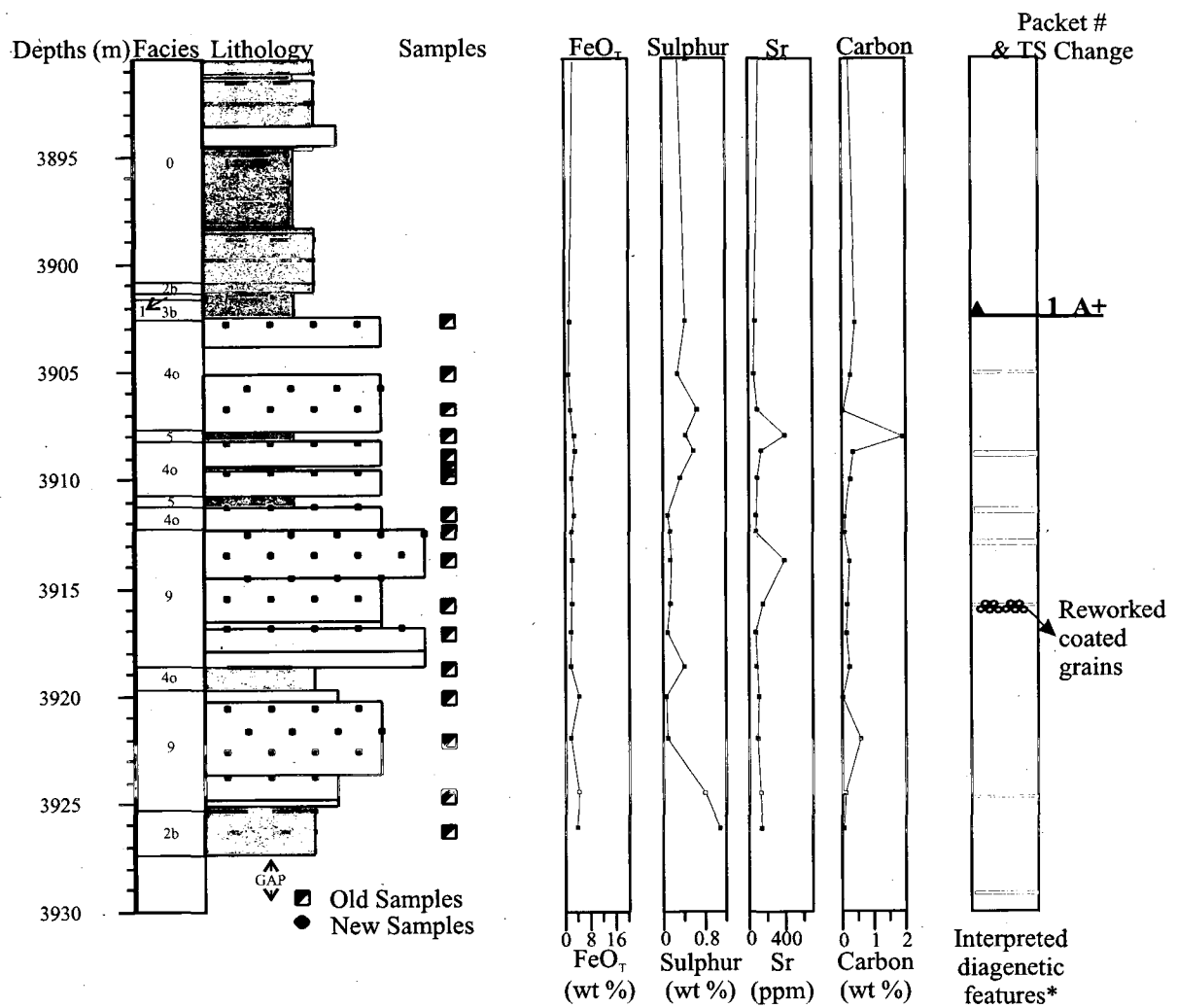
Sea-floor diagenesis results from changes in pore water composition driven by reduction and remineralization of organic carbon. As earlier discussed (Section 6.1), the Gould *et al.* (2010) hypothesis suggests that as a result of transgression, sea-floor diagenetic zones in prograding, high sedimentation rate sandstones tend to fossilize within the transgressive unit in low sedimentation rate transgressive sediments (Fig. 1.3). The effects of fossilization are recognized in this study by the presence of (a) early diagenetic minerals as found in coated grains precipitating above the TS (Fig. 4.1), (b) microscopic siderite cementation (Fig. 4.3E), (c) high Sr content corresponding to high carbonate cementation (Fig. 5.33), and (d) high Fe and P contents stratigraphically, in the Lower Mississauga (Figs. 5.26, 5.28). More importantly is the presence of higher FeO_T where there has been an abrupt and major environmental change in sedimentation rate (Fig. 6.5), which leads to high carbonate cementation.

A possible interpretation of packet 1 in Thebaud C-74 in terms of fossilization of the diagenetic profile is shown in Figure 6.6. This packet shows environmental change across the TS interpreted as A+, with rapid sedimentation of lithofacies 9 below the TS and a highstand facies 1 above it. Most samples below the TS are from sandstones. Sr (a proxy for Ca) and C are elevated between 4 and 18 m below the TS. Sulphur is mostly elevated between 0 and 8 m below the TS, but also shows higher values in muddy sediments at greater depths. FeO_T is elevated from 4 m below the TS. These observations may indicate fossilization of diagenetic minerals to depths of up to 20 m below the TS, but explicit evidence that this is the dominant process controlling diagenetic minerals is lacking.

A corresponding plot of packet 9 in Peskowsk is shown in Figure 6.7. This packet shows less environmental change, rated as B. Thin prodeltaic facies 0 and 9 and fluvial-estuarine facies 4 are overlain by tidal flat facies 5. There is a slight peak in sulphur down to 8 m below the TS, but no systematic variation in Sr and C, and overall carbonate is extremely low. The sulphur peak may merely reflect the presence of muddy sediments, since sulphur seems to correlate inversely with SiO_2 content of sediment (Fig. 5.34). There is no evidence for fossilization of a diagenetic profile in this packet.

6.7.1 The Sampling Problem

The data in this study are limited by the availability of core and the natural variability of rocks. They have been divided based on the different stratigraphic units (section 6.5), and then further divided in terms of the inferred magnitude of environmental change (section 6.6). We have used the distribution of diagenetic minerals (e.g. pyrite, siderite, and calcite) as a key to understanding the sea-floor diagenetic system within this data set. Some authors have carried out similar diagenetic studies (Taylor *et al.*, 1995 & 2000) in outcrop, and their findings have suggested that only subtle diagenetic difference or similarities can be expected. Hence the interpretation in this study may be limited by the available data sets.



* interpreted diagenetic features as seen in core face

Figure 6.6: Cores 4, 5 and 6 at Thebaud C-74 with interpreted core stratigraphy, lithofacies and identified diagenetic features, showing evidence of fossilization below the TS

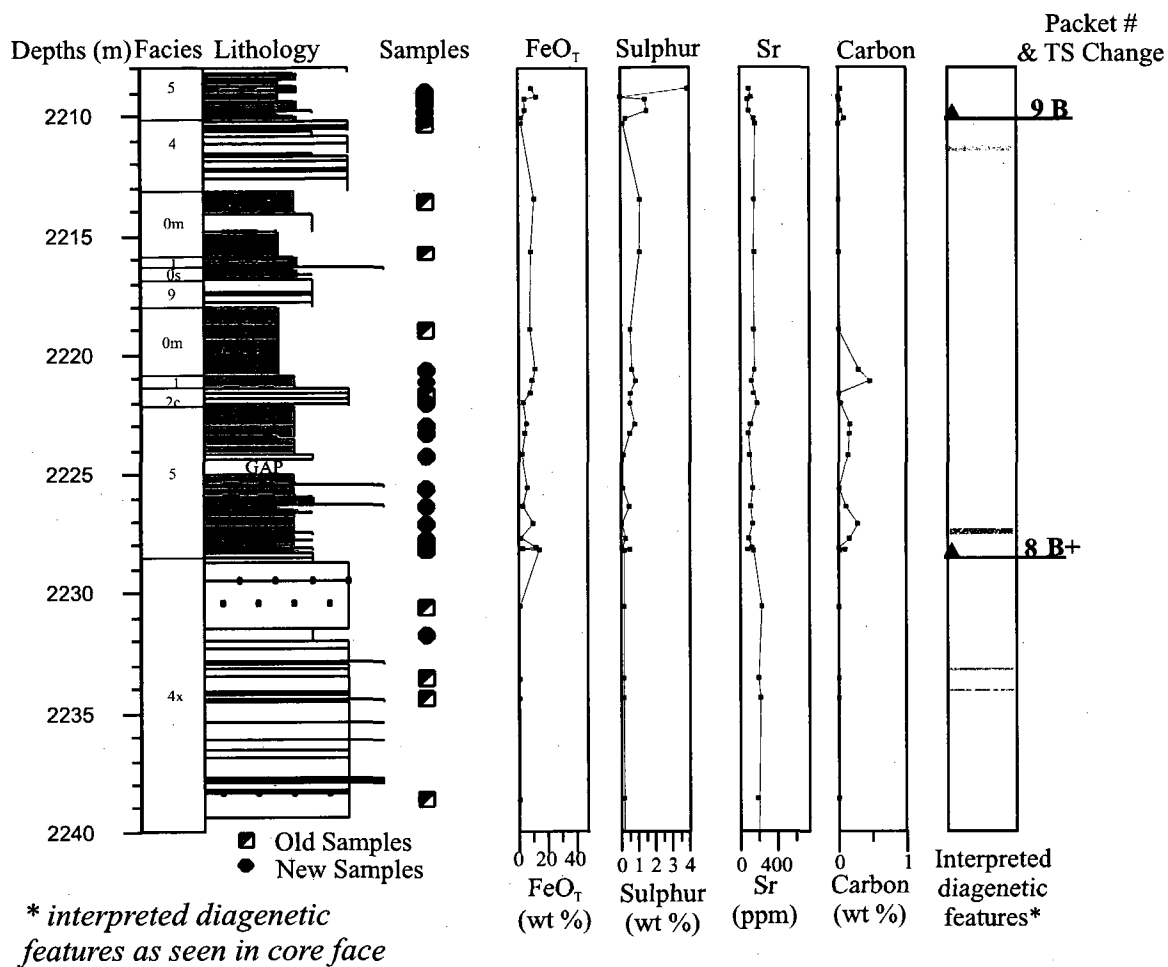


Figure 6.7: Cores 1 and 2 at Peskowesk A-99 with interpreted core stratigraphy, lithofacies and identified diagenetic features, showing evidence of the lack of fossilization below the TS in Core 2.

6.8 AN INTEGRATED DIAGENETIC MODEL

6.8.1 Introduction

A major objective of this study was to determine the nature of the early diagenetic system in the overall diagenesis of sandstone reservoirs in the Scotian Basin, with a focus on two wells: Thebaud C-74 and Peskowesk A-99. Because early diagenesis influences later diagenesis, it is important to understand the early diagenetic processes, especially in Fe-rich sea-floor environments. These processes are studied within minerals found at or near the sea-floor, and in coated grains, with interpretation of the stratigraphic, geochemical and geographic variations surrounding these minerals.

6.8.2 Distribution of Diagenetic Carbonates

At Peskowesk A-99, a prominent diagenetic feature is the early carbonate cementation (especially in the Mississauga and Mic Mac Formations), which has an economic impact on petroleum industries by degrading reservoir quality. As indicated in chapter 4, calcite usually forms during later recrystallization, perhaps through meteoric water or in the zone of methanogenesis. It is however possible that calcite in the coated grains in this study is of later diagenesis with an aragonite precursor. Early carbonate cementation is also present at Thebaud C-74 (predominantly Fe-calcite). For both wells early carbonate cementation is common beneath the TS, in shoreface sandstone where most Fe-rich coated grains have also been identified (chapter 4). Similar early carbonate correlation below transgressive surfaces is found in literature within the Upper Cretaceous Blackhawk Formation in Utah (Taylor *et al.*, 1995). In addition, the presence of Fe-calcite, siderite, and pyrite immediately beneath some TS (Section 4.3; Fig. 6.1) suggests

that these cements are precipitating within the sulphate reduction and methanogenesis zones (Coleman 1985; Curtis et al., 1986 in Taylor et al., 1995).

6.8.3 Principal Component of Whole-rock Geochemistry

From principal component analysis (PCA), K_2O at the Thebaud C-74 loads equally with both PC1 and PC2 (Fig. 5.3). Since no K-feldspar was identified at Thebaud (due to depth of burial, all K-feldspar may be dissolved and replaced by albite), it is suggested that the K_2O is all in glauconite. This would account for K_2O not correlating well with either detrital minerals or carbonate cements. For both wells, CaO behavior (Fig. 5.3 & 5.5) suggests high amounts of CaO, and for this study all CaO are considered calcite, and can be thus be interpreted as effects of calcite cementation, either early or late.

Based on the identified variations and correlations in PCA, it is suggested that CaO and MnO are both in carbonate cements because both oxides are not abundant in other minerals and they both also correlate with Sr, LOI and facies (Figs. 5.4 and 5.6). Fe and Mg going together is due to the presence of abundant chlorite, while the effects of detrital heavy minerals explains the PCA loading of Ti, Zr, and Cr. Ba from drilling mud loads with mean grain size (Mgs) (cluster b in Fig. 5.6), where all samples in the cluster are coarse-grained suggesting that the large pores of the coarser sands absorbs more drilling mud. This effect was also recognized by Gould (2007).

6.8.4 Depositional Model for Studied Wells

As earlier discussed in section 2.4, Thebaud C-74 is a well with a thick, sand prone unit (Fig. 2.5) in the central Sable Subbasin and Peskowesk A-99 is in the Abenaki Subbasin (Fig. 2.4) predominantly with shale and interbedded siltstone to coarse-grained sandstones. Based on the result from sedimentology, petrography and geochemistry and on recent work by Karim *et al.* (2010), a diagenetic model showing sediment accommodation (Fig. 6.8) is proposed for these wells.

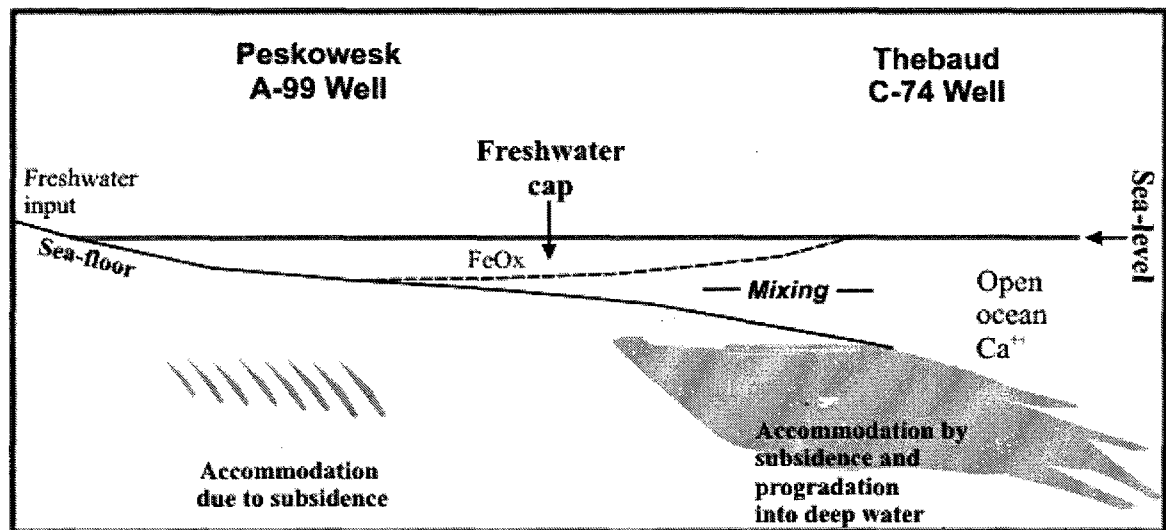


Figure 6.8: Accommodation and diagenesis model for both studied wells.

Paleogeographic studies confirmed that accommodation at the Thebaud C-74 well was provided by fault-related subsidence and progradation into deep water in the shelf-edge deltas (Cummings and Arnott, 2005). At Peskowesk A-99, accommodation is by subsidence on top the shelf. Note that sea-level rise may create temporary accommodation at both wells, by as much as 50 m. Hence, at Thebaud there will be much more opportunity for thick rapidly deposited successions.

At the Peskowsk A-99 well, water supply was dominantly fluvial to brackish in facies 4, 5, and 6 and mixed with ocean water on the shallow shelf in the less common facies 0, 1, 2 and 3. The fluvially-dominated water has higher inputs of Fe but lower Ca than expected in open ocean. Water supplied to the Mic Mac Formation, where there is less evidence of terrigenous input, is suggested to be poorer in Fe since the water available to the sediments should be well mixed with ocean water. In the freshwater zone at Peskowsk A-99 (Fig. 6.8), Fe^{++} is high and Ca^{++} is low, probably as a result of less ocean water influence. Figure 6.9 shows diagenetic minerals precipitating within the different pore-water profile zones. Due to a more Fe feeding the Fe-reduction zone, reduction will take more time, which results in the precipitation of more Fe-rich minerals.

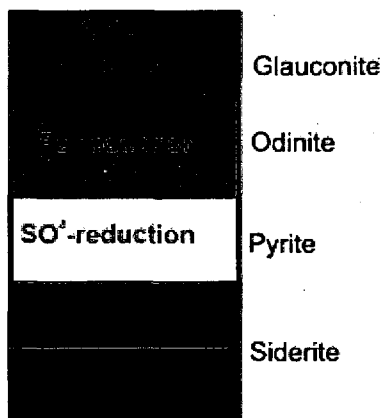


Figure 6.9: Diagenetic minerals within pore-water profiles in the Scotian Basin for the fluvially dominated Peskowsk A-99

In the mixing zone between both wells (Fig. 6.8), the Fe input reduces making the Fe-reduction zone thinner (Fig. 6.10). Note that the distribution of ions from the oxic zone through to the zone of methanogenesis can be controlled by mixing and/or diagenetic reactions. Usually, when Fe^{++} enters the system, it could be by bacterially mediated Fe-reduction or the breakdown of Fe-silicates.

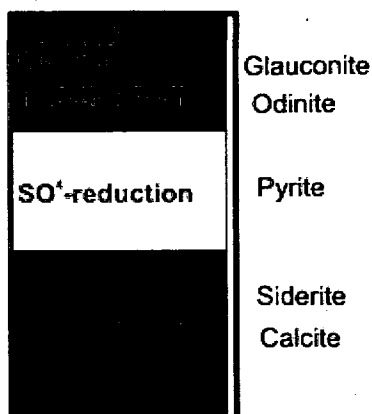


Figure 6.10: Diagenetic minerals within pore-water profiles in the Scotian Basin for the mixing zone between studied wells

At the deep water shelf-edge at Thebaud, fresh water would easily become fully mixed with ocean water, resulting in Ca and Mg enrichment (Fig. 6.11) and this extends the zone of methanogenesis. With these observations, it is suggested that the available water supply for early diagenetic reactions is dependent on paleogeography.

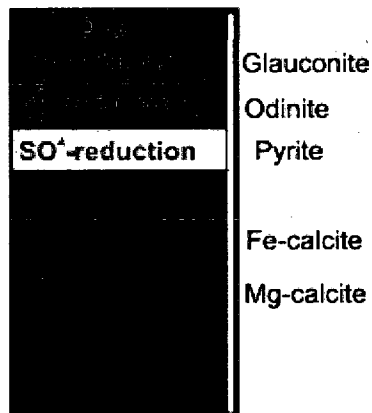


Figure 6.11: Diagenetic minerals within pore-water profiles in the Scotian Basin for the deep water shelf edge at Thebaud C-74

The difference between these wells can thus be associated with paleogeography e.g. abundant siderite at Peskowsk suggested to be as a result of freshwater, and the little siderite found at Thebaud C-74 could be due to marine water being dominant.

Furthermore, when evidence of diagenetic zone fossilization is integrated with coated grains types, a clearer difference can be seen between both studied wells (Fig. 6.12).

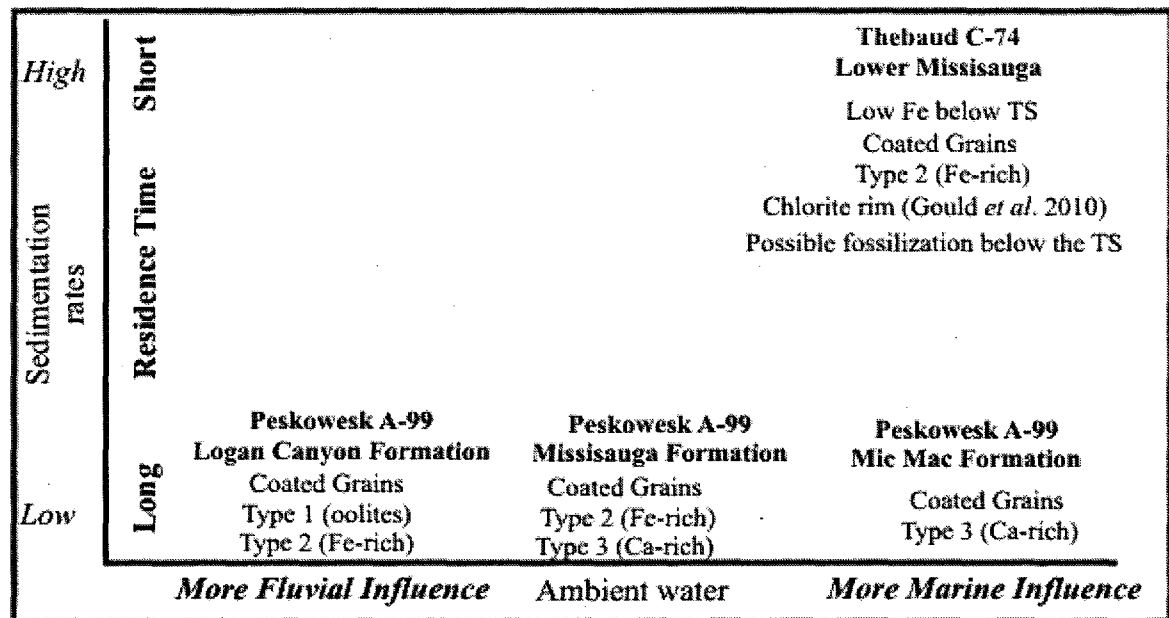


Figure 6.12: Integrated model for studied wells.

The nature of the early diagenetic systems for both wells is controlled by the sediment residence time within the early diagenesis zones (Taylor et al., 1995). Generally, carbonate cementation is widespread (i.e. siderite at Peskowesk vs. Fe-calcite at Thebaud). However carbonate cementation is more at Thebaud, and the early diagenetic minerals are Fe-rich (Fig. 6.11).

6.8.5 Reservoir Quality

The anticipated outcome of this study is a new understanding of the influence of sea-floor diagenesis on the later diagenetic history and reservoir quality in the Scotian Basin. For this study the focus was to fully understand early diagenetic processes, which would eventually influence later diagenesis, hence a detailed observation of later diagenesis is

not given. However, in terms of reservoir quality two diagenetic processes are directly related to this study: (a) late carbonate cementation, and (b) chlorite rims.

Late carbonate cementation is favored by early carbonate cementation. In recent work by Karim *et al.* (in prep), texturally early carbonate have isotope values of late carbonate cements. At Peskowsk, calcite (Fe and Mg-rich) have both been identified to be textually early, however it is possible that these carbonates are a later replacement. Chlorite rims have been identified by Gould (2007) at Thebaud. The chlorite rims are favored by a Fe-rich system and destroyed by the presence of meteoric water. Gould (2010) and Karim *et al* (2010) suggested that when sea-level lowers in the presence of meteoric water, this results in the presence of kaolinite in pores, destruction of precursors of chlorite (e.g. oodinite), alteration of feldspars, and the corrosion of pyrite. The Thebaud environment is suitable for the precipitation of chlorite rims on the basis of rapid subsidence of deltas. Meteoric water can be associated with the presence of kaolinite, which is more common at Peskowsk A-99.

6.9 CONCLUSIONS

Early diagenesis is influenced by pore-water chemistry. The chemistry of the pore-water in facies 3 sediments is very favorable to early diagenetic processes, specifically with regards to high Fe^{2+} content. All identified early diagenetic minerals in facies 3 (with its sub-facies) occur within type 2 (Fe-rich) coated grains in both wells, suggesting that facies 3 sediments are more Fe-rich, probably resulting in more early diagenetic reactions.

The early diagenetic system in both wells is similar in terms of identified lithofacies, petrography and geochemistry. However, the rate of sedimentation and the residence time are the driving forces of the diagenetic system in each well. Thus at Thebaud C-74 the large environmental change across transgressive surfaces and the occurrence of Fe-rich coated grains suggest higher rates of sedimentation and shorter residence time. At Peskowsk A-99, the presence of smaller environmental change across transgressive surfaces and the greater abundance of fluvial and tidal facies suggest greater influence of fresh compared with ocean water and a higher residence.

The fossilization of the diagenetic sequence as a result of change in sedimentation rates occurs only where such changes are large. This it has been recognized in the Thebaud C-74 well but not in the Peskowsk A-99 well.

The strong early diagenetic relationship between P and Ti proposed by Gould et al., 2010 has not been substantiated by the new data from these wells.

Two types of seawater influence the early diagenetic system, River water rich in colloidal iron (oxy)-hydroxide only partially mixes with seawater on the inner shelf and this resulted in predominant Fe-rich early diagenetic minerals in the Missisauga and Logan Canyon Formations at Peskowsk and in progradational sediments at Thebaud. At inactive shelf edge deltas and on the outer shelf during the Mic Mac Formation, open ocean seawater was little diluted by river water, as reflected by early diagenetic minerals richer in Ca and Mg in some facies 3 at Thebaud and in the Mic Mac Formation at Peskowsk.

REFERENCES

- Al-Ramadan, K., Morad, S., Proust, J.N., and Al-Aasm, I., 2005. Distribution of diagenetic alternations in siliciclastic shoreface deposits within a sequence stratigraphic framework: evidence from the upper Jurassic, Boulonnais, NW France. *Journal of Sedimentary Research*, Vol. 75, pp. 943-959.
- Berner, R.A., 1980. *Early Diagenesis: A Theoretical Approach*. Princeton University Press.
- Berner, E.K., and Berner, R.A., 1996. *Global Environment: Water, Air and Geochemical Cycles*. Prentice-Hall Inc.
- Buatois, L.A., Mangano, G., and Carr, T.R., 1999. Sedimentology and ichnology of Paleozoic estuarine and shoreface reservoirs, Morrow Sandstone, Lower Pennsylvanian of Southwest Kansas, USA. *Bulletin of the Kansas Geological Survey*, Vol. 243, Pt 1, pp. 35.
- Burdige, D.J., 2006. *Geochemistry of Marine Sediments*. Princeton University Press.
- Burns, S.J., 1997. Early diagenesis in Amazon Fan sediments. In: Flood, R.D., Piper, D.J.W., Klaus, A., and Peterson, L.C., (Eds), 1997. *Proceedings of the Ocean Drilling Program, Scientific Results*, Vol. 155, pp. 497-504.
- Catuneanu, O., Abreu, V., Bhattacharya, J.P., Blum, M.D., Dalrymple, R.W., Eriksson, P.G., Fielding, C.R., Fisher, W.L., Galloway, W.E., Gibling, M.R., Giles, K.A., Holbrook, J.M., Jordan, R., Kendall, C.S.St.C., Macurda, B., Martinsen, O.J., Miall, A.D., Neal, J.E., Nummedal, D., Pomar, L., Posamentier, H.W., Pratt, B.R., Sarg, J.F., Shanley, K.W., Steel, R.J., Strasser, A., Tucker, M.E., and Winker, C., 2009. Towards the standardization of sequence stratigraphy. *Earth Science Reviews* 92, pp. 1-33.
- Cha, H.J., Lee, C.B., Kim, B.S., Choi, M.S., and Ruttenberg, K.C., 2005. Early diagenesis redistribution and burial of phosphorus in the sediments of the southwestern East Sea (Japan Sea). *Marine Geology*, Vol. 216, pp. 127-143.
- Coleman, M.L., 1985. Geochemistry of diagenetic non-silicate minerals: kinetic considerations, *Philosophical Transaction of the Royal Society of London*, Vol. A315, pp. 39-56.
- Collin, P.Y., Loreau, J.P., and Courville, P., 2005. Depositional environments and iron ooid formation in condensed sections (Callovian-Oxfordian, south-eastern Paris Basin, France). *Sedimentology*, Vol. 52, pp. 969-985.
- Cummings, D.I., and Arnott, R.W., 2005. Growth-faulted shelf-margin deltas: a new (but old) play type, offshore Nova Scotia. *Bulletin of Canadian Petroleum Geology*, Vol. 53, No. 3, pp. 211-236.

Cummings, D.I., Hart, B.S., and Arnott, R.W., 2006. Sedimentology and stratigraphy of a thick, areally extensive fluvial-marine transition, Missisauga Formation, offshore Nova Scotia, and its correlation with shelf margin and slope strata. *Bulletin of Canadian Petroleum Geology*. Vol. 54, No. 2, pp. 152-174.

Davies, P.J., Bubela, D., and Ferguson, J., 1978. The formation of ooids. *Sedimentology*, Vol. 25, No. 5, pp. 703-729.

Curtis, C.D., Coleman, M.L., and Love, L.G., 1986. Pore water evolution during sediment burial from isotope and mineral chemistry of calcite, dolomite and siderite concretions. *Geochimica et Cosmochimica Acta*, Vol. 50, pp. 2321-2334.

Deflandre, B., Mucci, A., Gagne, J.P., Guignard, C., and Sundby, B., 2002. Early diagenetic processes in costal marine sediments distributed by a catastrophic sedimentation event. *Geochimica et Cosmochimica Acta*, Vol. 66, No. 14, pp. 2547-2558.

Dehler, S., Boutilier, R., Fensome, R., Jackson, R., Keen, C., MacMillan, B., Potter, P., Shimeld, J., Funck, T., Loudon, K., MacRae, A., and Upson, P., 2004. Geology of the Scotian Margin, Geological Survey of Canada, Atlantic. <http://www.nrcan.gc.ca>

Dickson, J.A.D., 2001. Diagenesis and crystal caskets: Echinoderm Mg-calcite transformation, Dry Canyon, New Mexico. *Journal of Sedimentary Research*, Vol. 71, No. 5, pp. 764-777.

Dickson, J.A.D., 2004. Echinoderm skeletal preservation: Calcite-aragonite seas and the Mg/Ca ratio of Phanerozoic oceans. *Journal of Sedimentary Research*, Vol. 74, pp. 355-365.

Droser, M.L., Jensen, S., and Gehling, J.G., 2002. Trace fossils and substrates of the terminal Proterozoic–Cambrian transition: implications for the record of early bilaterians and sediment mixing. *Proceedings of the National Academy of Sciences*, Vol. 99, pp. 12572–12576.

Drummond, K.J., 1992. Geology of Venture, a geopressed gas field, offshore Nova Scotia. In: M.T. Halbouty, ed., *Giant Oil and Gas Fields of the Decade 1978-1988: AAPG Memoir 54*, pp. 55-71.

El-ghali, M.A.K., Mansurbeg, H., Morad, S., Al-Aasm, I., and Ajdanlisky, G., 2006. Distribution of diagenetic alterations in fluvial and paralic deposits within sequence stratigraphic framework: Evidence from the Petrohan Terrigenous Group and the Svidol Formation, Lower Triassic, NW Bulgaria. *Sedimentary Geology*, Vol. 190, pp. 299-321.

El-ghali, M.A.K., Morad, S., Mansurbeg, H., Caja, M.A., Sirat, M., and Ogle, N., 2009. Diagenetic alterations related to marine transgression and regression in fluvial and

shallow marine sandstones of the Triassic Buntsandstein and Keuper sequence, the Paris Basin, France. *Marine and Petroleum Geology*, Vol. 26, pp. 289-309.

Essene, E.J. & Peacor, D.R., 1997. Illite and smectite - metastable, stable, or unstable? *Clays & Clay Minerals*, Vol. 45, pp. 116-122.

Fazio, A.M., Scasso, R.A., Castro, L.N., and Carey, S., 2007. Geochemistry of rare earth elements in early diagenetic Miocene phosphatic concretions of Patagonia, Argentina: Phosphogenetic implications. *Deep Sea Research Part II*, Vol. 54, pp. 1414-1432.

Fisher, J.B., 1982. Effects of macrobenthos on the chemical diagenesis of fresh water sediments. In: McCall, P.L., and Tevesz, M.J.S, Eds., *Animal-Sediment Relations. The Biogenic Alteration of Sediments*, Plenum Press, p. 635-644.

Froelich, P.N., Klinkhammer, G.P., Bender, M.I., Luedtke, N.A., Heath, G.R., Cullen, D., and Dauphin, P., 1978. Early oxidation of organic matter in pelagic sediment of the eastern equatorial Atlantic: suboxic diagenesis. *Geochimica et Cosmochimica Acta*, Vol. 43, pp. 1075-1090.

Froelich, P.N., Arthur, M.A., Burnett, W.C., Deakin, M., Hensley, V., Jahnke, R., Kaul, L., Kim, K-H., Roe, K., Soutar, A., and Vathakanon, C., 1988. Early diagenesis of organic matter in Peru continental margin sediments: phosphorite precipitation. *Marine Geology*, Vol. 80, pp. 309-343.

Gould, K.M., 2007. Chlorite diagenesis in reservoir sandstones of the Lower Missisauga Formation, offshore Nova Scotia. A thesis submitted to Saint Mary's University, Halifax Nova Scotia.

Gould, K., Pe-Piper, G., and Piper, D.J.W., 2010. Relationship of diagenetic chlorite rims to depositional facies in Lower Cretaceous reservoir sandstones of the Scotian Basin. *Sedimentology Journal*. Vol. 57, pp. 587-610.

Hansen, M.D., Shimeld, J.W., Williamson, M.A., and Lykke-Anderson, H., 2004. Development of a major polygonal fault system in Upper Cretaceous chalk and Cenozoic mudrocks of the Sable Subbasin, Canadian Atlantic Margin. *Marine and Petroleum Geology*, Vol. 21, pp. 1205-1219.

Haq, B.U., Hardenbol, J., and Vail, P.R., 1987. Chronology of fluctuating sea levels since the Triassic. *Science*, Vol. 235, No. 4793, pp. 1156-1167.

Ings, S.J. and Shimeld, J.W. 2006. A new conceptual model for the structural evolution of a regional salt detachment on the northeast Scotian margin, offshore eastern Canada. *AAPG Bulletin*, Vol. 90, pp. 1407-1423.

- Jansa, L.F., and Noguera-Urrea, V.H., 1990. Geology and diagenetic history of overpressured sandstones reservoirs, Venture gas field, offshore Nova Scotia, Canada, AAPG Bulletin, Vol. 74, pp. 1640-1658.
- Karim, A., Pe-Piper, G., and Piper, D.J.W., 2008. Distribution of diagenetic mineral in Lower Cretaceous sandstones and their relationship to stratigraphy and lithofacies: Glenelg, Thebaud and Chebucto fields, offshore Scotian Basin. Geological Survey of Canada, open file 5880.
- Karim, A., Pe-Piper, G., and Piper, D.J.W., 2010. Controls on diagenesis of Lower Cretaceous reservoir sandstones in the western Sable Subbasin, offshore Nova Scotia, Sedimentary Geology. Vol. 224, pp. 65-83.
- Kozłowska, A., 2003. Genesis of carbonate minerals in the Upper Carboniferous sandstones in central Poland. Polskie Towarstwo Mineralogiczne-Prace Specjalne Mineralogical Society of Poland- Special Papers. Vol. 22, pp. 115-118.
- Kretz, R., 1983. Symbols for rock-forming minerals. American Mineralogist, Vol. 68, pp. 277-279.
- Louchouart, P., Lucotte, M., Duchemin, E., and de Vernal, A., 1997. Early diagenetic processes in recent sediment of the Gulf of St. Lawrence: phosphorus, carbon, and iron burial rates. Marine Geology, Vol. 139, pp. 181-200.
- MacEachern, J.A., Bann, K.L., Bhattacharya, J.P., and Howell, C.D., Jr. 2005. Ichnology of deltas: Organisms response to the dynamic society of rivers, waves, storms, and Tides. Special Publication-Society of Sedimentary Geology, Vol. 83, pp. 49-85.
- MacLean, B.C., and Wade, J.A., 1993. Seismic markers and stratigraphic picks in Scotian Basin wells: Atlantic Geoscience Centre, Geological Survey of Canada, 276 p.
- McArthur, J.M., 1984. Francolite geochemistry: compositional controls during formation, diagenesis, metamorphism and weathering. Geochemica et Cosmochimica Acta, Vol. 49, pp. 23-35.
- Noguera, V.H., 1987. Geology and diagenetic history of over-pressured siliclastic reservoirs in the Lower Missisauga-Mic Mac Formations of the Venture gas field, Scotian Shelf, Nova Scotia. A thesis submitted to Dalhousie University, Halifax Nova Scotia.
- Ohta T. and Arai, H., 2007. Statistical empirical index of chemical weathering in igneous rocks: A new tool for evaluating the degree of weathering. Chemical Geology, Vol. 240, pp. 280-297.

- Pe-Piper, G., and Dolansky, L., 2005. Early diagenetic origin of Al phosphate-sulfate minerals (woodhouseite-crandallite series) interstitial sandstones, Nova Scotia, Canada. *American Mineralogist*, Vol. 90, pp. 1434-1441.
- Pe-Piper, G., and MacKay, R.M., 2006. Provenance of Lower Cretaceous sandstones onshore and offshore Nova Scotia from electron microprobe geochronology and chemical variation of detrital monazite. *Bulletin of Canadian Petroleum Geology*, Vol. 54, No. 4, pp. 366-379.
- Pe-Piper, G., and Weir-Murphy, S., 2008. Early diagenesis of inner shelf phosphorites and iron silicate minerals, Lower Cretaceous of Orpheus graben, southeastern Canada: implications of the origin of chlorite rims. *AAPG Bulletin*, Vol. 92, pp. 1153-1168.
- Pe-Piper, G., Piper, D.J.W., Dolansky, L.M., 2005. Alteration of ilmenite in the Cretaceous sands of Nova Scotia, southeastern Canada. *Clay and Clay Minerals*, Vol. 53, pp. 490-510.
- Pe-Piper, G., Triantafyllidis, S., and Piper, D.J.W., 2008. Geochemical identification of clastic sediment provenance from known sources of similar geology. The Cretaceous Scotian Basin, Canada. *Journal of Sedimentary Research*, Vol. 78, No. 9, pp. 595-607.
- Pe-Piper, G., Piper, D.J.W., Gould, K.M., and Shannon, J., 2006. Depositional environment and provenance analysis of the Lower Cretaceous sedimentary rocks at the Peskowsk A-99 well, Scotian Basin, Geological Survey of Canada, open file report 5383.
- Pemberton, S.G., and MacEachern, J.A., 1995. The sequence stratigraphy significance of trace fossils in examples from the Cretaceous of Alberta. In: Van Wagoner, J.A., and Bertram, G.T., eds. *Sequence Stratigraphy of Foreland Basin Deposits – Outcrop and Subsurface Examples from the Cretaceous of North America*, American Association of Petroleum Geologists Memoir, Vol. 64, pp. 429-447.
- Pemberton, S. G., Frey, R. W., Ranger, M. J., and MacEachern, J. A., 1992, The conceptual framework of ichnology. In: *Applications of Ichnology to Petroleum Exploration--A Core Workshop*, S. G. Pemberton, ed.: Society of Economic Paleontologists and Mineralogists, Core Workshop 17, p. 1-32.
- Piper, D.J.W., Pe-Piper, G., and Ingram, S.C., 2004. Early Cretaceous sediment failure in the southwestern sable Subbasin, offshore Nova Scotia. *AAPG Bulletin*. Vol. 88, pp. 991-1006.
- Piper, D.J.W., Nofall, R., and Pe-Piper, G., 2010. Allochthonous prodeltaic sediment facies in the Lower Cretaceous at the Tantallon M-41 well: Implications for the deep-water Scotian Basin. *AAPG Bulletin*, Vol. 94, No. 1, pp. 87-104.

- Posamentier, H.W., and Allen, G.P., 1999. Siliciclastic sequence stratigraphy: concepts and applications. *Concepts in Sedimentology and Paleontology*, Vol. 7, Society of Economic Paleontologists and Mineralogists (SEPM). 210 pp.
- Pucci, A.A., Szabo, Z., and Owens, J.P., 1997. Variations in pore-water quality, mineralogy, and sedimentary texture of clay-silts in the Lower Miocene Kirkwood Formation, Atlantic City, New Jersey. In: Miller, K.G., and Snyder, S.W. (Eds),. *Proceedings of the Ocean Drilling Program, Scientific Results*, Vol. 150X.
- Pufahl, P.K., Grimm, K.A., Abed, A.M., and Sadagah, R.M.Y., 2003. Upper Cretaceous (Campanian) phosphorite in Jordan: Implication for the formation of a south Tethyan phosphorite giant. *Sedimentary Geology*, Vol. 161, No. 3, pp. 175-205
- Pufahl, P.K., and Grimm, K.A., 2003. Coated phosphate grains: proxy for physical, chemical, and ecological changes in seawater. *Geology*, Vol. 31. No. 9, pp. 801-804.
- Rich, J.L., 1951. Three critical environments of deposition and criteria for recognition of rocks deposited in each of them. *Geological Society of America Bulletin*, Vol. 62, pp. 1-20.
- Rollinson, H.R., 1993. *Using Geochemical Data: Evaluation, Presentation, Interpretation*. Longman Group UK Limited, pp. 37-38.
- Rossi, C., Marfil, R., Ramseyer, K., and Permanyer, A., 2001. Facies-related diagenesis and multiphase siderite cementation and dissolution in the reservoir sandstones of the Khataba Formation, Egypt's Western Desert. *Journal of Sedimentary Research*, Vol. 71, No. 3, pp. 459-472.
- Ruttenberg, K.C., and Goñi, M.A., 1997. Depths trends in phosphorus distribution and C:N:P ratios of organic matter in Amazon fan sediments: indices of organic matter sources and burial history. In: Flood, R.D., Piper, D.J.W., Klaus, A., and Peterson, L.C. (Eds), 1997. *Proceedings of the Ocean Drilling Program, Scientific Results*, Vol. 188, pp. 505-517.
- Seeberg-Elverfeldt, J., Schlüter, M., Feseker, T., and Kölling, M., 2005. Rhizon sampling of pore-water near the sediment-water interface of aquatic systems. *Limnol. Oceanogr. Methods* 3, pp. 361-371.
- Smith, L.I., 2002. A tutorial on principal component analysis. http://www.cs.otago.ac.nz/cosc453/student_tutorials/principal_components.pdf, pp. 1-24.
- Stoll, H. M., and Schrag, D. P., 1996. Evidence for glacial control of rapid sea level changes in the Early Cretaceous. *Science*, Vol. 272, pp. 1771-1774.

Taylor, K.G., Gawthorpe, R.L., and Van Wagoner, J.C., 1995. Stratigraphic control on laterally persistent cementation, Book Cliffs, Utah. *Journal of the Geological Society*, London, Vol. 152, pp. 225-228.

Taylor, K.G., Gawthorpe, R.L., Curtis, C.D., Marshall, J.D., and Awwiller, D.N., 2000. carbonate cementation in a sequence-stratigraphic framework: Upper Cretaceous sandstones Book Cliff, Utah-Colorado. *Journal of Sedimentary Research*, Vol. 70, No. 2, pp. 360-372.

Toevs, G.R., Morra, M.J., Polizzotto, M.J., Strawn, D.G., Bostick, B.C., and Fendorf, S., 2006. Meta(lloid) diagenesis in mine-impacted sediments of Lake Coeur d'Alene, Idaho. *Environmental Science and Technology*. Vol. 40, pp. 2537-2543.

Tromp, T.K., Van Cappellan, P., and Key, R.M., 1995. A global model for the early diagenesis of organic carbon and organic phosphorus in marine sediments. *Geochimica et Cosmochimica Acta*, Vol. 59, No. 7, pp. 1259-1284.

Tucker, M. E., Wright, V. P and Dickson, J.A.D., 1990. *Carbonate Sedimentology*. Blackwell Science. pp. 2-3.

Wade, J.A., and MacLean, B.C., 1990. Aspects of the geology of the Scotian Basin from recent seismic and well data. In: M.J. Keen and G.L. Williams (eds.) *Geology of the Continental Margin off Eastern Canada: Geological Survey of Canada*, Vol. 2, pp. 87-137.

Wade, J.A., MacLean, B.C., and Williams, G.L., 1995. Mesozoic and Cenozoic stratigraphy, eastern Scotian shelf: new interpretations. *Canadian Journal of Earth Sciences*, Vol. 32, pp. 1462-1473.

Weir-Murphy, S. L., 2004. The Cretaceous rocks of the Orpheus Graben, offshore Nova Scotia. Saint Mary's University, Halifax N.S., Canada, M.Sc thesis, 168p.

Worden, R.H., and Burley, S.D., 2003. *Sandstone Diagenesis: the Evolution of Sand to Stone*. Blackwell Publishing, pp. 3-44.